

University of Alberta

**Process Analysis of Rockfalls with Stationary Terrestrial LiDAR and RockFall
Analyst**

by

James Andrew Russell

A thesis submitted to the Faculty of Graduate Studies and Research
in partial fulfillment of the requirements for the degree of

Master of Science

in

Geotechnical Engineering

Department of Civil and Environmental Engineering

©James Andrew Russell

Fall 2011

Edmonton, Alberta

Permission is hereby granted to the University of Alberta Libraries to reproduce single copies of this thesis and to lend or sell such copies for private, scholarly or scientific research purposes only. Where the thesis is converted to, or otherwise made available in digital form, the University of Alberta will advise potential users of the thesis of these terms.

The author reserves all other publication and other rights in association with the copyright in the thesis and, except as herein before provided, neither the thesis nor any substantial portion thereof may be printed or otherwise reproduced in any material form whatsoever without the author's prior written permission.

ABSTRACT

Rockfalls are a hazard concern for many transportation corridors in Alberta and British Columbia. A method of analyzing and further understanding rockfalls could help to reduce the hazard potential that rockfalls present. Rockfall hazard assessments are carried out in three steps: (1) identification of hazard zones, (2) site investigation to establish the site characteristics and rockfall source, and (3) empirical and numerical analyses. This study investigates the use of terrestrial LiDAR technology along highways in Southern Alberta for the second step of rockfall hazard assessment, and the RockFall Analyst software program on data obtained from a measured rockfall event at Tornado Mountain for the third step. The limitations of technologies involved are described, as well as the importance of the topography that describes rockfall trajectory and determines rockfall energy.

ACKNOWLEDGEMENTS

Dr. Derek Martin, my supervisor; for his advice and support in the completion of this thesis.

Mr. Renato Macciotta; for his help on site in both the summers of 2009 and 2010, as well as his insight into the possibilities of the studies conducted.

Alberta Infrastructure and Transportation; for the funding that they provided for the LiDAR survey and analysis, as well as providing a site tour (along with AMEC) of land movement concerns throughout southern Alberta.

Mr. Neil Kjelland; for guiding me through the AIT site tour.

Mr. Duncan Wyllie; for sharing his information and advice on the Tornado Mountain rockfall event.

Dr. Chris Bunce; for helping facilitate the site visit at Tornado Mountain.

CP Rail; for allowing us to investigate Tornado Mountain, as well as providing transportation to the site.

NSERC; for the funding provided towards the completion of this study.

TABLE OF CONTENTS

ABSTRACT

ACKNOWLEDGEMENTS

TABLE OF CONTENTS

LIST OF TABLES

LIST OF FIGURES

LIST OF SYMBOLS, NOMENCLATURE, AND ABBREVIATIONS

1. INTRODUCTION	1
1.1. Scope of Study	1
1.2. Research Objective	2
2. LITERATURE REVIEW	3
2.1. Rockfall Hazards.....	4
2.1.1. Rockfall Hazard Rating System.....	6
2.2. LiDAR	9
2.3. RTK GPS	13
2.4. RockFall Analyst	14
2.5. Coefficient of Restitution.....	16
2.6. Energy Absorption Capacity of Trees on Slope.....	20
2.7. Means of Mitigation.....	22
3. CHARACTERISTICS OF SEVERAL ROCKFALL SITES ALONG TRANSPORTATION CORRIDORS IN SOUTHWESTERN ALBERTA AND SOUTHEASTERN BRITISH COLUMBIA	23
3.1. Alberta Infrastructure and Transportation Sites.....	23
3.1.1. Highway 3 – Crowsnest Lake	23
3.1.2. Highway 541 – Highwood House Rock-Cut	29

3.1.3.	Highway 541 – East of Fir Creek Rock-Cut	34
3.1.4.	Highway 40 – Galatea Creek Through-Cut	36
3.1.5.	Highway 40 – Mt. Baldy Rock-Cut	39
3.1.6.	Old Man Dam	43
3.1.7.	Highway 724:02 – Spray Lake Site Gabion Wall.....	45
3.2.	Mapping a Rockfall Trajectory: Tornado Mountain	48
3.2.1.	Site Location	48
3.2.2.	Site Characteristics.....	49
3.3.	Summary	53
4.	EVALUATION OF TERRESTRIAL LIDAR.....	54
4.1.	Terrestrial LiDAR Using the Optech ILRIS-3D.....	54
4.2.	LiDAR Application.....	57
4.2.1.	Highway 3 – Crowsnest Lake	58
4.2.2.	Highway 541 – Highwood House Rock Cut.....	61
4.2.3.	Highway 541 – East of Fir Creek Rock Cut	63
4.2.4.	Highway 40 – Galatea Creek Through-Cut	65
4.2.5.	Highway 40 – Mt. Baldy Rock Cut.....	67
4.2.6.	Old Man Dam	68
4.2.7.	Highway 724:02 – Spray Lake Site (Gabion Wall)	69
4.3.	Terrestrial LiDAR in Future Site Reviews	70
4.3.1.	LiDAR data in Rockfall Analysis	70
4.3.2.	Application in Hazard Management	72
5.	ROCKFALL ANALYST/COEFFICIENTS OF RESTITUTION.....	74
5.1.	RTK GPS Survey of Tornado Mountain.....	74

5.2.	Three Dimensional Rockfall Analyses	81
5.2.1.	Initial Calibration Approach	84
5.2.2.	Rockfall Energy Calibration Approach.....	92
5.2.3.	COR Analysis	96
5.2.4.	Sensitivity of Analysis to Change in Friction	113
5.2.5.	Effect of Trees on RA and COR	116
5.3.	Summary of Three Dimensional Rockfall Analyses.....	119
6.	CONCLUSION.....	122
6.1.	Stationary Terrestrial LiDAR Surveys.....	122
6.2.	Tracking Rockfall Trajectories on Tornado Mountain	124
6.3.	Rockfall Simulations.....	125
6.4.	Future Studies and Applications	127
	REFERENCES	128
	APPENDIX A.....	132
	APPENDIX B.....	136
	APPENDIX C.....	142
C.1	Site Notes.....	142
C.2	GPS Survey Data	146
C.3	Rockfall Analysis Profiles	149

LIST OF TABLES

Table 2.1: Preliminary Rating System (Modified from Pierson and Van Vickle 1993, p18).....	7
Table 5.1: Slope Coefficient Parameters for Initial Calibration	85
Table 5.2: Rockfall Seeder Calibration Input Velocities with $\Theta=45^\circ$	94
Table 5.3: Rockfall Seeder Calibration Input Velocities with $\Theta=55^\circ$	94
Table 5.4: Rockfall Seeder Calibration Input Velocities with $\Theta=65^\circ$	94
Table 5.5: Rockfall Seeder Calibration Input Velocities with $\Theta=75^\circ$	95
Table 5.6: Values of COR for Sensitivity Analysis.....	100
Table 5.7: COR Values for RA Simulations.....	110
Table A.1: RHRS Field Data Sheet (Pierson and Van Vickle 1993, p16).....	132
Table A.2: Summary Sheet of Rockfall Hazard Rating System (Pierson and Van Vickle 1993, p26).....	133
Table A.3: RocScience Coefficient of Resitution (Modified from RocScience Website)	134
Table C.1: Observations and Notes of Tornado Mountain GPS Survey.....	143
Table C.2: RTK GPS Points	146

LIST OF FIGURES

Figure 2.1: Rockfall Source at Crowsnest Lake Site (photo by James Russell)	3
Figure 2.2: Schematic of Aerial LiDAR Process	10
Figure 2.3: RTK GPS Base Station at Tornado Mt. (photo by Renato Macciotta).....	14
Figure 2.4: Test Set up used in Wu’s Experiment (Modified from Wu 1985)	18
Figure 2.5: Normal Coefficient of Restitution from Slope Angle (Modified from Wu 1985)	19
Figure 2.6: Tangential Coefficient of Resitution from Slope Angle (Modified from Wu 1985)	19
Figure 3.1: Crowsnest Lake Rockfall Site (Taken From ILRIS-3D Camera)	24
Figure 3.2: GoogleMap Location of Crowsnest Lake Site	24
Figure 3.3: Gully/Erosion Path at Crowsnest Lake Site (photo by James Russell)	26
Figure 3.4: High Rock Face at Crowsnest Lake Site (photo by James Russell).....	26
Figure 3.5: Barrier Net at Crowsnest Lake Site (photo by James Russell).....	27
Figure 3.6: Large Boulder Behind Barrier Net at Crowsnest Lake Site (photo by James Russell)	28
Figure 3.7: Talus Pile to be Cleared at Crowsnest Lake Site (photo by James Russell)...	29
Figure 3.8: Highwood House Rock-Cut as Stitched Together from ILRIS-3D Camera ..	30
Figure 3.9: GoogleMap Location of Highwood House Rock Cut	30
Figure 3.10: Highwood House Rock-Cut (photo by James Russell)	31
Figure 3.11: Hazard Zone at Head of Highwood House Rock-Cut (photo by James Russell)	32
Figure 3.12: Ditch of Highwood House Rock-Cut (photo by James Russell)	33
Figure 3.13: Fir Creek Rock-Cut as Stitched Together from ILRIS-3D Camera Images	34
Figure 3.14: Talus Cone Formed Under Erosion Gully at Fir Creek Site (photo by James Russell)	35

Figure 3.15: Composite Image of Galatea Creek Through-Cut Stitched Together from ILRIS-3D Camera Images	36
Figure 3.16: GoogleMap Location of Galatea Through-Cut	37
Figure 3.17: Rock Bolts in Galatea Through-Cut East Rock Face (photo by James Russell)	39
Figure 3.18: Mt. Baldy Rock-Cut (Taken from ILRIS-3D Camera)	40
Figure 3.19: GoogleMap Location of Mt. Baldy	40
Figure 3.20: Crest of Rock Slope at Mt. Baldy Rock-Cut (photo by James Russell)	41
Figure 3.20: Material in Ditch at Mt. Baldy Rock-Cut (photo by James Russell)	42
Figure 3.21: Old Man Dam Rockfall Hazard Area (Taken from ILRIS-3D Camera)	43
Figure 3.22: GoogleMap Location of Old Man Dam and Location of LiDAR Station on Site	44
Figure 3.23: Spraylake Gabion Wall Site (Taken from ILRIS-3D Camera)	46
Figure 3.24: GoogleMap Location of Spraylake Gabion Wall Site	46
Figure 3.25: GoogleMap Location of Tornado Mountain Site	49
Figure 3.26: Barrier Wall and Catchment Area at Tornado Mt. (photo by James Russell)	50
Figure 3.27: Rock Fragments Along Slope at Tornado Mt. (photo by Renato Macciotta)	51
Figure 3.28: Large Past Rockfall Event on Slope at Tornado Mt. (photo by Renato Macciotta)	52
Figure 3.29: Likely Rockfall Source at Tornado Mt. (photo by Renato Macciotta)	52
Figure 4.1: ILRIS-3D Set-up In Field (Photo by Renato Macciotta)	55
Figure 4.2: Flow Chart of LiDAR Scan Procedure with ILRIS-3D	56
Figure 4.3: Crowsnest Lake Site Point Cloud Stitched in Polyworks with Different Colours Representing Each Scan	59
Figure 4.4: Surface Map and Cross-Section of Crowsnest Lake Site	60
Figure 4.5: Surface Map and Cross-Section of Highwood House Rock-Cut	62

Figure 4.6: Surface Map and Cross-Section of Fir Creek Rock-Cut	64
Figure 4.7: Rock Bolts Holding Rocks in Galatea Through-Cut (photo by James Russell)	65
Figure 4.8: Loose Rock Bolt in Galatea Through-Cut (photo by James Russell).....	65
Figure 4.9: Surface Map and Cross-Section of Galatea Through-Cut.....	66
Figure 4.10: Surface Map and Cross-Section of Mt. Baldy Rock-Cut	67
Figure 4.11: A) Old Man Dam (Taken from ILRIS-3D Camera). B) Point Cloud of Old Man Dam. C) Raster Hillshade Elevation Profile in ArcGIS from Selected Points in Point Cloud.....	68
Figure 4.12: Point Cloud of Spray Lake Site Demonstrating Shadowed Areas Due to Line-Of-Site Obstruction from Vegetation and Resulting Interpolated Surface Map	69
Figure 5.1: Rockfall Boulder Found Near CP Railway Tracks (Photos by Renato Macciotta)	74
Figure 5.2: Rockfall Impact Points (Photos by Renato Macciotta)	75
Figure 5.3: Rockfall Impact Craters A) General Bounce Profile, B) Tumbling Bounce Profile, C) Impact Causes Enough Loss in Energy to Result in Roll/Slide, and D) Boulder Comes to Rest	76
Figure 5.4: Trees Broken Along Rockfall Paths (Photos of Renato Macciotta and James Russell)	77
Figure 5.5: Fragments from Boulder at Impact Points Along Rockfall Path (Photos by Renato Macciotta).....	77
Figure 5.6: Increasing Talus Material Looking up Rockfall Path to Source Area (Photo by Renato Macciotta).....	78
Figure 5.7: Plan View of RTK GPS Survey of Tornado Mountain Rockfall Path	79
Figure 5.8: Profile View of Orange-flagged Rockfall Path at Tornado Mountain	79
Figure 5.9: Profile View of Yellow-flagged Rockfall Path at Tornado Mountain	80
Figure 5.10: Comparison of RTK GPS Survey to Duncan Wyllie’s Survey for Orange- flagged Rockfall Path.....	81
Figure 5.11: Tornado Mountain Rockfall Trajectory Superimposed on Raster from Geobase Data	82

Figure 5.12: Rockfall Source in Fractured Limestone Cliff Face at Tornado Mountain (Photo by Renato Macciotta)	83
Figure 5.13: Seeder Polylines for Tornado Mountain Rockfall Simulations.....	84
Figure 5.14: Material Polygons to Define COR in Tornado Mountain Rockfall Simulations	85
Figure 5.15: Initial Calibration of Rockfall Simulation with 15m/s Horizontal Velocity, 10m/s Vertical Velocity, 5m Drop Height, and Initial COR Values	86
Figure 5.16: A) Refined Seeder Polyline Set and B) Further Refined Seeder Polyline Set	87
Figure 5.17: Rockfall Simulation Calibration Tests with Initial Calibration Parameters and A) Redefined Polyline Seeder, B) Further Redefined Polyline Seeder, and C) Comparison of Rockfall Trajectories from Both Seeders	88
Figure 5.18: Rockfall Simulation Velocity Sensitivity with Initial Calibration Parameters and 5m Drop Height at A) 5m/s Horizontal and 0m/s Vertical, B) 10m/s Horizontal and 5m/s Vertical, and C) 15m/s Horizontal and 10m/s Vertical.....	90
Figure 5.19: Rockfall Simulation Drop Height Sensitivity with Initial Calibration Parameters and 5m/s Horizontal Velocity and 0m/s Vertical Velocity at A) 10m Drop Height, B) 25m Drop Height, and C) 50m Drop Height.....	91
Figure 5.20: Raster Image of Slope Angles for Tornado Mountain DEM.....	93
Figure 5.21: Rockfall Energy Calibration Visual Model	93
Figure 5.22: Rockfall Energy Calibration Simulation: Angle 45° Drop Height 60m.....	95
Figure 5.23: Rockfall Energy Calibration Simulation: Angle 55° Drop Height 70m.....	96
Figure 5.24: Rockfall Energy Calibration Simulation: Angle 65° Drop Height 70m.....	96
Figure 5.25: Typical COR Value Simulation (55° Slope Angle and 70m Drop Height). 97	
Figure 5.26: Typical COR Value Simulation (65° Slope Angle and 70m Drop Height). 97	
Figure 5.27: 2-Dimensional Rockfall Simulation Profile and RTK GPS Impact Point Comparison (Typical COR: Rn=0.3 Rt=0.8; Slope Angle 55°; Drop Height 70m)	98
Figure 5.28: 2-Dimensional Rockfall Simulation Profile and RTK GPS Impact Point Comparison (Typical COR: Rn=0.3 Rt=0.8; Slope Angle 65°; Drop Height 70m)	99

Figure 5.29: Reduced COR Value Simulation (55° Slope Angle and 70m Drop Height)	100
Figure 5.30: Reduced COR Value Simulation (65° Slope Angle and 70m Drop Height)	100
Figure 5.31: Reduced Normal Typical Tangential COR Value Simulation (55° Slope Angle and 70m Drop Height)	101
Figure 5.32: Reduced Normal Typical Tangential COR Value Simulation (65° Slope Angle and 70m Drop Height)	101
Figure 5.33: Typical Normal Reduced Tangential COR Value Simulation (55° Slope Angle and 70m Drop Height)	101
Figure 5.34: Typical Normal Reduced Tangential COR Value Simulation (65° Slope Angle and 70m Drop Height)	102
Figure 5.35: Greatly Reduced COR Value Simulation (55° Slope Angle and 70m Drop Height)	102
Figure 5.36: Greatly Reduced COR Value Simulation (65° Slope Angle and 70m Drop Height)	102
Figure 5.37: Greatly Reduced Normal Typical Tangential COR Value Simulation (55° Slope Angle and 70m Drop Height)	103
Figure 5.38: Greatly Reduced Normal Typical COR Value Simulation (65° Slope Angle and 70m Drop Height)	103
Figure 5.39: Typical Normal Greatly Reduced Tangential COR Value Simulation (55° Slope Angle and 70m Drop Height)	103
Figure 5.40: Typical Normal Greatly Reduced Tangential COR Value Simulation (65° Slope Angle and 70m Drop Height)	104
Figure 5.41: Median Rockfall Travel Distance in RA vs. the Assumed Drop Height at Source	106
Figure 5.42: Maximum Rockfall Travel Distance in RA vs. the Assumed Drop Height at Source	107
Figure 5.43: Median Rockfall Travel Distance in RA vs. the Assumed Slope Angle at Source	108
Figure 5.44: Maximum Rockfall Travel Distance in RA vs. the Assumed Slope Angle at Source	109

Figure 5.45: Maximum and Median Rockfall Travel Distance by COR Value.....	110
Figure 5.46: Maximum and Median Rockfall Travel Distance by Test Number	111
Figure 5.47: Cumulative Distribution of Typical COR Rockfalls for A) 45° Slope Angle, B) 55° Slope Angle, and C) 65° Slope Angle.....	112
Figure 5.48: Rockfall Simulation Friction Sensitivity Test with Increased COR for 45° Slope Angle, 60m Drop Height, and Friction of A) 25°, B) 20°, and C) 15°	114
Figure 5.49: Cumulative Distribution Curve of Rockfall Travel Distance for Friction Angle of Slope	115
Figure 5.50: Smashed and Scarred Trees (photo by Renato Macciotta).....	116
Figure 5.51: Fallen Trees Along Rockfall Path (photo by Renato Macciotta)	117
Figure B.1: A) Point Cloud at Crowsnest Lake Rock-Cut, B) View and Scale on XZ Plane, C) View and Scale on YZ Plane, and D) View and Scale on XY Plane.....	136
Figure B.2: Surface Map of Crowsnest Lake Site	137
Figure B.3: Surface Map of Highwood House Rock-Cut.....	138
Figure B.4: Surface Map of Fir Creek Rock-Cut (Rotated).....	139
Figure B.5: Surface Map of Galatea Through-Cut East Rock Slope (Rotated).....	140
Figure B.6: Surface Map of Mt. Baldy Rock-Cut (Rotated).....	141
Figure C.1: Rock Block from Orange Flagged Path.....	142
Figure C.2: Rockfall Simulation: $R_n = 0.33$ $R_t = 0.87$; Slope Angle 45°; Drop Height 10m	150
Figure C.3: Rockfall Simulation: $R_n = 0.33$ $R_t = 0.87$; Slope Angle 45°; Drop Height 20m	150
Figure C.4: Rockfall Simulation: $R_n = 0.33$ $R_t = 0.87$; Slope Angle 45°; Drop Height 30m	150
Figure C.5: Rockfall Simulation: $R_n = 0.33$ $R_t = 0.87$; Slope Angle 45°; Drop Height 40m	150
Figure C.6: Rockfall Simulation: $R_n = 0.33$ $R_t = 0.87$; Slope Angle 45°; Drop Height 50m	151

Figure C.7: Rockfall Simulation: $R_n = 0.33$ $R_t = 0.87$; Slope Angle 45° ; Drop Height 60m	151
Figure C.8: Rockfall Simulation: $R_n = 0.33$ $R_t = 0.87$; Slope Angle 45° ; Drop Height 70m	151
Figure C.9: Rockfall Simulation: $R_n = 0.33$ $R_t = 0.87$; Slope Angle 55° ; Drop Height 10m	152
Figure C.10: Rockfall Simulation: $R_n = 0.33$ $R_t = 0.87$; Slope Angle 55° ; Drop Height 20m	152
Figure C.11: Rockfall Simulation: $R_n = 0.33$ $R_t = 0.87$; Slope Angle 55° ; Drop Height 30m	152
Figure C.12: Rockfall Simulation: $R_n = 0.33$ $R_t = 0.87$; Slope Angle 55° ; Drop Height 40m	152
Figure C.13: Rockfall Simulation: $R_n = 0.33$ $R_t = 0.87$; Slope Angle 55° ; Drop Height 50m	153
Figure C.14: Rockfall Simulation: $R_n = 0.33$ $R_t = 0.87$; Slope Angle 55° ; Drop Height 60m	153
Figure C.15: Rockfall Simulation: $R_n = 0.33$ $R_t = 0.87$; Slope Angle 55° ; Drop Height 70m	153
Figure C.16: Rockfall Simulation: $R_n = 0.33$ $R_t = 0.87$; Slope Angle 65° ; Drop Height 10m	154
Figure C.17: Rockfall Simulation: $R_n = 0.33$ $R_t = 0.87$; Slope Angle 65° ; Drop Height 20m	154
Figure C.18: Rockfall Simulation: $R_n = 0.33$ $R_t = 0.87$; Slope Angle 65° ; Drop Height 30m	154
Figure C.19: Rockfall Simulation: $R_n = 0.33$ $R_t = 0.87$; Slope Angle 65° ; Drop Height 40m	154
Figure C.20: Rockfall Simulation: $R_n = 0.33$ $R_t = 0.87$; Slope Angle 65° ; Drop Height 50m	155
Figure C.21: Rockfall Simulation: $R_n = 0.33$ $R_t = 0.87$; Slope Angle 65° ; Drop Height 60m	155
Figure C.22: Rockfall Simulation: $R_n = 0.33$ $R_t = 0.87$; Slope Angle 65° ; Drop Height 70m	155

Figure C.23: Rockfall Simulation: $R_n = 0.33$ $R_t = 0.87$; Slope Angle 75° ; Drop Height 10m	156
Figure C.24: Rockfall Simulation: $R_n = 0.33$ $R_t = 0.87$; Slope Angle 75° ; Drop Height 20m	156
Figure C.25: Rockfall Simulation: $R_n = 0.33$ $R_t = 0.87$; Slope Angle 75° ; Drop Height 30m	156
Figure C.26: Rockfall Simulation: $R_n = 0.33$ $R_t = 0.87$; Slope Angle 75° ; Drop Height 40m	156
Figure C.27: Rockfall Simulation: $R_n = 0.33$ $R_t = 0.87$; Slope Angle 75° ; Drop Height 50m	157
Figure C.28: Rockfall Simulation: $R_n = 0.33$ $R_t = 0.87$; Slope Angle 75° ; Drop Height 60m	157
Figure C.29: Rockfall Simulation: $R_n = 0.33$ $R_t = 0.87$; Slope Angle 75° ; Drop Height 70m	157
Figure C.30: Rockfall Simulation: $R_n = 0.3$ $R_t = 0.8$; Slope Angle 45° ; Drop Height 50m	158
Figure C.31: Rockfall Simulation: $R_n = 0.3$ $R_t = 0.8$; Slope Angle 45° ; Drop Height 60m	158
Figure C.32: Rockfall Simulation: $R_n = 0.3$ $R_t = 0.8$; Slope Angle 45° ; Drop Height 70m	158
Figure C.33: Rockfall Simulation: $R_n = 0.3$ $R_t = 0.8$; Slope Angle 55° ; Drop Height 50m	159
Figure C.34: Rockfall Simulation: $R_n = 0.3$ $R_t = 0.8$; Slope Angle 55° ; Drop Height 60m	159
Figure C.35: Rockfall Simulation: $R_n = 0.3$ $R_t = 0.8$; Slope Angle 55° ; Drop Height 70m	159
Figure C.36: Rockfall Simulation: $R_n = 0.3$ $R_t = 0.8$; Slope Angle 65° ; Drop Height 50m	160
Figure C.37: Rockfall Simulation: $R_n = 0.3$ $R_t = 0.8$; Slope Angle 65° ; Drop Height 60m	160
Figure C.38: Rockfall Simulation: $R_n = 0.3$ $R_t = 0.8$; Slope Angle 65° ; Drop Height 70m	160

Figure C.39: Rockfall Simulation: $R_n = 0.27$ $R_t = 0.77$; Slope Angle 45° ; Drop Height 50m	161
Figure C.40: Rockfall Simulation: $R_n = 0.27$ $R_t = 0.77$; Slope Angle 45° ; Drop Height 60m	161
Figure C.41: Rockfall Simulation: $R_n = 0.27$ $R_t = 0.77$; Slope Angle 45° ; Drop Height 70m	161
Figure C.42: Rockfall Simulation: $R_n = 0.27$ $R_t = 0.77$; Slope Angle 55° ; Drop Height 50m	161
Figure C.43: Rockfall Simulation: $R_n = 0.27$ $R_t = 0.77$; Slope Angle 55° ; Drop Height 60m	162
Figure C.44: Rockfall Simulation: $R_n = 0.27$ $R_t = 0.77$; Slope Angle 55° ; Drop Height 70m	162
Figure C.45: Rockfall Simulation: $R_n = 0.27$ $R_t = 0.77$; Slope Angle 65° ; Drop Height 50m	162
Figure C.46: Rockfall Simulation: $R_n = 0.27$ $R_t = 0.77$; Slope Angle 65° ; Drop Height 60m	162
Figure C.47: Rockfall Simulation: $R_n = 0.27$ $R_t = 0.77$; Slope Angle 65° ; Drop Height 70m	163
Figure C.48: Rockfall Simulation: $R_n = 0.27$ $R_t = 0.8$; Slope Angle 45° ; Drop Height 50m	163
Figure C.49: Rockfall Simulation: $R_n = 0.27$ $R_t = 0.8$; Slope Angle 45° ; Drop Height 60m	163
Figure C.50: Rockfall Simulation: $R_n = 0.27$ $R_t = 0.8$; Slope Angle 45° ; Drop Height 70m	164
Figure C.51: Rockfall Simulation: $R_n = 0.27$ $R_t = 0.8$; Slope Angle 55° ; Drop Height 50m	164
Figure C.52: Rockfall Simulation: $R_n = 0.27$ $R_t = 0.8$; Slope Angle 55° ; Drop Height 60m	164
Figure C.53: Rockfall Simulation: $R_n = 0.27$ $R_t = 0.8$; Slope Angle 55° ; Drop Height 70m	164
Figure C.54: Rockfall Simulation: $R_n = 0.27$ $R_t = 0.8$; Slope Angle 65° ; Drop Height 50m	165

Figure C.55: Rockfall Simulation: $R_n = 0.27$ $R_t = 0.8$; Slope Angle 65° ; Drop Height 60m	165
Figure C.56: Rockfall Simulation: $R_n = 0.27$ $R_t = 0.8$; Slope Angle 65° ; Drop Height 70m	165
Figure C.57: Rockfall Simulation: $R_n = 0.3$ $R_t = 0.77$; Slope Angle 45° ; Drop Height 50m	166
Figure C.58: Rockfall Simulation: $R_n = 0.3$ $R_t = 0.77$; Slope Angle 45° ; Drop Height 60m	166
Figure C.59: Rockfall Simulation: $R_n = 0.3$ $R_t = 0.77$; Slope Angle 45° ; Drop Height 70m	166
Figure C.60: Rockfall Simulation: $R_n = 0.3$ $R_t = 0.77$; Slope Angle 55° ; Drop Height 50m	167
Figure C.61: Rockfall Simulation: $R_n = 0.3$ $R_t = 0.77$; Slope Angle 55° ; Drop Height 60m	167
Figure C.62: Rockfall Simulation: $R_n = 0.3$ $R_t = 0.77$; Slope Angle 55° ; Drop Height 70m	167
Figure C.63: Rockfall Simulation: $R_n = 0.3$ $R_t = 0.77$; Slope Angle 65° ; Drop Height 50m	167
Figure C.64: Rockfall Simulation: $R_n = 0.3$ $R_t = 0.77$; Slope Angle 65° ; Drop Height 60m	168
Figure C.65: Rockfall Simulation: $R_n = 0.3$ $R_t = 0.77$; Slope Angle 65° ; Drop Height 70m	168
Figure C.66: Rockfall Simulation: $R_n = 0.15$ $R_t = 0.5$; Slope Angle 45° ; Drop Height 50m	168
Figure C.67: Rockfall Simulation: $R_n = 0.15$ $R_t = 0.5$; Slope Angle 45° ; Drop Height 60m	169
Figure C.68: Rockfall Simulation: $R_n = 0.15$ $R_t = 0.5$; Slope Angle 45° ; Drop Height 70m	169
Figure C.69: Rockfall Simulation: $R_n = 0.15$ $R_t = 0.5$; Slope Angle 55° ; Drop Height 50m	169
Figure C.70: Rockfall Simulation: $R_n = 0.15$ $R_t = 0.5$; Slope Angle 55° ; Drop Height 60m	169

Figure C.71: Rockfall Simulation: $R_n = 0.15$ $R_t = 0.5$; Slope Angle 55° ; Drop Height 70m	170
Figure C.72: Rockfall Simulation: $R_n = 0.15$ $R_t = 0.5$; Slope Angle 65° ; Drop Height 50m	170
Figure C.73: Rockfall Simulation: $R_n = 0.15$ $R_t = 0.5$; Slope Angle 65° ; Drop Height 60m	170
Figure C.74: Rockfall Simulation: $R_n = 0.15$ $R_t = 0.5$; Slope Angle 65° ; Drop Height 70m	170
Figure C.75: Rockfall Simulation: $R_n = 0.15$ $R_t = 0.8$; Slope Angle 45° ; Drop Height 50m	171
Figure C.76: Rockfall Simulation: $R_n = 0.15$ $R_t = 0.8$; Slope Angle 45° ; Drop Height 60m	171
Figure C.77: Rockfall Simulation: $R_n = 0.15$ $R_t = 0.8$; Slope Angle 45° ; Drop Height 70m	171
Figure C.78: Rockfall Simulation: $R_n = 0.15$ $R_t = 0.8$; Slope Angle 55° ; Drop Height 50m	172
Figure C.79: Rockfall Simulation: $R_n = 0.15$ $R_t = 0.8$; Slope Angle 55° ; Drop Height 60m	172
Figure C.80: Rockfall Simulation: $R_n = 0.15$ $R_t = 0.8$; Slope Angle 55° ; Drop Height 70m	172
Figure C.81: Rockfall Simulation: $R_n = 0.15$ $R_t = 0.8$; Slope Angle 65° ; Drop Height 50m	172
Figure C.82: Rockfall Simulation: $R_n = 0.15$ $R_t = 0.8$; Slope Angle 65° ; Drop Height 60m	173
Figure C.83: Rockfall Simulation: $R_n = 0.15$ $R_t = 0.8$; Slope Angle 65° ; Drop Height 70m	173
Figure C.84: Rockfall Simulation: $R_n = 0.3$ $R_t = 0.5$; Slope Angle 45° ; Drop Height 50m	173
Figure C.85: Rockfall Simulation: $R_n = 0.3$ $R_t = 0.5$; Slope Angle 45° ; Drop Height 60m	174
Figure C.86: Rockfall Simulation: $R_n = 0.3$ $R_t = 0.5$; Slope Angle 45° ; Drop Height 70m	174

Figure C.87: Rockfall Simulation: $R_n = 0.3$ $R_t = 0.5$; Slope Angle 55° ; Drop Height 50m	174
Figure C.88: Rockfall Simulation: $R_n = 0.3$ $R_t = 0.5$; Slope Angle 55° ; Drop Height 60m	174
Figure C.89: Rockfall Simulation: $R_n = 0.3$ $R_t = 0.5$; Slope Angle 55° ; Drop Height 70m	175
Figure C.90: Rockfall Simulation: $R_n = 0.3$ $R_t = 0.5$; Slope Angle 65° ; Drop Height 50m	175
Figure C.91: Rockfall Simulation: $R_n = 0.3$ $R_t = 0.5$; Slope Angle 65° ; Drop Height 60m	175
Figure C.92: Rockfall Simulation: $R_n = 0.3$ $R_t = 0.5$; Slope Angle 65° ; Drop Height 70m	175
Table C.3: Maximum and Median Rockfall Travel Distances Based on COR, Drop Height, and Slope Angle	177
Figure C.93: Median Rockfall Travel Distance at 50m Drop Height	178
Figure C.94: Median Rockfall Travel Distance at 60m Drop Height	179
Figure C.95: Median Rockfall Travel Distance at 70m Drop Height	180
Figure C.96: Maximum Rockfall Travel Distance at 50m Drop Height	181
Figure C.97: Maximum Rockfall Travel Distance at 60m Drop Height	182
Figure C.98: Maximum Rockfall Travel Distance at 70m Drop Height	183
Figure C.99: Median Rockfall Travel Distance at 45° Slope Angle	184
Figure C.100: Median Rockfall Travel Distance at 55° Slope Angle	185
Figure C.101: Median Rockfall Travel Distance at 65° Slope Angle	186
Figure C.102: Maximum Rockfall Travel Distance at 45° Slope Angle	187
Figure C.103: Maximum Rockfall Travel Distance at 55° Slope Angle	188
Figure C.104: Maximum Rockfall Travel Distance at 65° Slope Angle	189
Figure C.105: Cumulative Distribution Curves for Increased COR at Assumed Slope Angles of A) 45° , B) 55° , and C) 65°	190

Figure C.106: Cumulative Distribution Curves for Reduced COR at Assumed Slope Angles of A) 45°, B) 55°, and C) 65°	191
Figure C.107: Cumulative Distribution Curves for Reduced Rn at Assumed Slope Angles of A) 45°, B) 55°, and C) 65°	192
Figure C.108: Cumulative Distribution Curves for Reduced Rt at Assumed Slope Angles of A) 45°, B) 55°, and C) 65°	193
Figure C.109: Cumulative Distribution Curves for Greatly Reduced COR at Assumed Slope Angles of A) 45°, B) 55°, and C) 65°	194
Figure C.110: Cumulative Distribution Curves for Greatly Reduced Rn at Assumed Slope Angles of A) 45°, B) 55°, and C) 65°	195
Figure C.111: Cumulative Distribution Curves for Greatly Reduced Rt at Assumed Slope Angles of A) 45°, B) 55°, and C) 65°	196

LIST OF SYMBOLS, NOMENCLATURE, AND ABBREVIATIONS

SYMBOLS

B	-	Scaling factor for Coefficients of Restitution
E	-	Energy
K_v	-	Constant value (ex. = 9.14m/s)
M	-	Mass
Rn	-	Normal Coefficient of Restitution
Rt	-	Tangential Coefficient of Restitution
V	-	Velocity
V_{n_r}	-	Normal component of velocity for rebound
V_{n_i}	-	Normal component of velocity for impact
V_{t_r}	-	Tangential component of velocity for rebound
V_{t_i}	-	Tangential component of velocity for impact
v_i	-	Initial velocity
v_h	-	Horizontal velocity
v_v	-	Vertical velocity
v_n	-	Normal velocity
v_t	-	Tangential velocity
α	-	Impact angle in Wu's experiment
	-	Angle of slope to rebound vector
θ	-	Slope angle

ABBREVIATIONS

AIT	-	Alberta Infrastructure and Transportation
COR	-	Coefficient(s) of Restitution
CP	-	Canada Pacific
CRSP	-	Colorado Rockfall Simulation Program
DEM	-	Digital Elevation Model
GIS	-	Geographic Information System
GPS	-	Global Positioning System
IDW	-	Inverse Distance Weighted
ILRIS-3D	-	Intelligent Laser and Ranging Imaging System – 3-Dimensional
IMU	-	Inertial Measurement Unit
LiDAR	-	Light Distancing and Ranging
NAD	-	North American Datum
NSTM	-	Numerical Single Tree Model
PDA	-	Personal Digital Assistant
PRF	-	Pulse Repetition Frequency
RA	-	RockFall Analyst
RHRS	-	Rockfall Hazard Rating System
RTK GPS	-	Real Time Kinematic Global Positioning System
TRIM	-	Terrain Resource Information Management
USB	-	Universal Serial Bus
UTM	-	Universal Transverse Mercator

1. INTRODUCTION

In steep mountainous terrain, rockfalls are a natural phenomenon. Rockfalls can vary both in size, and in the energy by which they travel down the slope. These natural phenomena can pose a serious hazard to the transportation corridors that pass through this terrain. Rockfalls have been responsible for delays in the transportation of goods, damage to both vehicles and infrastructure, and injury to people in the area (including fatal injury as mentioned in Hoek 2007). While it is true that rockfalls are naturally occurring, the frequency of rockfalls hazard can be increased by the over steepening of the rock slope and the poor blasting practice that was used to construct the transportation corridor. In both natural and man-made slopes, the identification and mitigation of rockfall hazards are important for maintaining the safety and functionality of such transportation corridors.

The occurrence of rockfalls can vary both spatially and temporally along a transportation corridor. Hence identifying a section of a transportation corridor as a rockfall hazard is outside the bounds of routine engineering analysis. Traditionally once a rockfall hazard is identified, usually based on historic records, remedial measures are evaluated. The process in a rockfall analysis has three steps: (1) identification of the rockfall hazard location, (2) investigation of the location to establish the rockfall source, and (3) determination of the site's geometry characteristics that can serve as the boundary conditions for the analysis. The output from such an analysis provides the energy associated with each rockfall, including the velocity and bounce height. The factors that impact this output are the parameters that control how the energy is absorbed and dissipated as the rock fall bounces, rolls and slides down the slope, and the three dimensional geometry that provides the slope on which these processes occur.

1.1. Scope of Study

Rockfalls occur in steep terrain and establishing the geometry of the slope on which these hazards occur is challenging. Remote survey techniques are typically preferred to establish the survey geometry of a steep rock slope. The line-of-sight survey technique that has become relatively popular in the past decade is Light Distancing and Ranging (LiDAR). While airborne LiDAR technology is now readily available, its application to rockfall prone terrain may be questioned as the geometric details of the slope that could influence the rockfall analysis may not be amenable to a line-of-sight technique; particularly when the source for the line-of-sight survey technique is positioned in a high-flying aircraft. Terrestrial LiDAR technology has also advanced and this technology can be applied if the rockfall source can be sighted from the rockfall impact. In this thesis terrestrial LiDAR technology was used to establish three dimensional digital elevation

models at several known rockfall sites in Southern Alberta. The digital elevation models created for these sites were evaluated as to their suitability for rockfall analyses.

The rockfall analyses discussed in this thesis utilize closed-form solutions to track the trajectory as the rockfall makes its way down the slope. The input parameters required for this analysis, such as the coefficients of restitution, are unknown and can only be estimated. They are unknown because there is no standard laboratory test that can be carried out to establish these parameters. In most rockfall analyses only the source location and the final location of the rockfall are known. Hence back analyses are poorly constrained because there are more unknowns than known inputs. In this thesis, in addition to the source and resting location for the rockfall, the trajectory of the rockfall event and impact locations are also known. These trajectory impact points were surveyed using an industrial quality Real-Time Kinematic Global Positioning System (RTK GPS); thus the number of unknowns in the rockfall analyses was significantly reduced. These analyses were used to establish if the typically reported input parameters recommended for rockfall analyses were suitable for analyses of rockfalls on treed natural mountain slope.

1.2. Research Objective

As a geomorphologic slope process, rockfall hazards are characterized by high energy and mobility despite their limited volume. Consequently the measures readily available to mitigate the hazard tend to be expensive. One objective of this research is to establish if the modern survey tools that are available today are suitable for adding value to traditional rockfall analyses. The second objective is to determine if the input parameters that are typically recommended for these analyses can be used to predict a rockfall trajectory to an acceptable level of accuracy for design of these mitigative measures.

2. LITERATURE REVIEW

Rockfall events occur when a failure takes place in the holding mechanism keeping a rock in place on a slope. With nothing to hold it back, the rock will fall down the slope until enough energy is lost to cause its movement to stop. Rocks can be classified with varying size, ranging from gravel (2mm – 75mm) to cobbles and boulders ($\geq 75\text{mm}$) (Das 2008, p65). The danger in any rockfall event occurs when people, or their works, intersect the path of the falling rocks. In the case of highway and railway maintenance, this is of particular concern since the rocks damage the road/track, and can become obstacles when resting on the road/track. Various methods of mitigation can be employed, but these ultimately benefit from the understanding of how rockfall events occur.



Figure 2.1: Rockfall Source at Crowsnest Lake Site (photo by James Russell)

Rockfall behaviours are affected by a number of factors:

- Slope geometry,
- Static and Dynamic frictions,
- Slope roughness,
- Resistance to rolling,
- Restitution characteristics of the rocks,
- Geometry of the rockfall patterns, and
- Rock's density (Richards et al 2001, p149)

Each of these factors affects the method, distance, and trajectory by which the rock progresses down the slope. Not all of these factors have been clearly defined in study,

and this makes analyzing rockfall hazards less precise. Mitigation methods can be improved by more clearly defining rockfall characteristics in actual field conditions.

2.1. Rockfall Hazards

The Western edge of Alberta and most of British Columbia is the rugged terrain of the Rocky Mountains. Transportation links cross through this mountainous terrain where they are exposed to a large number of landslide hazards. Hazards along both highways and railways arise from frequent, small rockfall events, and infrequent rock slide events. Along highway and railway corridors, the natural rock slopes are often undercut to form suitable roadbed grade. This slope cutting may expose unfavourably oriented rock joints, which can provide suitable conditions for both slide failures and rockfall events. Surface erosion and weathering can also loosen and undercut the slope, increasing the likelihood for similar rockfall hazard scenarios (Hung et al 1998). Rockfalls may not pose the same economic risk as the large scale slope failures, but rockfalls tend to result in fatalities at a rate equivalent to other forms of rock slope instability (Hoek 2007).

Obtaining quality data for assessing the rockfall hazards is essential for determining the actual hazard level. Records and databases exist for many landslide risk areas, as well as various data sources, publications, studies, etc. CN, in particular, keeps records based on warning fences, which have reports compiled each time they are triggered. However, the CN reports do not report a great deal of information on the volume of falling rocks (Hung et al 1998, p228). Data may be censored for analyses for varying reasons: (1) the underreporting of, or incomplete, record data (i.e. missing volume information), (2) the sample interval may also be too short to represent low frequency events adequately, and/or (3) the characteristics of the rockfall system being analyzed (i.e. ditches and barriers may intercept smaller rockfall events). Data gathering and censoring is unique to each rockfall site analyzed. Since each site analyzed will have unique data sets, it is important to attempt to process the data with an aim to reduce the censoring that is not a result of the characteristics of the rockfall system, thus keeping as much usable data for each site (Hung et al 1998, p228). Choosing a sample interval of data is important in this regard, since data with normal variation must be preserved, while abnormal variation intervals should be excluded as they tend to indicate censoring (Hung et al 1998, p231). Obtaining rockfall data is important in assessing a problem area; however, it is also necessary to understand the mechanisms and properties of rockfall events to deal with regions that do not have historical rockfall records.

Predicting where rockfalls may occur would be an ideal solution to many problems associated with rockfall events. However, while there are many obvious and visible hazard regions, it is not possible to locate all of the potential future event sites. Once a rock is freed from the slope surface, it will fall, but knowing where and when a rock will reach a point where such an event will occur is difficult, if not implausible, to discern. It is the unknown points of failure that lead to the most dangerous scenarios, and depending

on the particular section of rock being freed from the slope, larger rockfalls or slope failure events could rapidly follow.

As mentioned previously, rocks need to be freed from the slope surface in order to initiate a rockfall event. Typically, it is some physical or environmental event that changes the way that the rock is being held. Examples of these events are:

- Pore pressure increases (due to rainfall infiltration),
- Erosion of stabilizing material,
- Freeze-thaw processes,
- Chemical degradation, or weathering, and
- Vegetative root growth/leveraging.

Of course, any construction processes may also apply new forces to a rock slope. While the construction works are in progress, the chance of rockfall initiation increases significantly. When work is completed, new slope exposures are then subjected to the events above, and may be more susceptible to failure (Hoek 2007).

A rock, once released from the slope, is controlled mainly by the material and geometry of the slope it is falling down. Slopes composed entirely of hard bedrock material do very little to slow the rock movement, while slopes composed of talus, or gravel absorb greater energy on every impact. The ability of a slope material to slow and/or stop a rock is known as the coefficient of restitution, and is described in more detail in Section 2.5. Within slope geometry, the steepness of the slope is a concern for rock movement, but it is the irregularities in the slope that can provide the greatest cause for concern. A sharp dip face can result in the rock being launched off the slope with high horizontal velocities, allowing the rock to impact on locations at greater distances than just rolling and bouncing would normally allow. This is similar to the effect of a ski-jump (Hoek 2007). Other factors, such as the size and shape of falling rocks, frictional coefficients, fragmentation considerations, and vegetative cover, will affect rock movement to varying degrees. Vegetative cover would typically be considered with slope material, though it is not quantifiable in the same way as other materials to determine restitution.

In the case of highways, specifically, Bunce (1997) poses that rockfalls are hazardous in multiple ways:

- The rock may impact a moving vehicle on the highway,
- The rock may impact a stationary vehicle on the highway,
- A moving vehicle may collide with a rock that has obstructed the highway,
- Highway obstruction due to rockfalls may cause traffic delays, and
- The rock may damage the highway itself.

While all these scenarios suggest that the damages are limited to the vehicles on the highway and the highway itself, it should be noted that any object on or around the highway experiences the same level of risk. Rockfalls occur randomly (i.e. they don't fall in accordance with specific intent to impede traffic), and as such there is not always a risk to traffic. In this regard, it is better to calculate the probability that a rockfall will actually impact a specific object, either stationary or moving, and then how probable this is to cause death and injury. This leads into how we rate the hazardous impacts of

rockfalls, which can be used to determine whether or not preventative measures are required.

2.1.1. Rockfall Hazard Rating System

Geotechnical analysis tends to focus on major slope failures and overall slope stability, and therefore many highway slopes miss the benefit of a thorough rockfall analysis. Since it is impractical to carry out a full analysis on every slope, more reasonable methods by which to assess hazard levels have been developed. A rockfall hazard assessment method developed by the Oregon State Highway Division has become widely accepted. This method is known as the Rockfall Hazard Rating System (RHRS) (Pierson and Van Vickle 1993).

The RHRS was developed by combining and modifying two systems that had been developed previously. One system, developed by Brawner and Wyllie (1976) to rate rockfall hazards adjacent to railways was used as a means to provide a preliminary categorization of rockfall sites. Wyllie (1980) subsequently developed a more detailed system which uses an exponential scoring system and rating sheet to determine the hazard rating of a particular site. These systems were further modified from experience in both the development of the combined system, and in its application, with State Highway agencies moving to further improve the RHRS in July of 1989.

The features of the current RHRS system are (Pierson and Van Vickle 1993):

- Slope Inventory – produce a geographic database of rockfall locations.
- Preliminary Rating – grouping of rockfall sites into three broad categories.
- Detailed Rating – prioritizing rockfall sites from the most to least hazardous.
- Initial Design and Cost Estimation – adds remediation information into the rockfall database.
- Project Identification and Development – determining which rockfall mitigation projects shall be moved into the construction phase.
- Annual Review and Update – maintaining the database as necessary.

For this thesis, the main point of concern is how a rockfall site is determined to be hazardous. Therefore it is prudent to understand how rockfall locations are identified and rated.

Taking a survey of the slopes in the area to locate potential rockfall sites is the first step. This can be a difficult and time-consuming task, but is ultimately necessary and more efficient in the long run. In the RHRS, rockfall sections are defined as “any uninterrupted slope along a highway where the level and occurring mode of rockfall are the same” (Pierson and Van Vickle 1993, p14). Having some pre-conception as to the potential location of these sites is beneficial, as is having someone on hand who has a working knowledge of the sites. Any historic data on the site can provide insight into future rockfall events. Even with advance knowledge of the area, establishing rockfall

sections requires both skill and effort on the part of the surveyor. The information that needs to be gathered is:

1. Location of the rockfall activity
2. Frequency of the rockfall activity
3. The highest annual level of activity
4. Mass (either size or quantity) of rockfall per event
5. Physical characteristics of the rockfall material
6. Resting place of fallen rock material
7. Accident history
8. Opinion on the cause of the rockfall events
9. An estimated cost for maintenance response

An example of a data sheet that could be filled out for the RHRS is given in Table A.1 in Appendix A. Once this knowledge is gathered, it can be used to start the rockfall database, which requires a preliminary investigation on each site.

The preliminary investigation, as stated before, simply separates each identified rockfall site into one of three broader categories. In the case of the RHRS, these categories are defined as A, B, and C slopes. Table 2.1 demonstrates how each class is determined:

Table 2.1: Preliminary Rating System (Modified from Pierson and Van Vickle 1993, p18)

CLASS	A	B	C
CRITERIA			
ESTIMATED POTENTIAL FOR ROCKFALL ON ROADWAY	HIGH	MODERATE	LOW
HISTORICAL ROCKFALL ACTIVITY	HIGH	MODERATE	LOW

The “estimated potential for rockfall on roadway” is the controlling criteria, while “historical rockfall activity” is used to supplement the decision. The estimated potential is evaluated by:

1. Estimated size of material,
2. Estimated quantity of material,
3. Amount of material present that could fall, and
4. Effectiveness of ditch.

The historic activity is evaluated by:

1. Frequency of rockfall event on the highway,
2. Quantity of material that has fallen,
3. Size of fallen material, and
4. Frequency of clean-out.

The estimated potential will typically be used to categorize the site as A, B, or C, but if the site is not clearly defined, then historic activity will determine whether or not it rates a higher or lower rating. C rated slopes would be either unlikely to experience a rockfall event, or to have a rockfall event make it to the roadway; risk is non-existent to low. B slopes have a low to moderate risk, with possible rockfall events, but rocks rarely reach the roadway. An A slope is moderate to high risk, with frequent rockfall events, and a greater likelihood of a rock impacting/coming to rest on the roadway. In terms of the RHRS, A slopes will be further evaluated and given priority for rockfall mitigation

projects, B slopes may be evaluated as resources allow, and C slopes receive no further attention.

The detailed rating system differentiates the risk identified sites for sorting and prioritization. There are twelve categories by which the slopes are rated (each representing some significant contribution to rockfall events):

1. Vertical height of the slope,
2. Effectiveness of the ditch,
3. Average risk to passing vehicles,
4. Percent of distance by sight decision,
5. Roadway width (includes shoulders),
6. Structural condition for Class 1 geologic character,
7. Structural condition for Class 2 geologic character,
8. Rock friction (Class1),
9. Difference in erosion rates (Class 2),
10. Block size/volume of rockfall event,
11. Climate and water presence on/in slope, and
12. Rockfall history.

Table A.2 in Appendix A sums up these categories in a 3^x exponential point system. There are additional aids, such as graphs and equations, which can further define and help to qualify category selection. Each category is actually ranked from 1 to 100 rather than 3, 9, 27, and 81. As such, an experienced rater can use additional data, formula, or good judgment to better define the score, while a less experienced person conducting the rating would be better advised to rank with the simple table. Once all of the sites have been categorized via the detailed approach, it is possible to determine which sites need immediate attention, and then allocate funding to projects to mitigate rockfall damages.

It should be noted that not every agency will be able to make use of the RHRS as it is shown in Pierson and Van Vickle (1993). Therefore agencies must modify the RHRS to better suit the needs of their particular geology. Consistency in evaluation then becomes a primary concern, so the agency needs to be sure that all modifications are documented and observed in future implementation. Another limitation to be noted is that not every rockfall event can be predicted, and so if an event occurs, re-evaluation of that site is in order. A single event should not spark an overreaction, since it is simply a single event. Due process within the rating system, and re-evaluation via the detailed process should it be required, will determine if any additional protective measures are necessary.

The benefits of using the RHRS are threefold. (1) Knowledge gained from the system allows agency management to observe detailed site information of a uniform nature. Practical analyses can be made with this information that will aid in future decision making processes and the allocation of funding to rockfall site projects. (2) RHRS is beneficial for public perception. Since rockfalls cannot fall under the category of human error in highway driving conditions, it is within the rights of drivers to have a level of expectation that rockfalls are being taken care of. In this regard, the RHRS demonstrates due diligence to the public. (3) RHRS offers legal protection. In the same way the system shows due diligence to the public, it does so in court. While it is unreasonable to

expect that any one agency has the funding or manpower to resolve all rockfall issues immediately, it is expected that they have some plans set to deal with them as resources allow (Pierson and Van Vickle 1993).

2.2. LiDAR

Rockfall patterns are affected greatly by slope features and geometry, as mentioned in Section 2.1. Therefore it is necessary to have as accurate a description of the slope when performing a rockfall analysis. There are many ways to survey slopes to obtain this data, but new technologies are making it simpler and more efficient to capture this information.

LiDAR technology, also known as Light Detection and Ranging, has become increasingly useful in the fields of engineering and geology. A light emitting device sends pulses of light, or photons, towards a target area and then measures the return time of each pulse. As each pulse returns, the device translates the time it takes for the pulse to return into the distance an object is from the machine. Coupled with coordinate information from the machine, the programming of the device is able to calculate a 3-dimensional coordinate for the point from which the light was reflected. A cloud of these points is created by a sweep of these light pulses, and the net result is a measurement that is useful in determining the shape of a given target, be it bare earth geology, smoke plumes, or river ice flows.

There are four varieties of LiDAR to note: fixed-wing aerial LiDAR, non-fixed-wing aerial LiDAR, stationary terrestrial LiDAR, and mobile terrestrial LiDAR. The final output of each LiDAR device is a point cloud of XYZ data points, with differences stemming from point saturation and global positioning data. Each type of LiDAR is useful for various applications, often overlapping, but each offers something that the others do not.

The most common form of LiDAR used to date is the fixed-wing aerial LiDAR. This form of LiDAR device is comprised of a pulse laser scanner/receiver, a GPS unit, and an Inertial Measurement Unit (IMU). 150,000 pulses are emitted from the device every second and will return after they have reflected off of a sufficiently dense surface, such as the surface of the ground, buildings, and/or vegetation (Lewis 2006). As the airplane flies over the site, the return point data is referenced to the stationary GPS unit in the vicinity to label each point with a XYZ position. Figure 2.2 illustrates the mechanism of the plane mounted LiDAR device. This method is fast, cost effective, and provides an accurate map of the geometry of the ground surface.

Aerial LiDAR is used frequently, and has been applied to landslide inventory application, as seen with Glenn et al (2006) and Sato et al (2007). The XYZ points derived from the system are used to map the ground surface to create a Digital Elevation Model (DEM). The XYZ point cloud is converted first into a triangular mesh, and this is then

interpolated into a surface grid that forms the DEM. Since the DEM is formed by interpolation, it should be noted that it will be subject to error between each of the points, and therefore the most accurate representation from the surface is actually in the form of the XYZ point cloud. Having made this observation, Glenn et al (2006) note that the LiDAR device has a 16cm absolute vertical accuracy, with up to a 5cm discrepancy from point-to-point, which is a very small level of error. Sato et al (2007) found an accuracy of 15cm on bare earth, with errors of up to 0.42m in defoliated deciduous vegetation, and 1.02m in coniferous vegetation. The 15cm accuracy can be given as a saturation level of approximately 36pts/m². Other sources would label point saturation more conservatively at 10pts/m² (Lato et al 2009, p938), which is within the same order of magnitude as the previous saturation. A DEM is best formed when points are taken directly from the bare ground surface, but LiDAR can obtain bare earth images even with vegetation present, noting potential error as pointed out previously. The light pulses are classified as received as first pulse, last pulse, and any in between being noted as other pulses (Sato et al 2007). By ignoring the first and other pulses obtained within a given pulse area and only taking the last pulses, the bare earth image DEM is obtained. This bare earth DEM is very useful in noting surface roughness and sloping due to its high spatial resolution, and can be used to define a great many geomorphologic features. Sato et al (2007) found that, since LiDAR images directly measure the 3-dimensional ground coordinates, LiDAR-DEMs illustrate these geomorphologic features in better detail than when using the photogrammetric technique.

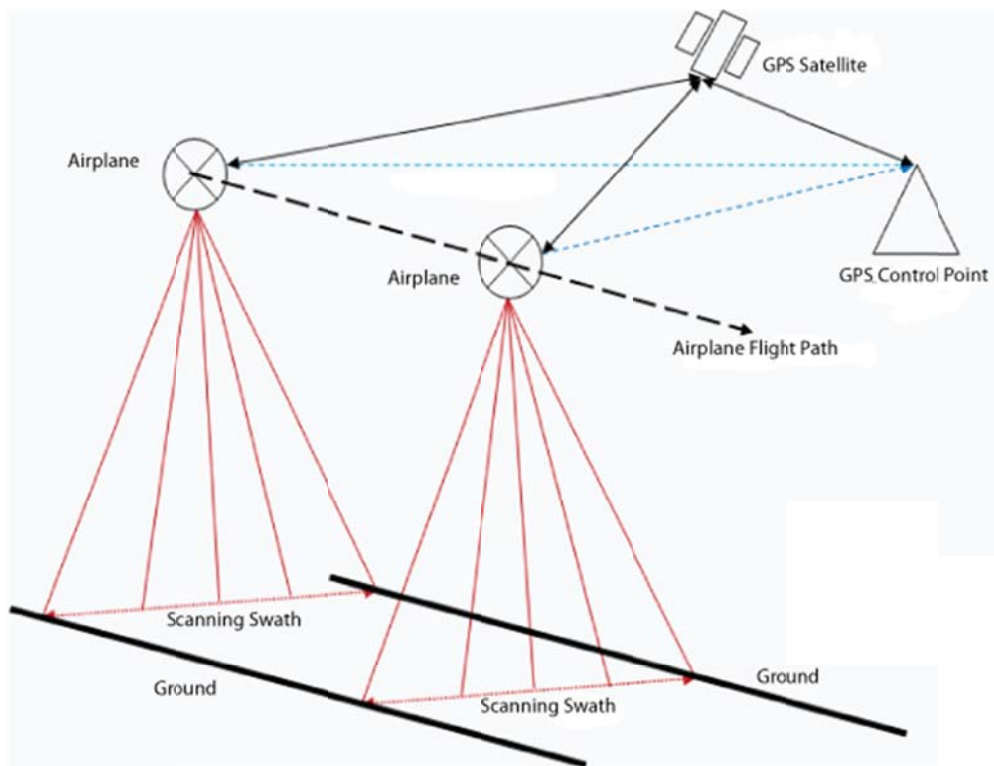


Figure 2.2: Schematic of Aerial LiDAR Process

In the case of rock-cut slopes, it is somewhat difficult to make good use of the fixed-wing aerial LiDAR. Since the slopes are generally quite steep, it is difficult to obtain an accurate geometry of the steep portions of the rock-cut slope. As stated previously, slope geometry is an important factor in determining how a rockfall will bounce/slide/roll down a slope. Therefore it is prudent to have a method that can obtain a precise image of the slope geometry.

Non-fixed-wing aerial LiDAR is similar in almost every respect to the fixed-wing format, except that it uses a helicopter rather than an airplane. Fixed-wing surveys are usually done by one specific company with the data being sold as required. Since the surveys are designed to cover large swaths of land, purchasing a particular location is not usually difficult since it is more than likely part of one of the survey flights. However, it is possible that the area was missed due to unfavourable conditions, or ranging issues. Whatever the reason, a helicopter has different access capabilities than an airplane, and certainly can be used to cover a more specific region if necessary. The listed coverable density of a helicopter is still within the same order of magnitude as the fixed-wing LiDAR at approximately 10pts/m² (Lato et al 2009, p938). Steep rocks slope images can be obtained with this technology. Limitations of non-fixed-wing aerial LiDAR would be safe site access, equipment availability, and expense.

Mobile terrestrial LiDAR functions by mounting the LiDAR station on a truck rather than an airplane or helicopter, while still maintaining the use of the same base station and satellite coordinating GPS technology. More care needs to be taken with the trucks location as it is subject to terrain based obstacles (swerves, bumps, and dips in the path of travel), and with line-of-site obstruction to GPS satellites (vegetation, canyon walls, rockfaces, cloud cover, etc.). The mobile LiDAR set up has four emitters and receivers around the station, gathering measurements at a full 360° around the truck. Each device has an effective range of about 200m, and gathers a point density of 50-500pts/m² depending on the speed of the truck, and the distance to the target (ideal speed is approximately 30km/hr) (Lato et al 2009). The convenience here is that surveyors can perform all checks and set ups in a safe environment, and only be exposed to the hazards they are investigating for a brief period of time. While more expensive than a stationary set up, it can cover ground more quickly, and may therefore prove more economical depending on man-time available. Additionally, it takes detailed measurements of near vertical rockfaces with better point saturation than the equivalent aerial LiDAR device. Sources do not indicate to what angle measurements can be performed. It would be reasonable to assume that different configurations of the device are possible, and with multiple sweeps of the site, a more complete image can be obtained.

Stationary terrestrial LiDAR has been used extensively for stationary surface analysis. The point saturation can be in excess of 10,000pts/m² (Lato et al 2009, 938), which is of significantly higher detail than any of the other methods of LiDAR analysis. Capturing the surface image of vertical, or near-vertical, rock faces is well within the capability of

the stationary terrestrial LiDAR system. The devices themselves are portable to allow movement from site to site, with a mass between 10-15 kg. Many devices are also equipped with digital camera that takes digital images of the same section to be analyzed, such as with Optech's Intelligent Laser and Ranging Imaging System (ILRIS-3D). These images can be analyzed separately or overlaid onto the point cloud using the Polyworks software from Innovmetric.

The ILRIS-3D is capable of a laser repetition rate of 2500 to 3500 Hz. This value is the effective and peak pulse repetition frequency (PRF), with the efficiency of the PRF being the ratio between the two. Optech Inc. reports the efficiency to be 100%. The wavelength of the laser itself is reported at 1535 nm. The return time for the laser pulses determines the XYZ coordinates in relation to the position of the ILRIS-3D. Intensities are also recorded for each data-point for the level of reflectivity of the surface material. This is based on the returned wavelength of the laser.

Stationary terrestrial LiDAR does have some noteworthy limitations. There is a theoretical maximum distance with which the device is effective. Depending on weather and atmospheric conditions, this distance is specified by Optech Inc. at a maximum of 1200m for the ILRIS-3D. The point accuracy ranges from plus/minus 3-10 mm depending on the distance of the taken reading, and conditions (Kememy 2005). Since the device is working at a higher resolution, vegetation is more difficult to remove, though the same first and last return pulses can be filtered, as was done in the airborne LiDAR. The major difference in this filter is that there will be a greater apparent area within which no points have been captured due to a shadowing effect of the obstacles, such as vegetation. For the system to work, the base needs to be stable, or the point cloud will have significant error, and any reference coordinate system will therefore be reported in error. This is not say that multiple locations for imaging cannot be used, but rather that each position should be stable to prevent errors from occurring. If a direct GPS coordinate system is needed, then known reference points will have to be found within each point cloud, a survey may need to be conducted to reference the locations, and/or the system itself will have to be described within a known coordinate system. The other forms of LiDAR had the advantage in this regard since location and direction were measured constantly and referenced to a known GPS base station. It has been previously noted that fixed-wing aerial LiDAR fails to capture detail in ground surface at angles oblique the device, such as vertical rock faces. Stationary terrestrial LiDAR exhibits this same difficulty, though the angles that are difficult to capture are those oblique to the current set up of the device. This can be resolved with system positioning and location, assuming that a stable, accessible standpoint is available, which may be constrained by the site.

Having made a note of limitations, when using the stationary terrestrial LiDAR technology, it is recommended to follow certain field and processing procedures. In the field, advised procedure would be:

- Ascertaining whether a site is suitable for a LiDAR survey,

- Checking scanning procedures for each site (number of scans, point spacing, image resolution, etc.),
- Surveying control points (if necessary),
- Capturing digital images of site (if necessary; i.e. no camera in LiDAR), and
- Collecting additional non-digital required information (field notes).

When processing the information obtained in the field, it is good to know what software and analysis procedures are to be used. Also, the LiDAR data should be available in multiple formats, including the raw scanner files, point cloud files, rendered surface files, and any calculations and interpretations made from any of the data.

2.3. RTK GPS

Rockfalls are noted for the damage or potential damages that they cause. Along the path of any rockfall, there are points where the rock will exhibit behaviours of bouncing, rolling, or sliding. The bounce points in particular leave impact points as notable areas of damage. A rockfall trajectory could be back-analyzed if these points are surveyed. Not every site has conditions favourable for many pieces of survey equipment, or for long-term survey safety conditions. In these cases, a portable GPS analysis may be favourable.

RTK GPS stands for Real-Time Kinematic Global Positioning System. Typical GPSs use satellites in order to triangulate the location of the receiver in terms of their relative position on the planet based on latitude and longitude gridlines. It takes time for a GPS to sync with satellites in order to accurately position the exact location of a point. The RTK system eliminates some of the time needed to map a series of points. By establishing a base point's position, each additional point recorded on a receiver can be related in terms of distance from the original base. There are a series of techniques that can be used to increase the accuracy of the gathered point, such as tying it in to geodetic survey markers. However, this is not entirely necessary if the error within the initial base position is acceptable based on the satellite triangulation alone.

The RTK GPS model used for the survey in this study, as available through the Civil and Environmental Engineering department at the University of Alberta, is the Trimble R6 GPS and R8 GNSS receiver. The receiver is made up of a GPS antenna, receiver, internal radio, and a battery. The unit can be mounted a pole which allows the user to rove the area taking GPS points. The system uses Bluetooth technology to communicate between the base station and the rover. There are numerous other models available, but each functions in essentially the same way. Additional information on the Trimble system can be seen in the manual where this information was obtained (Trimble User Guide 2006). Figure 2.3 shows an example of the set up for the RTK GPS as used at the Tornado Mountain site survey.



Figure 2.3: RTK GPS Base Station at Tornado Mt. (photo by Renato Macciotta)

2.4. RockFall Analyst

Programs have been designed for rockfall analysis that encompasses both the translation of data obtained on site, and in the assessment of the hazards imposed by rockfalls. Many programs exist, each offering different input values and output properties in a rockfall analysis, but not all of them are to be used here, or covered. ArcGIS, in particular, has been very useful in engineering as it can be adapted to analyze a wide variety of problem scenarios. Examples could include landslide hazard analyses in the Xiaojiang watershed in Yunnan, China (Lan et al 2004), or rock mass classification and fault zone analysis in tunnelling (Choi et al 2009). Lan et al 2007 develop an ArcGIS application to allow three-dimensional rockfall analysis using the Digital Elevation Model (DEM) created in ArcGIS.

As previously stated, slope properties and geometry determine how rocks bounce/slide/roll down a slope surface. RockFall Analyst allows the input of both the properties and geometry (DEM) of a slope surface. Derived surface rasters are created from the DEM to model the surface topography cell by cell. Rockfall simulations can then be run by “seeding” the slope at potential rockfall sources, followed by determining the rockfall trajectory and the process by which the rocks interact with the slope, i.e. rolling, sliding, bouncing, and free-falling (Lan 2007).

While it is true that the slope properties are important in considering how a rock falls, the shape of that rock is also a concern. While it is possible to model various 3-dimensional rock shapes and how they fall, this is difficult for two reasons. First, taking into account separate shapes and sizes for rocks requires a large amount of additional computational time, which becomes more strenuous as greater rockfall areas and regions are considered. Second, even a small area is unlikely to experience one particular rock shape, therefore each individual rock would have to be classified and analyzed prior to falling to cover the spectrum of shapes, sizes, and additional properties. This is highly impractical. RockFall Analyst, therefore, employs the “lumped mass” approach to handle rockfall trajectory simulation without considering the effect of the rock’s shape (Lan et al 2007, p265). Additionally, rock shape may change as the impacting rock fragments on the slope surface. It can be quite unreasonable to estimate the effect of this fragmentation on the distribution of the rockfalls, and is also difficult to qualify on a larger scale.

RockFall Analyst concentrates on the modeling of (1) free-falling, (2) bouncing, and (3) rolling/sliding motions of rocks on the 3-dimensional surface using kinematic algorithms that can account for each of these motions (Lan et al 2007, p265). When mapping the projectile motion of the rock, it is important to determine the point of impact and the end of the motion. The impact point is the intersection of the defined surface raster and the flight path parabola of the rock. At the impact point, the rebound velocity vector has to be calculated with the coefficient of restitution. Rolling/sliding will occur if this velocity is found to have decreased to some value, i.e. 0.5m/s, after impact. Should the rock maintain a higher velocity, it will bounce, continuing into a new parabolic projectile motion, and repeat the process. Rolling/sliding algorithms will take over when the projectile motion algorithms are exited, and rely on the slope geometry and surface properties (i.e. friction) in their calculation. The final stopping distance of the rock is determined by a zero exit velocity. This means that when the velocity of a rock reaches zero in a length shorter than the segment length of the slope it is travelling on, the simulation will end (Lan et al 2007, p266).

Theoretical walls and barriers can be built into the DEM to see how they impede the probabilistic movement of the falling rocks. Assuming that the starting conditions are rigorous enough, this is sufficient in determining best placement of barriers, and proper wall heights. This is especially useful with LiDAR derived surface maps, since the final results can be viewed on a surface model that is close to the actual slope surface.

In summation, the RockFall Analyst program extension in ArcGIS allows for:

- An integration of 3-dimensional process based physical modeling and raster based distribution modeling for rockfall hazard assessment and understanding.
- Modeling of all physical rockfall processes including sliding, rolling, bouncing, and free-falling (and all sub-processes therein) in a 3-dimensional system.
- The generation of quality prediction surfaces of rockfall hazards by taking into account the primary rockfall characteristics.
- Investigation of impact on structural surfaces, potential barrier analyses in changing the hazard distribution.
- Uncertainty modeling by throwing rocks in random directions for raster model generation via spatial statistics techniques.

While rockfalls are physical phenomena that occur on natural slopes, there is always uncertainty to be taken into account. Rockfall models should be calibrated to reflect the characteristics of the site, such as the rockfall source location(s) and the slope material properties, which is best done with first-hand field observations and case history data. Once properly calibrated, the model will have higher resolution and accuracy, and thus the results will be improved. (Lan et al 2007, p277-278)

2.5. Coefficient of Restitution

The Coefficient of Restitution (COR) describes the kinematic behaviour of a falling rock as it impacts against the slope surface. Every time a rock impacts against a slope surface, the characteristics by which it moves are changed. Hoek (2007) describes COR as the mathematical expression of the retarding capacity of a surface material when dealing with falling rocks. Each slope has unique properties, which vary from region to region along the slope. Each falling rock also has unique properties. It is, therefore, quite difficult to characterize the COR since each case has a unique set of properties. To simplify this, the COR is generalized to suit the behaviours of similar falling rocks down slopes that have understood parameters.

Restitution is most often defined as the velocity loss in both the normal and tangential directions to the surface of the slope (Richards et al 2001, p149). From this definition, the formula for the normal COR can be described:

$$R_n = V_{n_r} / V_{n_i} \quad (2.1)$$

where R_n = normal COR

V_{n_r} and V_{n_i} = normal component of velocity for rebound/impact

The tangential COR can also be described (Alajeno et al 2007):

$$R_t = V_{t_r} / V_{t_i} \quad (2.2)$$

where R_t = tangential COR

V_{t_r} and V_{t_i} = tangential component of velocity for rebound/impact

This equation is a general form measuring velocities, but can also be converted into other forms based on different assumptions. Ultimately, what is being described is the relationship of the energy remaining in the rebounded rock to the energy lost (or gained) from the impact with the slope. The general form of the equation relating energy to velocity is shown:

$$E = \frac{1}{2}mV^2 \quad (2.3)$$

or

$$V = \sqrt{(2E/m)} \quad (2.4)$$

where E = energy
m = mass
V = velocity

It should be noted that if the value for energy was substituted into equation 2.1 or 2.2 that the mass would cancel. This means that while the change in energy/velocity is needed to determine COR, the mass of the object in concern is irrelevant to the value.

Rocks impacting onto slope surfaces do not necessarily maintain their original shape and volume. In a rockfall event, fracturing should be expected, and a scaling factor must be considered to take into account the reduction to the normal COR. Rockfall analysis programs, such as the Colorado Rockfall Simulation Program (CRSP) and ROCKFAL3, take this into account with a scaling factor of B (Lee and Elliot 1998). The reduction in COR from B accounts for both the fracturing of the falling rock, and the cratering of the slope surface due to the rock's impact. B is described:

$$B = \frac{1}{(1+(Vn_i/K_v)^2)} \quad (2.5)$$

where B = scaling factor
K_v = constant value = 9.14m/s

Some programs allow a user to change the value of K_v if a different value is more suited to their scenario. The scaling factor, B, typically results in a reduction of the normal COR, in this case to approximately half of its value if Vn_i is equivalent to a K_v of 9.14m/s (Richards et al 2001, p150).

The normal COR has been estimated for rockfall analyses many times. Values for COR are obtained using assumptions, trajectory analysis calibrations, and programs utilizing both laboratory and field testing. Many of the values obtained from the different methods are identical, and most certainly comparable. Table 1 in the journal by Richards provides a compilation of COR values from a number of different tests conducted, and empirical observation (Richards et al 2001, p150). See attached Table A.3 from RocScience in Appendix A. These tables appear to focus on the slope parameters rather than on the falling rocks, therefore the differences that would rise between a granite and sandstone

rock are not considered. Tests that are able to account for the differences in rock material, however, are usually in situ, expensive, and perhaps impractical in terms of space and/or safety.

One experiment (Wu 1985) specifically was used to analyze the effect of rockfalls in how they pertained to highway safety issues. Wu posed four questions:

1. How effective is moving a road at reducing the number of rocks that reach the road?
2. Is an energy absorbing catchment area method effective at stopping rocks?
3. Where should catchment walls be located to be most effective?
4. How high should catchment walls be?

To answer these questions, one ultimately needs to understand the manner in which a rock interacts with the slope surface once it begins to fall. In this regard, Wu identified four mechanisms by which rocks move down a slope: rolling, sliding, bouncing, and free-falling. With the exception of free-falling, all move due to gravity with some resistance from frictional forces. Wu's experiment used two surfaces, an inclined wooden platform and actual rock slopes, to determine how rocks would bounce upon impact. The basic design for his experiment is shown in Figure 2.4. With the wooden platform, thirteen rocks were dropped from at four different angles to determine the effect of both rock size and slope inclination. This same experiment was repeated on three rock slopes of different angles, with each rock's trajectory and speed measured following its bounce. Wu ultimately determined the same equations for R_n and R_t as shown above. It was, however, Wu's conclusion that the impact angles had a significant effect on the restitution. Figures 2.5 and 2.6 illustrate the relationships that Wu derived from his experiments. The relationship in the figure is clearly linear, but it should be noted that Wu's experiments were only tested between 25° and 75° , and it is therefore difficult to determine if more extreme angles follow his suggested trend.

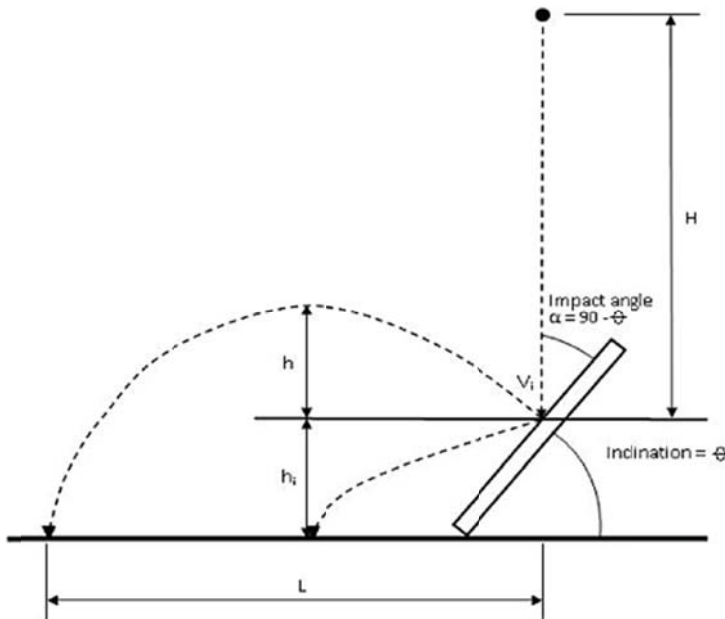


Figure 2.4: Test Set up used in Wu's Experiment (Modified from Wu 1985)

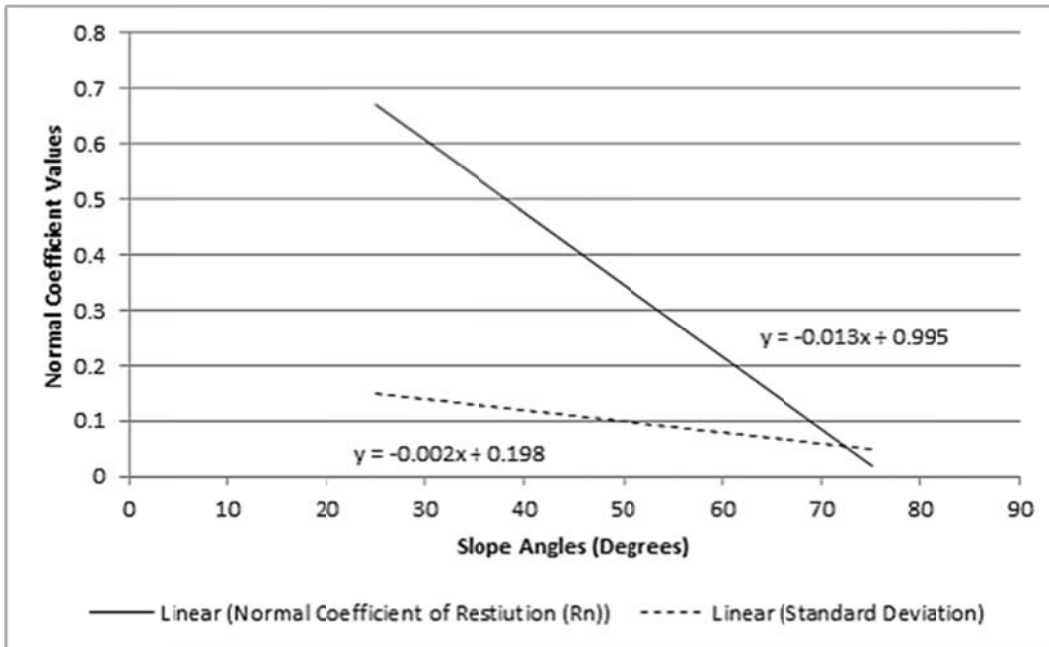


Figure 2.5: Normal Coefficient of Restitution from Slope Angle (Modified from Wu 1985)

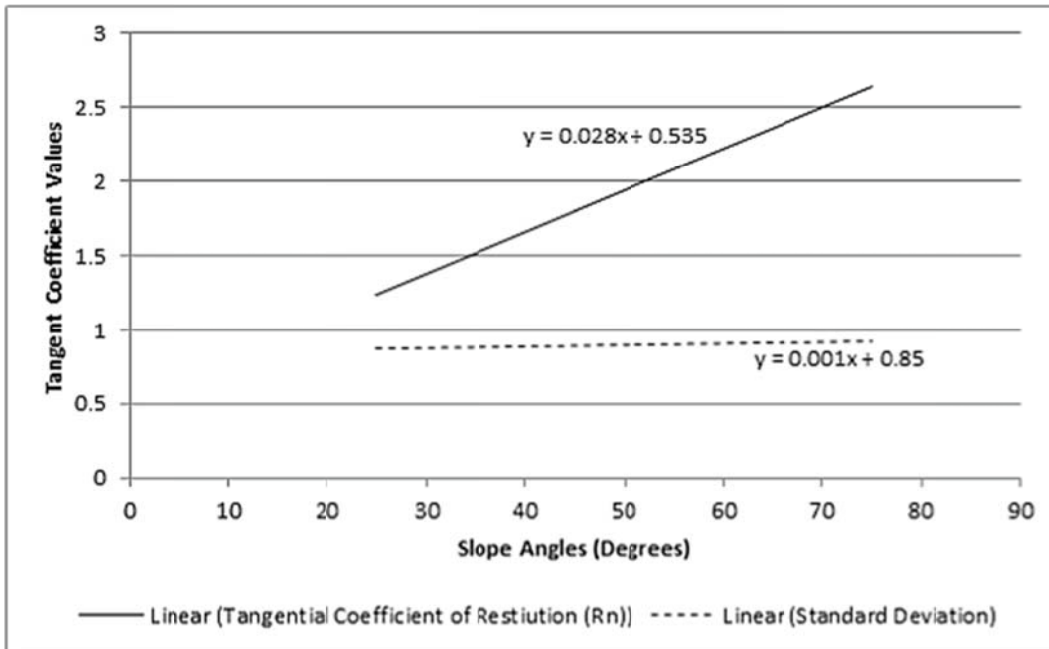


Figure 2.6: Tangential Coefficient of Restitution from Slope Angle (Modified from Wu 1985)

The Schmidt hammer test measures the rebound of a spring-loaded steel mass against a plunger. Rebound values obtained from the test can estimate the uniaxial compressive strength of a rock surface (Hoek and Bray 1981). This test has been used to determine the COR on grouted ceramic tiles as a quality check, but not specifically on rock (Bowman et al 1997). A test was performed by Rayudu (1997) to measure COR by dropping steel balls onto various rock slabs. Comparison with a Type L Schmidt hammer

test on the same rock slabs showed acceptable correlation in the COR values. While this does not test rock to rock impact restitutions, it does suggest that the Schmidt hammer test would be a useful device in estimating COR.

Chau et al (1999) also investigated COR, but with a focus on the shape of the impacting object. Where Wu had found that the impact angle was a sensitive concern to the normal COR, Chau et al found that the specimen shape was also a sensitive factor. This, however, is more difficult to measure under field conditions since the shape of a rock falling down the slope is indeterminate until one begins to fall, and the shape may change with each impact. However, it is useful to note that changing the shape of any falling rock will have impact on COR, and by finding which shape is the most significant as a hazard concern, a hazard analysis can be properly focused on such a rockfall event.

Tests carried out by Richards et al (2001) include dropping spherical balls onto smooth slabs, balls and blocks onto rough slabs, and drop test on debris/soil material. Field tests were also carried out. The test data appears to give a reasonable correlation between the obtained COR and the COR found using the Schmidt hammer test. As mentioned previously, Wu (1985) found that the impact angle significantly affected the normal COR. From Richards' (2001) tests, this result is not necessarily observed to be entirely correct. It could be surmised that normal velocities at impact account for the apparent changes in the normal COR (Richards et al 2001, p154).

Richards (2001) finds that the Schmidt hammer test can give a satisfactory prediction for COR. Hard rocks impacting on bedrock gave COR values up to, but not exceeding 0.30. Softer rocks could register values as low as 0.10. Normal COR on fragmental material will be less than 0.25 (typically 0.10) regardless of projectile characteristics, and compacted soils may have higher normal COR values compared to rock aggregates. Richards' conclusions result in lower COR properties than the rockfall simulation programs would typically suggest. The report suggests that the effect of velocity with respect to the slope angle is still to be further investigated. However, it is known that COR values in rockfall analyses are typically overestimating or conservative, and this leads to more costly mitigation procedures than may be necessary.

2.6. Energy Absorption Capacity of Trees on Slope

While it is true that rockfalls are a hazard in mountainous regions, it is not always necessary to provide a rigorous preventative measure to maintain an acceptable level of safety. Vegetation on the terrain itself aids in the prevention of rockfall dangers by absorbing energy and catching the rocks. To this effect, a forest located between the rockfall source and hazard area may be all that is needed to prevent the majority of the dangers. The question becomes, how well does vegetation actually absorb the energy of a falling rock? This question was taken up by Martin Jonsson in his Doctoral Paper for the Swiss Federal Institute of Technology in Zurich.

When investigating the effect of a forest in stopping falling rocks, there could be two general approaches to consider. One is to take the forest as a whole, and measure some energy absorption effect as a general standard of the distance the rock must travel through the vegetated area. Since vegetation is so varied in both its spacing and variety, it is difficult to quantify any forested area of having a simple energy absorption value. Also, individual plants may have varying effects on both the trajectory and overall behaviour of the rock that cannot be quantified by simply assuming a resistance factor. The other method of describing the effect of vegetation is therefore to quantify the effect of a single tree in dissipating energy during a rock impact. A tree can dissipate this energy in several different ways: rotation and translation of the roots system, deformation through the tree stem, and penetration of the rock into the tree on impact (Jonsson et al 2007, p359). The difficulty of analyzing a single tree is that slopes are populated with multiple trees, and it is therefore necessary to determine locations of said trees to form an accurate analysis. Depending on the necessary rigour of the analysis at hand, it may be simpler to consider one of the above approaches in favour of the other.

In Jonsson's analysis, a single tree approach is taken to better quantify the actual effect of a tree absorbing the impact of a falling rock, as well as winching and swaying tests. With trees, the root-soil plate is an important factor in both the rotation and translation of the impacted tree. The bending moment of this area is dependent on the ultimate mass of the roots and soil in contact, the general failure strength of the soil, and root resistances on both the windward and leeward side of the tree (Jonsson et al 2007, p359). In order to determine the energy absorption of the tree, one has to consider the impact point of the rock. Since trees carry most of their mass in and around the area of the root-soil plate, a rock impacting high above the ground surface will cause a different behaviour than one impacting on this area of higher mass near the ground surface. Also, if the rock was to impact the tree on its edges, there is less energy absorbed, and the rock's trajectory has now changed. Taking in these considerations, Jonsson's goal is to create a physical model that can realistically simulate behaviour during a tree-rock impact.

Impact tests were conducted using a trolley positioned to travel down adjustable wire lines to impact a tree. Accelerometers on both the trolley and the tree measure the effects of the impact, and cameras were set to catch the impact event. From the data obtained in these tests, a finite elements model was constructed. This model was simplified for the mass distribution to make the tree a simpler geometry for the analysis. Considerations were taken in the soil in and around the roots to properly ensure that the effects of the root-soil interaction were not lost. The trolley itself was corrected to assume a rigid material model for the impact. The process results in the creation of Jonsson's numerical single tree model (NSTM) (Jonsson et al 2007, p360-361).

Calibration of the NSTM took into account 4 separate trees, each having been tested in winching, swaying, and full-scale impact. It should be noted that the full-scale impact tests were performed at an energy level lower than would cause full penetration through

the tree. This allowed for multiple tests, and understanding of the energy absorption rates, but did not provide the full scope of the impact possibilities. Therefore, Jonsson applied the results of a similar study to validate the results of his NSTM (Jonsson et al 2007, p361).

The ultimate conclusion reached after analyzing the NSTM was that the model results corresponded with observations in nature and during the tests. This was even giving that the variables within and between the wood material, soil properties, and root-soil interactions can be quite great. It was believed that the most important parameters were attributed to the dynamic properties like the mass and inertia distributions for the tree, the root-soil plate, and the surrounding soil. Parameter studies were able to predict the energy absorption capacity of the tree as a function of the trees diameter at breast height, and the position of the impacting rock based on its impact height, eccentricity, and impact angle. However, using DBH to define the energy absorption capacity depends on all of these factors, which makes in less feasible in use with experiments that do not follow the actual track of the falling rock. Therefore the approach used with the NSTM model is more sufficient for analyzing the rock-tree interactions as it can be applied to different tree species with a reduced number of field experiments (Jonsson et al 2007, p363-364).

2.7. Means of Mitigation

Hoek (2007) makes note of several methods by which rockfall event damages may be reduced, controlled, or avoided entirely. Mentioned previously was prediction of rockfall hazard zones, but his is not entirely possible given current understanding and technology. Some of his noted methods are:

- Reducing excessive energy levels produced in excavation and construction,
- Physically restraining the rocks from falling,
- Berms,
- Rocksheds or avalanche shelters,
- Rock traps, and
- Catch fences or barrier fences.

None of these methods are applicable for every situation, and sometimes it is beneficial to combine them. The objective of each method is to reduce the chances of a rockfall event from becoming an economic or safety hazard. Therefore, it is best to analyze your current level of risk, analyze the particular features of merit for the given site, and then apply the solution(s) that best fits the scenario.

This study does not analyze the means of mitigation closely, only recognizes that the methods are important. Rockfall analyses are performed to determine their potential hazards, and based on the risk presented by a particular rockfall, the methods of mitigation may be employed. Noting that the following study is based on the methods of analysis rather than the final result, it is prudent to understand that the final use of the analysis may be determining a suitable means of mitigation for the hazard.

3. CHARACTERISTICS OF SEVERAL ROCKFALL SITES ALONG TRANSPORTATION CORRIDORS IN SOUTHWESTERN ALBERTA AND SOUTHEASTERN BRITISH COLUMBIA

This research is concerned with a number of rockfall sites in Alberta and British Columbia, Canada. Each of these rockfall sites has unique features and concerns. The first sites (Section 3.1) are associated with ongoing investigations by Alberta Infrastructure and Transportation (AIT) where rockfalls and slope failure have been known to affect nearby infrastructure. The remaining site (Section 3.2) is the Tornado Mountain area along the CP rail lines that was chosen for analysis due to its unique opportunity to survey a documented rockfall path.

3.1. Alberta Infrastructure and Transportation Sites

Each of the chosen sites is monitored by representatives from AIT and AMEC Earth and Environmental, compared with previous records, and then evaluated for risk level and appropriate maintenance practices. In the course of monitoring these sites, Light Distancing and Ranging (LiDAR) was considered as a method to characterize each slope face for yearly analysis and more rigorous risk assessment. However, it was found that due to the scale of each site, typical overhead LiDAR shot from an airplane would not provide sufficient detail, or would not be economically feasible. A survey to define steep rock slope characteristics using a truck-mounted mobile terrestrial LiDAR was attempted. For unforeseen reasons, this technology proved unable and/or insufficient to provide the desired data.

Following are several sites in Southern Alberta that were analyzed using the stationary terrestrial LiDAR device. The subsequent information is a combination of the AMEC report data provided for AIT through 2006-2008, and on-site observations.

3.1.1. Highway 3 – Crowsnest Lake

A persistent rockfall hazard has existed along the Crowsnest Pass, or Highway 3, for some time. Previous investigations in 1999 have led to construction of a concrete lock-block wall downslope of the outlet gully that is the point of concern for the rockfall hazard. Scaling of adjacent cut slopes was also performed. In 2003, an increase in both volume and frequency of rockfalls was noted, and an AMEC inspection led to the replacement of the wall with a rockfall barrier net in 2005. Figure 3.1 shows the site as seen from the LiDAR station on site.



Figure 3.1: Crowsnest Lake Rockfall Site (Taken From ILRIS-3D Camera)

Location

The Crowsnest Lake is found along Highway 3 when driving through Alberta to the B.C. border. A rockfall hazard around a gully outlet in a rock cut slope across the highway from the lake was identified as a problem. This site is approximately 4 km from the Alberta/B.C. border, west of the town of Coleman, AB. A GoogleMap image shown in Figure 3.2 provides a visual of the general location of the site.



Figure 3.2: GoogleMap Location of Crowsnest Lake Site

Site Topography

The rockfall hazard is centered around a gully outlet in the rock cut slope along Highway 3. This location is within the Rocky Mountains, so the terrain is steep and uneven. The toe of the gully outlet exits into a recess in the cut slope which has steep vertical to near-vertical walls all around. Above the rock cut slope, the gully cuts into a talus slope, which is likely the source of the majority of the rockfall debris feeding into the ditch. Further up the slope, a large rock face is visible. The face appears to be quite steep, and may also be a contributing factor/concern for future rockfall events.

Site Geology

The Crowsnest Lake rock cut is located in a thrust up bedrock formation. Specifically, the Paleozoic formation, undivided, that is composed primarily of limestone, dolomites, and shales (Hydrogeological Map: Lethbridge-Fernie, Alberta 1973). The slope in question exhibits a large portion of daylighted bedrock material. Further upslope, a talus slope is being eroded away, filtering rock material of varying size through one of two outwash gullies lower in the bedrock.

Vegetation at the ditch level and up the talus slope to the high rock face was non-existent. Trees, mosses, and some light scrub flanked the entirety of the area above the rock cut, leaving only the noted areas exposed.

Rockfall Hazard

The main area of concern for the rockfall hazard at this site would be the head of the gully formed in the talus slope (as seen in Figures 2.1 and 3.3). Groundwater springs have been noted on both the talus slope and rock cut slope behind the barrier, which is consistent with the seasonal groundwater discharge. It would appear that this seasonal water discharge, coupled with precipitation, and perhaps even freeze/thaw cycles, has led to a heavy amount of erosion in the talus slope. This can be clearly observed at site, and gravel to cobble-sized rockfalls can be noted quite frequently. It can also be noted that the clearing of the talus has revealed several larger boulders, that when fully exposed could be at risk of falling.



Figure 3.3: Gully/Erosion Path at Crowsnest Lake Site (photo by James Russell)

A higher rock face has been noted, as seen in Figure 3.4, and may be a concern for rockfalls in the future. At this time, it is unclear as to whether this face is contributing to the rockfall, but if it were, it would certainly present a present danger to the site, and increase the risk level.



Figure 3.4: High Rock Face at Crowsnest Lake Site (photo by James Russell)

The barrier net that was installed in 2005 would seem to have been functioning properly as of 2006 (See Figure 3.5). Recommendations there were to maintain proper maintenance of the net to maintain capacity and ensure that it remains up to standards. As of the 2007 AMEC report, the east anchor ropes of the net had been disconnected to allow access behind the barrier for the clearing of rockfall debris. Unfortunately, removing these anchors and leaving them as such has reduced the capacity of the barrier net by a large amount, thereby reducing the protection it offers to the highway. The anchors can be disconnected for maintenance under the assumption that they will be reconnected thereafter, which has not been done. As of the 2008 report, the barrier net design is still considered to be sufficient, but maintenance has not been properly conducted as per the 2007 report, thus the net is not performing to the intended design standards. It is to be noted that cleaning the debris behind the net is a necessity to maintain the design standards; therefore the concerns of the maintenance contractors should be noted for both safety and ease of access. However, the design standards are still to be maintained if the highway is to be kept at the lowest possible risk level.



Figure 3.5: Barrier Net at Crowsnest Lake Site (photo by James Russell)

Large boulders have struck the barrier net. One, measuring 2m x 1.8m x 1.1m struck and was retained by the net on April 4, 2006. There was damage to the supports and net, but the boulder was retained. Other rocks of size have been noted in the talus slope, as mentioned previously, and several have been removed pre-emptively with the intent to prevent any risk of their falling. One such boulder can be seen in Figure 3.6. Ensuring that the net is maintained properly is of paramount concern for a rockfall of this size.



Figure 3.6: Large Boulder Behind Barrier Net at Crowsnest Lake Site (photo by James Russell)

Ditch

The ditch is located behind the rockfall barrier net. Concern for this area is primarily with the removal of debris to ensure that the net continues to function to design standards. As a result, access to this area is level with the road to make it accessible for larger machines and equipment.

Water has been noted to pool in the ditch behind the net. A significant amount was noted in 2006, but this was not deemed to be a concern for the barrier net since it was built to be corrosion resistant. However, it was deemed prudent to maintain observation on these conditions to ensure that no damage is done to the net that would reduce its effectiveness, and thereby increase the rockfall hazard/risk level for the highway.

Remedial Measures

As already noted, the primary remedial measure for this site has already been implemented; the rockfall barrier net. Inspection, maintenance, and repairs of the net are to be completed regularly to ensure that it maintains capacity, and reduces the level of risk on site. Assuming that this is done on a regular basis, the requirements for annual inspections may no longer be needed. Clearing the talus slope that builds up behind the barrier net is a key maintenance requirement (talus can be seen in Figure 3.7).



Figure 3.7: Talus Pile to be Cleared at Crowsnest Lake Site (photo by James Russell)

It is noted that proper maintenance levels have not been maintained. As a result, the risk level of the site increased between 2006 and 2007 in the AMEC reports presented to AIT. The same recommendations have been maintained, with the addition that the east anchor ropes be reconnected and tensioned to return the net to acceptable design standards.

As of 2008 the cause of the maintenance recommendations had not been satisfactorily put into action, and thus the risk/hazard had not diminished. The barrier net is in need of further repair and maintenance. Assuming that the net is fixed on the short term basis, then the long term recommendations remain the same as before. It should be noted that the net appeared to have been in the same condition in the 2009 inspection as was noted in the 2008 inspection, suggesting that the repairs still need to be conducted.

3.1.2. Highway 541 – Highwood House Rock-Cut

Location

The Highwood House Rock Cut is located about 800m east of the junction between Highways 40, 541, and 940 on the north side of Highway 541. Highway 40 closes for the winter, but the closure gate is west of the junction, so the road passing under the cut is open all year round, and subject to rockfalls. A UTM reference has been provided in the 2006 AMEC inspection report:

Easting – 667719 Northing – 5584034



Figure 3.8: Highwood House Rock-Cut as Stitched Together from ILRIS-3D Camera

The image of the site can be seen in Figure 3.8, and Figure 3.9 is a GoogleMap location of the site.

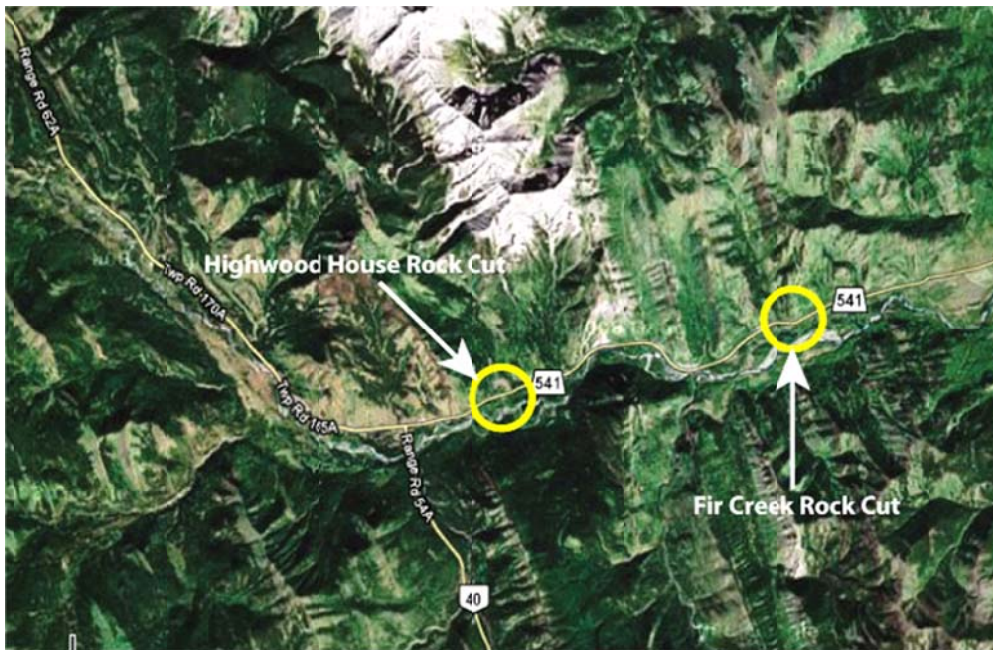


Figure 3.9: GoogleMap Location of Highwood House Rock Cut

Site Topography

Maximum vertical height is estimated to exceed 20m, with a slope of near-vertical to legitimately vertical along the length of the cut. The highway strikes at approximately 80° , while the rock strikes at 30° with a bedding angle of 55° . The opposite side of the highway drops off into a valley after several meters; therefore the hazard source for the rockfalls is only from the southward facing cut slope. Highway 541 and the rock-cut can be seen in Figure 3.10.



Figure 3.10: Highwood House Rock-Cut (photo by James Russell)

Site Geology

The exposed bedrock consists of shale, coal, and conglomerate, and is set in steeply dipping, alternating beds. Dip direction is roughly parallel to that of the highway alignment; down to the west. Soil and bedrock slopes above the cut incline at up to a 35° angle. A map consultation shows that the bedrock layer of this area is Undifferentiated Mesozoic, which is composed of a number of different rock formations. One grouping of rock formations in particular stands out; the Nikanassin and Kootenay formations, which are composed of fine- to coarse-grained, cherty sandstone, interbedded with shale, siltstone, and coal (Hydrogeological Map: Kanaskis Lakes, Alberta). This formation seems to agree best with the observed shale, coal, and conglomerate bedding pattern noted above.

Vegetation above the cut is mostly grass and scrub brush, with trees interspersed throughout. The ditch is mostly grass and weeds, and no vegetation is obvious on the cut face.

Rockfall Hazard

The rockfall hazards at this site seem to be mostly erosion based. Debris was typically found accumulated in talus cones beneath erosion gullies passing through the more easily erodable layers of the exposed bedrock. It should be noted that larger rocks have fallen from exposures in the rock slope, which are more likely from a freeze thaw cycle or failure along weak planes in the bedding. Additional rock is eroded from the rocky soil located at the crest of the slope, releasing larger sized rock masses that pose a greater threat than those released and deposited into the talus cones. These hazards can be seen in Figure 3.11.



Figure 3.11: Hazard Zone at Head of Highwood House Rock-Cut (photo by James Russell)

Ditch

When considering a rockfall ditch, the 20m height of this site suggests a recommended ditch sizing of 6.4m wide and 1.5-1.8m deep. The actual ditch at the site ranges from 5-6m wide and 1.5-1.75m deep. For the segments that reach or exceed 20m, the ditch is somewhat inadequate by the specified criteria. Debris and talus cones have accumulated in the ditch at this site under gullies eroded through weaker planes, as seen in Figure 3.12. Gravel sized rocks have been noted on the north shoulder and adjacent lane of the road, but damage to the road is minimal, suggesting that no rocks of significant size or velocity have actually impacted the road surface. Some rocks reaching up to 2m in

maximum dimension have been noted to have fallen into the ditch. These have fallen from exposures in the cut rock slope and/or have been eroded from the rocky soil face at the crest of the slope. However, these rocks were contained within the ditch at the west end of the site, and did not impact the road.



Figure 3.12: Ditch of Highwood House Rock-Cut (photo by James Russell)

Remedial Measures

Recommendations are to clean out the rockfall debris from the ditch to maintain capacity and prevent the talus cones from filling the ditch. This should be ongoing and completed as necessary to ensure the ditch meets standards. In addition to the removal of the small debris, the large rocks need also be removed to avoid new rocks falling on top, breaking, and launching smaller rock pieces onto the road.

Additional measures above general ditch maintenance include increasing the effective ditch size by either increasing the depth, or by adding jersey barriers (if acceptable by standards). Scaling the slope at the crest would also reduce the fall of rocky debris in the short term.

3.1.3. Highway 541 – East of Fir Creek Rock-Cut

Location

The location of the site is just east of the crossing over Fir Creek on Highway 541, about 5 km east of the Highway 542/ Highway 40/ Highway 940 junction. A UTM reference has been provided in the 2006 AMEC inspection report:

Easting – 673286 Northing – 5585665

Figure 3.13 shows the site as taken by the internal camera of the LiDAR device. The map location can be seen represented in Figure 3.9, east down Highway 541 from the Highwood House rock-cut location.



Figure 3.13: Fir Creek Rock-Cut as Stitched Together from ILRIS-3D Camera Images

Site Topography

The area of concern for this site is a rock cut along the north side of Highway 541 that reaches a maximum height of 20m for a near-vertical cut. An embankment, or natural rise, exists on the south side of the highway before dropping off into a valley. This site was ideal for LiDAR use since the embankment provided a perfect point of perspective for obtaining shots of the rock face.

Site Geology

The exposed bedrock consists of shale, coal, and conglomerate, and is set in steeply dipping, alternating beds. Dip direction is roughly parallel to that of the highway alignment; down to the west, while the strike is therefore perpendicular. This is the same bedding configuration noted in the Highwood House site nearby, and is likely from the same formation. It was noted that the Undifferentiated Mesozoic formation noted in the Highwood House does indeed meet the Fir Creek rock cut site, and therefore the exposed bedrock can indeed be considered the same.

Vegetation above the cut is mostly grass and scrub brush, with trees interspersed throughout. The ditch is mostly grass and weeds, with no growth is obvious on the cut

face itself. This matches same general description of the vegetation present at the Highwood House site.

Rockfall Hazard

A talus cone has built up beneath a notable erosional gully, which appears to be the largest source of debris at this site. However, damage to the road indicates that previous rockfalls have impacted the road. Cobble to boulder size debris in the ditch indicates that there may be additional erosion at the crest of the slope, or failure along the bedding planes. Freeze/thaw action cannot be ruled out as a factor.



Figure 3.14: Talus Cone Formed Under Erosion Gully at Fir Creek Site (photo by James Russell)

Loose rock has been noted on the cut slope face. During inspection, several minor rock falls were audible.

Ditch

The width of the ditch at this site is noted to be 4-5m with a depth of 1.5m. Recommendations for ditches suggest that this is acceptable for an 8-12m near-vertical cut, and not the 20m cut at this site. A rough test was conducted where-by cobble sized rocks were sent down the slope to determine the action that they would take. All rocks in this test landed in the ditch and did not roll onto the road surface.

Remedial Measures

Remedial measures for this site are to ensure that the debris in the ditch is cleared and to maintain further inspection to determine if the risk level of this site warrants further action.

3.1.4. Highway 40 – Galatea Creek Through-Cut

The Galatea Creek Through-Cut is composed of both an east and west cut slope flanking Highway 40 as it passes in the north/south direction. Studies by AMEC have been conducted on this site, and it is still currently under review and inspection. The study has found that it is the East Cut slope that presents the greater hazard level, and therefore the East Cut slope is the point of study hereafter. Figure 3.15 shows a composite image of the entirety of the East Cut slope.



Figure 3.15: Composite Image of Galatea Creek Through-Cut Stitched Together from ILRIS-3D Camera Images

Location

The location of the site is just north of the Galatea Provincial Recreation Area on Highway 40, about 32 km south of the Highway 1/ Highway 40 junction. A UTM reference has been provided in the 2006 AMEC inspection report:

Easting – 628365 Northing – 5636456

Figure 3.16 shows the map location of the through-cut.



Figure 3.16: GoogleMap Location of Galatea Through-Cut

Site Topography

The highway curves through the through-cut, entering along a bearing of 040 and exiting along a bearing of 346, passing through the north-south alignment at the midway point (bearing 000). Maximum height of the cut slope from toe to crest is approximately 16m.

Site Geology

The Galatea Creek Through-Cut is located within the mountainous region of southwestern Alberta where the foothills end and the Rocky Mountain Range begins. Exposed bedrock at the site is composed of dark grey shale to siltstone, noting that there are also quartz veins found throughout. Rock bedding strikes somewhere between 140 to 150° and has a dip ranging between 35 and 45° downwards to the southwest. This would suggest that the bedding is sloping downwards towards the road on the East Cut, which is not a favourable situation for the risk of rockfalls. (Information found in AMEC 2006 report)

Further investigation reveals that this site is located bordering two bedrock formations: the Banff Formation (includes Exshaw Formation), and the Rundle Group. (Geology of the Seebe-Kanaskis Area, 1971)

Vegetation is typical of the mountainous regions in south-western Alberta. Coniferous trees are growing on the slopes above the cuts, as well as grasses and scrub brush. The actual cut face exhibits occasional plant growth in the form of weeds or small flowering plant, but has no permanent rooted vegetation, i.e. it is clear of vegetation.

Rockfall Hazard

Rockfall hazard issues on the East Cut are due to:

- Weathering and freeze/thaw cycles on the exposed rock
- Release of rocks from the exposed soil at the crest of cut slope
- The unfavourable bedding orientation of the site which lends to risk of block sliding, wedge, and toppling failures

There is also risk of rockfalls from an area higher above the cut slope on the East Cut where boulder sized rocks have rolled down slope due to power line construction and have become wedged/embedded along the upslope side of trees. Without the trees, these rocks would have rolled onto the highway, but this is not indicative of a current hazard, rather it should be noted for potential future concern.

Ditch

The East Cut ditch measures, at certain segments, less than 4m from the edge of the pavement to the toe of the slope. Depth when compared to the road surface level is between 0.5 to 0.75 m.

The ditch has been successful in catching debris, and exhibits cobble-sized debris for the most part, with boulder sized rocks being noted as well. As per the previous section, it has been judged that the majority of the debris found in the ditches is the result of weathering and freeze/thaw cycles.

Damage to the pavement has been noted, and cobble-sized debris has been found as far as the centerline of the road. This would suggest that the ditch is not entirely successful in its purpose of containing the rockfalls, and therefore a risk analysis is called for.

Remedial Measures

A risk analysis has been conducted on the East Cut, and a recommended Risk Level of 45 has been provided by AMEC.

In order to manage the risk level associated with the site, the accumulated rockfall debris should be cleared regularly to maintain ditch capacity. Additionally, the road should

remain free of debris at all times, which may require visual inspection on an ongoing basis, and the removal of debris by hand until the next clean-up is scheduled for the ditches.



Figure 3.17: Rock Bolts in Galatea Through-Cut East Rock Face (photo by James Russell)

To reduce risk, the ditch capacity could be increased in accordance with the ditch sizing criteria. Jersey barriers on the east side of the road would create a greater effective depth of the ditch, but need to meet AIT requirements for installation. Cleaning of the ditch would still be necessary. Scaling of the slope face would also reduce the loose rock that is at risk of falling, and would also likely require the removal of the rocky soil at the crest of the slope to a certain degree.

Rockbolts have already been placed along the East Cut to counter the unfavourable bedding orientation mentioned earlier (See Figure 3.17). However, it is clear that some fracturing has occurred, numerous rockbolts are no longer in proper contact with the rock face, and some rocks have actually broken free from their respective rockbolts and fallen away from the area of installation.

3.1.5. Highway 40 – Mt. Baldy Rock-Cut

Location

The Mt. Baldy Rock Cut is located on the east side of Highway 40 about 4.75 km south of the junction between Highway 40 and Highway 68. Highway 40 closes for the winter,

so this site is not a problem year round, but a “Watch For Fallen Rock” sign is posted to alert northbound traffic. A UTM reference has been provided in the 2006 AMEC inspection report:

Easting – 635202 Northing – 5652672

Figure 3.18 shows the rock face at the site, and Figure 3.19 shows the map location.



Figure 3.18: Mt. Baldy Rock-Cut (Taken from ILRIS-3D Camera)



Figure 3.19: GoogleMap Location of Mt. Baldy

Site Topography

This site reaches a maximum height of 8-10m with a near-vertical cut slope. A soil layer is exposed at the crest of the slope with a thickness estimated between 3-4m. Rocks up to boulder size have been noted exposed in this soil layer. The west side of the road has some meters of clearance before dropping of into a valley at either end of the site. Near the centre of the site, the drop-off is quicker, hence a guard-rail has been placed.

Site Geology

A map investigation reveals that the Mt. Baldy site is located within the Middle and Upper Cambrian Rock Layers. These layers include the Arctomys, Waterfowl, Pika, Eldon, Stephen Cathedral, and Mt. Whyte Formations. (Geology of Seebe-Kanaskis Area 1971)

Vegetation at the crest of the slope is primarily composed of coniferous trees. The ditch is mostly grass, or barren. No vegetation is obvious along the cut slope.

Rockfall Hazard

It would seem that the greatest hazard at this site exist with the exposed rock in the soil at the crest of the slope, rather than from the slope itself. Therefore erosional cycles are the primary source of concern, and freeze/thaw effects would also contribute to the loosening of rock within the exposed soil layer. Indications do not suggest that the face itself poses a major threat to the site, but it is a near vertical layer exposed to the elements, and will as a result contribute to the rockfall numbers.



Figure 3.20: Crest of Rock Slope at Mt. Baldy Rock-Cut (photo by James Russell)

Ditch

The Mt. Baldy ditch is approximately 4m wide and 0.75m deep. For the maximum height of the site, the rockfall ditch sizing criteria indicates that a minimum width of 4.3-4.7m with a minimum depth of 1.15-1.3m is necessary. This means that the ditch is not to standards for the segments of the cut that range at the maximum height levels.



Figure 3.20: Material in Ditch at Mt. Baldy Rock-Cut (photo by James Russell)

The AMEC inspection in 2005 noted that the rockfall debris accumulation in the ditch appeared to reduce the ditch depth by a significant amount. This debris included some boulder sized rocks within 1m of the road, though no rocks had actually reached the pavement. Some possible sign of damage were noted on the road surface, which could be attributed to previous rockfalls.

Remedial Measures

Clearing the debris from the ditch is a top priority. In clearing the debris, the effective ditch size is increased, and if kept clean, may lower the associated risks for this site. Scaling the rock slope and the exposed soil face would also reduce the number of rocks that could fall in the short term, or perhaps even a few years to come. The ditch would still need to be cleaned, and especially so upon completion of the scaling procedure.

3.1.6. Old Man Dam

The Old Man Dam falls under the jurisdiction of Alberta Infrastructure and Transportation (AIT) for investigation and maintenance. As a result, when erosion along one of the embankments caused rockfall concerns, with a particular focus on down slope equipment damage, AIT launched an investigation. Areas of concern for the rockfalls are clearly evidenced upon observation, and it was deemed that an analysis of the site would be beneficial for determining remedial measures and potential future risks. The zone of interest on the dam can be seen in Figure 3.21.



Figure 3.21: Old Man Dam Rockfall Hazard Area (Taken from ILRIS-3D Camera)

Location

The Old Man Dam is located in southern Alberta, just North of Pincher Creek and Highway 3 (See Figure 3.22).



Figure 3.22: GoogleMap Location of Old Man Dam and Location of LiDAR Station on Site

Site Topography

The area surrounding the Old Man Dam is in the foothills of Southern Alberta, with high terraces and deep valleys. Water from the dam filters into the original Old Man River valley, while the reservoir fills the upstream portion of this valley.

Site Geology

Area is sedimentary material deposited in the Southern Alberta region. The area will also include glacial deposits, as with most of the rest of Alberta. Dam is an earth fill embankment. Rocks are being exposed along the edge of the spillway. If we are to assume that this is exposed bedrock material, then it would be of the Willow Creek Formation, which is largely composed of sandstones and shales (Hydrogeological Map: Lethbridge-Fernie, Alberta 1971).

Vegetation in the area would appear to be mostly grass and scrub brush, with sparse growth of trees. Grass is growing on the embankment slope. In the area of concern for rockfalls there is evidence of grass on the slope. However, the area directly around the points of erosion and rockfalling are barren of vegetation, which is likely indicative of the consistent movement of the earth in those areas.

Rockfall Hazard

The actual source point of the rock is clearly in evidence at this site. The rock layer being revealed via erosion is falling after its surrounding support is lost, and this is causing equipment damage. The real question is not whether the rocks will continue to fall, it is how to mitigate or prevent damage.

Remedial Measures

As mentioned previously, mitigation or prevention of damage is the key. Preventing slope erosion is certainly one solution. Scaling the slope would be one short term solution. If this solution were to be combined with a shotcrete facing of the slope, the rockfall hazard would likely be neutralized. However, there would need to be an analysis on how this would affect the drainage and functionality of the dam before it could be implemented. There is also the question as to whether this is economically feasible, or even necessary.

Mitigating the damage caused is as simple as providing rockfall protection down slope. Barriers have already been erected, though they are a temporary measure. The purpose of the analysis of this site is to determine the legitimate risk to the down slope area, and to determine the design requirements to prevent damage. While this would not provide a solution to the actual rockfall problem, it would prevent the damage caused and likely be more economical in the long term.

3.1.7. Highway 724:02 – Spray Lake Site Gabion Wall

This site is not a rockfall hazard per se, but rather a concern with a man-made gabion wall designed to provide support for the road passing through the area. A recreational trail and rock-climbing area exist below the gabion wall, and thus the concern when the wall began to fail was that the gabions would either topple down as a whole or empty their rock baskets down the slope. As it stands, a portion of the gabion wall has already failed and been removed. This has created an additional concern in that the geogrid support layer behind the gabion wall has now been exposed. When a geogrid is exposed to UV light, which is given off by the sun, it degrades, which further degrades the support for the road. Resulting failure of the wall is now a risk for both the highway and the recreational area down slope, and therefore the issue must be resolved properly.



Figure 3.23: Spraylake Gabion Wall Site (Taken from ILRIS-3D Camera)

Location

The Spray Lake Gabion Wall Site is found south of Canmore, AB on Highway 742:02. From the Canmore Nordic Centre turn-off, the site approximately 3.8km to the south. Highway 742:02 is an unpaved narrow gravel surface with no ditches, but there is a guardrail. The gabion wall is upslope of the Grassi Lakes Provincial Recreation Area, more specifically the Upper Grassi Lakes Trails, and immediately downstream of North Whiteman's Dam. The Map location of the site can be seen in Figure 3.24.

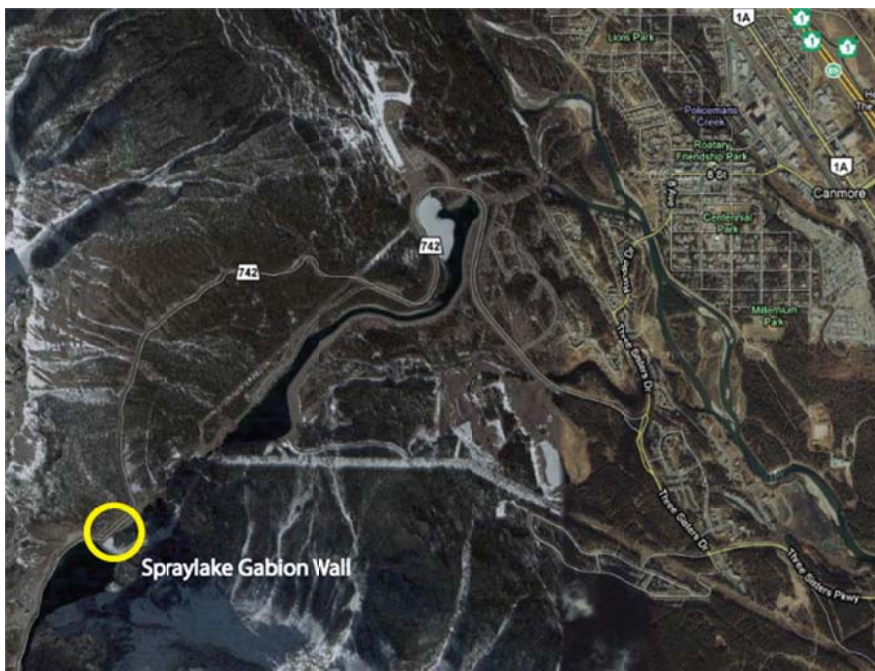


Figure 3.24: GoogleMap Location of Spraylake Gabion Wall Site

Site Topography

The road itself is cut into a mountain slope, specifically the lower portions of the eastern side of Mt. Rundle. A steep rock cut slope exists to the right side of the road when following Highway 742:02 southbound, while the left side drops past the vertical gabion wall to another steep slope, followed by another vertical drop. As previously mentioned, the North Whiteman's Dam is just upstream of the site.

Site Geology

The highway is oriented along a bearing of 050/230 (i.e. northeast/southwest) along a bedrock slope. The segment of the highway directly behind the gabion wall appears to be constructed on a fill embankment across a swale in the bedrock slope. A map investigation suggests that the bedrock is of the Pleistocene and Recent layers (Geology of the Seebe-Kanaskis Area).

Coniferous trees are growing both on the slope leading up to the gabion wall, and above the rock cut slope flanking the other side of the road. The trees appear to be well established, though some damage has been noted in the surrounding area due to combinations of both rockfalls and avalanches.

Rockfall Hazard

As previously mentioned, this site is not concerned with rockfalls in a traditional sense, but rather with failure of the man-made gabion wall and highway embankment. It was judged that groundwater exiting the slope at the west end of the wall caused surface erosion and gulying, undermining the base of the wall. A volunteer group of rock climbers scaled the slopes and removed the loose gabion baskets and rocks, exposing the embankment and geogrid behind, but reducing the risk of further failure from the wall. It would appear that the gabion wall was not designed to structurally support the embankment, but rather prevent its erosion. Therefore, assuming that further problems do not arise, the embankment and wall should be recoverable.

Erosion is certainly the primary concern at this site. Groundwater discharge and surface run-off will continue to cause gulying and degradation of the embankment. It is also possible that the gabion wall will experience further degradation if surface run-off is not properly controlled. As long as the erosional concerns remain, the site will certainly be at risk of rockfalls from the embankment, and potentially the wall.

A note is made that the collapse of the western gabion wall section does not significantly increase the pre-existing, natural rockfall hazard.

Remedial Measures

Short term maintenance to the site should include preventing further erosion, and repairing damage. Erosion could be reduced by a number of means, such as installing an impermeable berm to prevent surface run-off from flowing below the guardrail, but rather to either side of the wall area. Whatever method is used, care must be taken to ensure that wherever the water is directed, it does not cause a new erosional issue. The damage repair is removal of debris (taken care of already) and the application of a repair to the collapsed segment, such as shotcrete. This would also cover the exposed geogrid, preventing its further degradation.

Long term plans must insure that further failure does not occur along the wall. The gabion wall will either need to be infilled with concrete, or underpinned as a preventative nature. Annual site inspections by AIT and AMEC personnel are also recommended to continue.

3.2. Mapping a Rockfall Trajectory: Tornado Mountain

The next site to be investigated was a concern for CP Rail. Rockfalls affect their tracks on a daily basis, and there is a great deal of interest in rockfall prediction and prevention as a result. Two concerns from the rail perspective are rocks obstructing the track line, and rocks impacting against the trains themselves. If an accurate prediction method is possible, then the rail companies can either avoid troublesome areas, or take measures to mitigate the problems. Sometimes, however, there are rockfall scenarios that pass under the radar until it is too late to prevent the event. Such an event took place at Tornado Mountain, and a site analysis was called for. The site analysis taken in this study was not the first to be conducted, with a previous survey and study done by CP and Mr. Duncan Wyllie.

3.2.1. Site Location

The Tornado Mountain site, located approximately 2 miles down the CP rail-line from the Line Creek Mine in British Columbia, is the site of some notable rockfalls. Large rock faces at the head of the slope release boulders that move down the slope; where they occasionally cross the rail line. As a result of the risk associated with the rockfalls, a barrier wall was built adjacent to the track, perpendicular to the slope and the rockfall path. It was two particular rocks that initiated the recommendation for this wall, and additionally, it is these two rocks that are the interest in additional studies on rockfall movement.

The Line Creek Mine can be accessed off of Highway 43 between Sparwood and Elkford. The base station from the GPS survey is located at UTM 11N, 5531778N and

654855.5E. In Figure 3.25, both the location of the site, and the general bounds of the rockfall area can be seen.

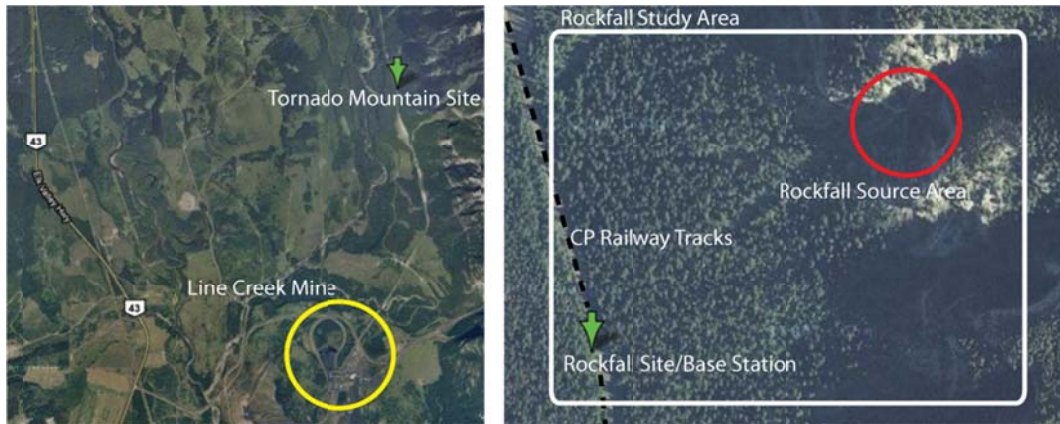


Figure 3.25: GoogleMap Location of Tornado Mountain Site

3.2.2. Site Characteristics

The Tornado Mountain site is located within an undeveloped area within the Rocky Mountain range in British Columbia. Only the rail lines, and potentially logging roads, provide access to the site area. At the rail line itself, the area is covered with gravel, placed on site to provide a space for any small rocks to loss energy before approaching the rail line. This catchment area failed to contain the two rocks in question, and so a barrier wall was installed soon after adjacent to the tracks. The wall was present only during this study, and was not there during previous studies of the rockfall that had determined the necessity of the wall. The wall and catchment area can be seen in Figure 3.26.



Figure 3.26: Barrier Wall and Catchment Area at Tornado Mt. (photo by James Russell)

After leaving the catchment area, the slope becomes heavily vegetated, and is covered in soft soil. Plants consist of both coniferous and deciduous trees, most with relatively small trunk diameters, which likely suggest a smaller depth of soil. There is also a large amount of moss, scrub brush, and smaller vegetation over the ground.



Figure 3.27: Rock Fragments Along Slope at Tornado Mt. (photo by Renato Macciotta)

The slope itself progresses at a steady angle of $\sim 27^\circ$ (ranging from 25° to 45°) and most, with very small areas being flat or steeper. Progress up the slope was relatively simple, so these angles were the most prevalent. Upon reaching the talus slope further up site, the slope became much steeper, to the point of impeding further progress with the equipment on hand.

Rock material was found more and more frequently as movement progressed up the slope. It is clear that rockfalls are a frequent event in the area, only they do not usually progress so far down slope as the rail lines. Figures 3.27 and 3.28 show both small deposits and large rocks along the main rockfall path. The rock material was composed of limestone, and little other material was noted on site. The slope face where the rockfall material was likely falling from was located from the final point of progress up the slope. The face was noted to also be composed of limestone (or apparently

composed), with large unweathered sections, suggesting recent rockfall. This face can be seen in Figure 3.29.



Figure 3.28: Large Past Rockfall Event on Slope at Tornado Mt. (photo by Renato Macciotta)



Figure 3.29: Likely Rockfall Source at Tornado Mt. (photo by Renato Macciotta)

3.3. Summary

For the sites investigated with AIT, there were several repeated characteristics at each site that are of interest to this study. Each of these sites, in particular, exhibited steep slope faces ranging from 50° to 90°. This steepness makes capturing and quantifying the slope faces with aerial LiDAR difficult. Also, the rock faces and slopes at these sites are exposed earth, mostly bare of vegetation. The nature of these sites is ideal for the terrestrial LiDAR survey in this study.

The Old Man Dam site, Section 3.1.6, and the Spraylake Gabion Wall site, Section 3.1.7, both have a unique rockfall hazard source visible within the scan area. The other sites do not exhibit clear and/or unique rockfall sources. Most of the sites exhibit erosional rockfall deposition, with larger rocks being freed during erosional processes. There are indications of other rockfall sources upslope depositing larger boulders, such as with the Crowsnest Lake site, Section 3.1.1. A rockfall analysis benefits from having a clear rockfall source location in addition to slope data.

The Tornado Mountain site would not benefit from a terrestrial LiDAR scan due to the large amount of vegetation, relatively shallow slope (25°-35°), and length of slope to cover. The site exhibits clear indication of rockfalls from impact points, wrecked vegetation, and rockfall deposits. There also appears to be a clear rockfall source further upslope, see Figure 3.29, though it is difficult to reach the area near the source due to steepening slope. For this study, an RTK GPS survey will be conducted to document rockfall impact points, though an aerial LiDAR survey would be of benefit for further defining the overall slope characteristics.

4. EVALUATION OF TERRESTRIAL LIDAR

Several sites, as mentioned previously in section 3, were investigated to establish the feasibility of using terrestrial based LiDAR to create digital elevation models that can be used in rockfall analyses. The sites chosen were based on either a need at that site to better quantify a rockfall hazard, or for their probable use in demonstrating the effectiveness of LiDAR technology. Each site was then further investigated with a stationary terrestrial LiDAR station. The following sections better clarify the choice of analysis, and the results, thereby, obtained.

Stationary terrestrial LiDAR was chosen for this analysis for two reasons. (1) The steepness of the rock faces at the sites being analyzed by AIT was such that aerial LiDAR was not feasible for total analysis. (2) The mobile terrestrial LiDAR had already been investigated for its use, and was determined to be either insufficient or unsuitable by AIT.

4.1. Terrestrial LiDAR Using the Optech ILRIS-3D

The stationary terrestrial LiDAR device used for the LiDAR surveys was the ILRIS-3D from Optech Inc.. The ILRIS-3D is a yellow box with a camera and light emitter on one side, and a screen, USB port, and cable connection ports on the other. Also included were batteries, the pan/tilt accessory, connecting cables, a tripod mount, and a PDA with the control software. Using a tripod base, this device can be set up anywhere the device can be carried. All of the equipment was transported in sturdy, protective travel cases, and assembled on site.

Equipment set-up is simple once a site has been chosen. The tripod is placed on the desired location with the mount, and then levelled. The ILRIS-3D is secured on top of this, with the pan/tilt accessory attached if it is required. Cables are connected between the devices and the batteries to ensure proper power is maintained throughout the scanning process. A USB is inserted into the ILRIS-3D for data storage, and the PDA is activated and connected to the device in order to begin scanning. The total time to set-up the equipment is relatively short, within 5 to 15 minutes depending on conditions. Figure 4.1 shows the set-up of the ILRIS-3D on site.



Figure 4.1: ILRIS-3D Set-up In Field (Photo by Renato Macciotta)

In order to use the ILRIS-3D, it must be centred on the location to be scanned. If the pan/tilt is attached, this is made simpler, since the device can then be tilted to capture images above or below the level of the device, and the device sweeps a 360° arc with the pan. An image of the area to be scanned appears on the PDA and rear screen of the ILRIS-3D. If the screen image is not clear, the lighting setting may be off. There are several settings that the ILRIS-3D camera can be changed to, which improve the displayed images. Using the PDA, an area for the scan can be selected, which can crop out much of the picture, and in the case of a panned site, many of the unnecessary images. Once an area has been selected, the level of detail required from the scan is input. By changing the level of detail, the time for completion is also changed. If higher level of detail is necessary, the site scan will take much longer, whereas a quick scan sacrifices the ultimate detail. Each site will have different goals for the survey, so the amount of detail required and/or time spent on each scan should reflect those goals. Once an acceptable compromise has been reached, a name for the scan is input and the ILRIS-3D begins capturing the point data for the site. Most single scans took between 5 and 10 minutes as chosen on site. This produced a detail of between one point every 2mm and one point every 2cm depending on the distance. Scans that required a pan of the site could take up to 45 minutes with the same detail. A file will be produced on the USB stick under the name input into the PDA which includes the raw data from the scan, and all pictures taken by the camera. Figure 4.2 shows the basic order of task in performing a LiDAR survey with the ILRIS-3D.

there are other reasons to run multiple scans. Rock outcroppings, erosions channels into the slope, and/or vegetation all have the effect of obscuring the scanned surface. The noted effect is a “shadow” within the point cloud data. If a second set up is positioned in such a way to define this area in the scan, the shadow can be removed by overlapping the two point-clouds. The final number of set-ups required at any given site is up to how much detail is required from the slope surface and the discretion of the LiDAR operator.

Data obtained from the ILRIS-3D is not immediately viewable. The file format needs to be checked in an applicable program and then converted into the format needed for future analysis. Parser.exe was used to view the initial data, and then to convert the data into a form usable in programs designed to perform point data stitching, surface interpolation, and rockfall analysis. If the initial data is poor, the site will need to be reanalyzed. It is therefore important to verify the acceptability of the data at the end of each day, or each site if possible.

After the point data is converted from the raw data given by the ILRIS-3D, it still needs additional processing. Polyworks, by Innovmetric, allows the converted data to be viewed and processed. The two main purposes of using Polyworks in this study were to stitch together the separate point data files from each site, and to clean up extraneous points. Most of the sites scans resulted in multiple data clouds, one at least for each set up of the ILRIS-3D. Stitching these images together required that there were points of commonality between the two point clouds, which is why overlapping scans are important. A minimum of three common selected points allows the program to fit the two point clouds together. More common points results in smaller error in the data alignment. The pan feature and a function in the parser program set the points from each scan in relation to one another so that stitching may not be required when the data is imported into Polyworks. Extraneous points can include reflections from the road surface, passing vehicles, vegetation, power lines, and surfaces beyond the scope of the analysis. These points can be selected and deleted within Polyworks to improve the efficiency of later tasks in the analysis.

In Section 3.1, a series of sites were investigated to determine if further analysis with the ILRIS-3D system would be beneficial for a study. Section 4.2 covers the results of applying the procedure in this section to those sites. Observations are noted for each on what needed to be done to complete the scanning to what was considered an acceptable level of detail at the time of the survey.

4.2. LiDAR Application

The stationary terrestrial LiDAR station was set up at each of the sites selected for investigation. Each site had different requirements for where the LiDAR device could be set up, and should be set up, in order to acquire the necessary data.

4.2.1. Highway 3 – Crowsnest Lake

For the Crowsnest Lake site, Highway 3 was a major concern. There is a great deal of traffic passing the site area, and this poses a potential hazard to any site investigators. The site also experiences frequent rockfall activity, with nearly constant small rock movement. Certainly large boulders are a major concern for traffic and safety, but enough build-up of small material is just as much a detriment. Additionally, the increased build-up of small rock material actually increases the probability of large rock material making it past the barricades which have been built to protect the highway. Even with this protection and regular maintenance, constant monitoring of the site is conducted to note changes to the site's hazard potential. In summation, the site is hazardous, but those hazards make site investigation a necessity.

It is for this reason that a LiDAR analysis was selected for this site. The constant level of risk associated with this site could be better quantified if the differences in the site from year to year could be identified. There are notable erosion areas on the slope, a large talus zone, and a high rock face, all of which contribute, or most likely contribute, to the rockfall problem. The ILRIS-3D can produce a surface map of the site with a great amount of detail. These maps can be produced each year, assuming repeatable set up procedures are used. Surface maps can be compared using constant points present in each, and then analyzed for their overall differences. Programs such as Polyworks from InnovMetric are able to perform this function. Once the differences are noted, the areas of greatest contribution to the rockfall hazard can be categorized, quantified, and responded to.

LiDAR set up on site was limited in space since the highway runs between a lake and the rock face. Setting up on the highway is out of the question without closing it down, but a service road exists between the highway and the lake. It was determined that two locations on this service road would suffice to provide the necessary coverage of the site with the exception of the ditch area behind the catchment fence. These set ups involved a pan of the site at eye level and then once again with a tilt to cover the visible range of the slope rising above eye level. An additional set up was attempted to capture the ditch behind the fence, which was located at the maintenance access to the catchment area on the east side of the site. There were concerns of rockfalls at this location, so only one set up and capture was attempted to minimize the potential risk. A point cloud was generated for each of the pan-tilt segments, which were then stitched together using Polyworks. The fully stitched, original point cloud can be seen in Figure 4.3, with the various colours representing the individual scans taking from the LiDAR as the device panned across the site.

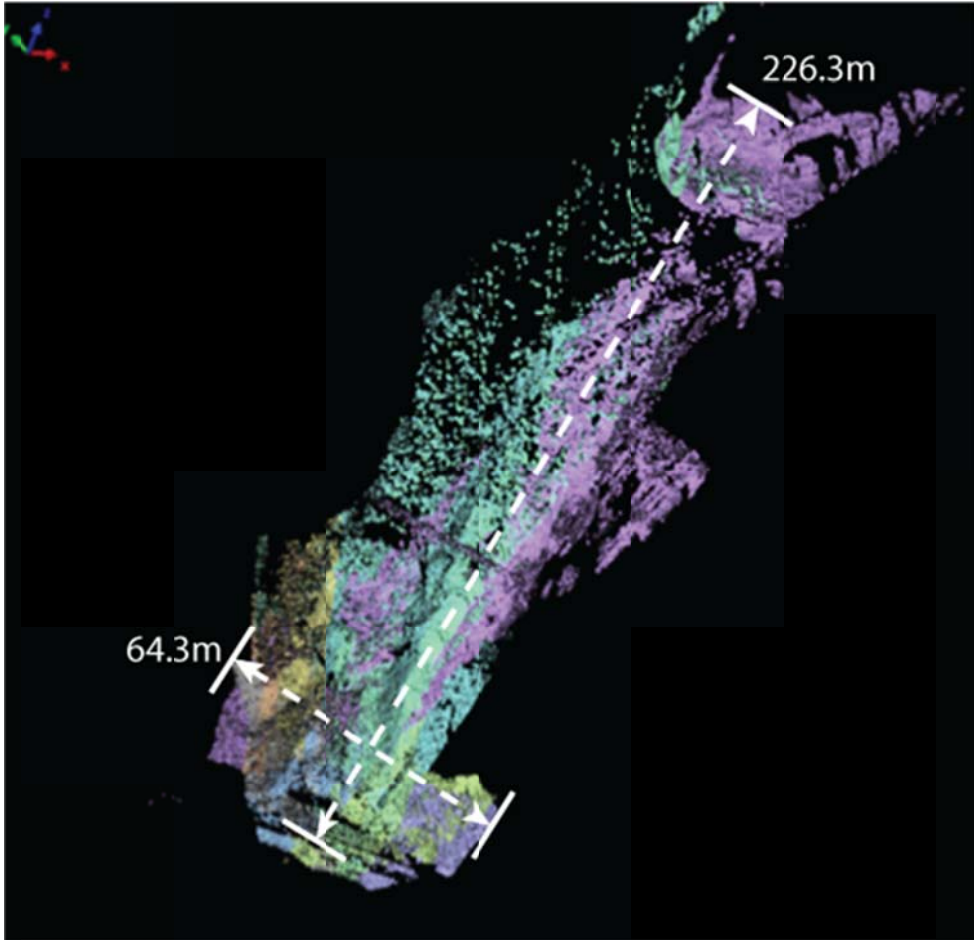


Figure 4.3: Crowsnest Lake Site Point Cloud Stitched in Polyworks with Different Colours Representing Each Scan

Additional representation of the scale of this figure can be seen in Figure 4.4 following, and in Appendix B, Figure B.1.

As seen from the figure, the point cloud covers quite a great deal of surface area, and due to the scale, it can be difficult to make assessments on slope properties without zooming in to particular areas of concern. Much of this data is vegetation or unnecessary point coverage. Further analysis can be facilitated by removing much of this data before interpolating a surface map from the points. The data of the point cloud as a whole still exists, but a simpler analysis can be performed by having another file with the points cut down to those deemed necessary to the analysis. The surface map produced follows the main rockfall paths, but if needed, the removed points are still available to increase the scope of the analysis. The surface map of the point cloud (after the extraneous points have been removed) can be seen in Figure 4.4 along with a sample cross-section of the slope taken along the centre of the surface map.

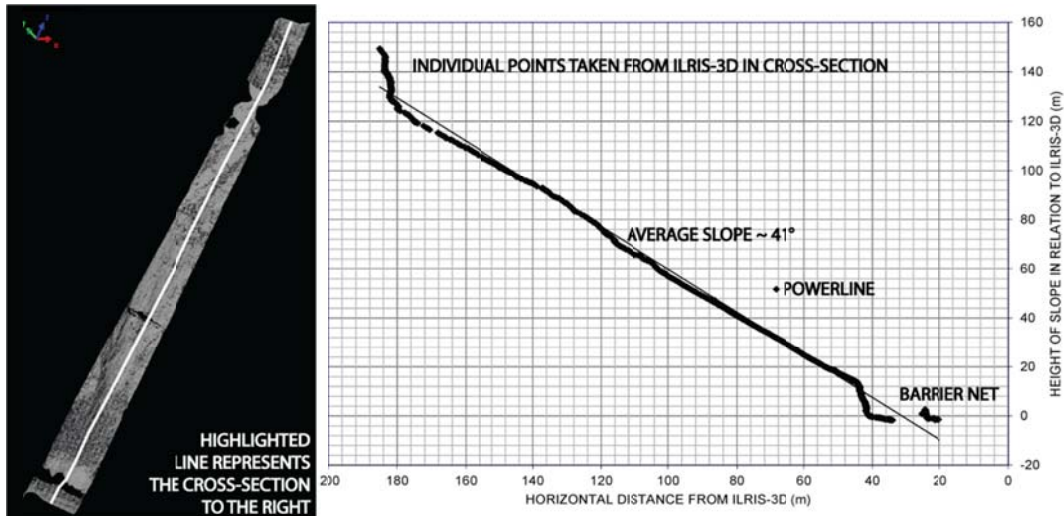


Figure 4.4: Surface Map and Cross-Section of Crowsnest Lake Site

Figure B.2 in Appendix B shows the above surface map enlarged.

Within the cross-section a few points are visible that should be noted. There is one obvious outlier at approximately 70m up the slope length, and sitting above 50m in elevation. This point is about 20m above the actual slope surface. These were powerlines crossing the site area captured by the LiDAR station. On the point cloud and surface map, there are notable shadows caused by these lines. Additionally, there is a gap in the area at the base of the slope. This area is the ditch in the catchment area behind the fence and barricade. The fence and barricade are shown as the initial points at the base of the slope, and the next set thereafter is an actual representation of the rock slope surface. Finally, it should be noted on the point cloud that the areas of higher elevation are more sparsely populated with points. This is because the slope angle became too steep for the stationary device to read any direct returns. The result is that these areas have to be entirely interpolated by analysis programs, or filled in with previous site data, such as that captured by an aerial survey. Without this process, these blank zones provide a greater level of uncertainty. This uncertainty could be an issue as the less detailed data is positioned within the talus zone, and near the upper rock face, where the rockfall source(s) is located.

This site demonstrates several limitations of a stationary LiDAR system survey. There are concerns of safety due to the nearby highway and rockfalls; which cannot be avoided due to the required set up distance of the station. With such a high slope that reaches angles nearly equivalent to the tilt of the station, many points will be lost or obscured. Man-made obstructions, such as the powerlines and catchment nets, have to be considered since they obscure data collection.

However, it should be noted that the ILRIS-3D did produce a viable surface map for rockfall analysis. Additionally, with the service road, the analysis is repeatable year to year, so there are applications for comparing the surface map results each year to

determine discrepancies in the rock slope. The cross-sections obtained are also usable in various rockfall analyses which do not require the same level of detail as the full 3-dimensional analysis.

4.2.2. Highway 541 – Highwood House Rock Cut

The Highwood House rock cut is not as potentially hazardous as the Crowsnest Lake site. However, there is reason to continue checking the site based on the potential risk that it does present. At this site, there are no barrier walls or fences to protect the nearby highway, only a ditch. The ditch itself catches a large amount of rock material, ranging from gravel to sizable chunks of rock approximately 30cm³. The cut wall itself could be the source of some of the rock material, but it is likely that much of it comes from the exposed erosion surface and slope above.

The size of the rock face made it difficult to capture the entirety of the rock slope from just one tilt angle. Two tilt angles were used to capture the whole of the rock cut, each covering two pans of the device. This means that it was possible to capture the surface of the site from only one set up of the ILRIS-3D. There was also room to capture part of the ditch in this effort, which was attempted. While the majority of the point cloud data provided an excellent map of the rock-cut surface, the data from the ditch set up exhibited a strange skew as it progressed further in distance from the ILRIS-3D. The points closest to the station lined up quite easily with the other point cloud data sets, but the references further along the rock face did not match with an increasing amount of error. The majority of these points were neglected for this reason, with only those located nearest the LiDAR device actually taken into consideration. It has not yet been determined why there was such a difference in the way in which the measured points were recorded with the parallel set up as compared to the perpendicular set up to the rock face. The surface map and a sample cross-section can be seen in Figure 4.5 with the enlarged surface map in Appendix B, Figure B.3.

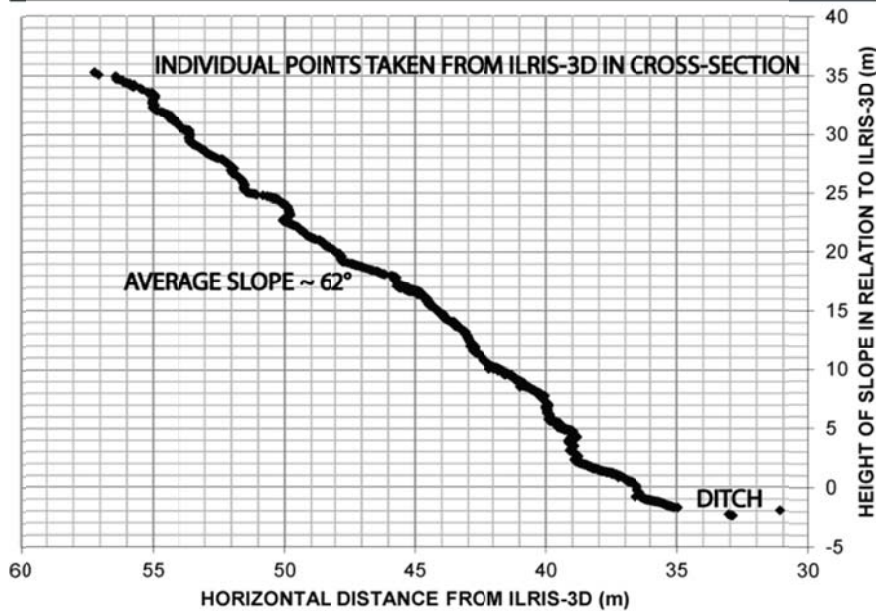
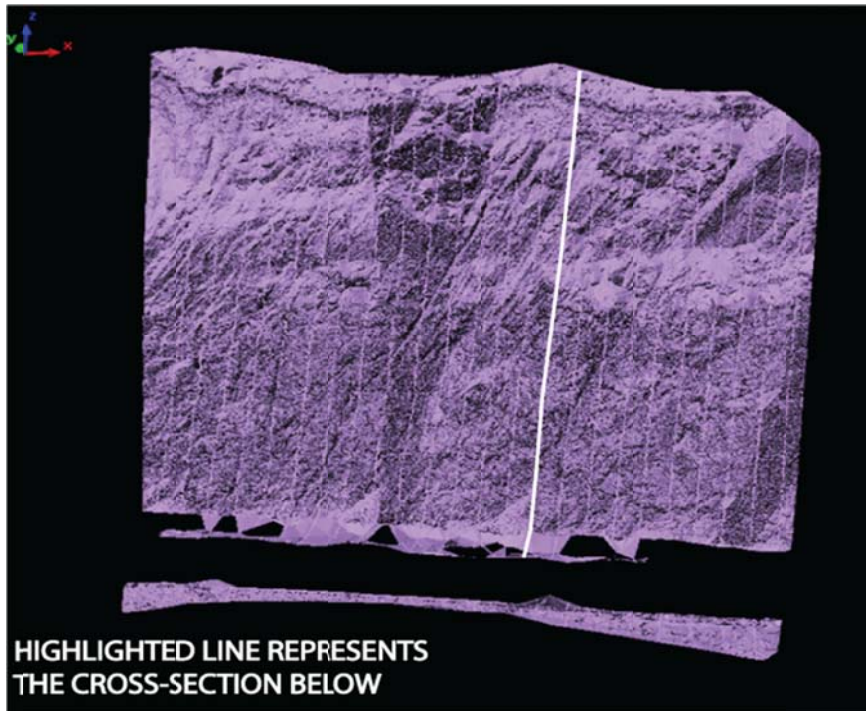


Figure 4.5: Surface Map and Cross-Section of Highwood House Rock-Cut

Finding suitable locations to capture the slope characteristics is a notable concern for stationary LiDAR devices. In this case, there was a grassy area adjacent to the highway opposite of the rock-cut wall before a steep dip into a valley. The area was lower than the highway level, which was not a problem for capturing the rock-cut surface given the height of the tripod base for the ILRIS-3D, but it was a concern in capturing ditch information. Additionally, the actual rockfall concerns at the site are not tied only to the rock-cut surface, but to sources in the slope above as well. As with the Crowsnest Lake site, the slope angle prevents accurate capture of the slope surface. Additional set ups to

the east and west of the wall may have helped in determining more of these upslope characteristics, but each angle would still have resulted in numerous blind spots of data that would require a more direct angle to capture. Finally, while it is not necessarily as great an issue with this particular site, the higher levels of vegetation located above the rock-cut face obscure the slope returns, and provide additional noise in the point cloud data. Due to the higher concentration of points with terrestrial LiDAR stations, slopes with heavy vegetation may not be as feasible as they are more prone to exhibit shadowing over the actual true slope surface. This is even when considering removing points of first return, which functions well in aerial LiDAR in removing vegetation and structural information. Ideally, combining the terrestrial data with aerial data would give the best definition of the site, though this depends upon the amount of detail required for the particular analysis being performed.

4.2.3. Highway 541 – East of Fir Creek Rock Cut

The rock-cut slope near fir creek shares the same overall characteristics as the one located nearby at Highwood House. AIT and AMEC's tour did not officially cover investigating this site at the time. It is, however, an interesting site for a LiDAR analysis since the area opposite the slope across the highway is a gentle elevation. This terrain was very suitable for the ILRIS-3D, and so it was chosen as much for a control site to test and compare the results from the device as for a rockfall hazard analysis survey.

Due to the way that the site was cut to allow the highway to curve around it, it was decided that multiple set ups of the ILRIS-3D would be more appropriate than using the pan function. Also, as mentioned previously, the elevated location of the set up allowed the site to be captured without the use of the tilt function. The ditch was more easily captured at this site due to the higher elevation of the LiDAR station. Since the station was above the level of the ditch and therefore granted line-of-site visibility of the ditch features, the majority of the ditch was captured without need for any additional set up. Figure 4.6 shows the resulting surface map of the rock-cut, and a sample cross-section. Figure B.4 in Appendix B shows the same surface map, but enlarged.

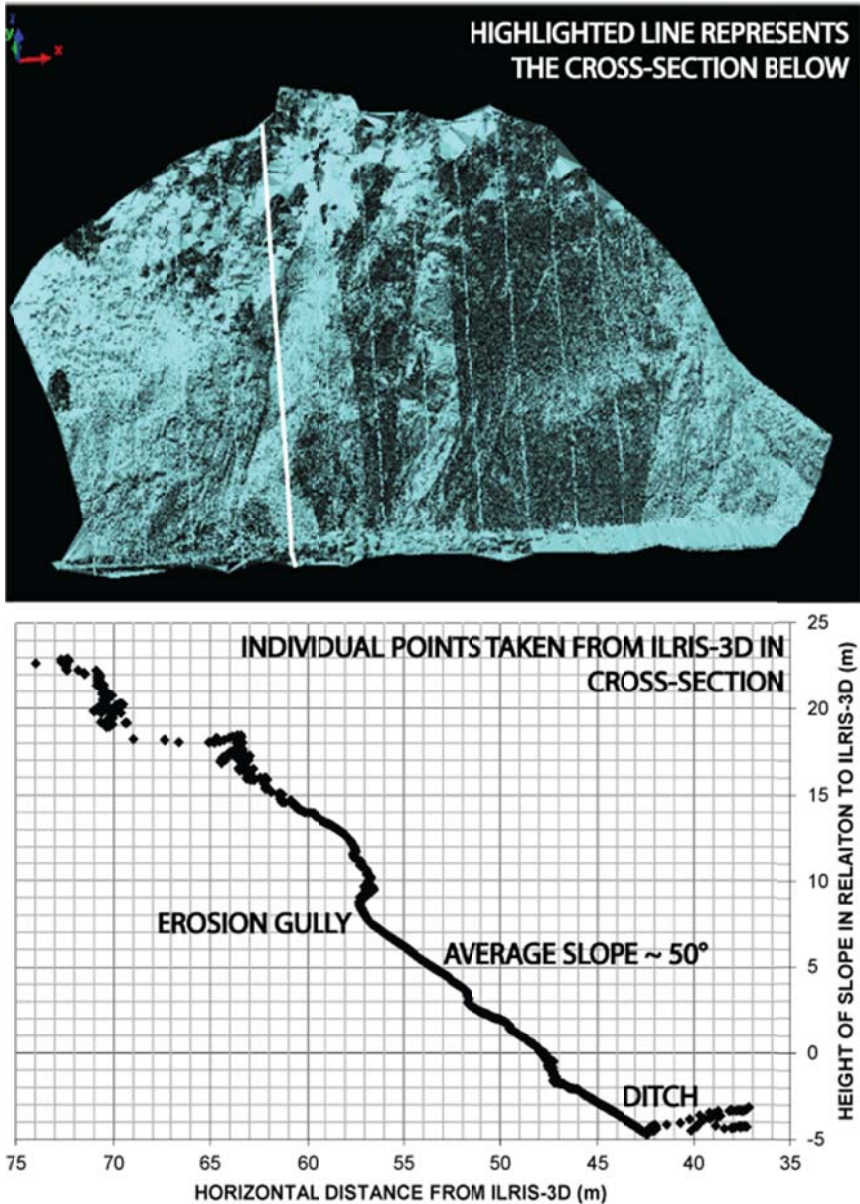


Figure 4.6: Surface Map and Cross-Section of Fir Creek Rock-Cut

This rock-cut showed that the right perspective from the initial set up can make quite a difference in the LiDAR return results. It is true that additional data upslope is obscured by vegetation and awkward angles, but much of the ditch was captured due to the location of the ILRIS-3D. With each site, strategic locations of the LiDAR stations are important. This site had ideal features which made the analysis significantly easier, but other sites are rarely so ideal. Advance knowledge of the site is most certainly a benefit for this type of analysis, as well as checking on past experience with each site if it is available.

4.2.4. Highway 40 – Galatea Creek Through-Cut

The Galatea Through-Cut has a rock face on either side of the highway. Both sides were steep faces with large blocks and fracture planes visible. The East side of the cut is the section that runs into the slope, and several large blocks seem to be at risk of movement. Rock bolts are placed at regular intervals along this face, aiding in holding back much of the rock mass, which can be seen in Figure 4.7. However, it was observed that one of the rock bolts was sitting quite loose, as if the block it had been holding was no longer present, which can be seen in Figure 4.8. This site, while at risk of small rock movement, certainly has a risk of large rock movement as well. There may be additional hazards upslope, but it was difficult to determine that due to the heavy vegetation.



Figure 4.7: Rock Bolts Holding Rocks in Galatea Through-Cut (photo by James Russell)



Figure 4.8: Loose Rock Bolt in Galatea Through-Cut (photo by James Russell)

The west side of the through-cut was easily accessible from the north and south, and was relatively even in grade. Since the through-cut was quite long, it was necessary to set up the ILRIS-3D multiple times, with each set up using both the pan and tilt feature of the station. Three locations above the west wall were chosen for maximum coverage, which allowed the whole East face and ditch to be captured in a point cloud. Figure 4.9 is a surface map and sample cross-section derived from a portion of the through-cut.

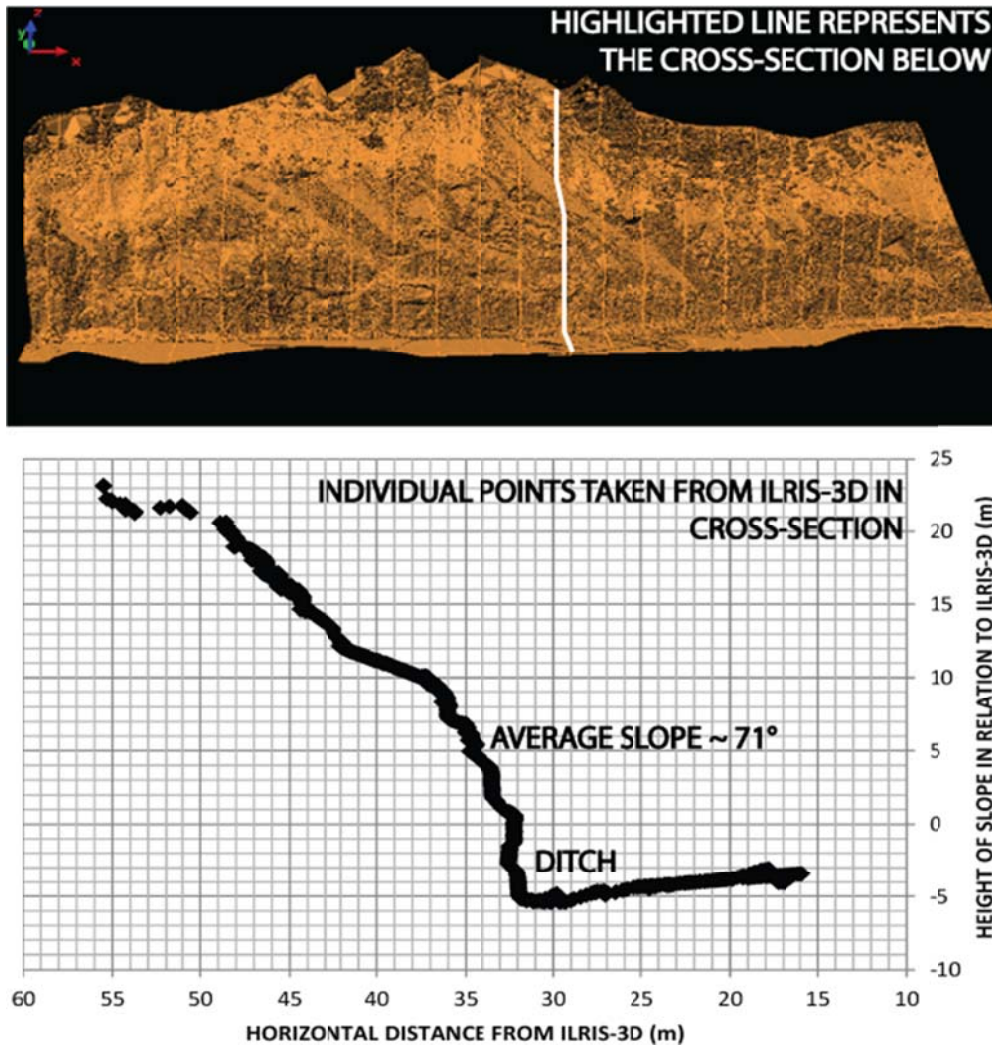


Figure 4.9: Surface Map and Cross-Section of Galatea Through-Cut

Appendix B, Figure B.5 shows the same surface map image enlarged.

As mentioned previously, knowing locations to set the LiDAR station is important. These three locations provided ample data for the East side rock cut, but to capture the West side cut, the positioning ILRIS-3D may not have been possible. Additionally, the vegetation directly above this site was so thick that capturing true earth points of the rest of the slope would be incredibly difficult.

4.2.5. Highway 40 – Mt. Baldy Rock Cut

The Mount Baldy Rock Cut does not present any new observations beyond those stated before. There was ample room to set up the ILRIS-3D to obtain the LiDAR data. Obstacles faced were similar to those before, such as upslope vegetation, and requiring multiple set ups to fully develop the point cloud. Following is Figure 4.10, which is a representative portion of the rock cut's surface map and a sample cross-section derived from that surface map. Figure B.6 in Appendix B provides an enlarged image of the surface map.

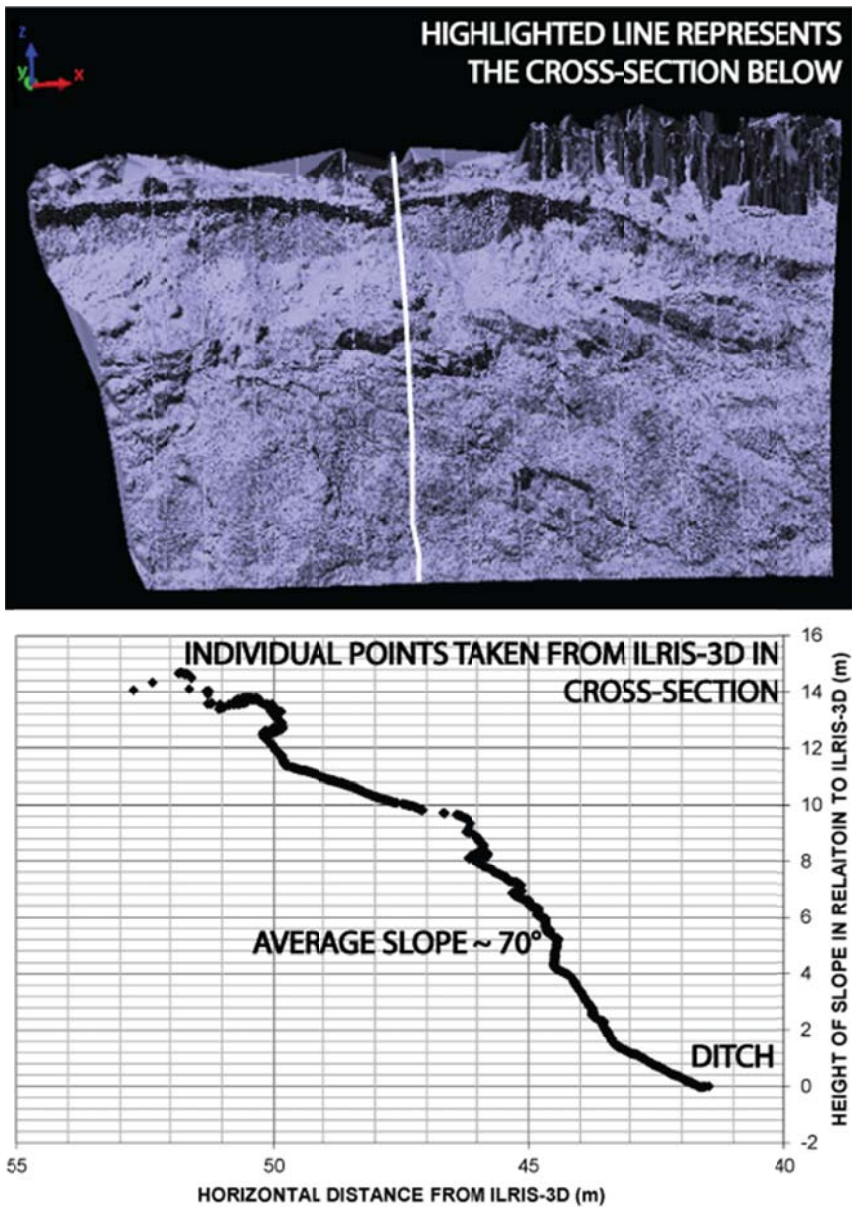


Figure 4.10: Surface Map and Cross-Section of Mt. Baldy Rock-Cut

4.2.6. Old Man Dam

As was stated in section 3, there is a rockfall hazard at the Old Man Dam which threatens the dam's monitoring equipment. Methods to mitigate this problem are being reviewed, but having a means by which to assess and analyze the situation may be of additional benefit. This site has a convenient observation point overlooking the hazard area. From this point, taking the LiDAR image is simple. The actual location of the ILRIS-3D was marked in Section 3.1.6, Figure 3.22. One set up of the ILRIS-3D is enough to fully capture the slope from rockfall source to the monitoring equipment.

Figure 4.11 is (A) the image captured by the ILRIS-3D's internal camera and (B) the point cloud obtained from the scan. The area in red shown in the point cloud is the area of concern that is to be further analyzed. Looking at the point cloud, there is a large area where the points remain undefined due to the wall of the dam blocking the surfaces behind. However, this area is unimportant for the analysis. The red marked area of the point cloud includes all the points to be analyzed. This area is quite well defined, with a point every 2cm. Programs, such as ArcGIS, can then be used to convert and analyze the data as a raster format DEM, as seen in Figure 4.11 (C).

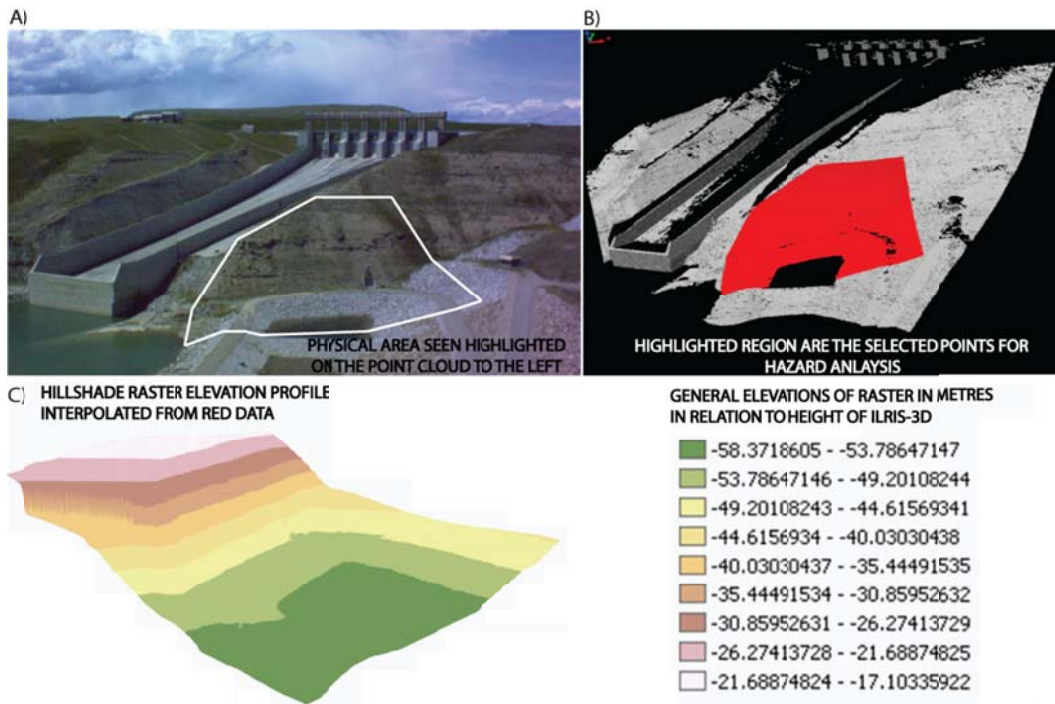


Figure 4.11: A) Old Man Dam (Taken from ILRIS-3D Camera). B) Point Cloud of Old Man Dam. C) Raster Hillshade Elevation Profile in ArcGIS from Selected Points in Point Cloud

4.2.7. Highway 724:02 – Spray Lake Site (Gabion Wall)

The Spray Lake site is located near a dam and a series of recreational hiking and climbing areas. While the site is not a rockfall hazard in the strictest sense, if the gabion wall at this site continues to fail, more rocks will be sent down into this recreational area. The dam itself is not likely at risk due to this issue, and was actually found to be of benefit in analyzing the site. The ILRIS-3D can be set up on the opposite side of the valley after crossing over the dam, which provides an exact line of site to the gabion wall. However, it should be noted that there are trees in this area that also fall into this line of site, and on the slope below the gabion wall itself (see shadows across point cloud in Figure 4.12). Since the analysis here is to determine how the rocks will fall if the gabion wall is not fixed, these trees create two points of interest. (1) They make it more difficult to define the slope itself as they create a significant shadow in the point data. This problem could be made less of a concern by adding another set up at an angle closer to the dam, if line of site can be maintained to the wall, and then stitching the images together to fill the shadowed space. (2) The trees will act either as a stop, or as a point of redirection in any rockfall scenario. Including the trees in the analysis as rockfall obstacles adds additional accuracy to the simulation. However, when attempting to create a DEM for the site, the points representing the full tree are not beneficial. Removing most of the extraneous points leaves a virtual stump. However, the interpolation of the surface does not always separate the slope points from those of the stump. That is to say, the mathematics within the program cause the stump points to angle more gently into the slope rather than project straight upwards like the tree does. In simulation, this causes the rocks to either catch or move in directions that would not occur in reality, and therefore these points become problematic. It may be possible that with the additional LiDAR data from another angle being stitched in to the DEM, that the stumps would become more clearly defined. Although, this may require as many as two to three additional angles to fully define the stump, and not all of the angles required to obtain this definition are feasible set up locations.

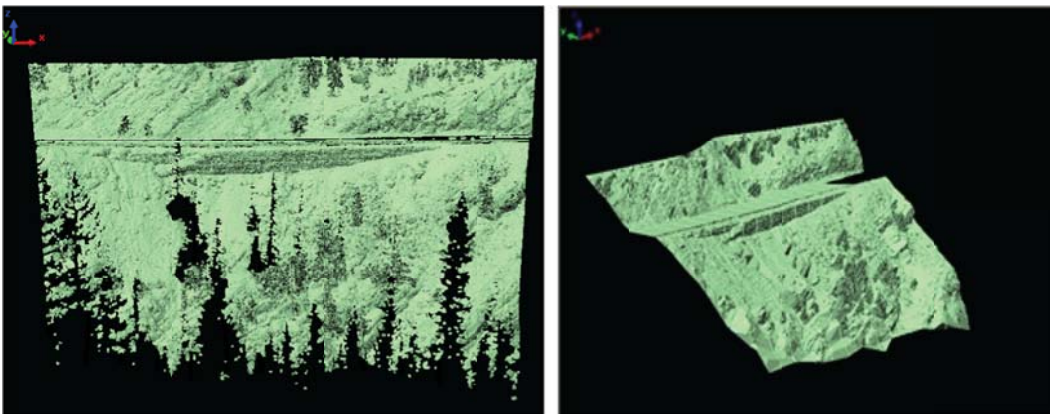


Figure 4.12: Point Cloud of Spray Lake Site Demonstrating Shadowed Areas Due to Line-Of-Site Obstruction from Vegetation and Resulting Interpolated Surface Map

4.3. Terrestrial LiDAR in Future Site Reviews

There were a number of things learned from each of the sites when using terrestrial based LiDAR technology. The objective of this research was to determine if stationary terrestrial LiDAR could produce repeatable results for future studies, and if any information to this effect is useful. However, the use of the analysis programs is also a concern when analyzing the point cloud data obtained from the ILRIS-3D LiDAR device. Since the point clouds contain millions of points, it is difficult for many programs to use the data effectively. Therefore, in addition to determining whether the survey is feasible, it is also important to determine whether the data obtained is useful. Polyworks, by Innovmetric, is one program that is quite effective for preparation and analysis of point clouds.

4.3.1. LiDAR data in Rockfall Analysis

The LiDAR data obtained needs to be complete and useful for analysis. For completion, the actual number and location of the points captured is the concern. For analysis, it is whether or not those points have some way of being interpreted, typically with the use of a computer program.

Each of the sites analyzed provided a different insight into the methodology and usefulness of the data obtained. Certainly location of the station was a defining factor for most of the sites. Two questions in particular are raised: (1) Is the station able to capture the necessary point(s) from a given location? (2) How many set up locations are needed? Each site has a limitation on where the stations can be located, either from pure spacing issues, or as a matter of safety. Once appropriate set up locations are determined, it is then useful to see whether blind spots are still being created on the point cloud. If these shadowed points can be defined with more scans from different set ups, then more set ups are necessary. It should be noted that some set up locations, particularly those running parallel to the slope surfaces, have exhibited curious skews in the point data. Avoiding parallel scanning locations, or performing additional scans from other locations may either mitigate or eliminate this issue.

Other factors to consider are the obstacles that obscure data. These can be vegetative cover or slope angles that do not allow measurable returns. Unless there are locations to see around light vegetation, or create more oblique angles to these slopes, there is little that can be done from a static station. The vegetation is generally removed from the point data, and any points remaining behind it are then useful in defining some of the slope, though it may be difficult to determine if these points are true earth points, or more vegetation. The slope obscured data can either be taken into account through interpolation within an analysis program, or filled in with additional data, such as known DEMs, or aerial surveys.

The aerial survey data may be combined with the terrestrial data, but that requires known points, or GPS locations. If possible, GPS locating the site of each set up could eliminate this problem and allow for simple stitching of the two sets together. However, if the set up points are being located by GPS, it may be necessary to stake the exact location of each set up to ensure repeatability of later scans. This is not necessary if each site analysis is GPS located individually. Additionally, placing reference points in the survey area could also serve this purpose. The reference point, which could be a stake with a dome or reflector on top, can be located with the GPS. With multiple GPS reference points on site, the rest of the point cloud can be referenced in relation. The reference points also have the additional benefit of making it easier to stitch multiple point clouds together, especially those that are taken from more extreme angles.

As stated previously, the point clouds created from a LiDAR scan contain millions of points. A stationary terrestrial system, like the ILRIS-3D, provides a significant amount of detail in a given small area. The first step of any useful rockfall analysis is to convert these points into a usable frame of reference. Any number of programs can be used to view the points, ArcGIS and Polyworks being two of note.

Two different analysis methods can benefit from the derived point clouds: one being a simple 2-dimensional analysis, and the other being a full 3-dimensional analysis. The 2D analysis only requires a cross-section in order to perform a rockfall simulation. This means that the data manipulation of the point clouds is much simpler, and the programs needed to calculate the trajectories are less complex. If the point cloud is in a viewable format, then two things can be done to obtain the cross-section. The first is to simply cut the data, thus obtaining any and all points along the cut lines, which can then demonstrate the slope cross-section. This method was used in the previous cross-sections, with the point data transferred to Excel where it can be viewed and further analyzed. The other method is to select a particular line and retrieve the data from there. This is more useful when a known rockfall path is visible in the cross-section, and can then be taken directly as viewed. If there are any erosion paths or channels in the slope, this is a likely place that rocks will be funnelled through. One way to tell if this is the case, when it is not apparent, is to note the talus piles at the base of the slope. If they are formed in a conical shape, they are likely being fed from a particular channel with consistent rockfall. Both of these methods only require that the program be able to view the point cloud and output selected point data. If stitching is required to align the point clouds properly, then a more rigorous program, like Polyworks, will be required even for the 2D analysis.

A 3D analysis requires additional program capability. This is the ability to interpolate a DEM from the point cloud data. Both Polyworks and ArcGIS can perform this task. Once a DEM is created, additional programming is required to determine how the rocks will interact with the slope model. RockFall Analyst (RA) is a program function addition to ArcGIS that performs this task. Based on a rockfall source point, the slope properties, and a number of physical parameters, it can determine probable ways in which a rock will move down slope. If the source is unknown, it is also possible to create a scenario where

a rock of a given mass and energy can enter the known slope area and travel down that slope. This requires a number of assumptions on the rock's starting energy and direction of travel. With enough repetition and consideration of starting location, this can provide the desired result.

A third benefit of the point cloud data is determining whether certain rockfall sources are at risk of becoming hazards. If a given section of slope is noted to have a fracture plane, or has experienced past movement, then it is possible to take two point clouds of that spot, taken at different dates, and compare them against each other. Polyworks has a series of tools that first allow point alignment, and then allow for comparison and discrepancies in those points to be noted. If the areas of concern show movement between surveys, then it is possible to stop this movement by either removing the offending area, or bracing it. Such a survey may be useful at the Galatea Through-Cut, noting both the loose rock bolts and the additional fracture planes along the site, and at the Crownest Lake site, with the high talus slope and the erosion channels forming within it.

All of these analysis methods are useful in verifying rockfall hazards. However, not all of them are necessary for projects to be completed. It may be that only the 2D analysis is required for the creation of cross-sectional data to determine a basic rockfall pattern for ditch and/or barrier wall dimensions. Therefore, the usefulness of the data is also dependent on the required purpose of the study. If more detail is needed, then more rigorous field surveys and analysis programs are needed.

Ultimately, a stationary terrestrial LiDAR survey is beneficial for repeated site analysis. Assuming that there are proper tools in office to complete the analysis, the LiDAR data can define rock faces and slopes very well. If the terrestrial LiDAR station reaches its limitations, then combining it with additional data, such as an aerial LiDAR survey, would be recommended.

4.3.2. Application in Hazard Management

Obtaining LiDAR data is one step of the process, but application is another. Knowing how a rock travels down a slope does not determine whether it will actually do so. Using LiDAR data to provide a surface to track bounce patterns and the energy of a falling rock is part of the design process that assists in determining the placement and cost of barriers and stop-gaps. However, tracking rockfalls is also about probabilities. In one year, the frequency of rockfall events may be large, while the next year may see very little activity. LiDAR data cannot predict the frequency of rockfalls. However, there are applications for LiDAR in hazard management.

Simply knowing probable rockfall paths is of assistance. If a rock is likely to hit the road, it increases the level of risk for that site. However, if the data shows that the rocks

are consistently entering the ditch, then maintenance efforts are likely all that are needed to maintain site safety. Tracking bounce patterns, and how these patterns intersect with infrastructure, is the first key point in LiDAR's usefulness in hazard analysis. While it is true that this does not reflect the frequency of rockfalls, site history should provide that data. By knowing where the rocks are likely to impact or come to rest, it can be determined if mitigative efforts are adequate, necessary, or need to be improved. The impact/resting points help determine the severity of the hazard, which enables the delivery of priority and cost assessment data to the projects on hand. In summation, the LiDAR data adds clarity to hazard assessment.

It was also mentioned that repeated LiDAR survey of a site could indicate areas of movement on a slope and/or rock face. Knowing potential hazard areas, rate of movement, and the estimated mass of moving material is very useful in a hazard assessment. Also, the knowledge of potential rockfall sources can determine whether removal is a priority, or if more passive methods will be sufficient to contain the potential hazard. The data obtained in this study could be useful as a baseline for repeated surveys at each of the sites, as well as for comparative data in future rockfall studies.

Since many transportation corridors experience rockfalls, a method that can be used to characterize the hazard is useful. In this regard, LiDAR is very useful. Many of these scenarios are easily covered in aerial surveys, but rock cut slopes, and other steep faces, are better surveyed via terrestrial means. With all of this taken into account, repeatable LiDAR surveys of potential hazard areas is recommended as long as both the data obtained is useful, and the costs are feasible.

LiDAR is most useful, then, in the characterization of a site for determining rockfall hazards. However, it does not reach its full potential without a means by which to model a potential rockfall. Further in this thesis is work on an analytical rockfall program that predicts rockfall trajectories down slopes similar to those captured in a LiDAR survey. While the Tornado Mountain slope analyzed is not suited for a terrestrial LiDAR analysis, many of the principles used from that study can be applied to data obtained from the LiDAR surveys in this section.

5. ROCKFALL ANALYST/COEFFICIENTS OF RESTITUTION

5.1. RTK GPS Survey of Tornado Mountain

As discussed in Section 2, the parameters that are used to describe the behaviour of a rockfall progressing down a slope are seldom measured for naturally occurring rockfalls. The Tornado Mountain site provides an opportunity to back analyze a measured rockfall trajectory while constraining the values of the parameters needed in the rockfall analyses. Two rockfall trajectories on Tornado Mountain were initially mapped by Mr. Duncan Wyllie for Canadian Pacific Railway. These surveys were carried out with a chain and compass, and at the time of the surveys, both the trajectories, final resting locations, and the two rockfall boulders were available. The impact points of the rockfall were flagged. The author resurveyed these impact locations using the Trimble RTK GPS system to establish the three dimensional coordinates of each impact point. The survey was conducted on June 22-23rd, 2010. The weather ranged from sunny with cloudy skies in the morning, to sunny with clear skies in the afternoon on both days. At the time of this site investigation, a rockfall-barrier wall had been built upslope of the railway tracks, and vegetation had grown on the mountain, obscuring some of the original rockfall impact points.

One of the two large rockfall-boulders had been removed by the time of this survey. The other rockfall boulder was readily apparent on the opposite side of the tracks from the slope (Figure 5.1). All flagged impact points were surveyed. Additional locations which could have been related to the rockfall paths, but were not marked with the flagging, were also surveyed. These points were noted as being unflagged, as possible points for comparison in further analysis.



Figure 5.1: Rockfall Boulder Found Near CP Railway Tracks (Photos by Renato Macciotta)

To begin the survey of the rockfall impact locations, a GPS base station was set alongside the CP Rail tracks and the resting place of one of the two rockfall boulders. This station was designed to provide a reference point for the roaming GPS receiver used to measure each point up the mountain slope. The GPS reading at the base station was very exact both days, with thirteen satellites to verify its position. The roaming GPS receiver was subject to communication error due to vegetative cover and increasing distance from the base station. Changing weather and satellite movement was also noted as the day progressed. These conditions could lead to variance in the readings. It should be noted here that the impact locations were generally quite large, often with more than a meter clearance in each direction (See Figure 5.2), which allows variance in measurements from the receiver. For consistency, each reading was taken to approximately the same level of error as noted on the GPS display. This was done by holding the GPS in place for an appropriate length of time, which ranged anywhere from 10 seconds to 5 minutes at each location. The average time was in the range of 30-60 seconds, with the error being no more than 10cm.



Figure 5.2: Rockfall Impact Points (Photos by Renato Macciotta)

Several different shapes and depths were noted in the impact points on Tornado Mountain. Some of the differences are due to the slope material, the energy of the incoming boulder before impact, and the rotation of the boulder. Slope material determines the amount of energy to be maintained after impact, which is defined in the coefficients of restitution. Softer material will also demonstrate deeper impact craters, while harder materials will exhibit shallower craters and rock fragments. The energy before impact will determine how hard the boulder hits the slope surface, which has a similar effects to those listed for the slope material. Additionally, if the boulder loses enough energy, it will not bounce, but will instead roll/slide from the impact crater, or even come to rest. The rotation of the rock may result in tumbling or change in trajectory, which also affects the shape of the crater. Some representations of the impact craters seen on site can be seen in Figure 5.3.

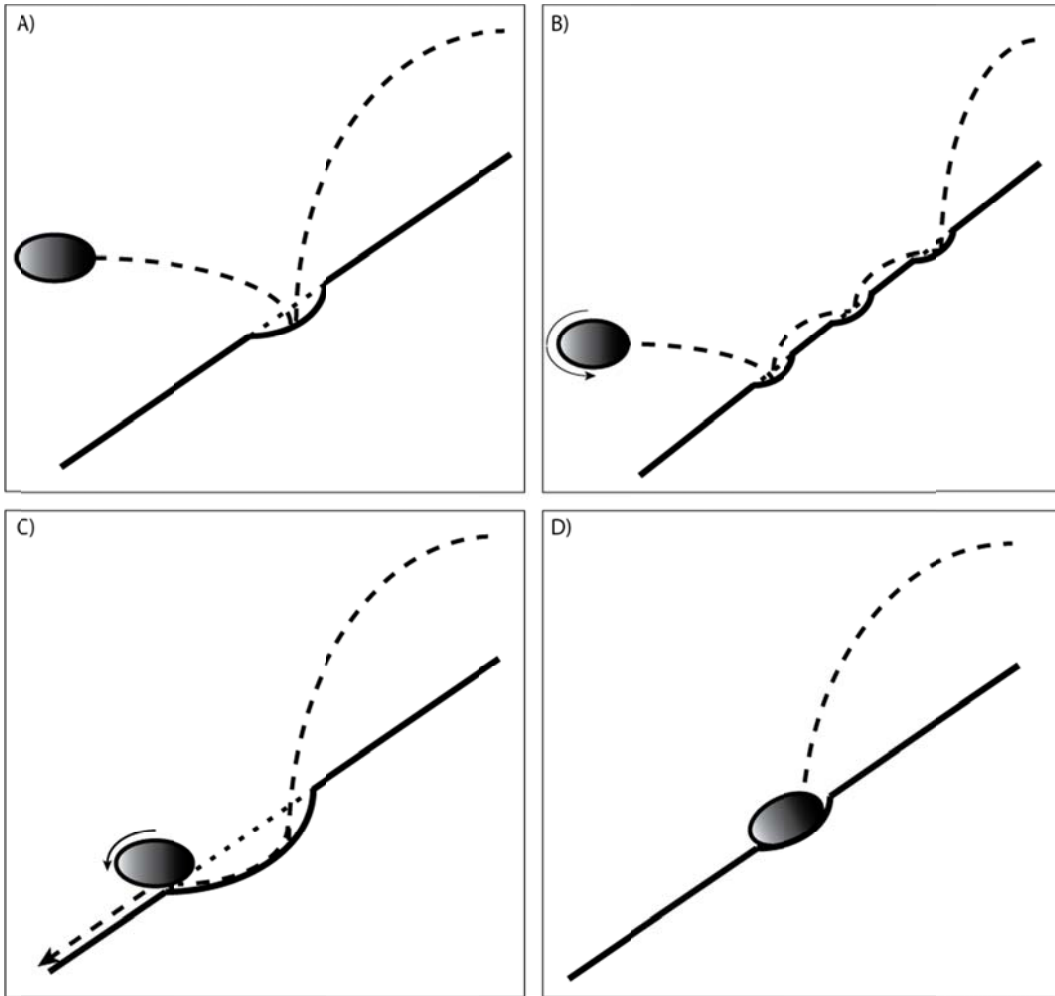


Figure 5.3: Rockfall Impact Craters A) General Bounce Profile, B) Tumbling Bounce Profile, C) Impact Causes Enough Loss in Energy to Result in Roll/Slide, and D) Boulder Comes to Rest

As previously mentioned, the trajectories of the Tornado Mountain rockfall events crossed the CP Rail line, which resulted in the construction of a barrier wall to prevent potential future damage of tracks and trains. The boulder sited near the tracks had an observable path, marked with orange flagging, progressing up the slope on the opposite side of the tracks. Travel up the mountain on the 22nd followed the orange flags, with each flagged point measured with the RTK GPS (additional points were recorded where it seemed prudent, see Appendix C.1: Site Notes). Additional rockfall activity was noted further upslope, such as broken branches and fallen trees (See Figure 5.4), and signs of fragmentation with fresh rock pieces of the same composition as the large boulder (See Figure 5.5). These fragments were unweathered and likely from recent rockfall events, potentially the same boulder given their location at the impact sites. There were other rock fragments in the area, more weathered than these pieces, likely having come down in previous rockfall events. This observation does beg the question of how many of these pieces were directly related to the rockfall event, and how many of these impact points were caused by the same rockfall event? Further travel up the slope makes these

questions more difficult to answer as additional boulders ranging from fresh to weathered are observed more frequently, and the smaller rock pieces and fragments are far more abundant. The flagging turned to yellow, and from this point, many fallen rocks were visible, and the rock face that was likely the source of the boulders became apparent. It is difficult to tell whether these impact points were directly related to either of the two rockfall boulders. Eventually, progress up the mountain became impractical with the equipment on hand, and it should be noted that this is where the flagging also apparently ended. From this point onward, fresh rock material was in heavy abundance, and it would be very difficult to separate any one rockfall impact point from another (See Figure 5.6). The path following only the orange flags was likely caused by the one rock, but anything higher up the slope is difficult to identify with any certainty.



Figure 5.4: Trees Broken Along Rockfall Paths (Photos of Renato Macciotta and James Russell)



Figure 5.5: Fragments from Boulder at Impact Points Along Rockfall Path (Photos by Renato Macciotta)



Figure 5.6: Increasing Talus Material Looking up Rockfall Path to Source Area (Photo by Renato Macciotta)

During the second day (June 23rd), the yellow flagging was followed back down the slope towards to the final impact point of the second boulder. This path demonstrated a far larger number of fallen trees, but the aging of these trees made it difficult to determine whether they were recently felled, or had been broken by previous rockfall events. The flagging was not nearly as consistent as the orange path, and the points of impact less obvious in many cases. In fact, some of the likely points seemed to be unmarked, while others that appeared to veer off the likely rockfall path were marked. For comparative purposes, both these points were taken for many of the cases noted. Additionally, a large number of boulders were discovered along the slope, which could have been previous rockfalls, fragmentations from this boulder, or the actual source of many of the points flagged. Unfortunately, the actual boulder was never identified for the yellow path, so the question as to which of these points were directly related to this particular rockfall cannot be answered with certainty from the observations made in this study.

Actual site data was recorded by Renato Macciotta, who labelled each point and provided observations. His notes were entered electronically and can be seen in Appendix C.1. Along with the notes gathered on site is the returned data collected at each point by the RTK GPS, which can be seen in Appendix C.2. Figure 5.7 is a visual representation of the points mapped from the GPS survey. The profiles of the rockfall trajectories are seen in Figures 5.8 and 5.9.

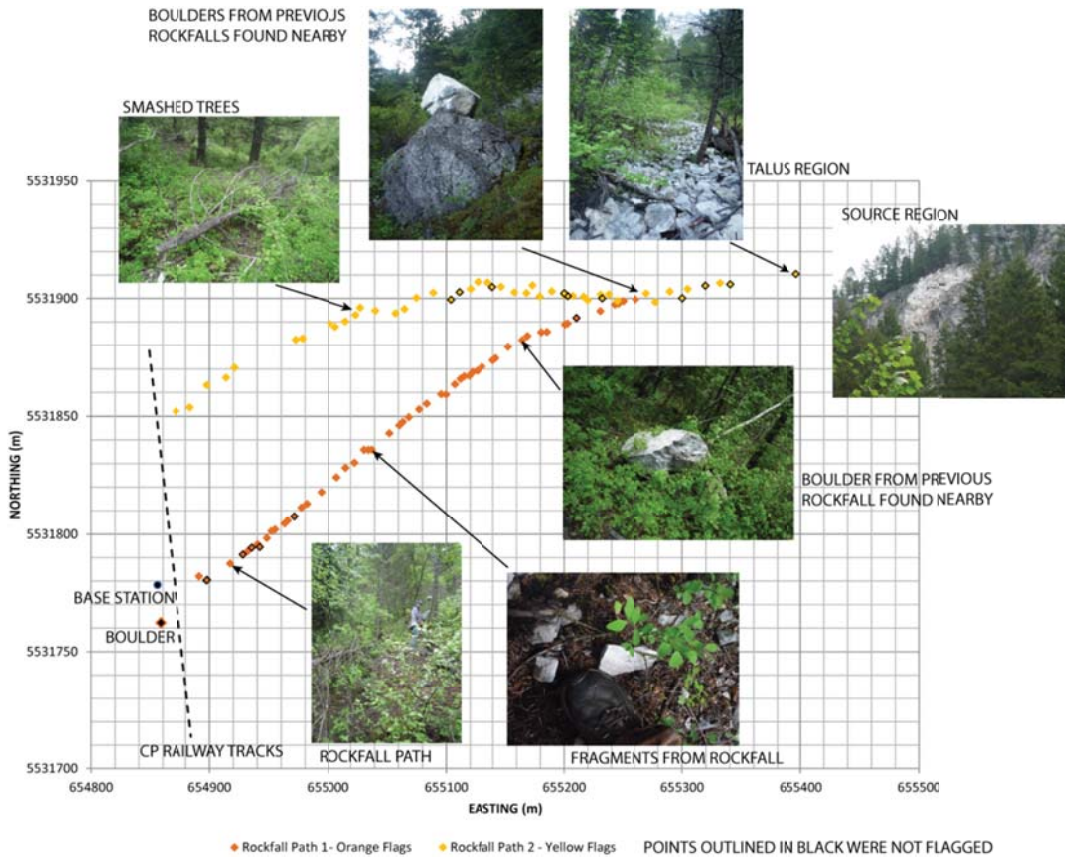


Figure 5.7: Plan View of RTK GPS Survey of Tornado Mountain Rockfall Path

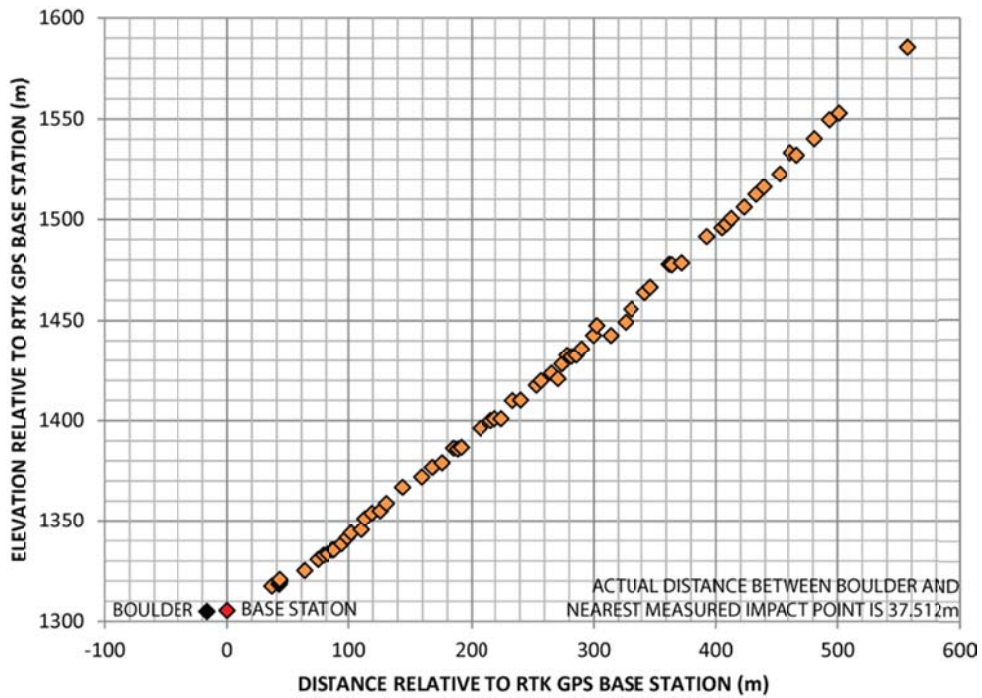


Figure 5.8: Profile View of Orange-flagged Rockfall Path at Tornado Mountain

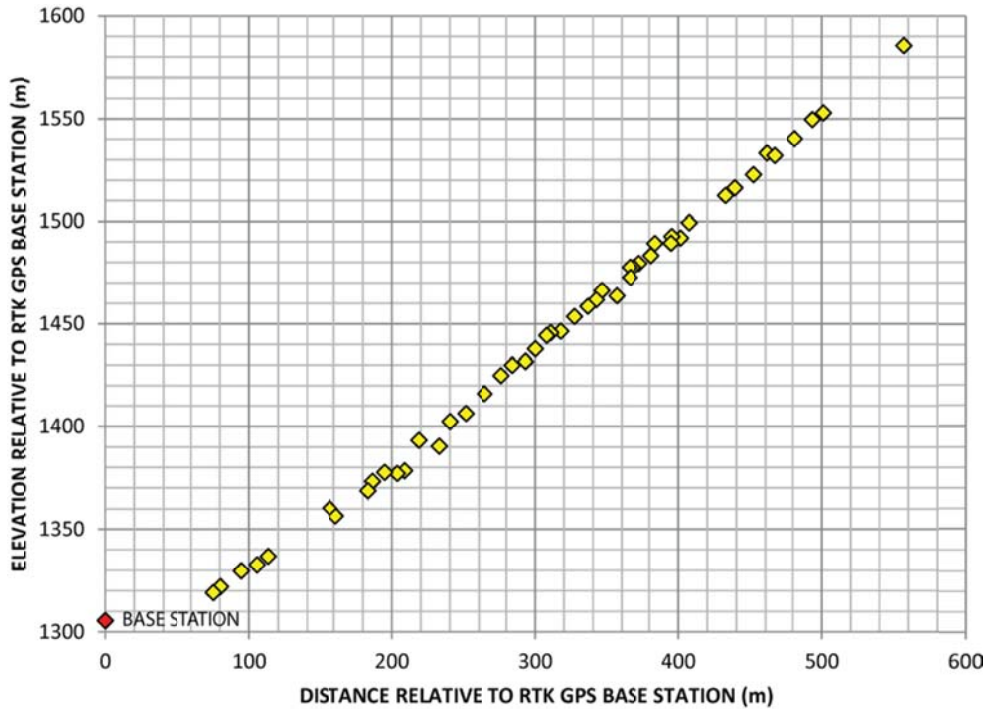


Figure 5.9: Profile View of Yellow-flagged Rockfall Path at Tornado Mountain

Information on the rockfall path provided by Mr. Duncan Wyllie was compared to the data obtained in the RTK GPS survey (See Figure 5.10). Though the survey methods were different between the analyses, there is reasonable agreement in the data sets within the two dimensional plane. There are 69 points in the Wyllie survey, and 64 in the RTK GPS survey. At least 6 points are not included in the RTK GPS survey at the track area and near the rockfall source. Additional discrepancies may be from taking into account possible additional points with the RTK GPS, obscuring of points by weathering and vegetation, and loss of flagging. Point pairing is evident within the data, with some error in elevation and distance. There are a number of points that exhibit elevation differences (at least three points notably greater) in the RTK GPS survey. These discrepancies are most likely due to the differing methods with which the data was gathered. Confirmation of data should become a priority in future studies; with some suggestions to achieve this confirmation of data being to take additional readings in and around each impact point. Additional readings could be used to reduce potential measurement errors, and would further define the site characteristics. The rockfall source location can be estimated even lacking the RTK GPS data point by following the curvature of the measured GPS path with the distance measured in Wyllie’s survey.

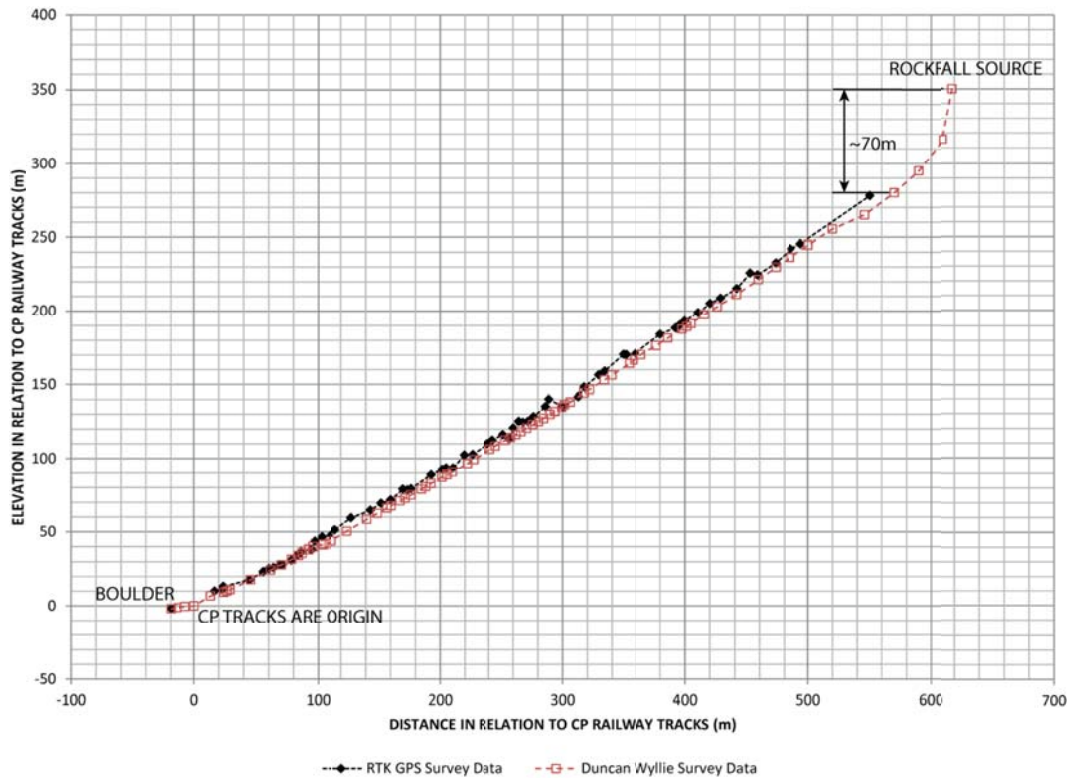


Figure 5.10: Comparison of RTK GPS Survey to Duncan Wylie's Survey for Orange-flagged Rockfall Path

5.2. Three Dimensional Rockfall Analyses

Most rockfall analyses are conducted using two dimensional models. While this can provide a reasonable estimate of rockfall behaviour, it eliminates many of the slope features that define rockfall behaviour. Three dimensional models require additional data, but are able to provide additional rockfall trajectories and insight into the slope because they do not constrain the rockfall system. The following section examines the use of a three dimensional rockfall analysis program, RockFall Analyst, using the data collected from Tornado Mountain. Since additional data is required for three dimensional analyses, integration, calibration, and use of that data will be discussed, as well as sensitivity to various input parameters.

RockFall Analyst requires a three dimensional digital elevation model (DEM) as the base geometry for rockfall analyses. The DEM used for this study was derived using the data obtained from the Geobase website, map section 082g15. Geobase provides maps in 1:250,000 and 1:50,000 scale. The map taken here is 1:50,000 scale within the North American Datum of 1983 (NAD1983). The data obtained was from sources in Alberta and B.C. (such as TRIM data). Both of the sources state horizontal accuracy within 10m and vertical accuracy within 5m. Point data within ArcGIS showed 10m separation between individual points. The data file opened within ArcGIS was referenced to

NAD1983 UTM 11N. The RTK GPS data was referenced to the same NAD1983 UTM 11N. With the spatial reference parameters in agreement, the measured data is imposed over and agrees with the Geobase map data (see Figure 5.11).

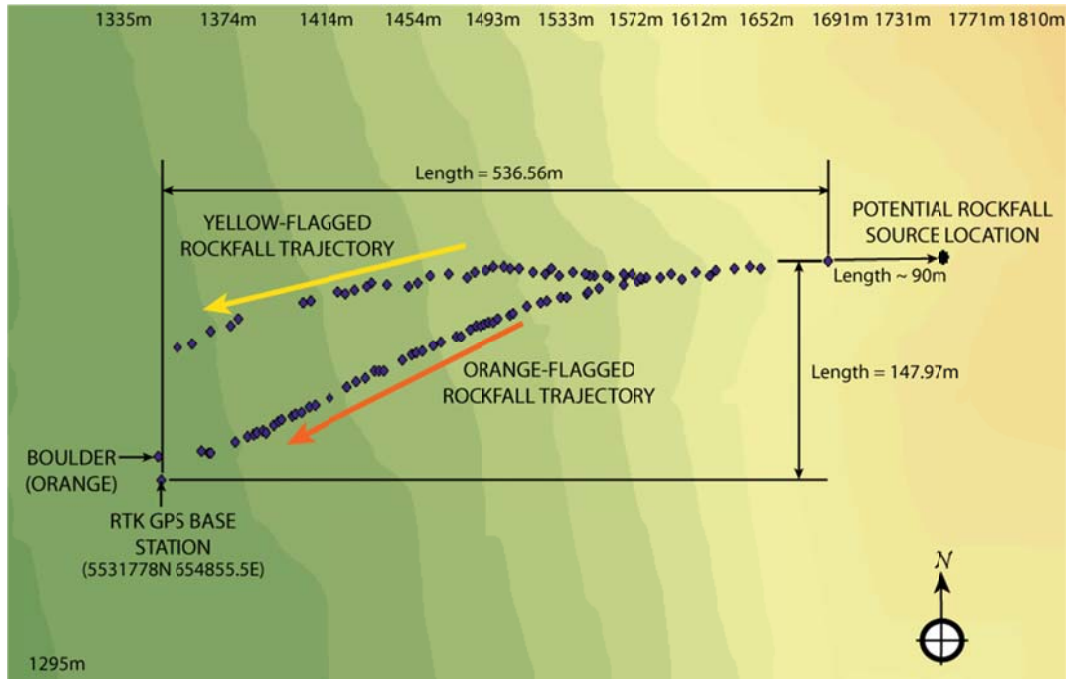


Figure 5.11: Tornado Mountain Rockfall Trajectory Superimposed on Raster from Geobase Data

All subsequent figures that include the Tornado Mountain DEM and RTK GPS data will refer to Figure 5.11 for scale.

To derive the DEM from the point data obtained, the data was converted into raster format within ArcGIS. Several options are available for the conversion to raster format, however there are considerations in the selection of one. The Kriging method is generally used for dense data sets and provides a large amount of detail around every point. The Inverse Distance Weighted (IDW) method is for sparser data sets, and considers the points surrounding each individual data point being analyzed to create a smoother trend. Kriging is more accurate in a denser data set, but the points obtained Geobase are not dense enough to make full use of this method. The DEM used for this analysis was created using the IDW method. Slope data proved to be smoother and more consistent with observations made on site.

The DEM in Figure 5.11 was interpolated using the GPS point data as well as the Geobase data points. Since the data was so sparse, the inclusion of the GPS data sets would provide extra slope detail lost between the Geobase points. However, since the RTK GPS was used to measure points within impact craters, the points were generally lower than the Geobase set. With the Kriging method, there left visible trenching along the GPS point trajectory. With the IDW method, there was little visible effect from the

GPS points since the slope geometry was derived from a wider trending in the points. It should be noted that the RTK GPS points were not entirely lower in elevation, with many higher by 2-3 meters. Because these points suggested a different slope trending than the sparser Geobase points suggested, they were included, as mentioned previously, for the extra detail.

The rockfall source must be identified in order to perform any simulation of rockfall trajectories. During the field survey, the likely source of the rockfall was identified, see Figure 5.12. By comparing Wyllie's survey, mentioned in Section 5.1, to the GPS survey, the distance to the rockfall source looking back from the measured trajectory was found to coincide with a steep slope section on the DEM. This coincides with the source being observed on a cliff face. However, this method only estimates the location of the rockfall source rather than clearly identifying it. Since the distance estimation suggests an area rather than a point for the rockfall source, a series of analyses using polylines is the more logical choice. The polylines allow multiple potential rockfall sources to be analyzed over an area. Once a simulation is completed, the simulated trajectories exhibiting behaviour most similar to the measured rockfall can be identified. By tracing these lines back to their seeder source point, the more likely rockfall source areas are clarified for the next analysis set.



Figure 5.12: Rockfall Source in Fractured Limestone Cliff Face at Tornado Mountain (Photo by Renato Macciotta)

Initial rockfall simulation tests were run using the identified source as a seeder location for the rockfalls. The volume of the observed rock was approximately 4m^3 , therefore the mass, assuming the boulder is entirely limestone, should be approximately 10444kg. The initial calibrations were carried out to verify the source location and the initial properties to ensure that the rockfall boulders had sufficient energy to deliver it down the slope to the railway tracks. Once these initial parameters are established the final step was to determine the sensitivity of the prediction to the assumed coefficients of restitution.

5.2.1. Initial Calibration Approach

While the general source of the rockfalls was identified during the field work, there is no way to identify the actual source of the rockfall boulder that was tracked down the mountain. RockFall Analyst provides options for locating the rockfalls as a point source or as a polyline source. Given the uncertainty in the actual source location, it was decided to analyze the site using a series of polyline seeders stretching out in both directions from the assumed source (See Figure 5.13 for the locations of the polylines). This provided additional observations on potential source areas.

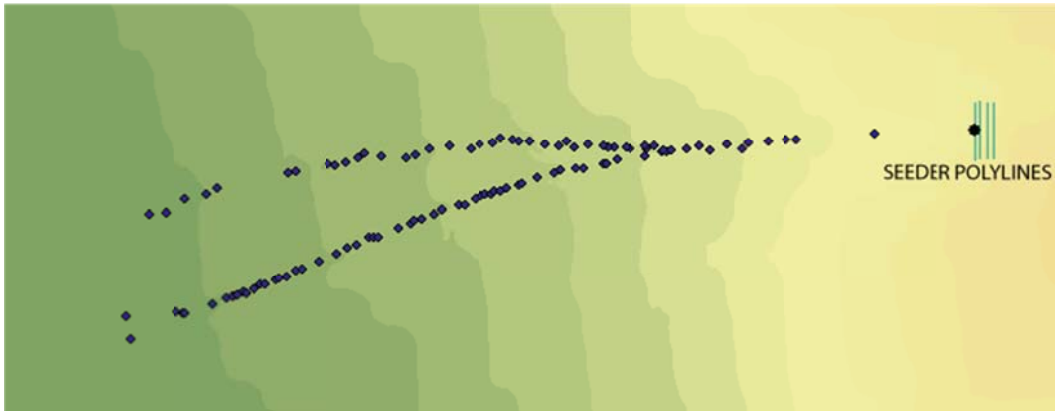


Figure 5.13: Seeder Polylines for Tornado Mountain Rockfall Simulations

Seeder parameters are important to develop in RA before performing a rockfall simulation. With any point seeder the parameters include horizontal velocity, vertical velocity, drop height, mass of rock, number of rocks, and degree deviation of rocks. The mass of the rock has already been defined for this test. The number of rocks and degree deviation describes how many rocks will be simulated for a given seeder point, and how many degrees will separate each as a starting direction. Multiple simulations at each seeder point prevent oversight of the direction of the rockfall's initial trajectory. The dip angle of the slope is the what determines the starting trajectory, but with additional variables to consider, it is better to consider additional rockfalls at various starting angles. The horizontal velocity, vertical velocity, and drop height are to provide starting energy for the rockfall within the simulation. There is a typical starting parameter set of 5m/s in the horizontal, 0m/s in the vertical, and a 5m drop height. Additionally, with polyline seeders, the separation between points along the line is a parameter. For example, a 10m

line with 2m point separation will have five individual seeder points. Each seeder point takes into consideration all of the previous parameters individually.

As discussed in Section 2.5, the type of material that rockfall boulder impact can influence the coefficients of restitution. Rather than assuming the default setting in RA for COR, a series of polygons representing the differing slope materials that the rockfall boulders encountered was created. Three polygons were used to represent limestone rock, talus, and the vegetated cover. The locations of these polygons coincide with the points in the site notes where the slope material changed, and seen in Figure 5.14. The initial properties of these polygons are given in Table 5.1. The actual material zones cannot be defined with rectangular polygons, but the rectangles do match the trending of materials on the slope.

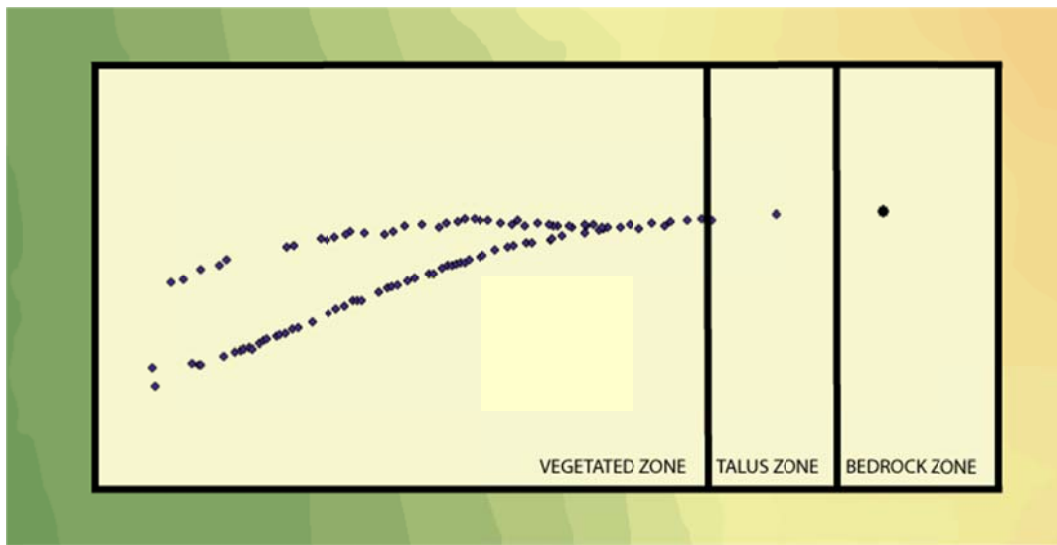


Figure 5.14: Material Polygons to Define COR in Tornado Mountain Rockfall Simulations

Table 5.1: Slope Coefficient Parameters for Initial Calibration

	Rn	Rt	Friction Angle
Limestone	0.315	0.712	20
Talus	0.33	0.82	20
Vegetated Cover	0.33	0.87	20

The coefficients of restitution Rn and Rt were taken from those compiled by Rocscience (In Rocscience Coefficient of Restitution table, Appendix A, Table A.3) with the exception of the values selected for the vegetated cover. The vegetated cover is the largest area that any rockfall will travel through. To ensure that the rocks travel the distance noted in the RTK GPS survey during the initial calibration, the Rn and Rt coefficients for the vegetated cover are increased from the values noted in Table A.3.

Initial rockfall simulations are used to confirm or refute assumptions, and to verify the DEM and input parameters. For the first of these simulations, the rockfall source is assumed to be within the area of the polylines. To confirm this assumption, the trajectory

of the falling rock is the most important point of observation. Rocks that follow one, or both, of the observed trajectories can be traced back to a point that coincides with the rockfall source. The actual energy of the rockfall does not need to be exact in these trials, but the rocks do need to follow the trajectory to some end point past those observed. Back analyzing the simulated trajectory should verify and/or zoom in on the potential rockfall source. Figure 5.15 shows an initial simulation to verify the rockfall source point. The rockfall path highlighted in blue is the trajectory of greatest interest for backanalysis to the rockfall source.

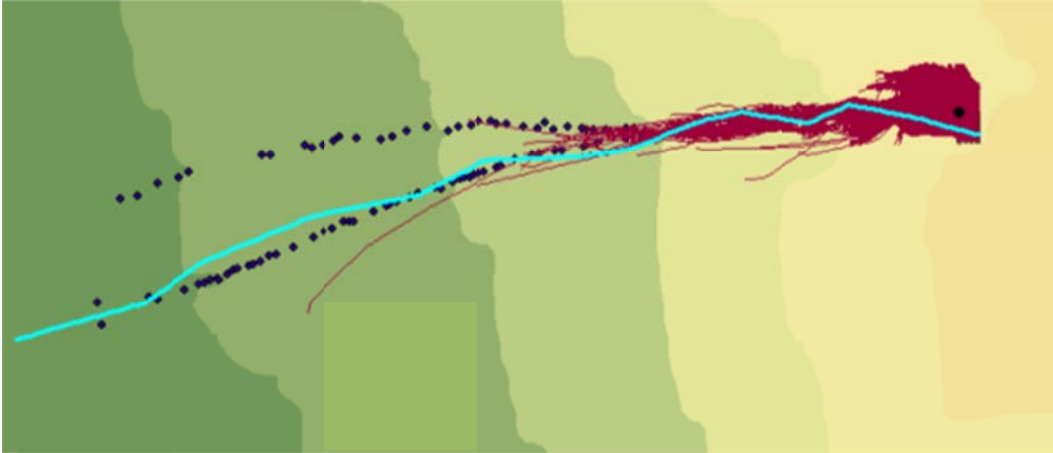


Figure 5.15: Initial Calibration of Rockfall Simulation with 15m/s Horizontal Velocity, 10m/s Vertical Velocity, 5m Drop Height, and Initial COR Values

Had agreement with the assumed rockfall source and the rockfall trajectory been achieved, then the initial calibration can be used as the baseline analysis for the rest of the rockfall simulations. When agreement is not reached, further calibration is necessary. The rockfall trajectory can be traced back to its starting point within the polyline seeder set. Two potential scenarios are possible at this junction: (1) The rockfall source can be located within the mass of the polyline seeder set, and (2) the rockfall source can be located at the edge of the polyline seeder set. If the source is within the mass, then the response is to reduce the number of seeder points being considered to speed up processing of the rockfall simulations. If the source is on the edge of the seeder set, then a new polyline seeder grid needs to be applied with that source point being centred within. In both cases the goal is to verify the source location and reduce the number of seeder points in the analysis. A seeder set, such as the one used in Figure 5.13, considers over 6000 possible rockfall trajectories and must calculate and process each individually. The time to finish this simulation ranges between 5 and 8 hours. Decreasing simulation time allows for a greater number of simulations to be run with varying parameters.

With a new polyline seeder set established, the calibration tests continue. The process follows the same pattern as suggested in the above paragraph until such time as both a suitable test duration and source definition are achieved. Figure 5.16 shows two seeder grids established to improve test duration and source definition using the same

parameters as the initial calibration test. Figure 5.17 shows the simulations run with these grids.

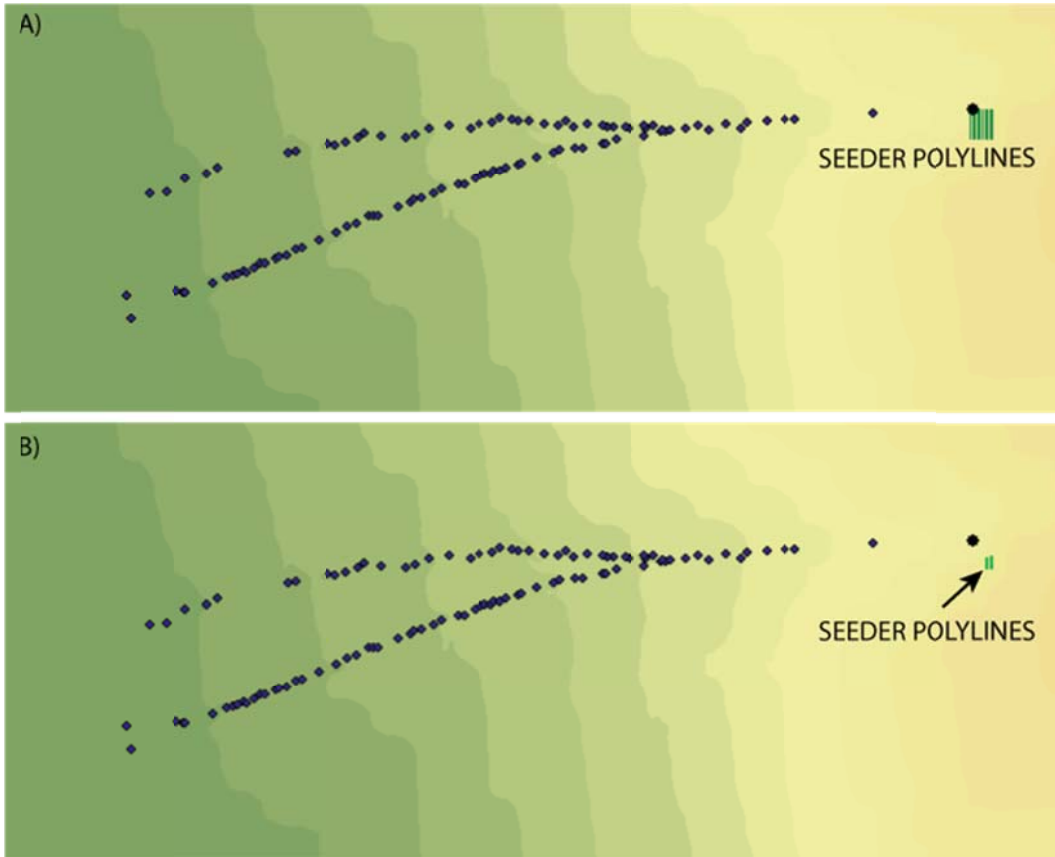


Figure 5.16: A) Refined Seeder Polyline Set and B) Further Refined Seeder Polyline Set

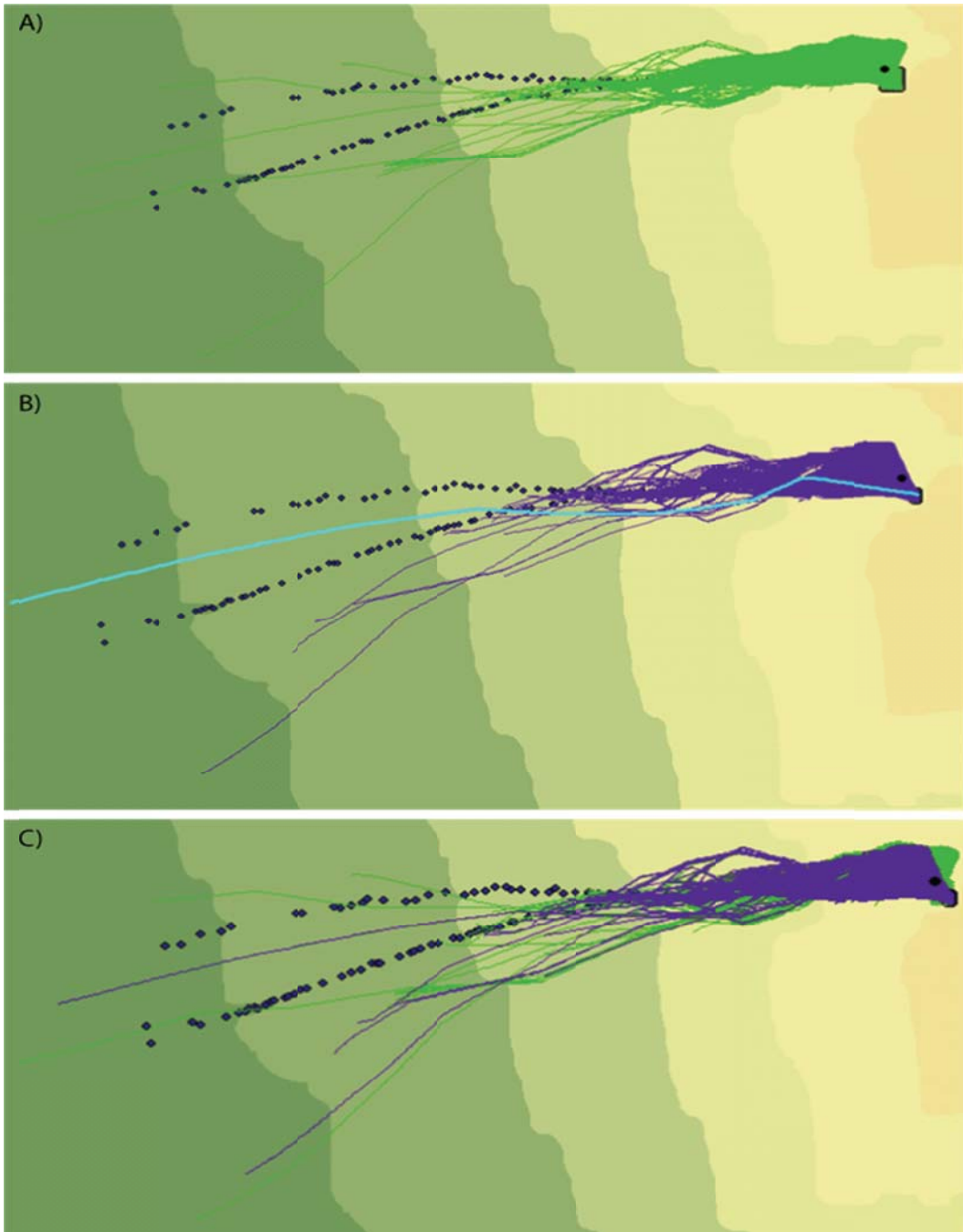


Figure 5.17: Rockfall Simulation Calibration Tests with Initial Calibration Parameters and A) Redefined Polyline Seeder, B) Further Redefined Polyline Seeder, and C) Comparison of Rockfall Trajectories from Both Seeders

One difference to note between the results of Figures 5.15 and 5.17 is that 5.15 demonstrates a simulated rockfall trajectory that more closely matches the measured rockfall trajectory. When calibrating the rockfall source, it should be noted that polyline seeders place the individual seeder points along the polyline, and not on specific locations. If an exact match for repetition of results is desired, then greater care must be

taken in choosing the polyline configuration to replicate the exact seeder locations. This task is not a necessity until more finely tuned calibration is required.

Once the source location has been defined to an acceptable level, the initial energy parameters of the rockfall need to be calibrated. A rock is not likely to launch from a cliff face with 15m/s horizontal velocity, and 10m/s vertical velocity. However, the conditions that cause a rock's release from the slope are not clearly defined or measured. Additionally, the DEM is not a true earth representation of the slope. The energy needs to be both realistic and capable of allowing the rockfall to overcome inconsistencies within the DEM. Three parameters are considered once a source location is defined: (1) the horizontal velocity, (2) the vertical velocity, and (3) the drop height. Each slope is sensitive to these parameters in unique ways. A series of simulations is of benefit to determine what these may be.

Considering the further redefined polyline seeder, as shown in Figure 5.17B, additional tests on the sensitivity of the input parameters can be conducted. Figure 5.18 demonstrates the effect of different velocity inputs. Figure 5.19 demonstrates the effect of different drop heights. All of these tests were conducted with fewer rockfall simulations at each individual seeder.

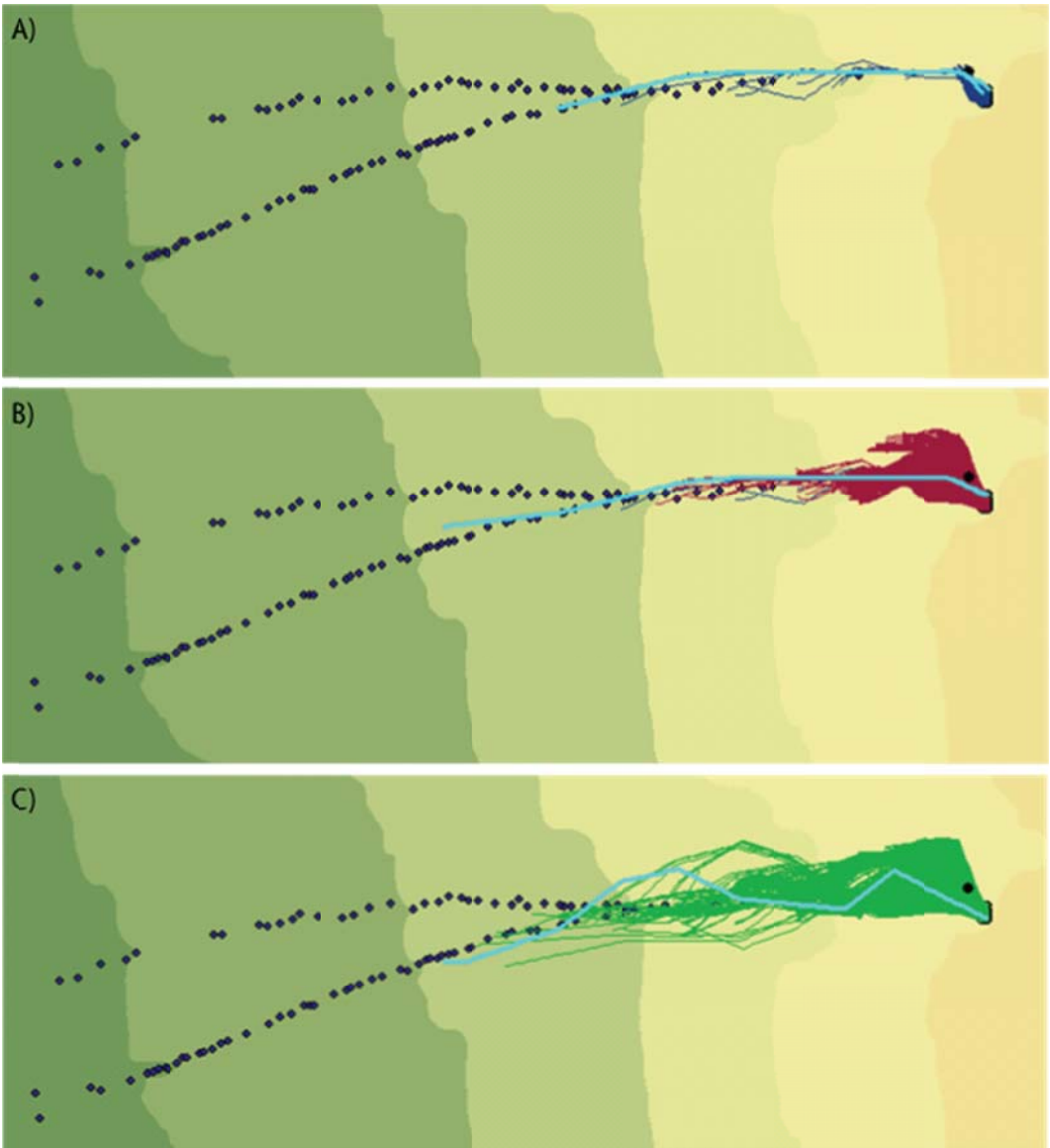


Figure 5.18: Rockfall Simulation Velocity Sensitivity with Initial Calibration Parameters and 5m Drop Height at A) 5m/s Horizontal and 0m/s Vertical, B) 10m/s Horizontal and 5m/s Vertical, and C) 15m/s Horizontal and 10m/s Vertical

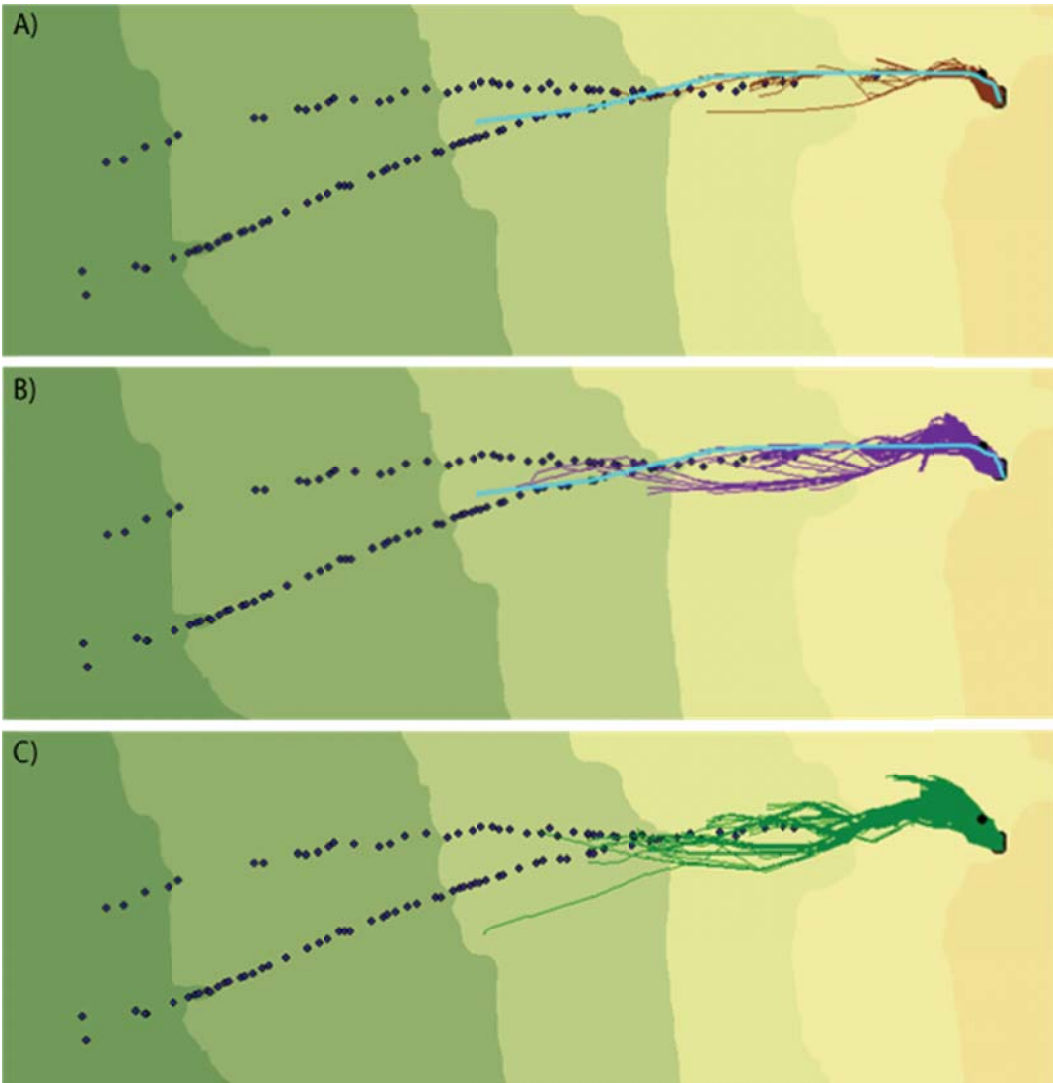


Figure 5.19: Rockfall Simulation Drop Height Sensitivity with Initial Calibration Parameters and 5m/s Horizontal Velocity and 0m/s Vertical Velocity at A) 10m Drop Height, B) 25m Drop Height, and C) 50m Drop Height

Within the analyses of sensitivity to starting velocities and drop heights, relationships can be observed to determine a likely starting energy for the additional rockfall simulations. If a realistic rockfall energy is determined based on the source location, further tests to verify the slope material parameters and trajectories can be conducted. Should there be conditions preventing a realistic determination of the starting energy, other methods may be considered to conduct the rockfall analysis. Such conditions were encountered in this study, and another calibration approach was considered.

5.2.2. Rockfall Energy Calibration Approach

Rockfall simulations in RA do require a seeder point for the rockfall, but this seeder point does not need to be the actual rockfall source. A defined rockfall source with an understood method of release is ideal, but not always attainable. Any point along the observed rockfall trajectory can also be used as a seeder point. Only a realistic amount of energy needs to be considered to make this approach feasible for rockfall analysis. To determine a realistic source of energy, the topography of the rockfall source area should be taken into consideration.

Mr. Duncan Wyllie's survey noted the approximate height of the rockfall source in relation to the last surveyed point. This point corresponds to the last point measured in the RTK GPS survey, as well as being located near the talus and vegetated slope border. It can be assumed that the rock will have a potential energy based on the height of the source area when compared to the final surveyed rockfall impact point. The height difference between the source and the last rockfall impact point is approximately 70m. Additionally, the cliff face that this boulder will drop from is an indeterminate height above the slope surface. The boulder will most likely impact the slope before reaching the chosen seeder point. It can be approximated that the boulder will retain a good deal of its energy as it bounces down this slope area. Consideration for the starting energy will be taken as though the boulder were dropped from a height ranging from 10m to 70m onto a limestone bedrock surface with varying slope angles.

Slope angles can be determined with ArcGIS. Raster conversions within the program can be output in a number of ways. The raster format used and shown thus far has been hillshade, which divides the slope into varying levels of elevation, similar to a contour map, but with elevation ranges defined by colour rather than discrete contours. Another output format is slope angle, which produces a colour image where the varying intensities of colour represent changes in slope. Figure 5.20 demonstrates the IDW raster conversion of the DEM into slope angle. The slope angles at and above apex of the measured rockfall trajectory range from approximately 45° to 75°.

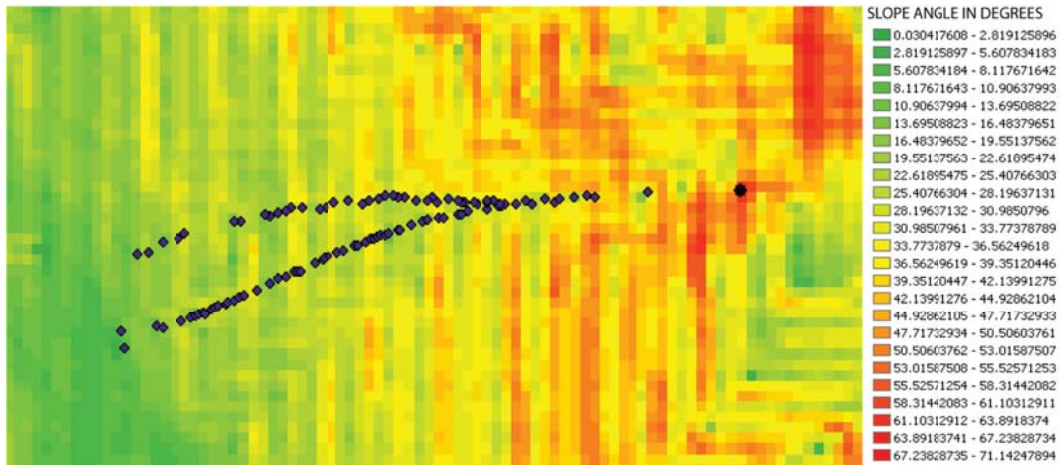


Figure 5.20: Raster Image of Slope Angles for Tornado Mountain DEM

The assumptions for this calibration are (1) the rock will be released from a vertical cliff, (2) the rock will impact nothing until it reaches the slope at the determined height and angle, and (3) no additional energy will be lost in the rockfall travel to the seeder point. With these assumptions, the energy of the rock will be maximized at the point where the seeder is placed, but is also subject to reasonable physical behaviour. Two of the assumptions are based on the observed topography of the rockfall source, and it is the topography that should determine what behaviour is reasonable. For the calibration, the input parameters of Table 5.1 apply. See Figure 5.21 for the visual model of the assumptions.

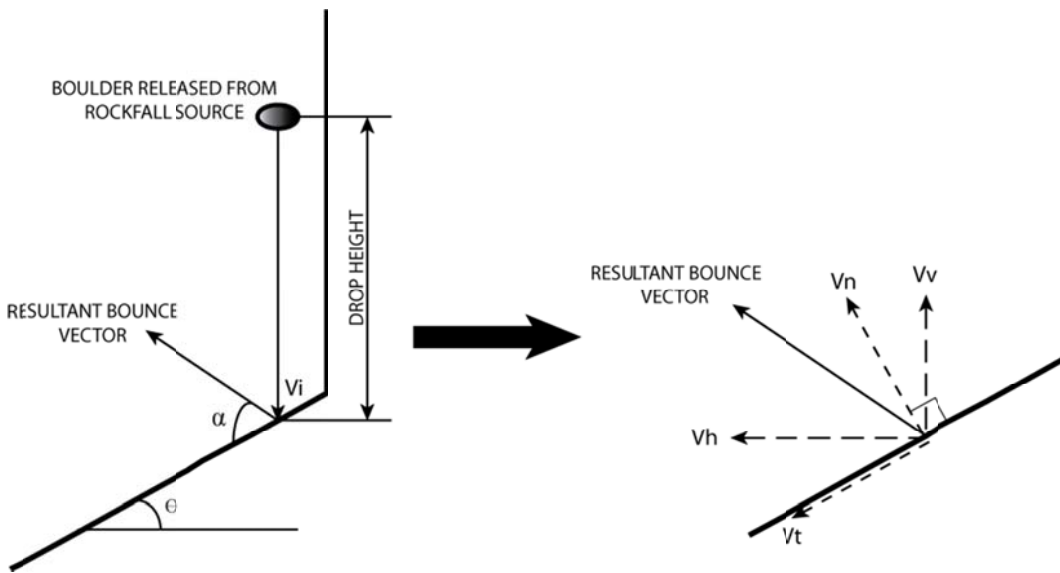


Figure 5.21: Rockfall Energy Calibration Visual Model

Initial velocity, defined here as v_i , is calculated based on the assumed height above the slope from which the rock initially falls. The resulting velocities after impact are arranged based on normal, tangential, horizontal, and vertical, respectively shown as v_n ,

v_t , v_h , and v_v . The slope angle is defined as Θ . To determine normal and tangential velocity, there are the equations:

$$v_n = v_i \cdot \cos(\Theta) \cdot R_n \quad (5.1)$$

$$v_t = v_i \cdot \sin(\Theta) \cdot R_t \quad (5.2)$$

Horizontal and vertical velocity can be determined using vector geometry conversions from the normal and tangential velocities. The horizontal and vertical velocities are used as parameters for the rockfall seeder. Tables 5.2 – 5.5 show the calculated velocities for input from the different assumed drop heights and slope angles.

Table 5.2: Rockfall Seeder Calibration Input Velocities with $\Theta=45^\circ$

Drop Height	v_n	v_t	v_h	v_v	α
10	3.12	7.06	7.20	-2.79	-21°
20	4.41	9.98	10.18	-3.94	
30	5.40	12.22	12.46	-4.82	
40	6.24	14.11	14.40	-5.56	
50	6.97	15.77	16.08	-6.22	
60	7.64	17.27	17.61	-6.81	
70	8.25	18.66	19.03	-7.36	-21°

Table 5.3: Rockfall Seeder Calibration Input Velocities with $\Theta=55^\circ$

Drop Height	v_n	v_t	v_h	v_v	α
10	2.53	8.17	6.76	-5.24	-38°
20	3.58	11.55	9.56	-7.42	
30	4.38	14.15	11.70	-9.08	
40	5.06	16.34	13.52	-10.48	
50	5.66	18.27	15.12	-11.72	
60	6.20	20.01	16.56	-12.84	
70	6.70	21.61	17.88	-13.86	-38°

Table 5.4: Rockfall Seeder Calibration Input Velocities with $\Theta=65^\circ$

Drop Height	v_n	v_t	v_h	v_v	α
10	1.86	9.04	5.51	-7.41	-53°
20	2.64	12.78	7.79	-10.47	
30	3.23	15.66	9.54	-12.83	
40	3.73	18.08	11.02	-14.81	
50	4.17	20.21	12.32	-16.55	
60	4.57	22.14	13.50	-18.13	
70	4.93	23.91	14.57	-19.59	-53°

Table 5.5: Rockfall Seeder Calibration Input Velocities with $\Theta=75^\circ$

Drop Height	v_n	v_t	v_h	v_v	α
10	1.14	9.63	3.59	-9.01	-68°
20	1.62	13.62	5.09	-12.74	
30	1.98	16.69	6.23	-15.61	
40	2.28	19.27	7.19	-18.02	
50	2.55	21.54	8.04	-20.15	
60	2.80	23.60	8.81	-22.07	
70	3.02	25.49	9.51	-23.84	-68°

The additional column of data in the tables, α , is the angle of the resultant vector after impact. If this angle was equal to Θ , then the boulder would be rolling rather than bouncing.

One additional parameter is needed to define the starting energy for the rockfall simulation. Drop height has been considered in this calibration as a means to determine the velocities of the rockfall, but this is not the drop height input parameter. The drop height input parameter is the offset in elevation over the specific point where the seeder is placed. Considering drop height for a rockfall exhibiting a parabolic trajectory is reasonable as long as the seeder is not placed directly over an impact point where there would be no offset height. The simulations run in this study assumed an offset height, and therefore the seeder point was placed at a point approximately 15m upslope from the final point. In addition, this point was chosen for the dip direction of the slope that affects the starting trajectory of the rockfall simulations.

Simulations were run with the assumptions and inputs determined for the rockfall energy calibration. The entire set of results can be seen in Appendix C.3. Figures 5.22, 5.23, and 5.24 show the most promising rockfall trajectories in comparison to the measured points.



Figure 5.22: Rockfall Energy Calibration Simulation: Angle 45° Drop Height 60m



Figure 5.23: Rockfall Energy Calibration Simulation: Angle 55° Drop Height 70m



Figure 5.24: Rockfall Energy Calibration Simulation: Angle 65° Drop Height 70m

It is apparent that the rockfall simulations do not demonstrate movement along both recorded rockfall trajectories. The simulations do, however, show agreement along the orange-flagged trajectory. These results are acceptable for calibrating the energy input parameters and model since reasonable agreement with repeatable results can be achieved. With the energy parameters set, there is a chance for further analysis on the effect of COR on the rockfall trajectory.

5.2.3. COR Analysis

The travel of a rockfall down a slope is determined by the geometry of the slope, the geometry of the rock, the characteristics of the slope, and the characteristics of the rock. RA considers the rock as a “lumped mass” to remove the consideration of the rock’s characteristics from the closed-form equations (Lan et al 2007, p265), with the exceptions of the starting energy of the rock. With all of the additional calculations for three dimensional analysis, as well as the uncertainty in the rock’s shape and features from a natural rockfall as it progresses from the source to its final resting position, the lumped mass approach retains an efficiency in rockfall calculation. The DEM defines the slope geometry, so only the characteristics need be defined. Slope friction and the coefficients

of restitution (COR) are the two characteristics for maintaining rockfall energy that RA considers. The CORs determine how much energy a rock retains mathematically after each impact. Any simulation that calculates multiple bounce points may demonstrate significant error for incorrect values assigned to these coefficients. To this point, tests of the COR have been empirical or lab based. This rockfall simulation comparison within RA to a natural rockfall trajectory provides an opportunity to verify those results, to determine the importance of COR to rockfall simulations, and even to determine which factor governs the movement of rocks down slope.

The calibrations in Section 5.2 were chosen to obtain a reasonable starting energy for the rockfall simulation. To determine if the values of COR are also reasonable in the RA simulations, the COR must be reset to typical values for the vegetative cover. Typical COR values for vegetative cover are $R_n = 0.3$ and $R_t = 0.8$. These values fall within the ranges provided in the RocScience table (Table A.3), and are consistent with the values given by Richards et al (2001). The tests were run again with the angles and drop heights determined in the initial simulations. The angles chosen were 45° , 55° , and 65° , and the drop heights for each ranged from 50m to 70m. The results for the 55° and 65° angles at the 70m drop height are given in Figures 5.25 and 5.26. These results were consistent with observed trajectory. All additional simulations, based on the energy assumptions from Tables 5.2 to 5.5, are to be found in Appendix C.3.



Figure 5.25: Typical COR Value Simulation (55° Slope Angle and 70m Drop Height)



Figure 5.26: Typical COR Value Simulation (65° Slope Angle and 70m Drop Height)

All of the results are consistent with the drop paths noted in previous simulations. The major difference between the simulations is that the rocks in the simulation with typical COR values do not progress as far down the slope. As noted in Section 2.5, there is thought that the values for COR are conservative, but the observations in these simulations do not necessarily support that claim.

The blue highlighted lines in Figures 5.25 and 5.26 represent the rockfall trajectories with the greatest travel distance. These trajectories can be viewed as 2-dimensional profiles along with the cross-sectional slope of the DEM. Figures 5.27 and 5.28 are the 2-dimensional rockfall profiles compared to the measured impact points from the RTK GPS survey.

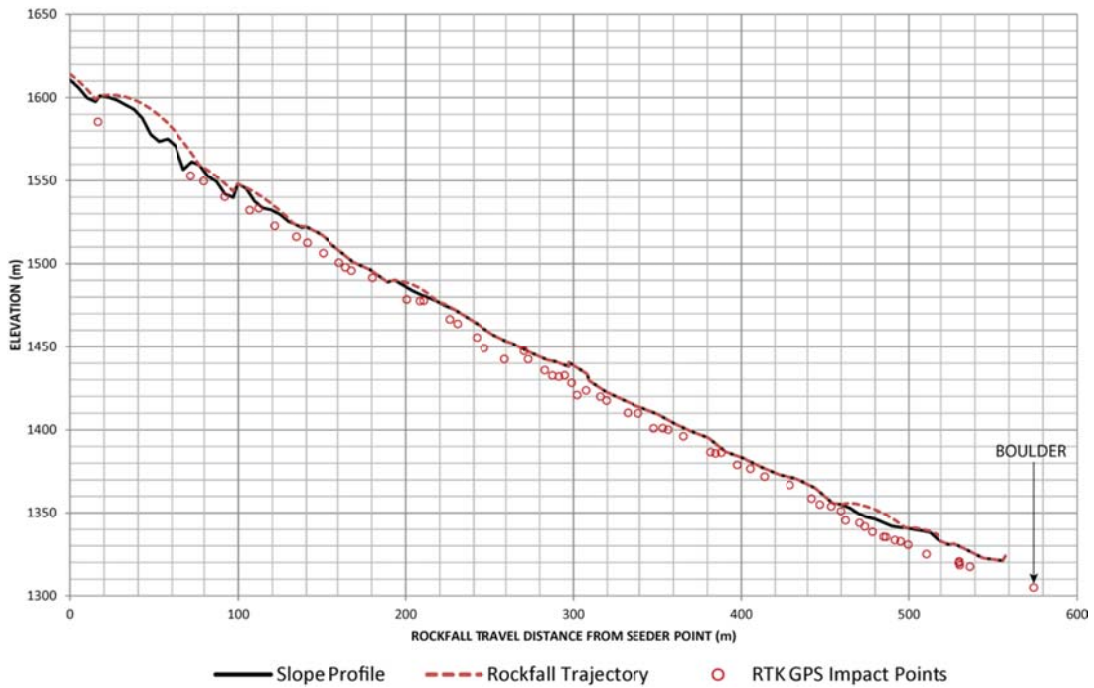


Figure 5.27: 2-Dimensional Rockfall Simulation Profile and RTK GPS Impact Point Comparison (Typical COR: $R_n=0.3$ $R_t=0.8$; Slope Angle 55° ; Drop Height 70m)

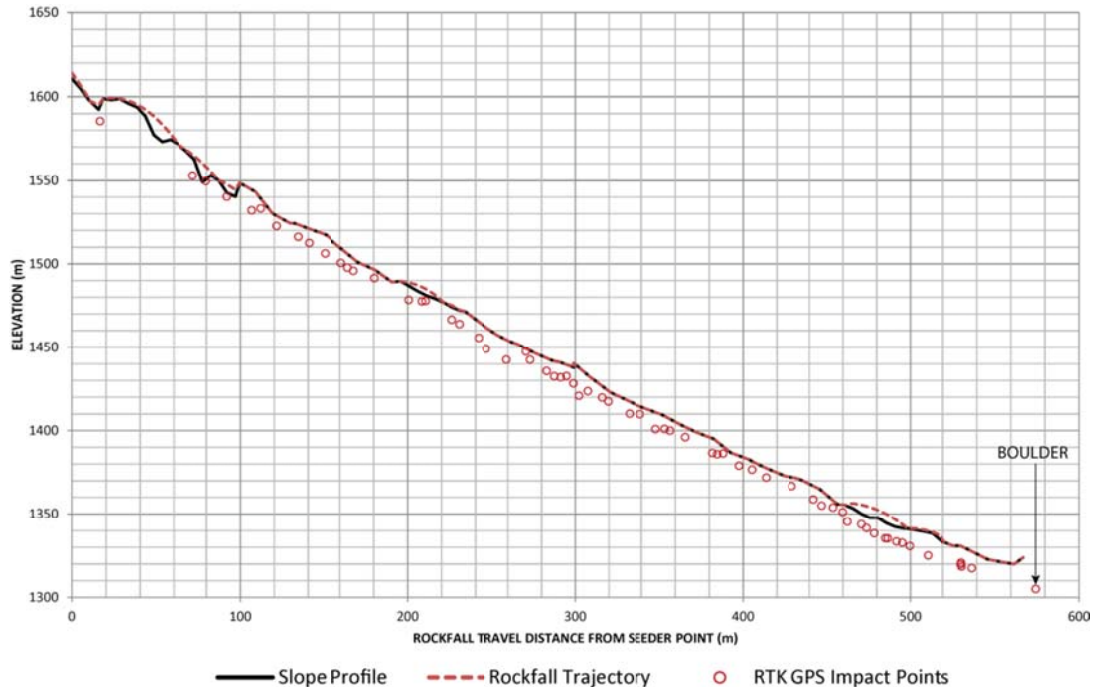


Figure 5.28: 2-Dimensional Rockfall Simulation Profile and RTK GPS Impact Point Comparison (Typical COR: $R_n=0.3$ $R_t=0.8$; Slope Angle 65° ; Drop Height 70m)

Two observations from the profile comparisons: (1) the RTK GPS impact points are consistently lower than the slope profile, and (2) the rockfall trajectory seems to be exhibiting rolling/sliding behaviour rather than bouncing behaviour. The surveyed points do not coincide directly with either trajectory, so the fact that they do not align perfectly with the elevation is not unreasonable. Another reason for the discrepancy is that the RTK GPS points were measured within impact craters. Finally, the Geobase data did demonstrate higher elevations, and therefore the common trend for the interpolated DEM would have slightly higher elevations. The comparison should be with the points of impact, which do not necessitate equal elevation. However, the simulated trajectories are showing more rolling/sliding behaviour than bouncing. This may be because the scale is too large to note smaller bounce profiles, the threshold for frictional model behaviour within RA is too high, and/or the topographic accuracy of the DEM is too smooth, leading to less launching in the rockfall trajectory.

At this point the values of COR have been tested at above normal and typical values. A sensitivity analysis would assist in verifying these results, as well as in determining the effect COR has on rockfall movement. To determine the sensitivity of COR within the simulation, lower COR values can be input. Reducing both the tangential and normal COR first provides a baseline, and then reducing only the normal/tangential properties respectively gives the individual sensitivity of the values. Lowering the COR values by two sets of variance provides a distinction for the analysis from which observations can be made. The selected values and their test orders can be seen in Table 5.6.

Table 5.6: Values of COR for Sensitivity Analysis

COR	Rn	Rt
Typical Values	0.3	0.8
Reduced Values	0.27	0.77
Reduced Rn – Typical Rt	0.27	0.8
Typical Rn – Reduced Rt	0.3	0.77
Greatly Reduced Values	0.15	0.5
Greatly Reduced Rn – Typical Rt	0.15	0.8
Typical Rn – Greatly Reduced Rt	0.3	0.5

Simulations were performed for each of the values of COR in Table 5.6. The initial energy input of these settings are the values used in Tables 5.2 to 5.5. All the plan views of the simulations run can be seen in Appendix C.3. Figures 5.29-5.40 show the simulations from the COR values in Table 5.6 with the slope angle and drop height demonstrating the most consistent results to the measured trajectory (the 55° and 65° slope angles at the 70m drop height).



Figure 5.29: Reduced COR Value Simulation (55° Slope Angle and 70m Drop Height)



Figure 5.30: Reduced COR Value Simulation (65° Slope Angle and 70m Drop Height)



Figure 5.31: Reduced Normal Typical Tangential COR Value Simulation (55° Slope Angle and 70m Drop Height)



Figure 5.32: Reduced Normal Typical Tangential COR Value Simulation (65° Slope Angle and 70m Drop Height)



Figure 5.33: Typical Normal Reduced Tangential COR Value Simulation (55° Slope Angle and 70m Drop Height)



Figure 5.34: Typical Normal Reduced Tangential COR Value Simulation (65° Slope Angle and 70m Drop Height)



Figure 5.35: Greatly Reduced COR Value Simulation (55° Slope Angle and 70m Drop Height)

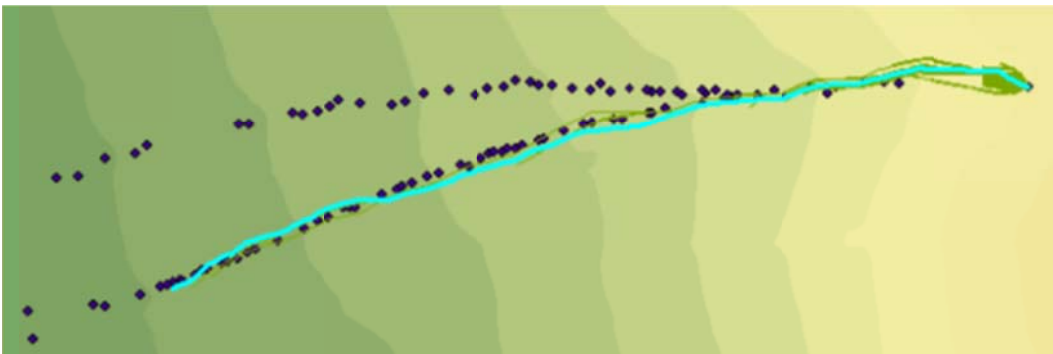


Figure 5.36: Greatly Reduced COR Value Simulation (65° Slope Angle and 70m Drop Height)



Figure 5.37: Greatly Reduced Normal Typical Tangential COR Value Simulation (55° Slope Angle and 70m Drop Height)



Figure 5.38: Greatly Reduced Normal Typical COR Value Simulation (65° Slope Angle and 70m Drop Height)



Figure 5.39: Typical Normal Greatly Reduced Tangential COR Value Simulation (55° Slope Angle and 70m Drop Height)



Figure 5.40: Typical Normal Greatly Reduced Tangential COR Value Simulation (65° Slope Angle and 70m Drop Height)

If the rockfall simulations are sensitive to changes in the COR values, then a slight drop in the COR value should result in a lower rockfall travel distance. This was noted to have occurred in the 55° slope angle simulations, as compared between Figures 5.25 and 5.29. However, there was no significant change in the travel distance in the 65° slope angle simulation, as compared between Figures 5.26 and 5.30. Simulations shown in Appendix C for the 65° slope angle show that there is no change throughout the various drop height when comparing the reduced and typical COR values. The 55° slope angle does show change between values of COR, though the results change based on drop height. Since drop height and slope angles are being used to define the initial velocities of the rockfall boulder at the seeder point, this may suggest that the rockfall energy is a greater concern than the varying COR. These observations may also suggest that there is a difference in the effect of the slope angle, which distributes the energy between the two COR vectors.

Since COR is divided into normal and tangential vectors that are considered separately in calculation, one of the coefficients may have more effect on the simulations than the other. When only the normal COR is reduced, there is still no change noted at the 65° slope angle, but the 55° slope angle does show a slightly different trajectory the progresses farther down the slope (see Figure 5.30). When only the tangential COR is reduced, there are a greater number of rockfalls that progress further downslope near the seeder in the 55° simulation, and one rockfall progresses as far as in the typical COR simulations (see Figure 5.33). The 65° slope angle still exhibits no change. If slope angle is the key concern here, then a lower slope angle would likely exhibit more normal COR to tangential COR. This would appear a reasonable assumption since the 55° slope angle exhibits more travel when the normal COR is greater, and the effects of the tangential COR are lowered.

The greatly reduced COR value simulations (Figures 5.35 and 5.36) exhibit more of the expected behaviour to the rockfall travel distance (i.e. they shorten the maximum travel distance). The actual difference noted in the rockfall travel distance is between 25m-50m, depending on the starting energy. Comparison of the results within the additional tests (seen in Appendix C.3) shows that this trend is consistent. However, looking at the 45° slope angle simulations in Appendix C.3, there is little difference noted in the

trajectories or final rockfall travel distance between the typical and greatly reduced COR values. Starting rockfall energy, and the direction of this energy, seems to have a greater, more consistent effect on the rockfall simulations than the changes presented by the COR. This also does not discount the observation of the effect of the starting slope angle.

In the reduced normal COR value simulation there was not a significant change in the rockfall travel distance within the 65° slope angle rockfall energy scenario. With the greatly reduced normal COR value, the 65° angle scenario demonstrates the same drop in travel distance as noted when both COR values were changed (see Figure 5.38). The 55° scenario was less affected by the change, nearly matching the 65° scenario (see Figure 5.37). When the tangential COR value was greatly reduced, no changes in rockfall travel distance were noted compared to reducing both COR values with either of the chosen slope angles. The results in Appendix C.3 show that the different drop height simulations demonstrate a greater change in the rockfall travel distance with the COR values at this level of reduction. The exception to this is the 45° scenarios, which still remain mostly unchanged regardless of COR or drop height.

All the simulations involving the 55° and 65° slope angles at the 70m drop height only exhibited a decrease of 25m-50m in rockfall travel distance. When determining if the boulders will cross the tracks, this is quite a large distance. However, the total travel distance of the boulders over 600m. 50m is less than a tenth of the total travel distance in either of these two rockfall events. The tests in COR may not suggest that the values are conservative, but this distance is small enough to suggest a potential hazard to the railway.

These conclusions are qualitative; based on the differences shown within the simulations for the varying COR values, concentrating specifically on the 55° and 65° slope angle with the 70m drop height. Figures in Appendix C.3 show that there is more consistent activity for the rockfall trajectories within the 45° slope angle, and that distances can be quite variable even at lower heights and angles. To present a quantitative view of the sensitivity of the model to the COR value, the actual rockfall travel distances for each simulated rock can be investigated and compared. Each of the conducted simulations contained 100 rockfall trajectories, with varying maximum rockfall travel distances, median rockfall travel distances, and distribution of rockfalls. Figures 5.41 and 5.42 show the median and maximum rockfall travel distances, respectively, vs. varying drop height. Figures 5.43 and 5.44 show the median and maximum rockfall travel distances with respect to the assumed slope angle at the rockfall source. In all of these figures, the lines represent a point corresponding to the other variable (i.e. either the drop height, or the slope angle). The same data can be seen in Appendix C.3 for each drop height and slope angle specifically.

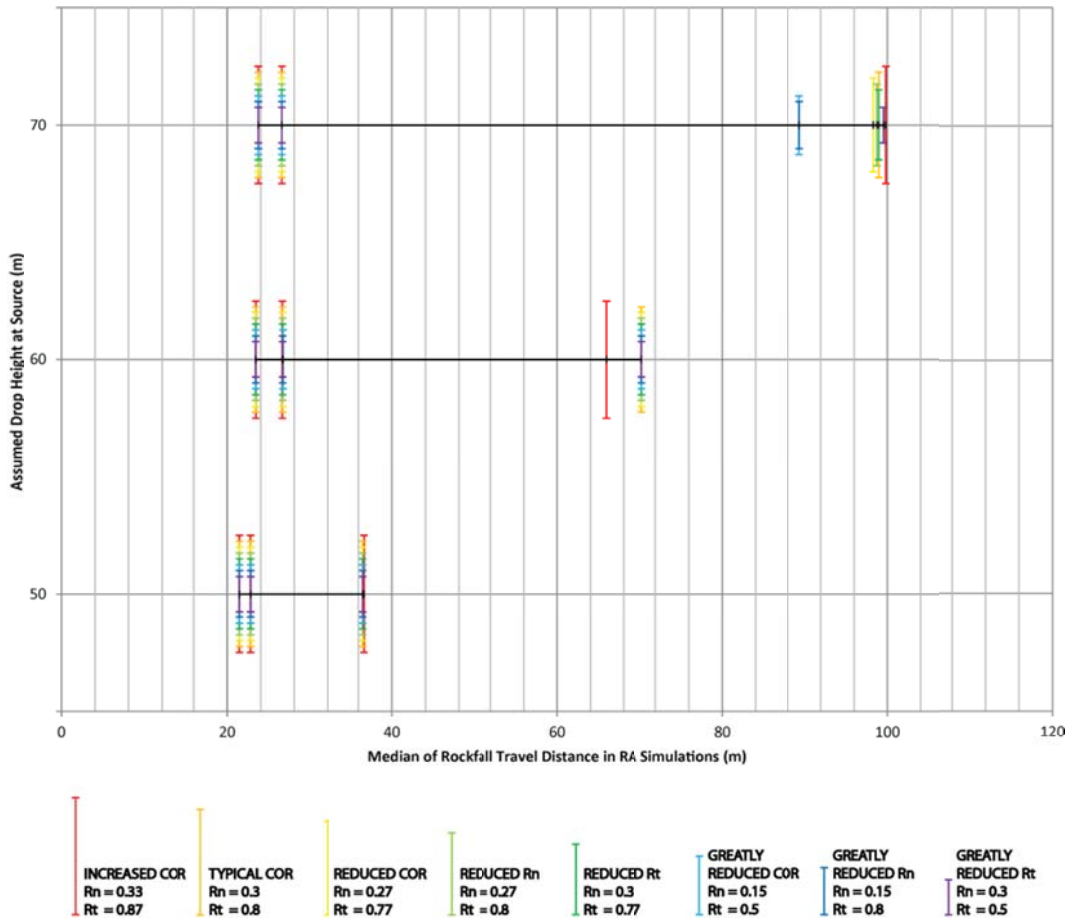


Figure 5.41: Median Rockfall Travel Distance in RA vs. the Assumed Drop Height at Source

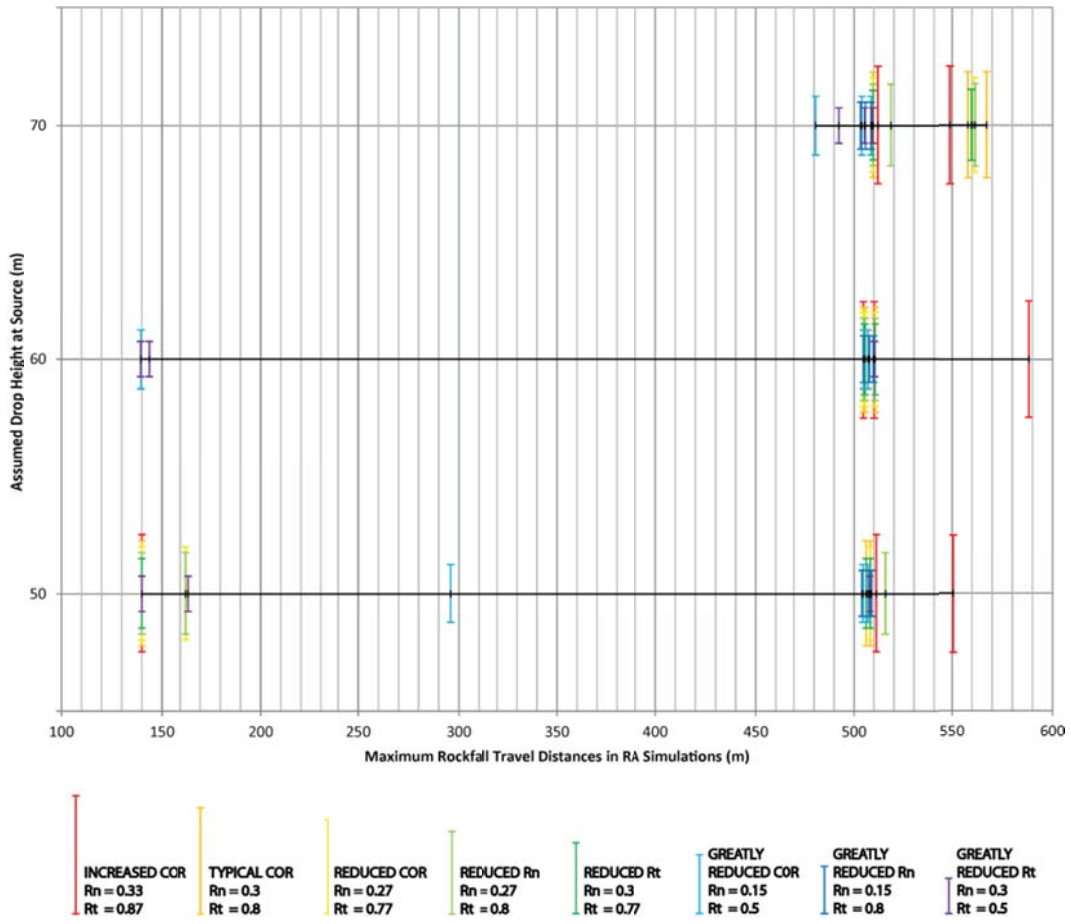


Figure 5.42: Maximum Rockfall Travel Distance in RA vs. the Assumed Drop Height at Source

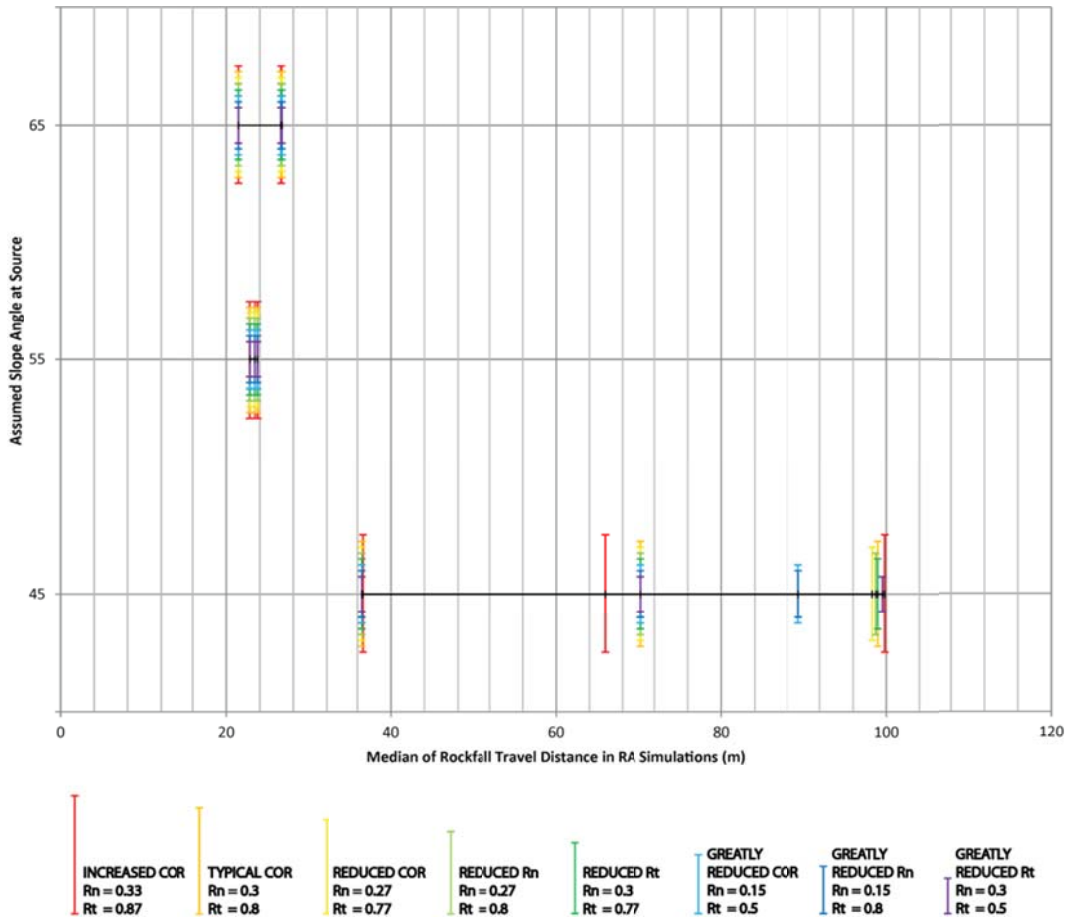


Figure 5.43: Median Rockfall Travel Distance in RA vs. the Assumed Slope Angle at Source

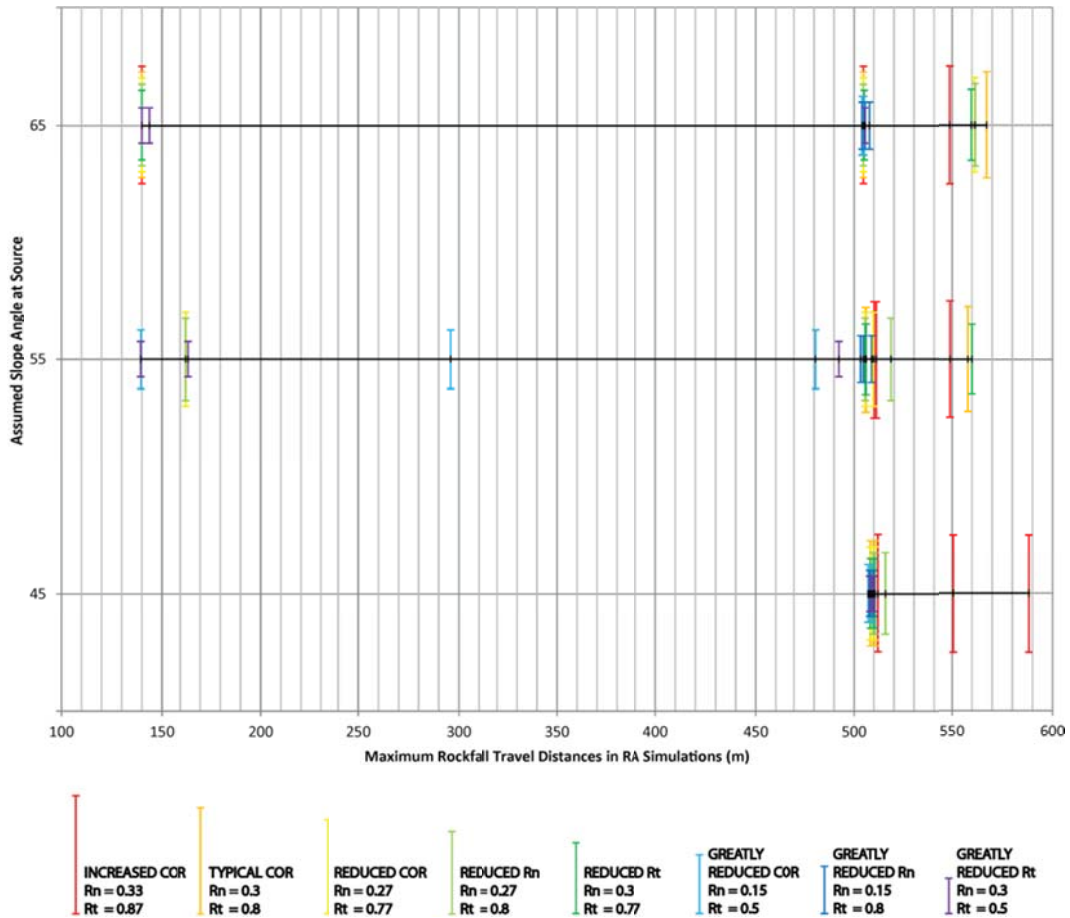


Figure 5.44: Maximum Rockfall Travel Distance in RA vs. the Assumed Slope Angle at Source

The difference in median rockfall travel distance is not overly pronounced when changing the COR. Both the change in drop height and slope angle at the source result in varying distribution patterns, but the COR values have little effect. This suggests that the rockfall distribution is less affected by the changing COR, and more affected by the source conditions and topography. The maximum distance rockfall figures show a greater spread due to the COR values, but, with some exceptions, the spread is within meters rather than hundreds of meters. The values that do demonstrate a greater deviation for the 500m plus travel distance are varied between all the values of COR chosen. Figure 5.45 demonstrates both the observations for the median and maximum cases purely based on travel distance and COR (see also Table 5.7).

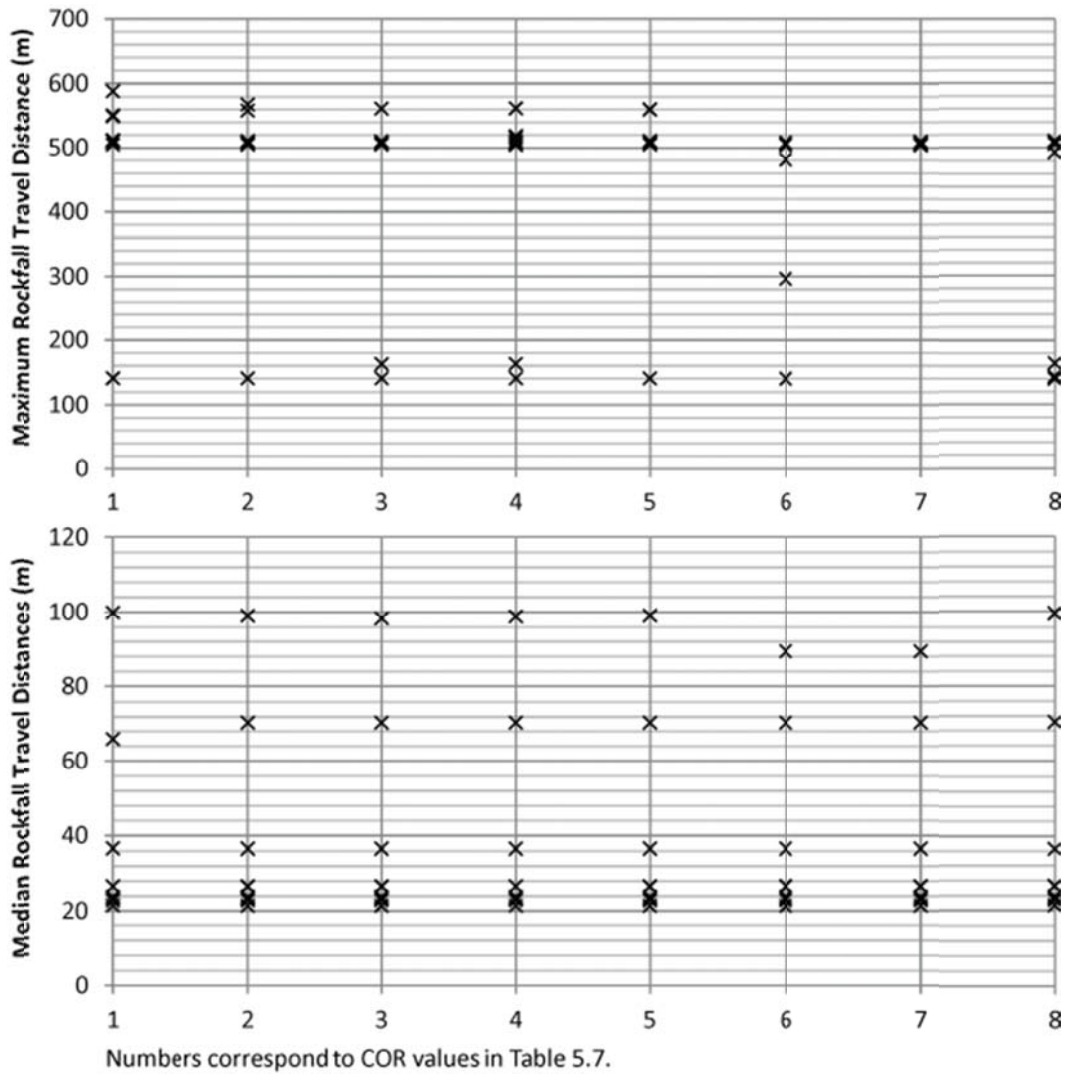


Figure 5.45: Maximum and Median Rockfall Travel Distance by COR Value

Table 5.7: COR Values for RA Simulations

#	COR	Rn	Rt
1	Increased	0.33	0.87
2	Typical	0.3	0.8
3	Reduced	0.27	0.77
4	Reduced Rn	0.27	0.8
5	Reduced Rt	0.3	0.77
6	Greatly Reduced	0.15	0.5
7	Greatly Reduced Rn	0.15	0.8
8	Greatly Reduced Rt	0.3	0.8

The maximum rockfall travel distances are consistent at two values: (1) ~500m, and (2) ~140m. Most of the rockfall activity falls within these zones regardless of COR. It should be noted that as COR values lower, the greatest maximum values do show a consistent decrease. This suggests that COR does have some effect, but not to the extent

previously expected. The median values are very consistent across the COR values. Table 5.46 shows the same data separated by test number rather than COR value.

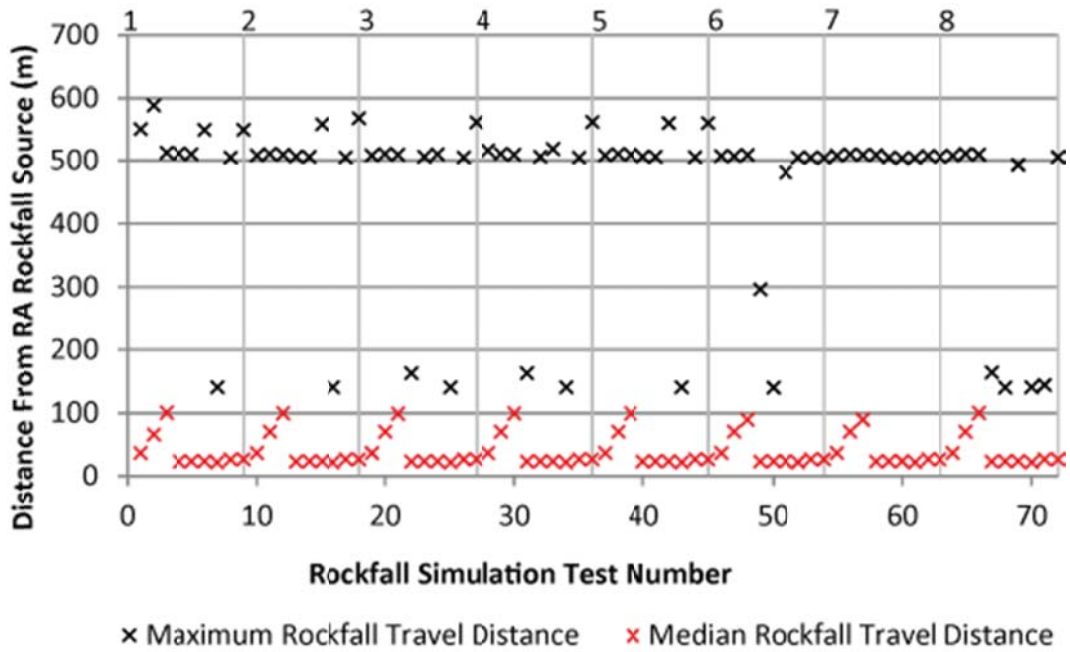


Figure 5.46: Maximum and Median Rockfall Travel Distance by Test Number

As in the previous figure, the results are consistent along the same values of ~140m and ~500m. However, by separating the individual tests, it becomes apparent in the median samples that there is a pattern being followed as the source energy parameters are changed. The pattern is consistent regardless of the COR, and therefore it is the energy and topography that dominates the movement in rockfalls.

The 140m and 500m marks on the rockfall trajectory should demonstrate some topographic consistency that slows rockfall movement. Noting Figures 5.27 and 5.28, at the 140m mark there are small areas of slightly shallower slope, and at the 500m mark, the same, but more pronounced than at the 140m mark. However, this only demonstrates a two dimensional thought process, and if these slope variations are truly so critical, then there should be other points exhibiting similar behaviour. In this regard, the three dimensional profile should be noted. The rockfall trajectory is not a straight line, as the two dimensional profile suggests, but is curved. This means that there is a slope feature that rocks must consistently curve around to pass while following the rockfall trajectory. This 140m mark is located approximately where the two rockfall trajectories diverge and the orange path starts to curve. Observations on site at this area noted a large amount of deposited rockfall material. There is no similar curvature at the 500m mark, but the amount of energy lost in the total rockfall trajectory, combined with a shallower slope section in this area, could account for simulations predicting a stopping point.

The cumulative distribution of the rockfalls for the typical COR can be seen in Figure 5.47. All of the distributions follow similar curves, which is consistent with the results in the figures above. The additional cumulative distribution curves can be seen in Appendix C.3.

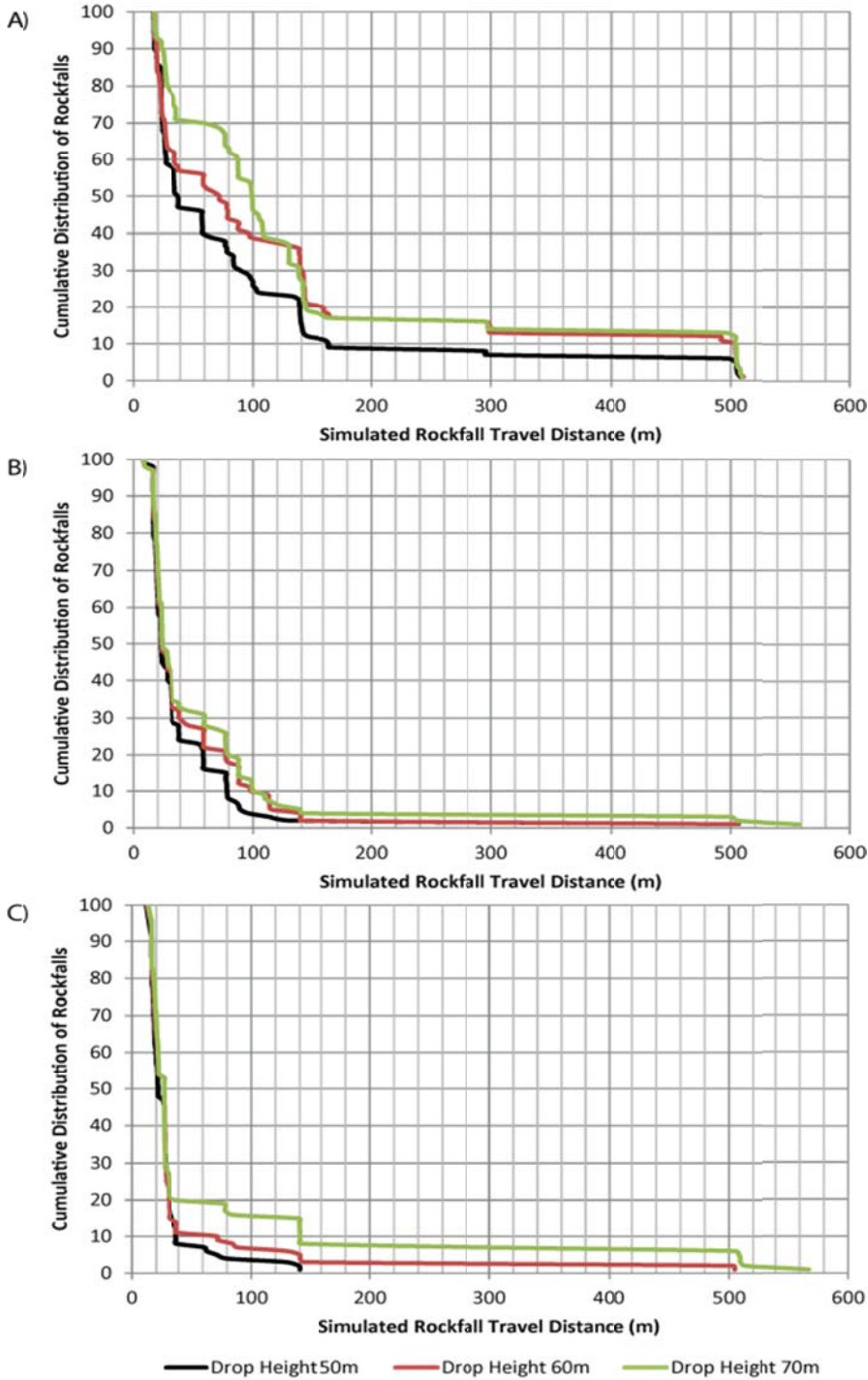


Figure 5.47: Cumulative Distribution of Typical COR Rockfalls for A) 45° Slope Angle, B) 55° Slope Angle, and C) 65° Slope Angle

There was some discussion previously regarding the effect of slope angle on rockfall travel and/or the comparative value of the normal and tangential COR. The rockfall distributions demonstrate that higher slope angles result in a greater number of rocks progressing shorter distances down slope. Observing Tables 5.2-5.5 in Section 5.2.2, it can be noted that the ration of horizontal velocities to vertical velocities decreases with each slope angle increase. This means that higher slope angles translate more motion into the tangential and vertical vectors, which results in smaller distances between initial impact points, and a greater amount of surface contact with the rock. Energy dissipation will rise with each moment of surface contact. Therefore the rocks at higher slope angles are dissipating their energy faster, which is why fewer travel as far down slope. This would be an example of how slope geometry determines rockfall behaviour while noting that the slope characteristics (COR and friction) determine the rate of energy loss due to that behaviour.

As an additional note, there was the possibility of defining the COR by constraining it between the points noted within the RTK GPS. This may have provided a more accurate COR for the site, which could have further been used to determine what is truly exhibited in a natural rockfall event versus what we see within lab experiments and empirical studies. However, it was found that the number of variables required to define the equation were greater than what could be defined on site; the most important of these variables being the starting energy properties for the rockfall analysis. Additionally, the each pair of impact points requires separate consideration for energy and rock movement behaviour (i.e. rolling or bouncing). This method of determination was deemed to be impractical with the given information.

5.2.4. Sensitivity of Analysis to Change in Friction

Rockfall simulations in RA use three variables to calibrate the slope properties. These three variables have been noted as the Normal COR, R_n , the Tangential COR, R_t , and the slope friction. For all of the previous analyses, the slope friction has been taken at 20° , which is likely greater than what is actually true for the friction of the slope on Tornado Mountain. As bounds for the analysis, a friction angle of 20° works well; however, the effect of friction should be noted as when the rock is not bouncing, it will enter into frictional calculation models.

The increased COR analysis with 45° slope angle and 60m drop height demonstrated the furthest rockfall travel distance of 588.2m (See Table C.3, Appendix C.3). By increasing and decreasing the slope friction an increment of 5° , this particular simulation can be used to demonstrate the effect of friction on the simulation. Figure 5.48 shows the rockfall trajectories based on the changing angle of friction.

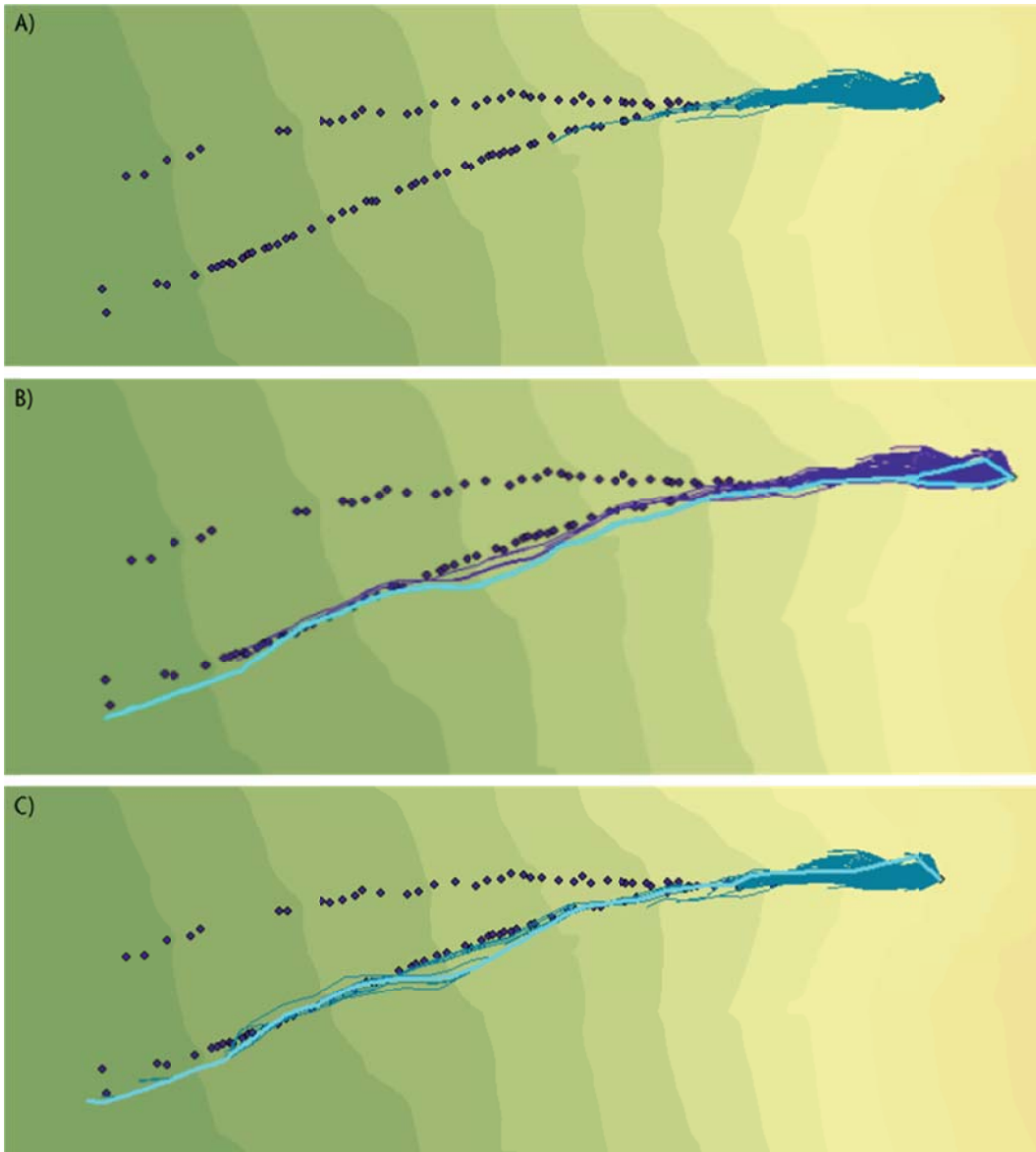


Figure 5.48: Rockfall Simulation Friction Sensitivity Test with Increased COR for 45° Slope Angle, 60m Drop Height, and Friction of A) 25°, B) 20°, and C) 15°

The maximum length for the 25° friction scenario is 272.7m, while the maximum length for the 15° friction scenario is 606.8m. While it is unlikely that the slope will exhibit a 25° friction angle, the change due to both increasing and decreasing the friction does follow the expected behaviour. When increasing friction, the travel length decreases, and when decreasing friction, travel length increases. Additionally, it is apparent that there are more rocks traveling further when friction is lowered. This is shown well in a cumulative distribution curve seen in Figure 5.49.

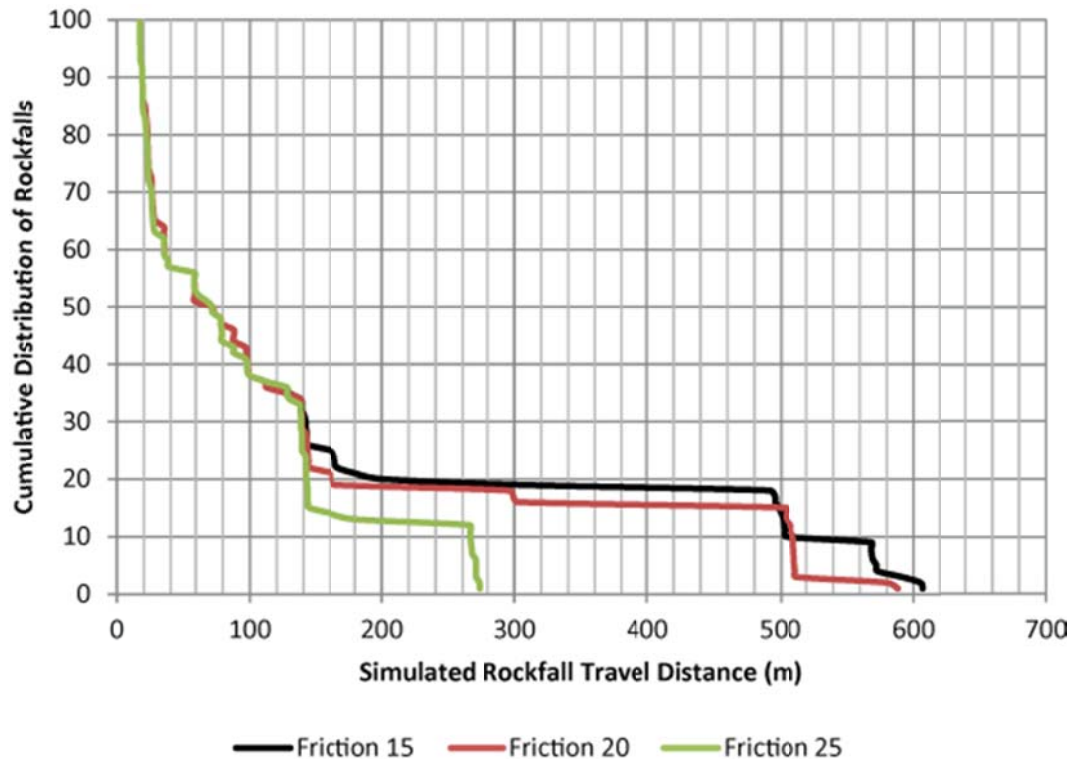


Figure 5.49: Cumulative Distribution Curve of Rockfall Travel Distance for Friction Angle of Slope

The curves are nearly identical for the majority of the simulated rockfall. However, at the point when 30% of the rocks are passing the 140m mark, the curves start to change. The curves also show similarities at the 500m mark. These two points were noted previously as being significant in the COR analysis. Up to the point of 140m, the rockfall behaviour consistent, but at that point, a large number of rocks are being caught. This is the same observation made previously where these points likely correspond to an area where an energy change is exhibited. The previous suggestion was that a topographic feature was responsible for this behaviour, with the curve in the three-dimensional profile and on site observation of rockfall distribution corroborating this assumption. Since the behaviour is comparable between the bouncing/skipping model that COR defines and the the rolling/sliding model that friction defines, the slope geometry must be the determining variable.

In conclusion, it is clear that friction does have an effect on the model, and it seems more pronounced than the effect of COR. The effect of friction is as would be expected, with greater rockfall travel distance for lower friction values, and decreased travel distance for higher values. Observations of the 140m and 500m marks, which were noted previously, suggest that there are other features that affect the rockfall simulations that exhibit greater effect regardless of the changing values of COR and friction.

5.2.5. Effect of Trees on RA and COR

COR tables, such as the RocScience Table (See Table A.1, Appendix A), include values that account for vegetated slopes. However, COR is meant to be useful when measuring the energy lost on impact with the ground surface. This means that COR should only account for vegetation that coincides with the point of impact. Any contact with vegetation during the periods of projectile motion is not related to COR. In Section 2.6, a paper and thesis by Dr. Martin Jonsson discussed the effect of trees in absorbing energy from rockfalls. His studies were directly related to boulders impacting against trees in mid-air rather than impacting the ground surface. There is some concern as to how the values of COR would change if the mid-air impact points could be accounted for in rockfall analyses.

There were numerous broken trees noted on site in the RTK GPS survey of Tornado Mountain. It is clear that rocks impacted against them, directly or only glancing, during rockfall events (see Figures 5.50 and 5.51).



Figure 5.50: Smashed and Scarred Trees (photo by Renato Macciotta)



Figure 5.51: Fallen Trees Along Rockfall Path (photo by Renato Macciotta)

Given that boulders were impacting against trees in the region, it is reasonable to assume that there was energy lost in each impact separate from that lost on the ground in the COR. RA does not have the means to account for this separate source of energy loss. COR for a vegetated slope would therefore be assumed to include all sources of energy loss up to, and including, the point of impact. An issue arising from this assumption is that different varieties of vegetation (specifically trees) will affect the energy loss of a rockfall event. The species and age of a tree affect trunk/branch size as well as its material properties. Therefore each slope would have a unique COR just to account for the trees. Additionally, the population density of the trees has an effect on how often a rockfall will experience mid-air impacts. It is also possible that a vegetated slope will have no trees, only ground based vegetation. A general COR value for a vegetated slope is fine so long as the value remains consistent regardless of the changing vegetation.

It could be possible to account for trees within an analysis program like RA. There are two possible ways to go about accounting for trees: (1) include the treed area as an

additional material zone through which rocks have to travel, similar to a frictional model, and/or (2) populate the area with tree like obstacles that have properties reflecting the actual trees on site. It would not be required to know the exact tree locations from site for either of these models, though the second could if it were possible to map out the exact location of the trees. If the trees could be mapped out exactly, then this would also improve the trajectory modelling of the analysis program. Accounting for trajectory change due to impacts against trees is currently not effective for a slope of this size in RA.

Accounting for the trees in some way would allow the COR to be kept separate within RA for calculations. It would also be a means of noting the different bounce patterns that become associated with impact. Trees can also have a significant effect based on the rock size. A large mass impacting the tree is likely to cause significant damage with perhaps minor change in direction, while a smaller rock may stop entirely, embed itself, or experience drastic trajectory change. The mass of the tree and its root bulb should also be considered when a rock impacts. Larger trees, or trees with stronger root systems, will be affected differently by the rock impacts (Jonsson et al 2007, p359). All of these concerns would require a detailed understanding of the trees in the area, which additionally would need to be updated as trees are living organisms. As stated previously, considering them as individual obstacles is impractical for RA.

The first model approach is reasonable, with tree population density, species, and growth taken into account as the material properties. While it would not reflect changes in trajectory, the effect of energy loss that is probable to experience along a given distance could be quantified. The only additional requirement on site would be to determine the average distance between the trees, the average trunk size (as is suggested within Jonsson's research), and the species of tree most prevalent. The species is particularly important because that determines the tree's material properties, and likely size of the root bulb. Assuming that this data could be collated into a reasonable series of numbers and input into the analysis program, then the trees could be considered separate from the COR.

Further study could be conducted if the results obtained by Perret (2004) could be converted to a 3-dimensional model simulation. In Perret's study, rocks dropped in a 2-dimensional modelling program showed comparable results to those of rocks dropped in various "types" of forested slopes. It was proven that rocks dropped in the forested slopes showed reduced velocity and energy when compared to those that had not encountered trees along the slope path. If a similar model could be applied to both the trajectory and frictional model in RA, then it is possible that the COR could be defined with greater independence from the vegetation.

Taking COR into account separately from vegetation is not currently possible within RA. However, the agreement shown between the measured trajectory and the trajectory of the rockfall simulations suggests that the values chosen for COR are reasonable. In future

studies, consideration should still be given for the vegetated slope COR value as it may vary due to differing vegetation on the slope. When vegetation becomes possible to consider as a separate variable, the values for COR will need to be reanalyzed.

5.3. Summary of Three Dimensional Rockfall Analyses

Predictive rockfall programs, such as RA, are useful when they give reasonable rockfall hazard predictions. It is unlikely that the inputs into the program will match observed conditions on site, but the model needs to be as accurate as possible. With a good model a predictive program like RA will output a rockfall solution that can be viewed in both 2D and 3D as required, as was demonstrated in this section. Each of the figures in this section, and those in Appendix C, have the RTK GPS survey points overlaid on the DEM. In addition to the rockfall path noted in the figures, there were observations made on site as to where additional rocks were located along the slope (Appendix C.1). The distribution of the rockfalls within the RA program matches the on-site observations to where the majority of the rockfall material was being distributed. Also, while the surveyed points were not followed directly, several of the trajectories are reasonable approximations both in path and overall travel distance. These correlations between the simulations, on-site observations, and measurements speak to the effectiveness of RA, and its potential use in future studies as a three dimensional rockfall analysis program.

The RTK GPS survey provided three dimensional locations of the rockfall boulder impact points for comparison with simulation technology. Two rockfall trajectories were measured and input into ArcGIS to be compared to a rockfall simulation. In order to run the simulation, several parameters need to be defined, such as the rockfall source location, the initial starting energy of the rockfall, and the slope characteristics, like the coefficients of restitution (COR). The values for COR are of interest since they have only been defined with empirical data and lab studies, and not with a natural rockfall event, but they cannot be studied without defining the starting parameters.

The rockfall source location was not clearly defined from the site survey, and this proved to be a challenge in producing repeatable results in the rockfall simulations. Even with an appropriate source location, the starting energy has quite an effect on the rockfall trajectories. To quantify the starting energy, there has to be reasonable physics involved. If a rock is released from a cliff, there will be some energy of release, but the bulk of energy is due to its drop height. Once the boulder impacts the slope, how will it behave? How the boulder bounces, rolls, or slides will depend on how much energy it retains from the drop, and will then determine how far the boulder is likely to travel down slope. Assumptions made on the physical processes are key in determining if the starting energy is reasonable, and these processes depend greatly on the topography of the area surrounding the rockfall source. With a rockfall source point and starting energy defined, then COR can be studied.

COR is the value that quantifies how much energy will be retained upon impact depending on the slope material. Since values for COR have been determined from empirical evidence and lab tests, there is some question as to how realistic or conservative they may be. With a measured rockfall trajectory to be compared to the simulated models, these values can be tested. The slope at Tornado Mountain was vegetated soft soil for the majority of the rockfall travel distance. Given the assumptions that the DEM adequately described the site, and that the starting energy was accurate, then the results suggest that the COR values given are reasonable. The simulated rockfalls followed the measured trajectory and observations made on site consistently, with travel distances near to those measured. Rather than suggesting the values of COR should be re-evaluated, it appears that they provide reasonable results.

This work depends on the accuracy of the model being used. The more accurate the model, the more likely it is that the simulation will produce usable results. Survey point data from the RTK GPS was input into the DEM data obtained from Geobase. This was done to ensure that there would be greater detail in the model, but it could also be said that it causes bias in the rockfall path. It was observed that the simulated rockfall trajectories did consistently follow one of the measured trajectories. However, if there was unreasonable bias in the model, then the rockfalls should have been observed to follow both trajectories. Also, the simulated rockfall trajectories should have exhibited less deviance around the path.

A comparison of the trajectories in profile to the impact points showed that the impacts measured consistently below the DEM slope surface. The data interpolation method (IDW) was chosen because it smoothed points into more of a slope trend, which this result demonstrates. While the point data from the RTK GPS does affect the model, it does not appear to bias it greatly.

The trajectory noted to have been followed in the simulations was the measured trajectory following the orange-flagged path from Mr. Duncan Wyllie's survey. The yellow-flagged trajectory was not travelled in the majority of the rockfall simulations. Simulations using the polyline seeders for the rockfall source did exhibit rockfalls that crossed, or travel nearer to the yellow-flagged trajectory. The rockfall simulations using the last GPS point as the seeder did not exhibit trajectories that followed the yellow-flagged trajectory. The rockfall source and starting energy play an important role in determining the rockfall trajectory. By removing some of the potential travel area, some of the potential changes in the rockfall trajectory are removed. While it was determined that the yellow and orange trajectories start at the same point coinciding with the last GPS point, it is possible that the trajectories did not both start from this point.

In a future analysis, based on the results of this study, the focus would be slightly different. Obtaining a comprehensive ground model from which to make the DEM would be ideal. If an aerial LiDAR survey of the area cannot be found or performed, then additional RTK GPS survey points around, but not inside, each of the impact points

should be obtained. An exact location of the rockfall source would be highly important, as well as more data on the location (i.e. photographs, LiDAR, topographic information, expert opinion, etc.). With the rockfall source better understood, the initial rockfall energy could be described. The most important information for performing a rockfall analysis seems to be the rockfall source and starting energy, then a more detailed ground model, and finally the slope parameters (such as COR). The actual given values for COR do appear to be reasonable, and the simulations appeared to be more sensitive to the factors affected by the topography of the slope.

6. CONCLUSION

Rockfall hazard assessments are carried out in three stages: (1) identification of hazard zones, (2) site investigation to establish the site characteristics and rockfall source, and (3) empirical and numerical analyses. In this thesis, terrestrial based LiDAR surveys were evaluated as part of the second stage, while RockFall Analyst (RA) was used in the third stage to evaluate the predictions provided by these analytical approaches compared with measured field data. To the author's knowledge, this is the first time such a comparison has been carried out for a rockfall on a natural slope.

6.1. Stationary Terrestrial LiDAR Surveys

LiDAR surveys are becoming increasingly popular for establishing 3-dimensional elevation models. This study evaluated the application of terrestrial based LiDAR for mapping rockfall slopes around rock cuts along highways in Southern Alberta.

Terrestrial LiDAR technology is line-of-sight, and therefore to capture the ground characteristics, the LiDAR must have a direct view of the ground surface to be defined. Each site provides unique challenges in this regard. For example, a highway that has no shoulders will provide little to no space within which to establish a useful LiDAR set up. The Crowsnest Lake Site investigated in this study is an example of site with limited space for set up, which required the use of the pan/tilt feature of the ILRIS-3D LiDAR station to fully capture the site. Elevation difference also plays a role in what can be easily captured, as was seen comparatively in the Highwood House and Fir Creek rock-cuts. Highwood House had a lower elevated shoulder to set up on that obscured the ditch, and necessitated the tilt function. The Fir Creek rock-cut had an elevated shoulder that allowed the ditch to be more easily defined, and the site captured in its full height without the use of the tilt function. The Old Man Dam also demonstrates this as the hazard area was easily captured in one set up of the ILRIS-3D at one advantageous location. Most of the sites conducted, however, required multiple station set ups, even with the pan function being used to define the entirety of the site. This was both because of the scope of the sites, and because each set up resulted in small areas of the slope remaining undefined due to their being shadowed by outcroppings or oblique angles in the line-of-site. The further upslope one is required to take measurements, the less reliable the LiDAR becomes for the same reason of oblique angles. Additional set ups at angles more appropriately located to capture these surfaces would be beneficial, but are not always feasible due to the natural constraints at the site (i.e. no safe, stable, and effective locations available). Additionally, outcroppings are not the only source that can cause shadows on the site surfaces. Vegetation was found to be a concern as well. It is possible to discount the first readings of vegetation, and only take the ground surface into account, but with the amount of detail being significantly decreased. On sites like the Spray Lake Gabion Wall, the trees obstructing the line-of-site leave a significant shadow over the slope surface. The point data on the vegetation can also obscure results by being

defined in the DEMs as sudden changes in elevation that do not necessarily represent the true geometry of the vegetation in question.

Number of set ups are dependent on two things: (1) the area of the site to be surveyed, and (2) the amount of detail required from the survey. If the site is large then it is likely that multiple set ups will be required. This is especially true when distance from the available set up space to the ground surface to be surveyed is small. Many of the sites investigated in this study required between 2 and 5 set ups to capture the site completely, with an average of 3. The pan/tilt feature of the ILRIS-3D greatly reduced the number of required set ups, or the number would have been much higher. Amount of detail required for each survey means that there cannot be shadowed areas within the zone of interest. Rock outcroppings, curvature of the slope, and a number of other obstacles can obstruct view of the ground surface, which requires a new angle from which to view the site. Many of the set ups on the sites investigated were capture the extra details obscured by portions of the slope itself.

Point density within the scans is another detail that it is important to consider. Each survey will have a required level of definition for the slope imaging. Distance from the site will have some effect on the level of detail obtained, but even at the 800m range, the ILRIS-3D system should be able to return detail at a point density of 2cm. The number of points captured in each scan increases the time it takes to complete the scan. Most of the surveys performed in this study were close range (within 100m) with detail ranging from a few millimeters to 2 cm. The time it took to complete this surveys was approximately 10-15 minutes. As the range increased, and thus the number of points captured in each survey, the time to completion increased to 30-45 minutes. Decreasing detail will decrease the time to scan completion, but this should be taken into consideration only if lower detail is acceptable for the survey.

Noting that line-of-site is the key consideration in any LiDAR survey, these limitations can be overcome. Multiple set ups when possible, use of the pan/tilt feature, and proper removal of garbage points (i.e. foliage in vegetation) can greatly improve the data obtained by the LiDAR. Having knowledge of the site to be investigated, and a plan on where to set up the device is important. Also, one should recognize that the device will not capture every possible slope aspect. A combination of various forms of LiDAR survey may be more advantageous if more than just the rock-cut face is required for analysis. The final point to recognize is that the data to be obtained should also be affected by the desired amount of detail. The less detail required, the less strict the LiDAR survey needs to be, the fewer set ups are required. Vice versa, if more detail is required, a better plan should be thought of in advance, and a longer survey should be implemented to properly capture the desired data.

The stationary terrestrial LiDAR station is a practical analysis method in determining slope characteristics for rockfall analysis. However, to ensure that it is useful to those who desire to utilize it as a method of site investigation, two things are necessary. (1)

Ensure that the limitations mentioned above are taken into consideration at each site, and (2) have a properly robust program with which to analyze the data further. A LiDAR survey assumes that the second stage of investigation is going to move into the third stage, or that the data will be compared from year to year. In both cases, being able to convert the data to a viewable form is a necessity, and so a program such as InnovMetric's Polyworks is recommended.

6.2. Tracking Rockfall Trajectories on Tornado Mountain

The 3-dimensional paths of two rockfall boulders, having crossed the CP Railway tracks at Tornado Mountain, were mapped using a Trimble Real-Time Kinematic Global Positioning System (RTK GPS). The data obtained from the survey mapping was input into a point file obtained from Geobase to create a DEM for the Tornado Mountain area.

Only one of the two boulders was present on site at the time of the RTK GPS survey. The boulder was approximately 4m³ of limestone material. The travel distance for this boulder was in the range of 640m-660m. A limestone cliff face with fresh, unweathered rock apparent on its surface was determined to be the most likely source of the rockfall boulders. The approach to the rock face was quite steep, and so the only data collected on it comes from a distance of 80m-100m. Slope material near the rockfall source was a limestone talus, though more exposed bedrock was becoming apparent.

The majority of the rockfall trajectory travelled through a vegetated zone of soft slope material. Impact points were generally large, with an average diameter of 2m and depths ranging from 0.25m-1m. Many of the impact points were discrete craters, though some were shallower and spaced closely, suggesting a tumbling motion, and others were elongated and deeper on the upslope side, suggesting that the boulder began to roll or slide at those points. Smashed trees in the area attest to the energy of the rockfall boulder, and fragments at many of the impact points appeared to have been broken off of the boulder at the point of impact.

The RTK GPS points were measured from the centre of each of the impact points. Data from the RTK GPS was referenced to the location of the base point to provide a Northing, Easting, and elevation in the UTM 11N coordinate grid of the NAD 1983 spatial referencing system. The Geobase data was referenced to the same system. Reconciling these two sets of data points in ArcGIS only required ensuring that both were input with the spatial reference parameters siting NAD 1983 UTM 11N. Satellite images of the area confirm that the reconciling was accurate to within meters.

6.3. Rockfall Simulations

There are several software programs, including RockFall Analyst (RA), designed to analyze rockfall trajectories. RA, developed at the University of Alberta, is unique in that it utilizes a 3-dimensional elevation model as the input geometry for the rockfall analyses. This aspect of the analysis removes any uncertainty related to the geometry of the slope surface impacted by the rockfall on the results.

A series of trials were conducted to determine reasonable starting parameters for the rockfall, and then the rockfall predictive method was tested under standard slope parameter settings. The results of which were that the simulated rockfalls reached a distribution with most of the rocks in areas of the slope that were observed to have large amount of rockfall material, while some followed the measured trajectory at close to the same total travel distance. This suggests that RA is effective in mapping possible rockfall pathways, and would be useful in future studies. Further studies and measurements would also be beneficial in validating the data obtained, even more so than when considering site observations and apparent trajectory agreement through the numerous simulations conducted. More recent and accurate site data, like that obtained from an aerial LiDAR survey, would have the additional benefit of showing the rockfall material distribution on site over the survey data, which confirms the validation from the on-site observations.

In determining the starting parameters for the rockfall analysis, determining the rockfall source was a very important factor. The most likely rockfall source was identified visually on site, and had been noted in the previous survey by Mr. Duncan Wyllie. However, it was not surveyed directly, nor was much of the last 90m leading up to its approximate location. Calibrating the model to provide reasonable rockfall trajectories relies on accurate source information. If the rockfall source has a known location on an accurate DEM, then it can be used directly as the seeder point for subsequent rockfall simulations. If the rockfall source location is unknown, then it must be estimated reasonably, with consideration for other possible locations in the rockfall simulations, such as when using a polyline seeder. The model accuracy has an effect on the rockfall source's usefulness in the program as well. The source at Tornado Mountain was noted to have been on a cliff face, while the equivalent area in the DEM was represented by very steep slopes ($\sim 70^\circ$). There is a potential difference of 20° between the observation and the model, which affects how the rock will react at the point of release within the DEM versus from the actual cliff face. Even if the rockfall source location is not a clearly defined location, it is possible to perform rockfall simulations using an understanding of the physics that are reasonable for the rockfall based on the site topography. A calibration approach that uses the rockfall energy relies on a starting point that follows the rockfall trajectory and on reasonable assumptions of the processes bringing the rockfall to that point. The topography of the rockfall source, and the area up to the point being investigated, is what drives the starting energy from this point. In conclusion, the topographic information of the rockfall source is very important to any

successful rockfall prediction, even if the source itself is not being used directly in the simulations.

The model accuracy has additional effect along the entirety of the rockfall trajectory. Topographic features drive the direction and energy of the rockfall down the slope. It was noted that the simulations followed the orange-flagged rockfall trajectory in preference to the yellow-flagged trajectory. This could be because of lack of information on slope geometry where the path diverged, or it can be due lack of definition of the rockfall source and its effects on energy and trajectory. The topographic detail that was present in the analysis did result in the demonstration of curvature in the rockfall trajectory similar to that noted in the measured trajectories, which followed a valley shape within the mountain slope.

To supplement the rockfall predictions in RA, the values for the coefficients of restitution (COR) were investigated. COR has default values in RA, but different slope material has a different effect on energy loss at each impact point, so defining COR for the site is important. Separating the slope into regions based on slope material, and then assigning these materials COR values improves the accuracy of the rockfall simulation.

Once the starting energy parameters were reasonably defined, the values of COR were adjusted several times to determine RA's sensitivity to this parameter. The simulated rockfalls behaved reasonably, consistently traveling approximately 500m along the orange-flagged trajectory, even as the COR values were varied. Differences between the adjusted values of COR were not a clear linear decrease in the rockfall travel distance. Rather, the decrease seemed dependent on the starting direction and energy of the rockfall. This suggests that RA is more sensitive to the energy input parameters, and therefore to the rockfall source information, than it is to COR.

Additional observations from the simulation on the rockfall trajectory show that three dimensional slope geometry also has an effect on the rockfall movement that is cannot be considered in two dimensional slope analyses. At approximately the 140m distance in the simulated trajectories, a large amount of rock material was deposited, which corresponds to a curve in the slope. Elements of the slope geometry associated with the curve and the energy loss caused by it would not be considered in a two dimensional analysis.

As well as COR being investigated as a slope characteristic, slope friction was also checked. Increasing friction decreased rockfall travel distance, and decreasing friction increases travel distance. This is expected, but like COR, the actual observed changes are not significant to the rockfall behaviour. Also, the rockfall behaviour exhibited when changing friction followed the patterns observed in the COR analysis, which further suggest the importance of the energy input parameters and detailed slope information.

RA predicted the trajectory and distribution of the rocks in simulation well in comparison to the measured trajectory and observed distributions. This confirms RA as a useful tool in future site analysis. It would be interesting to have a chance to compare RA with a site that has less vegetation to further evaluate the sensitivity of the program to vegetation, topographic factors, friction of the slope, and the values of COR.

6.4. Future Studies and Applications

The LiDAR survey was concentrated primarily on the steep rock cuts and faces, and not on the slopes above. To create a complete rockfall assessment of these sites, the additional slope information would be very useful, as well as identifying rockfall sources. If possible, obtaining an aerial LiDAR survey to combine with the terrestrial LiDAR data would improve and expediate the survey method. This would require obtaining GPS data during the terrestrial survey to ensure that data points can be matched in the computer software. If it is not possible to obtain the aerial LiDAR data, then the limits of the terrestrial station should be testing in attempting to obtain as much of the slope data as possible.

The RockFall Analyst study made it clear how important the rockfall source region and topography are for the 3-dimensional rockfall analysis. In a future site survey, additional concentration should be placed on obtaining the rockfall source region, and thoroughly describing that area. The office study should work to improve the overall DEM and the understanding of the processes that describe the initial rockfall energy.

Rockfall analysis is a hazard management concern. There are already many mitigative and preventative efforts in place in rockfall hazard areas. Improving analysis and predictive techniques will improve the methods of mitigation and prevention, as well as make them more economical and efficient. RockFall Analyst can also be used to determine wall height for barriers along any point in the rockfall path. If the predictions given by the program are proven to be accurate through measured comparison, then it can also be used as a design program for determining optimal height and location of rockfall barriers.

REFERENCES

- Alajeno, L.R., B. Pons, F.G. Bastante, E. Alonso, H.W. Stockhausen. 2007. Slope geometry design as a means for controlling rockfalls in quarries. *International Journal of Rock Mechanics & Mining Sciences* 44: 903-921.
- Alberta Research Council. Hydrogeological Map: Lethbridge-Fernie, Alberta. 1971. 1:250,000. Surveys Branch, Alberta Department of Highways and Transport, Edmonton.
- Alberta Research Council. Hydrogeological Map: Kananaskis Lakes, Alberta. 1:250,000.
- Alberta Society of Petroleum Geologists. Geology of the Seebe-Kananaskis Area. 1971. 1in:2miles. R.G. Salloway Consulting Ltd.
- ArcGIS® Version 9. 2006. ESRI.
- Bidwell, A.. 2006. Geohazards Review: Highway 40/Highway 541 Corridor Southwestern Alberta. Consulting Report submitted by AMEC Earth & Environmental, submitted to Alberta Infrastructure and Transportation.
- Bowman, R., P. Westgate, and E. Maliwat. 1997. Coefficient of restitution as an indication of impact resistance. *CSIRO Division of Building Construction & Engineering*. Australia.
- Brawner, C.O. and D. Wyllie. 1976. Rock slope stability on railway projects. *Am Railway Eng Assoc Bull* 656: 449-474.
- Bunce, C.M., D.M. Cruden, and N.R. Morgenstern. 1997. Assessment of the hazard from rock fall on a highway. *Canadian Geotechnical Journal* 34: 344-356 (1997).
- Chau, K.T., R.H.C. Wong, J. Liu, J.J. Wu, and C.F. Lee. 1999. Shape effects on the coefficients of restitution during rockfall impacts. *Proceedings 9th International Congress on Rock Mechanics*. Paris: Balkema, 541-544.
- Choi, Y., S.Y. Yoon, and H.D. Park. 2009. Tunneling Analyst: A 3D GIS extension for rock mass classification and fault zone analysis in tunneling. *Computers & Geosciences* 35: 1322-1333.
- Das, B.M.. 2008. Fundamentals of Geotechnical Engineering: Third Edition. Chapter 3: Weight-Volume Relationships, Plasticity, and Soil Classification. Cengage Learning, Stamford, Connecticut.

- GeoBase. <http://geobase.ca/geobase/en/find.do?produit=cded>. (Accessed September 17, 2010)
- Glenn, N.F., D.R. Streutker, D.J. Chadwick, G.D. Thackray, and S.J. Dorsch. 2006. Analysis of LiDAR-derived topographic information for characterizing and differentiating landslide morphology and activity. *Geomorphology* 73: 131-148.
- Hoek, E.. 2007. Practical Rock Engineering. Chapter 9: Analysis of rockfall hazards. http://www.rocscience.com/hoek/pdf/9_Analysis_of_rockfall_hazards.pdf (Last Accessed April 21, 2010).
- Hoek, E., and J.W. Bray. 1981. *Rock Slope Engineering*. London: Institution of Mining & Metallurgy.
- Hungr, O., S.G. Evans, and J. Hazzard. 1998. Magnitude and frequency of rock falls and rock slides along the main transportation corridors of southwestern British Columbia. *Canadian Geotechnical Journal* 36: 224-238 (1999).
- ILRIS Summary Specification Sheet. Optech Incorporated. http://www.optech.ca/pdf/ILRIS_SpecSheet_110309_Web.pdf (Last Accessed May 12, 2011)
- Jonsson, M.J.. 2007. *Energy absorption of trees in a rockfall protection forest*. Dissertation submitted for Doctor of Sciences. Swiss Federal Institute of Technology, Zurich
- Jonsson, M.J., A. Volkwein, and W.J. Ammann. 2007. Quantification of energy absorption capacity of trees against rockfall using finite element analysis. *Rock Mechanics: Meeting Society's Challenges and Demands*: 359-363. Taylor and Francis Group, London.
- Kememy, J., K. Turner, and B. Norton. 2005. LIDAR for Rock Mass Characterization: Hardware, Software, Accuracy and Best Practices. American Rock Mechanics Association.
- Lan, H.X.. 2007. Manual for RockFall Analyst: 3D Rockfall Modeling Extension to ArcGIS 9.x, 2nd Edition. University of Alberta: Centre for Risk Assessment for Geohazard Studies.
- Lan, H.X., C.D. Martin, and C.H. Lim. 2007. RockFall analyst: A GIS extension for three-dimensional and spatially distributed rockfall hazard modeling. *Computers & Geosciences* 33: 262-279.

- Lan, H.X., C.H. Zhou, L.J. Wang, H.Y. Zhang, and R.H. Li. 2004. Landslide hazard spatial analysis and prediction using GIS in the Xiaojiang watershed, Yunnan, China. *Engineering Geology* 76: 109-128.
- Lato, M., J. Hutchinson, M. Diedrichs, D. Ball, and R. Harrap. 2009. Engineering monitoring of rockfall hazards along transportation corridors: using mobile terrestrial LiDAR. *National Hazards and Earth System Sciences* 9: 935-946.
- Lee, K., and G. Elliott. 1998. Rockfall: Application of computer simulations to design of preventative measures. *Planning, design and implementation of debris flow and rockfall hazards mitigation measures*. Hong Kong: Association of Geotechnical Specialists & HK Institution of Engineers.
- Lewis, D.. 2006. Understanding LIDAR. *Cascadia: News and information from the Oregon Department of Geology & Mineral Industries* V.4 #2: 4. www.OregonGeology.com
- Parser.exe Version 1.7. 2002. Copyright © 1996-2002 Norbert H. Doerry.
- Perret, S., F. Dolf, and H. Kienholz. 2004. Rockfalls into forests: Analysis and simulation of rockfall trajectories – considerations with respect to mountainous forests in Switzerland. *Landslides* 1: 123-130.
- Pierson, L.A. and R. Van Vickle. 1993. Rockfall Hazard Rating System Participant's Manual. Federal Highway Administration (FHWA) Publication No. FHWA-SA-93-057. FHWA, U.S. Department of Transportation.
- Polyworks® Version 10.0. 2007. InnovMetric Software Inc..
- Rayudu, D.P.. 1997. *Computer simulation of rockfalls: application to rockfalls at Fox Glacier, West Coast, New Zealand*. MSc thesis. Lincoln University, New Zealand.
- Richards, L.R., B. Peng, and D.H. Bell. 2001. Laboratory and Field Evaluation of the Normal Coefficient of Restitution for Rocks. In *Rock Mechanics – a Challenge for Society*, ed. Särkkä and Eloranta, 149-155. Swets & Zeitlinger Lisse, ISBN 90 2651 821 8.
- Rocscience Coefficient of Restitution Table.
http://www.rocscience.com/downloads/rockfall/webhelp/RocFall.htm#baggage/rn_rt_table.htm (Last Accessed April 19, 2010).
- Sato, H.P., H. Yagi, M. Koarai, J. Iwahashi, and T. Sekiguchi. 2007. Progress in Landslide Science. Chapter 17: Airborne LIDAR Data Measurement and

Landform Classification Mapping in Tomari-no-tai Landslide Area, Shirakami Mountains, Japan. Springer Berlin Heidelberg.

Trimble® R6/R7 GPS Receivers Trimble R8 GNSS Receiver: User Guide Revision A. 2006. Trimble Navigation Limited Engineering and Construction group.

Wu, S.S.. 1985. Rockfall Evaluation by Computer Simulation. *Transportation Research Record* 1031: 1-5.

Wyllie, D.C.. 1980. Topping Rock Slope Failures – Examples of Analysis and Stabilization. *Rock Mechanics* 13: 89-98.

APPENDIX A

Table A.1: RHRS Field Data Sheet (Pierson and Van Vickle 1993, p16)

RHRS FIELD DATA SHEET

HIGHWAY:		REGION:	
HIGHWAY # _____	Beginning M.P. _____	L / R _____	Ending M.P. _____
COUNTY # _____	DATE _____	NSW _____	Rated By _____
CLASS A B	ADT _____	UPDATE _____	Speed Limit _____

CATEGORY	REMARKS	CATEGORY SCORE
Slope Height _____ ft		SLOPE HEIGHT _____
Ditch Effectiveness G M I W		DITCH EFFECT _____
Average Vehicle Risk %		AVR _____
Sight Distance _____ ft		SIGHT DISTANCE _____
Percent Decision Site Distance %		
Roadway Width _____ ft		ROADWAY WIDTH _____
GEOLOGIC CHARACTER		GEOLOGIC CHARACTER
CASE 1		CASE 1
Structural Condition D C/F R A		STRUCT COND _____
Rock Friction R I U P C - S		ROCK FRICTION _____
CASE 2		CASE 2
Differential Erosion Features P O N M		DIF ER FEATURES _____
Difference in Erosion Rates S M L E		DIF ER RATES _____
Block Size/Volume _____ ft ³		BLOCK SIZE _____
Climate		
Precipitation L M H		CLIMATE _____
Freezing Period M S L		
Water on Slope M I C		
Rockfall History F O M C		ROCKFALL HISTORY _____
COMMENTS:		TOTAL SCORE _____

Table A.2: Summary Sheet of Rockfall Hazard Rating System (Pierson and Van Vickle 1993, p26)

CATEGORY		RATING CRITERIA AND SCORE				
		POINTS 3	POINTS 9	POINTS 27	POINTS 81	
SLOPE HEIGHT		25 FEET	50 FEET	75 FEET	100 FEET	
DITCH EFFECTIVENESS		Good catchment	Moderate catchment	Limited catchment	No catchment	
AVERAGE VEHICLE RISK		25% of the time	50% of the time	75% of the time	100% of the time	
PERCENT OF DECISION SIGHT DISTANCE		Adequate sight distance, 100% of low design value	Moderate sight distance, 80% of low design value	Limited sight distance, 60% of low design value	Very limited sight distance 40% of low design value	
ROADWAY WIDTH INCLUDING PAVED SHOULDERS		44 feet	36 feet	28 feet	20 feet	
G E O L O G I C	C A S E 1	STRUCTURAL CONDITION	Discontinuous joints, favorable orientation	Discontinuous joints, random orientation	Discontinuous joints, adverse orientation	Continuous joints, adverse orientation
		ROCK FRICTION	Rough, Irregular	Undulating	Planar	Clay infilling, or slickensided
C H A R A C T E R	C A S E 2	STRUCTURAL CONDITION	Few differential erosion features	Occasional differential erosion features	Many differential erosion features	Major differential erosion features
		DIFFERENCE IN EROSION RATES	Small difference	Moderate difference	Large difference	Extreme difference
BLOCK SIZE VOLUME OF ROCKFALL/EVENT		1 Foot 3 cubic yards	2 Feet 6 cubic yards	3 Feet 9 cubic yards	4 Feet 12 cubic yards	
CLIMATE AND PRESENCE OF WATER ON SLOPE		Low to moderate precipitation; no freezing periods; no water on slope	Moderate precipitation or short freezing periods or intermittent water on slope	High precipitation or long freezing periods or continual water on slope	High precipitation and long freezing periods or continual water on slope and long freezing periods	
ROCKFALL HISTORY		Few falls	Occasional falls	Many falls	Constant falls	

Table A.3: RocScience Coefficient of Resitution (Modified from RocScience Website)

RN (Normal)				RT (Tangential)				Type
Min	Max	Mean	Standard Deviation	Min	Max	Mean	Standard Deviation	
0.37	0.42			0.87	0.92			Hard surface paving
0.33	0.37			0.83	0.87			Bedrock or boulders with little soil or vegetation
0.3	0.33			0.83	0.87			Talus with little vegetation
0.3	0.33			0.8	0.83			Talus with some vegetation
0.28	0.32			0.8	0.83			Soft soil slope with little vegetation
0.28	0.32			0.78	0.82			Vegetated soil slope
		0.315	0.064			0.712	0.116	Limestone face
		0.303	0.08			0.615	0.17	Partially vegetated limestone scree
		0.315	0.064			0.712	0.116	Uncovered limestone blast pile
		0.251	0.029			0.489	0.141	Vegetated covered limestone pile
		0.276	0.079			0.835	0.087	Chalk face
		0.271	0.018			0.596	0.085	Vegetated chalk scree
		0.3837	0.1326			0.6865	0.1303	Wood platform slope at 45 degrees was used as a control for the field tests they did.
		0.2				0.53		Dolomitic limestone boulders on rocky surfaces and on talus desoposits
		0.1				0.2		Remolded pyroclastic from the terraces situated at the base of the cliff
		0				0.24		Impacts on detritus of the fans present at the foot of a rock cliff
		0.393				0.567		Soil
		0.453				0.737		Shotcrete
		0.487				0.91		Rock slope
		0.5				0.95		Bedrock
		0.35				0.85		Bedrock covered by large blocks
		0.3				0.7		Debris formed by uniform distributed elements
		0.25				0.55		Soil covered by vegetation
		0.53				0.99		Clean hard bedrock
		0.4				0.9		Asphalt roadway
		0.35				0.85		Bedrock outcrops with hard surface, large boulders
		0.32				0.82		Talus cover

		0.32				0.8		Talus cover with vegetation
		0.3				0.8		Soft soil, some vegetation
0.37	0.42							Smooth hard surfaces and paving
0.33	0.37							Most bedrock and boulder fields
0.3	0.33							Talus and firm soil slopes
0.28	0.3							Soft soil slopes
					0.87	0.92		Smooth hard surfaces such as
								pavement or smooth bedrock surfaces
					0.83	0.87		Most bedrock surfaces and talus with no vegetation
					0.82	0.85		Most talus slopes with some low
								vegetation
					0.8	0.83		Vegetated talus slopes and soil slopes with sparse vegetation
					0.78	0.82		Brush covered soil slope
		0.53	0.04			0.99	0.04	Clean Hard Bedrock
		0.35	0.04			0.85	0.04	Bedrock outcrop
		0.32	0.04			0.82	0.04	Talus cover
		0.32	0.04			0.8	0.04	Talus with vegetation
		0.4	0.04			0.9	0.04	Asphalt paving
		0.53	0.04			0.99	0.04	Clean Hard Bedrock
		0.35	0.04			0.85	0.04	Bedrock outcrop
		0.48	0.19			0.53	0.17	Concrete
		0.47	0.3			0.55	0.23	Weathered Rock
		0.48	0			0.53	0	Concrete
		0.47	0			0.55	0	Weathered Rock
		0.85	0			0.53	0	Concrete
		1	0			0.55	0	Weathered Rock
		0.53	0.04			0.99	0.04	Bedrock
		0.5	0.06			0.7	0.06	Blockfield
		0.5	0.06			0.65	0.06	Blockfield with bushes and small
								trees
		0.5	0.06			0.5	0.06	Blockfield with forest
		0.3	0.06			0.8	0.06	Top-soil with vegetation
		0.4	0.04			0.9	0.04	Asphalt paving
		0.35	0.04			0.85	0.04	Gravel road
		0.5				0.8		Sparsley forested slope is covered by a veneer of very fine weathered talus derived from weak shistose units underlying the limestone cap.
		0.5				0.8		Limestone on bare uniform talus slope formed of basalt fragments with a modal size of 5 cm.
		0.7				0.9		rectangular bolder of metamorphosed tuff on bare rock and a steep snow covered shelf.

APPENDIX B

The Figures in this Appendix are related to Section 4 of the thesis and reflect the data captured with the ILRIS-3D LiDAR device from Optech Inc.. The following figure is a demonstration of the scale view of a point cloud

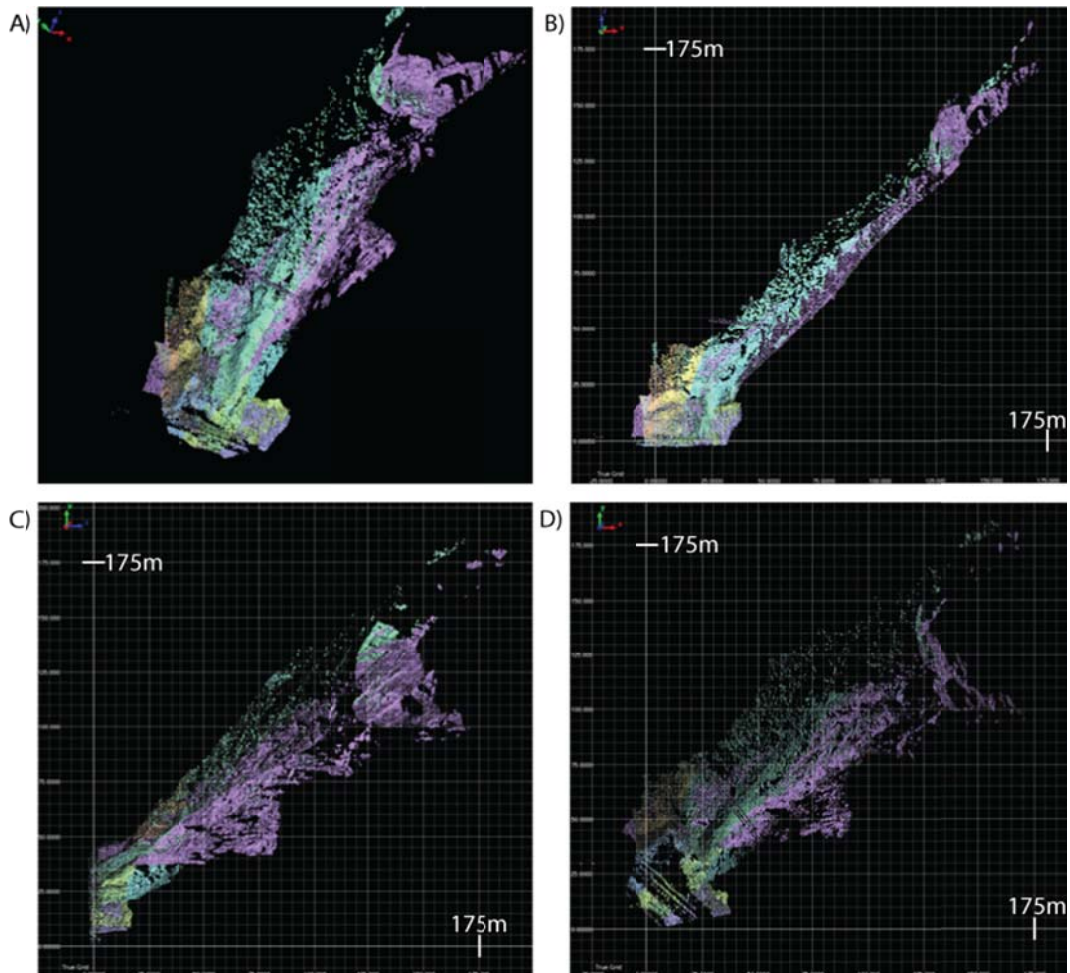


Figure B.1: A) Point Cloud at Crowsnest Lake Rock-Cut, B) View and Scale on XZ Plane, C) View and Scale on YZ Plane, and D) View and Scale on XY Plane.

The following figures are the enlarged images of the surface maps interpolated within Polyworks from the ILRIS-3D XYZ point cloud data.

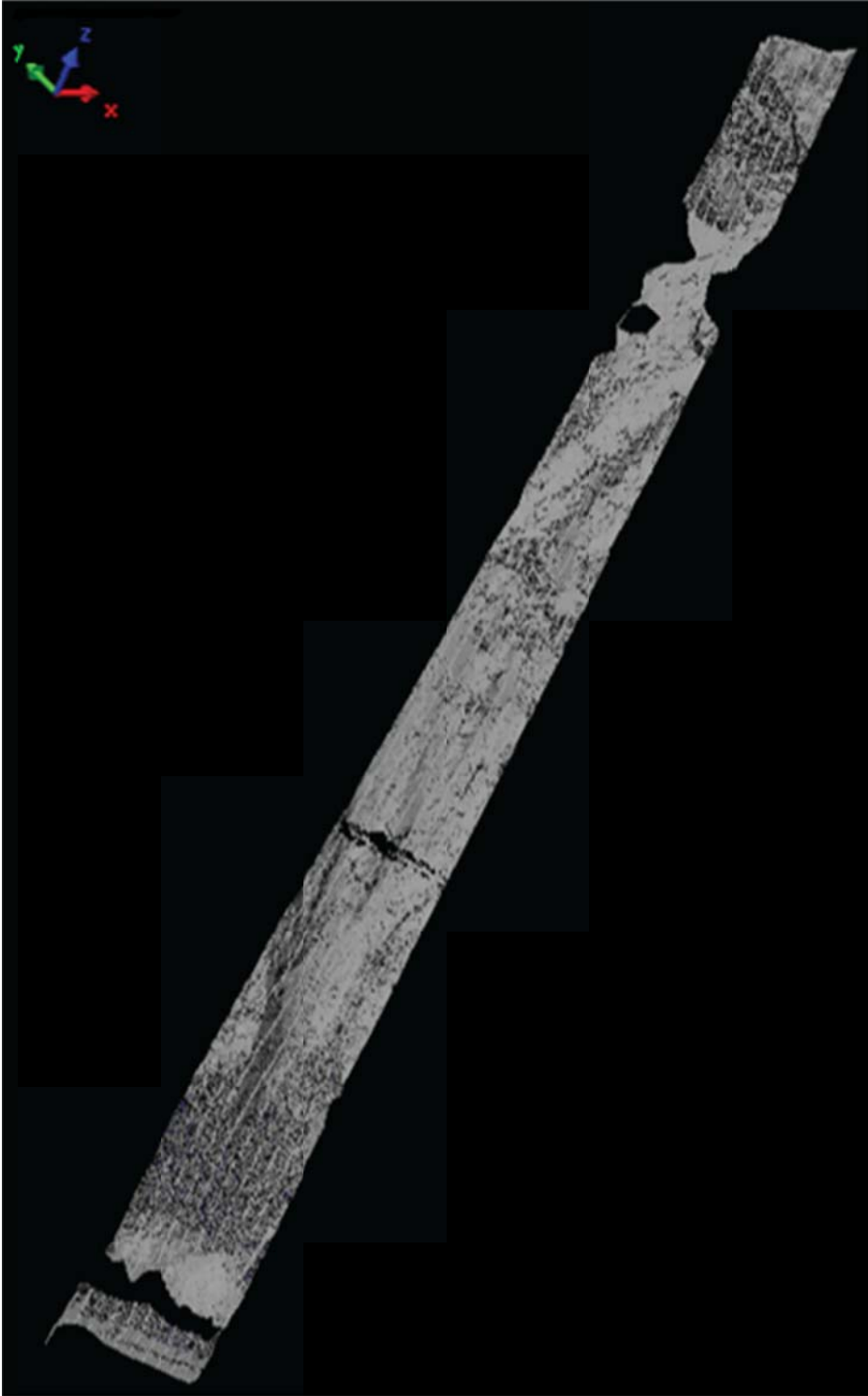


Figure B.2: Surface Map of Crowsnest Lake Site

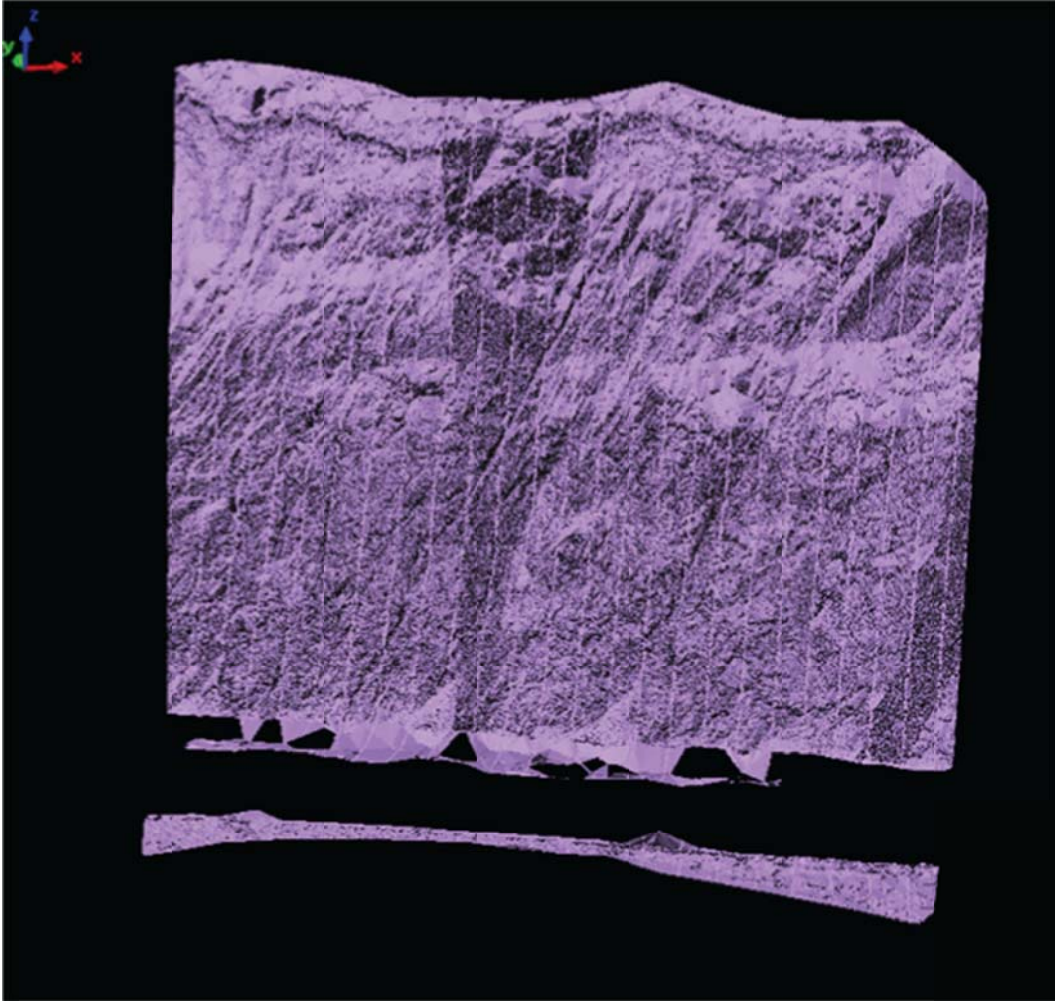


Figure B.3: Surface Map of Highwood House Rock-Cut

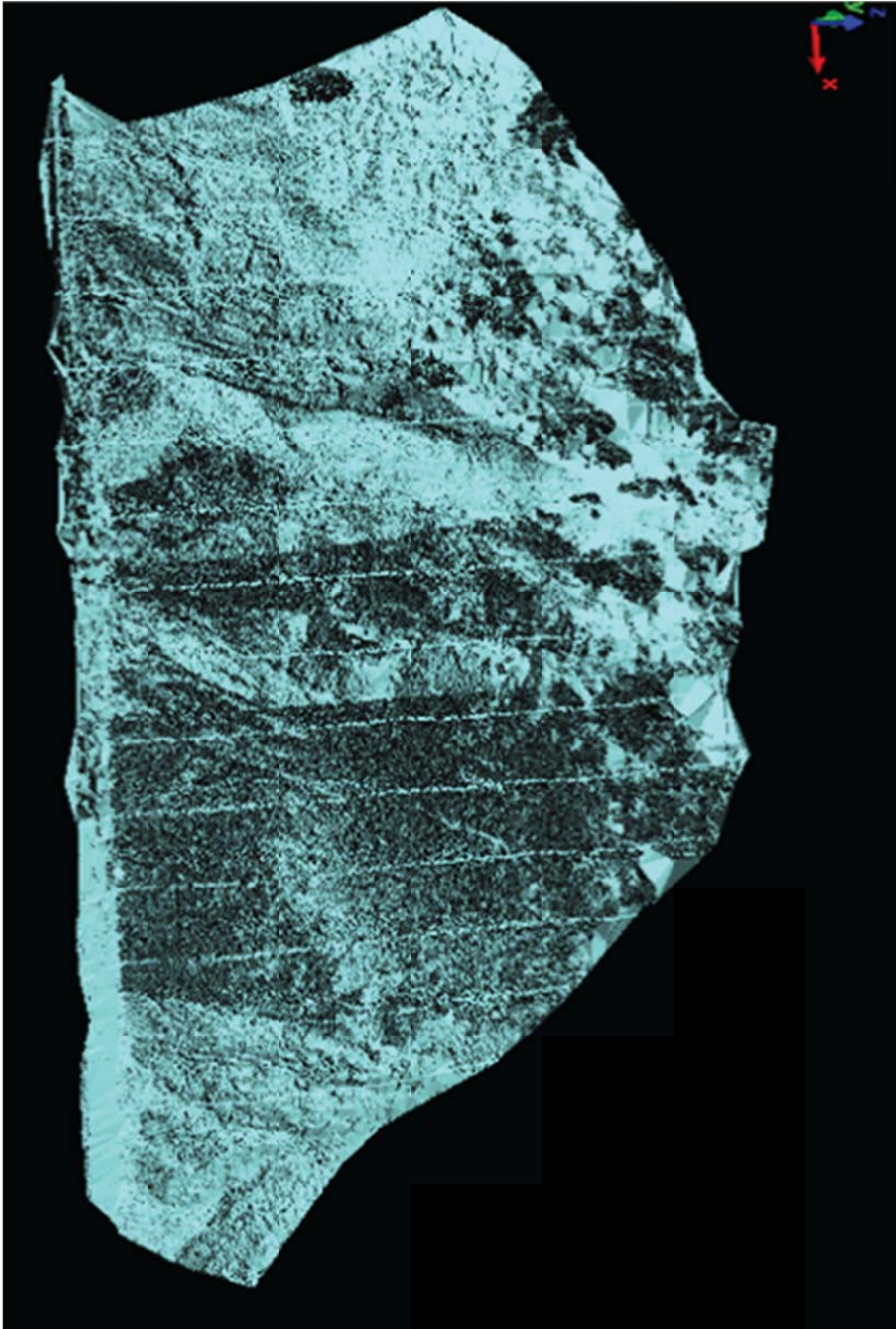


Figure B.4: Surface Map of Fir Creek Rock-Cut (Rotated)

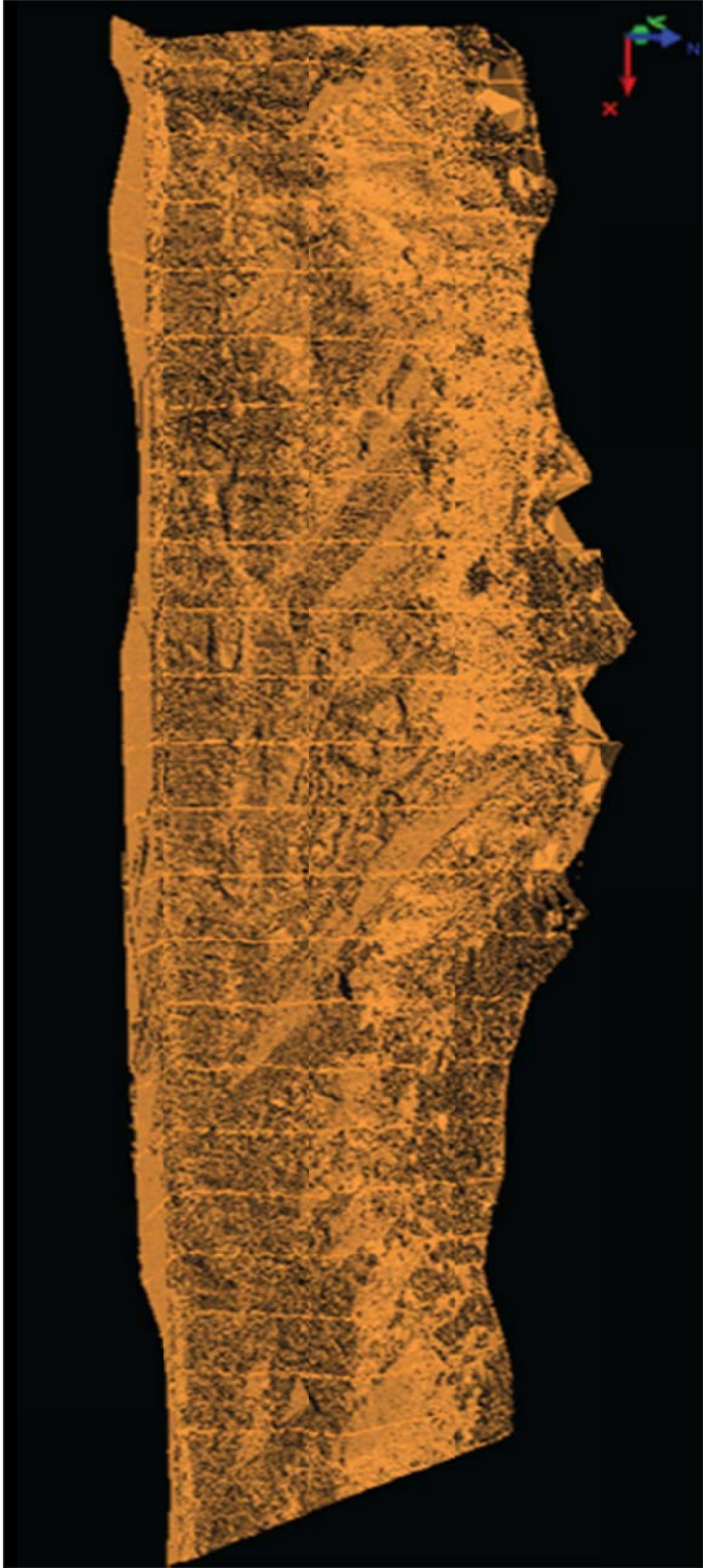


Figure B.5: Surface Map of Galatea Through-Cut East Rock Slope (Rotated)

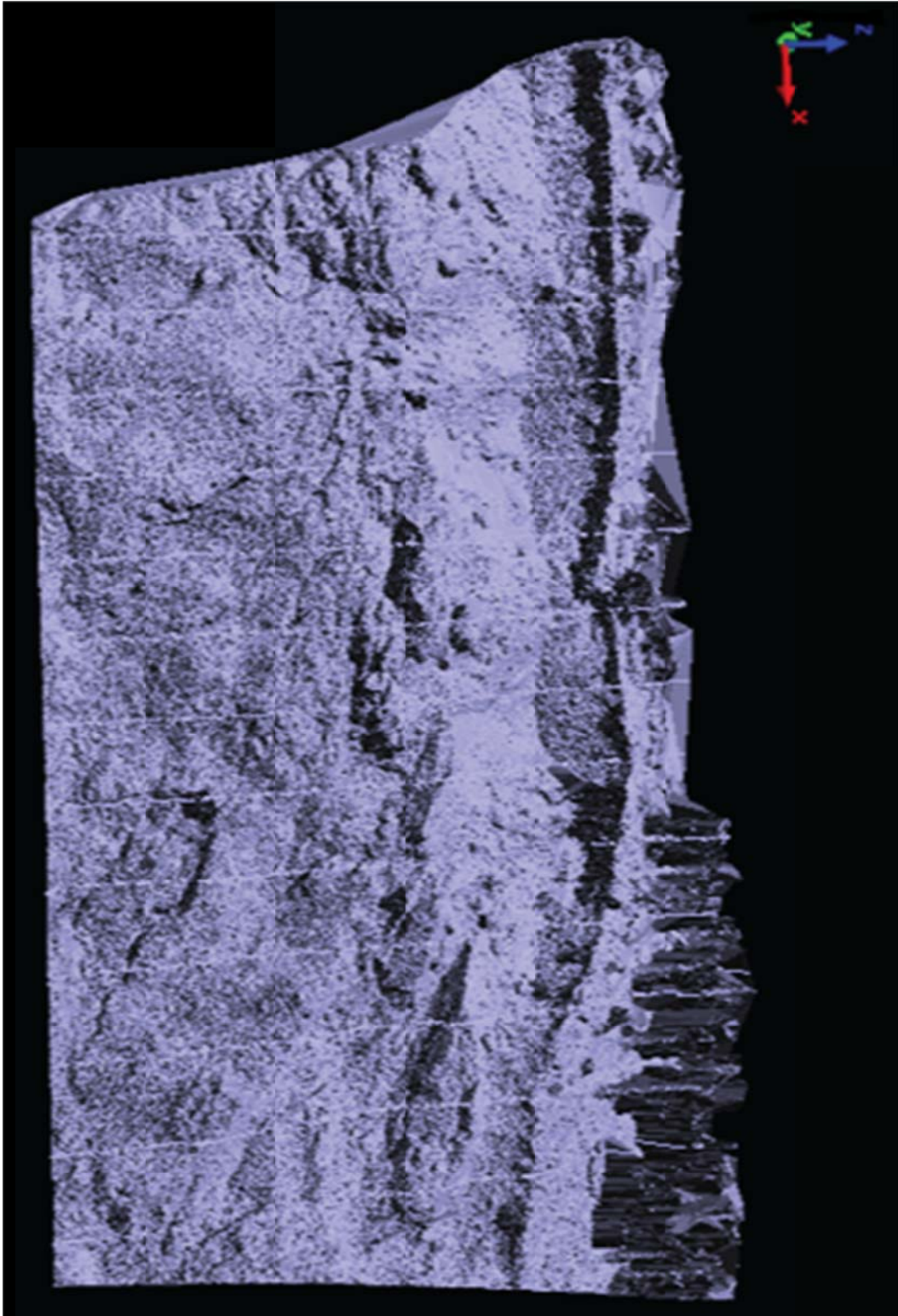


Figure B.6: Surface Map of Mt. Baldy Rock-Cut (Rotated)

APPENDIX C

C.1 Site Notes

The following are the observational notes taken on site on June 22nd and 23rd during the RTK GPS survey.

- Boulder downslope from track: about 6 m from railway. 2.2 m x 1.8 m x 1.0 m. Boulder was stopped by 2 trees (Figure C.1). Rock block looks fresh limestone with trace quartz like intrusions and veins. Jointed with spacing between 2 to 15 cm (less where seemed to be impacted) and depending on the joint set orientation. (some foliation can be seen?). A smaller, 0.7 x 0.4 x 0.2 m, rock block (maybe detached from bigger) 3 to 4 m upslope, still downslope from railway.



Figure C.1: Rock Block from Orange Flagged Path

- Several blocks and footprints of rockfall history along the slope. Fresh to weathered blocks, bigger ones up to 2 m in diameter found. Rock chips (fresh and weathered, sign of fragmentation while falling) can be found all over the place.
- Vegetation was starting to cover the footprints of the paths under investigation.

- All footprints had a topsoil cover with crashed branches and leaves. No signs of sliding of the blocks or have been covered.
- Toe of rock wall on the head of the slope was observed. Limestone heavily jointed. 5 – 10 and 15 cm spacing depending on the joint set for the most damaged zones. Scars of fresh rock blocks (un-weathered areas) can be seen. Characteristic joint orientations are 1) sub-vertical with trend sub-parallel to face contour, 2) sub-vertical almost perpendicular to face and 3) sub-horizontal.
- Debris accumulation fan (left side the most noticeable) with blocks from 10 cm diameter up to 30 to 40 cm diameter. Weathered and fresh blocks.

Table C.1: Observations and Notes of Tornado Mountain GPS Survey

Point	Flagged?	Observation
5001	Y	A bit off if path is followed.
5002	N	Lowest observed depression near 5001. Looks like lowest depression in a rolling path before block jump. Linked to points 5003 and 5004.
5003	N	Middle depression of apparent rolling path.
5004	N	Upper depression of apparent rolling path.
5005	Y	Smashed bushes.
5006	N	Looks like impacts 1 m apart (impact – roll – jump sequence?)
5007	Y	Smashed bushes.
5008	N	Similar footprint noted and within the path. Smashed vegetation.
5009	Y	
5010	N	About 2m next to point 5009.
5011	Y	Footprint 1.5 to 1.8 m long, 10 – 20 cm deep. Rock chips and blocks.
5012	Y	Crushed bushes with small footprint 0.5 to 1 m long. Hard to determine. Bushes crushed between points 5011 and 5012.
5013	Y	0.8 m long footprint. 10 – 20 cm deep.
5014	Y	30 to 20 cm deep footprint. Smashed bushes in the area.
5015	Y	1.2 m long, 0.8 m wide, 30 m deep footprint. Rock pieces found.
5016	N	Damaged tree with recent scars (in the direction of the path looking upslope) 0.8 m long, 10 – 20 cm deep footprint. Fresh rock blocks and chips found.
5017	Y	1.5 m long, 0.8 m wide, 20 to 30 cm deep footprint. Fresh rock chips and rock blocks (15 cm diameter) found.
5018	Y	2 m long, 0.8 m wide, 30 cm deep footprint. Damaged tree. Fresh rock chip accumulation 5 m upslope.
5019	Y	1.5 m long footprint. Fresh and weathered rock chip accumulation.
5020	Y	1.2 m long, 0.8 – 1 m wide, 30 – 40 cm deep footprint. Fresh rock chips found.
5021	Y	2 m long, 1.2 m wide, 30 – 35 cm deep footprint.
5022	Y	2 – 2.2 m long, 1.2 m wide, 30 – 35 cm deep footprint. Fresh rock chips and 15 cm diameter blocks found.
5023	Y	0.8 m diameter footprint.

5024	Y	0.8 m diameter footprint.
5025	Y	1.5 m long 0.6 m wide, 40 cm deep footprint.
5026	Y	1.5 – 1.8 m diameter, 30 cm deep footprint. Fresh rock blocks found (15 to 30 cm diameter and smaller).
5027	Y	1.2 m long, 0.8 m wide, 35 cm deep footprint. Fresh rock blocks (15 – 30 cm diameter).
From this point on all footprints had accumulation of fresh and weathered rock chips and 15 to 30 cm diameter rock blocks.		
5028	Y	2 m long, 1 m wide, 35 to 40 cm deep footprint.
5029	Y	2 m long, 0.6 m wide, 30 cm deep footprint.
5030	Y	2.2 m long, 1 m wide, 30 to 40 cm deep footprint.
5031	Y	0.8 m long, 0.4 m wide, 20 cm deep footprint.
5032	Y	2.2 m long, 1.2 m wide, 30 cm deep footprint.
5033	Y	1.5 m long, 0.6 m wide, 35 cm deep footprint.
5034	Y	1.8 m long, 0.5 m wide, 20 cm deep footprint. Smashed tree.
5035	Y	2 m long, 0.7 m wide, 20 cm deep footprint.
5036	Y	2.2 m long, 1 m wide, 30 cm deep footprint. Smashed tree.
5037	Y	Possible deviant point. Not same dimensions (40 – 50 cm diameter and 15 cm deep footprint).
5038	Y	2.2 m diameter, 35 cm deep footprint. Several 1 to 1.6 m diameter blocks, fresh and weathered, in the area.
5039	Y	2 m long, 0.8 m wide, 25 to 30 cm deep footprint. Smashed trees.
5040	Y	0.8 m diameter, 35 to 40 cm deep footprint.
5041	Y	1.6 m long, 0.6 m wide, 35 cm deep footprint.
5042	Y	1.6 m long, 0.6 m wide, 40 cm deep footprint.
5043	Y	1.5 m long, 0.6 m wide, 25 to 30 cm deep footprint.
5044	Y	1.5 m long, 0.6 m wide, 25 to 30 cm deep footprint.
5045	Y	1.6 m long, 0.8 m wide, 35 to 40 cm deep footprint. Underneath smashed tree trunk.
5046	Y	Crushed tree.
5047	Y	Possible deviant point as no noticeable footprint was found (might have been covered).
5048	Y	0.6 m diameter, 30 to 35 cm deep footprint. Bushes smashed.
5049	Y	1.2 m long, 0.6 m wide, 25 to 30 cm deep footprint.
5050	Y	0.6 m diameter, 20 cm deep footprint.
5051	N	2 m long, 0.7 m wide, 35 to 40 cm deep footprint.
5052	Y	1.2 m diameter footprint.
5053	Y	2.2 m long, 0.8 m wide, 35 to 40 cm deep footprint.
5054	Y	0.6 m diameter, 20 cm deep footprint.
5055	Y	2.2 m long, 0.6 to 0.8 m wide, 35 to 40 cm deep footprint.
Flags change color from orange to yellow - second path – looks like shared (accounted as very similar) with first path for the upper most footprints.		
5056	Y	2.2 m long, 0.8 m wide, 40 cm deep footprint, smashed tree.
5057	Y	2.2 m long, 0.8 m wide, 40 cm deep footprint.
5058	Y	Possible deviant point due to different size of footprints with yellow flag 1.5 m diameter. Smashed trees.
5059	N	Similar footprint 2.2 m long, 0.8 m wide, 40 cm deep. 1.5 m diameter blocks just 30 m down slope.
5060	Y	2.2 m long, 0.8 m wide, 40 cm deep footprint.

5061	N	2 m long, 0.8 m wide, 30 to 35 cm deep footprint.
5062	Y	Possible deviant point, difficult to define. Several impacts in the area can be inferred from smashed trees and footprints and old weathered and fresh blocks.
5063	N	Possible deviant point, difficult to define. Several impacts in the area can be inferred from smashed trees and footprints and old weathered and fresh blocks. Footprint about 2 m long, 0.8 m wide.
5064	N	No more clear impact scars found that could have been caused by the particular event. Likely impact zone given the subsequent path of the block and source area, and considering the blocks and debris found.
5065	Y	2.5 to 3 m long, 0.8 m wide, 40 cm deep footprint.
5066	Y	Looks like rolling path 8 to 10 m long, 0.8 m wide, 20 to 30 cm deep. Path marked by points 5066 through 5068.
5067	N	Looks like rolling path 8 to 10 m long, 0.8 m wide, 20 to 30 cm deep. Path marked by points 5066 through 5068.
5068	Y	Looks like rolling path 8 to 10 m long, 0.8 m wide, 20 to 30 cm deep. Path marked by points 5066 through 5068.
5069	Y	2 m long, 0.8 m wide, 50 cm deep footprint. Smashed tree trunk.
5070	Y	Possible deviant point, not easy to define footprint dimension, looks like rolling path after it.
5071	Y	2 m long, 1 – 1.2 m wide, 50 cm deep footprint. Smashed tree.
5072	N	1.6 m long, 1 m wide, 35 cm deep footprint.
5073	Y	0.8 m diameter, 20 to 30 cm deep footprint. Continues like a rolling path up to point 5074.
5074	N	Path from 5073 has here a marked 4 m long, 0.8 m wide 20 cm deep footprint. Path continues for a couple more metres. Smashed trees.
5075	Y	2 m long, 1.6 m wide, 50 cm deep footprint.
5076	Y	2 to 2.2 m long, 1 m wide, 40 cm deep footprint.
5077	Y	1.3 m long, 1 m wide, 30 cm deep footprint. Not very reliable as seems to be smaller impact.
5078	Y	2 m long, 0.8 m wide, 50 cm deep footprint.
5079	Y	2 m long, 1.6 m wide, 50 to 60 cm deep footprint. Smashed trees up slope and down slope. Damaged trees from here to point 5080.
5080	Y	1.8 – 2 m long, 1 m wide, 30 cm deep footprint. Smashed tree.
5081	N	1.3 to 1.6 m long, 0.6 m wide, 30 cm deep footprint. Not very reliable due to different dimensions. Tree smashed.
5082	Y	Not very noticeable, under tree trunk (did a later event smashed the tree and covered the footprint?).
5083	Y	1.5 m long, 0.8 to 1 m wide, 30 cm deep footprint. Hard to define, not very noticeable.
5084	Y	Not noticeable, looks like part of a rolling path.
5085	N	2 m long, 1 m wide, 25 to 30 cm deep footprint. Smashed tree on top.
5086	N	2 m long, 0.8 to 1 m wide, 30 cm deep footprint.
5087	Y	1.5 m long, 0.7 m wide, 30 cm deep footprint.
5088	Y	2 m long, 0.6 m wide, 25 m deep footprint.

5089	Y	1.5 m long, 0.7 m wide, 30 cm deep footprint.
5090	Y	1 m diameter, 20 cm deep footprint. Not very reliable due to difference in dimensions.
5091	Y	1.8 – 2 m long, 0.8 – 1 m wide, 30 cm deep footprint. Smashed trees.
5092	Y	No footprint found.
Several 0.8 to 1.5 m diameter blocks found from this point on around the area. Weathered and fresh.		
5093	Y	Footprint seen under a smashed tree. Hard to get dimensions. Not very reliable.
5094	Y	1.5 m long, 0.3 m wide, 10 cm deep footprint. Not reliable due to dimensions. Many 0.8 m diameter boulders down slope from it.
Many scars from previous events around the points can be seen from this point on.		
5095	Y	1.5 m long, 0.3 m wide, 10 cm deep footprint. Not reliable due to dimensions.
5096	Y	Smashed tree, hard to notice dimensions. Not very reliable.
5097	Y	1.6 m long, 0.6 m wide, 10 cm deep footprint. Not easy to determine.
5098	Y	1.6 m long, 0.5 m wide, 15 to 20 cm deep footprint. Not easy to determine.
5099	Y	Not able to see any sign of impact here.
5100	Y	Not able to see any sign of impact here.
5101	Y	1.5 m long, 1 m wide, 15 to 20 cm deep footprint. Not easy to see.
5102	Y	1.6 m diameter, 15 cm deep footprint, not easy to notice.
5103	Y	1.5 m diameter, 15 cm deep footprint, not easy to notice.

C.2 GPS Survey Data

The following table is the GPS point data located using the RTK GPS at Tornado Mountain. Orange marked points were mapped with orange flags on site by Duncan Wyllie’s previous survey. Similarly, the yellow boxes reflect points marked by yellow flags. There are some points that were marked with both, and those can be noted in Renato’s site notes in C.1. The orange flags followed one specific boulder, while the yellow flags followed the other. There is a common origin point for both boulders. The white boxes are noted points on the RTK GPS survey which were likely rockfall points, but were unflagged. These points were taken to improve the dataset, and as a precaution in the event that the flags were simply lost between surveys.

Table C.2: RTK GPS Points

	North	East	Elevation	
BASE100	5531778	654855.5	1305.462	CP
5000	5531762	654858.4	1304.961	GRD
5001	5531782	654891.4	1317.425	GRD
5002	5531780	654897.6	1318.393	GRD
5003	5531781	654898.1	1319.597	GRD

5004	5531780	654897.9	1320.691	GRD
5005	5531787	654917.5	1325.056	GRD
5006	5531791	654928	1330.715	GRD
5007	5531793	654932.2	1332.794	GRD
5008	5531794	654935.4	1333.447	GRD
5009	5531796	654940.4	1335.313	GRD
5010	5531795	654942.1	1335.426	GRD
5011	5531798	654948.1	1338.413	GRD
5012	5531801	654952.1	1341.627	GRD
5013	5531802	654955	1343.839	GRD
5014	5531805	654963	1345.419	GRD
5015	5531806	654965.5	1351.034	GRD
5016	5531808	654971	1353.86	GRD
5017	5531811	654977	1354.961	GRD
5018	5531813	654981.7	1358.662	GRD
5019	5531818	654993.8	1366.767	GRD
5020	5531824	655008.2	1371.891	GRD
5021	5531828	655015.8	1376.63	GRD
5022	5531830	655023.2	1378.91	GRD
5023	5531836	655031.3	1386.245	GRD
5024	5531836	655034.9	1385.809	GRD
5025	5531836	655037.9	1386.557	GRD
5026	5531843	655052.5	1396.081	GRD
5027	5531846	655060.8	1399.958	GRD
5028	5531848	655063.6	1400.931	GRD
5029	5531850	655068.7	1400.843	GRD
5030	5531853	655077.3	1409.818	GRD
5031	5531855	655083.6	1410.109	GRD
5032	5531859	655095.8	1417.475	GRD
5033	5531859	655099.7	1419.841	GRD
5034	5531863	655107.2	1423.624	GRD
5035	5531866	655111.9	1420.782	GRD
5036	5531867	655115	1428.184	GRD
5037	5531867	655119.3	1432.669	GRD
5038	5531869	655122.4	1431.981	GRD
5039	5531869	655126.3	1432.586	GRD
5040	5531871	655130.4	1435.784	GRD
5041	5531874	655139.9	1442.547	GRD
5042	5531875	655142.3	1447.476	GRD
5043	5531879	655152.9	1442.554	GRD
5044	5531882	655164.8	1449.139	GRD

5045	5531884	655169.2	1455.56	GRD
5046	5531886	655180.8	1463.824	GRD
5047	5531886	655185.6	1466.466	GRD
5048	5531889	655200.7	1477.767	GRD
5049	5531889	655202.9	1477.574	GRD
5050	5531892	655210.4	1478.458	GRD
5051	5531895	655230.6	1491.512	GRD
5052	5531897	655242.7	1495.763	GRD
5053	5531898	655246.2	1497.708	GRD
5054	5531899	655250	1500.498	GRD
5055	5531900	655260.8	1506.18	GRD
5056	5531902	655270	1512.492	GRD
5057	5531898	655277.7	1516.178	GRD
5058	5531903	655289.8	1522.625	GRD
5059	5531900	655300.2	1533.18	GRD
5060	5531904	655304.7	1532.054	GRD
5061	5531905	655319.6	1540.21	GRD
5062	5531907	655332.1	1549.627	GRD
5063	5531906	655340.3	1552.891	GRD
5064	5531910	655396.3	1585.438	GRD
5065	5531899	655244.7	1499.263	GRD
5066	5531902	655237.7	1491.821	GRD
5067	5531900	655232	1492.594	GRD
5068	5531902	655230.8	1489.328	GRD
5069	5531899	655219.9	1489.259	GRD
5070	5531901	655216.5	1483.2	GRD
5071	5531901	655207.5	1479.421	GRD
5072	5531901	655203	1477.553	GRD
5073	5531902	655200.2	1477.622	GRD
5074	5531902	655200.1	1472.527	GRD
5075	5531903	655189.8	1463.656	GRD
5076	5531901	655179.5	1466.238	GRD
5077	5531906	655173.4	1461.661	GRD
5078	5531902	655168.5	1458.531	GRD
5079	5531903	655158.2	1453.549	GRD
5080	5531905	655146.9	1446.296	GRD
5081	5531905	655139.4	1445.628	GRD
5082	5531907	655135.4	1444.222	GRD
5083	5531907	655126.7	1437.714	GRD
5084	5531904	655120.5	1431.689	GRD
5085	5531903	655111	1429.787	GRD

5086	5531900	655104	1424.769	GRD
5087	5531902	655089.1	1416.013	GRD
5088	5531900	655075	1406.344	GRD
5089	5531895	655065.1	1402.333	GRD
5090	5531894	655057.7	1390.309	GRD
5091	5531895	655040.6	1393.197	GRD
5092	5531896	655027.9	1378.263	GRD
5093	5531893	655024.1	1376.922	GRD
5094	5531890	655015.4	1377.525	GRD
5095	5531888	655007	1373.046	GRD
5096	5531889	655001.9	1368.496	GRD
5097	5531883	654978	1356.421	GRD
5098	5531882	654972.2	1360.293	GRD
5099	5531871	654921.1	1336.625	GRD
5100	5531866	654914	1332.56	GRD
5101	5531863	654897.9	1329.604	GRD
5102	5531854	654883.5	1321.941	GRD
5103	5531852	654871.6	1319.043	GRD

C.3 Rockfall Analysis Profiles

This section contains all of the rockfall analysis profiles conducted once the final measurement parameters were decided upon. All of these points follow the same seeder positioning within the RA program, while the starting parameters are varied to allow observations on the resulting rockfall trajectories. These parameters are the important concern in each of these test series, and so they will be listed prior to their use.

Following is the first set of rockfall trajectories which were tested with starting parameters set to determine the bounding conditions, and to ensure that reasonable results were attainable. One parameter that remains unchanged in all of the following tests is friction, which is set at 20°. The figure names relate the initial drop height and slope angle, and therefore provide those parameters. The changing parameter in each case is the COR. For these tests, the COR values are:

$$\begin{aligned} R_n &= 0.33 \\ R_t &= 0.87 \end{aligned}$$

These COR values only reflect the changes in the vegetated slope cover. There are additional values for the talus slope zone and the limestone bedrock zone. These values were taken from the RocScience table in Appendix B, and can be seen listed in Section 5.2. Scale for these figures is the same as seen in Section 5, Figure 5.11.



Figure C.2: Rockfall Simulation: $R_n = 0.33$ $R_t = 0.87$; Slope Angle 45° ; Drop Height 10m



Figure C.3: Rockfall Simulation: $R_n = 0.33$ $R_t = 0.87$; Slope Angle 45° ; Drop Height 20m



Figure C.4: Rockfall Simulation: $R_n = 0.33$ $R_t = 0.87$; Slope Angle 45° ; Drop Height 30m



Figure C.5: Rockfall Simulation: $R_n = 0.33$ $R_t = 0.87$; Slope Angle 45° ; Drop Height 40m



Figure C.6: Rockfall Simulation: $R_n = 0.33$ $R_t = 0.87$; Slope Angle 45° ; Drop Height 50m



Figure C.7: Rockfall Simulation: $R_n = 0.33$ $R_t = 0.87$; Slope Angle 45° ; Drop Height 60m



Figure C.8: Rockfall Simulation: $R_n = 0.33$ $R_t = 0.87$; Slope Angle 45° ; Drop Height 70m



Figure C.9: Rockfall Simulation: $R_n = 0.33$ $R_t = 0.87$; Slope Angle 55° ; Drop Height 10m



Figure C.10: Rockfall Simulation: $R_n = 0.33$ $R_t = 0.87$; Slope Angle 55° ; Drop Height 20m



Figure C.11: Rockfall Simulation: $R_n = 0.33$ $R_t = 0.87$; Slope Angle 55° ; Drop Height 30m



Figure C.12: Rockfall Simulation: $R_n = 0.33$ $R_t = 0.87$; Slope Angle 55° ; Drop Height 40m



Figure C.13: Rockfall Simulation: $R_n = 0.33$ $R_t = 0.87$; Slope Angle 55° ; Drop Height 50m

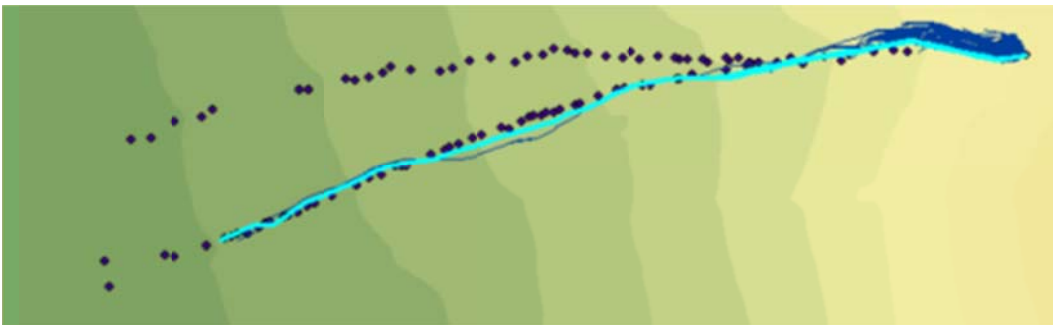


Figure C.14: Rockfall Simulation: $R_n = 0.33$ $R_t = 0.87$; Slope Angle 55° ; Drop Height 60m



Figure C.15: Rockfall Simulation: $R_n = 0.33$ $R_t = 0.87$; Slope Angle 55° ; Drop Height 70m



Figure C.16: Rockfall Simulation: $R_n = 0.33$ $R_t = 0.87$; Slope Angle 65° ; Drop Height 10m



Figure C.17: Rockfall Simulation: $R_n = 0.33$ $R_t = 0.87$; Slope Angle 65° ; Drop Height 20m



Figure C.18: Rockfall Simulation: $R_n = 0.33$ $R_t = 0.87$; Slope Angle 65° ; Drop Height 30m



Figure C.19: Rockfall Simulation: $R_n = 0.33$ $R_t = 0.87$; Slope Angle 65° ; Drop Height 40m



Figure C.20: Rockfall Simulation: $R_n = 0.33$ $R_t = 0.87$; Slope Angle 65° ; Drop Height 50m



Figure C.21: Rockfall Simulation: $R_n = 0.33$ $R_t = 0.87$; Slope Angle 65° ; Drop Height 60m



Figure C.22: Rockfall Simulation: $R_n = 0.33$ $R_t = 0.87$; Slope Angle 65° ; Drop Height 70m



Figure C.23: Rockfall Simulation: $R_n = 0.33$ $R_t = 0.87$; Slope Angle 75° ; Drop Height 10m



Figure C.24: Rockfall Simulation: $R_n = 0.33$ $R_t = 0.87$; Slope Angle 75° ; Drop Height 20m



Figure C.25: Rockfall Simulation: $R_n = 0.33$ $R_t = 0.87$; Slope Angle 75° ; Drop Height 30m



Figure C.26: Rockfall Simulation: $R_n = 0.33$ $R_t = 0.87$; Slope Angle 75° ; Drop Height 40m



Figure C.27: Rockfall Simulation: $R_n = 0.33$ $R_t = 0.87$; Slope Angle 75° ; Drop Height 50m



Figure C.28: Rockfall Simulation: $R_n = 0.33$ $R_t = 0.87$; Slope Angle 75° ; Drop Height 60m

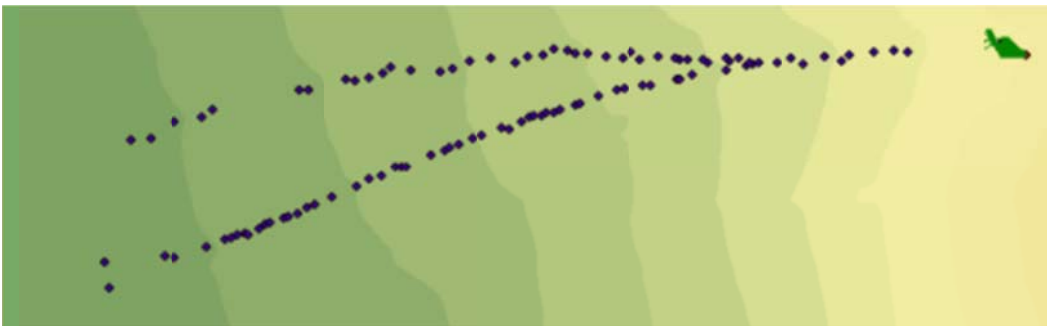


Figure C.29: Rockfall Simulation: $R_n = 0.33$ $R_t = 0.87$; Slope Angle 75° ; Drop Height 70m

These simulations suggest that the rockfall event noted at Tornado Mountain experienced a starting energy similar to that found in the ranges of 45° - 65° at drop heights of 50m-70m. Limiting further study to these ranges, the COR is changed to the typical values noted in the literature and RocScience table. These values are:

$$\begin{aligned} R_n &= 0.3 \\ R_t &= 0.8 \end{aligned}$$



Figure C.30: Rockfall Simulation: $R_n = 0.3$ $R_t = 0.8$; Slope Angle 45° ; Drop Height 50m



Figure C.31: Rockfall Simulation: $R_n = 0.3$ $R_t = 0.8$; Slope Angle 45° ; Drop Height 60m



Figure C.32: Rockfall Simulation: $R_n = 0.3$ $R_t = 0.8$; Slope Angle 45° ; Drop Height 70m



Figure C.33: Rockfall Simulation: $R_n = 0.3$ $R_t = 0.8$; Slope Angle 55° ; Drop Height 50m



Figure C.34: Rockfall Simulation: $R_n = 0.3$ $R_t = 0.8$; Slope Angle 55° ; Drop Height 60m

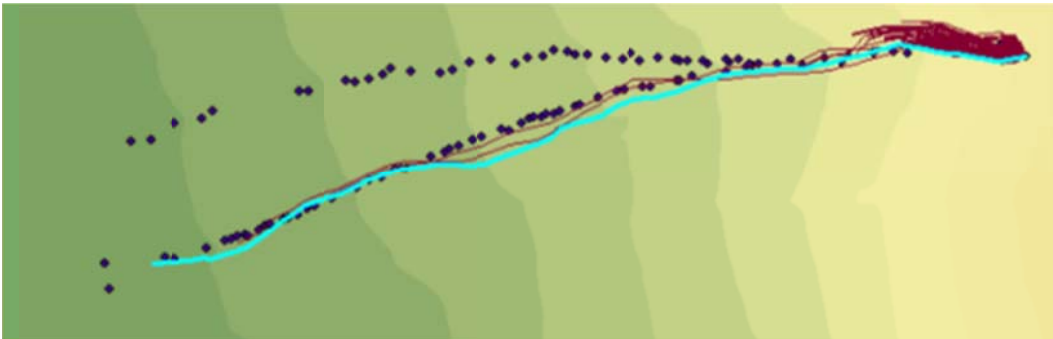


Figure C.35: Rockfall Simulation: $R_n = 0.3$ $R_t = 0.8$; Slope Angle 55° ; Drop Height 70m



Figure C.36: Rockfall Simulation: $R_n = 0.3$ $R_t = 0.8$; Slope Angle 65° ; Drop Height 50m



Figure C.37: Rockfall Simulation: $R_n = 0.3$ $R_t = 0.8$; Slope Angle 65° ; Drop Height 60m



Figure C.38: Rockfall Simulation: $R_n = 0.3$ $R_t = 0.8$; Slope Angle 65° ; Drop Height 70m

Repetition of results is noted in the trajectories of the above simulations. Following tests lower values of COR, as if the ground surface was absorbing more impact energy, to test the sensitivity in RA to this change. The reduced COR values are:

$$\begin{aligned} R_n &= 0.27 \\ R_t &= 0.77 \end{aligned}$$



Figure C.39: Rockfall Simulation: $R_n = 0.27$ $R_t = 0.77$; Slope Angle 45° ; Drop Height 50m



Figure C.40: Rockfall Simulation: $R_n = 0.27$ $R_t = 0.77$; Slope Angle 45° ; Drop Height 60m



Figure C.41: Rockfall Simulation: $R_n = 0.27$ $R_t = 0.77$; Slope Angle 45° ; Drop Height 70m



Figure C.42: Rockfall Simulation: $R_n = 0.27$ $R_t = 0.77$; Slope Angle 55° ; Drop Height 50m



Figure C.43: Rockfall Simulation: $R_n = 0.27$ $R_t = 0.77$; Slope Angle 55° ; Drop Height 60m



Figure C.44: Rockfall Simulation: $R_n = 0.27$ $R_t = 0.77$; Slope Angle 55° ; Drop Height 70m



Figure C.45: Rockfall Simulation: $R_n = 0.27$ $R_t = 0.77$; Slope Angle 65° ; Drop Height 50m



Figure C.46: Rockfall Simulation: $R_n = 0.27$ $R_t = 0.77$; Slope Angle 65° ; Drop Height 60m



Figure C.47: Rockfall Simulation: $R_n = 0.27$ $R_t = 0.77$; Slope Angle 65° ; Drop Height 70m

With COR being a dual parameter, both normal and tangential, there is a question as to which the rockfall simulation is more sensitive to. The following tests are taken with a typical tangential COR and a reduced normal COR:

$$\begin{aligned} R_n &= 0.27 \\ R_t &= 0.8 \end{aligned}$$

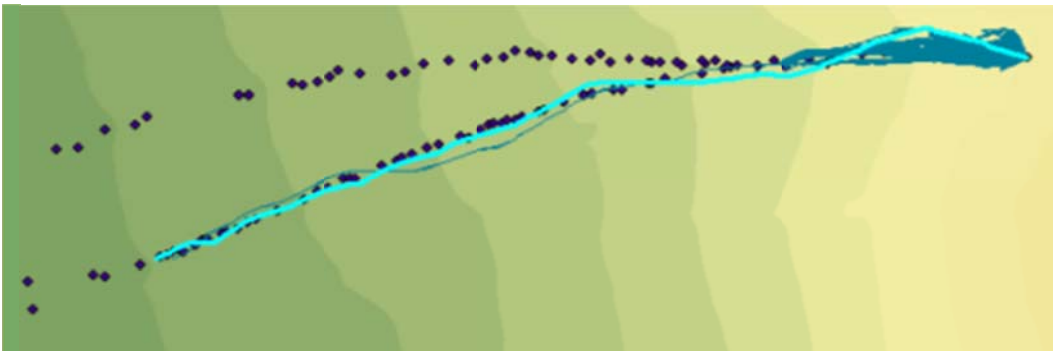


Figure C.48: Rockfall Simulation: $R_n = 0.27$ $R_t = 0.8$; Slope Angle 45° ; Drop Height 50m



Figure C.49: Rockfall Simulation: $R_n = 0.27$ $R_t = 0.8$; Slope Angle 45° ; Drop Height 60m



Figure C.50: Rockfall Simulation: $R_n = 0.27$ $R_t = 0.8$; Slope Angle 45° ; Drop Height 70m



Figure C.51: Rockfall Simulation: $R_n = 0.27$ $R_t = 0.8$; Slope Angle 55° ; Drop Height 50m



Figure C.52: Rockfall Simulation: $R_n = 0.27$ $R_t = 0.8$; Slope Angle 55° ; Drop Height 60m

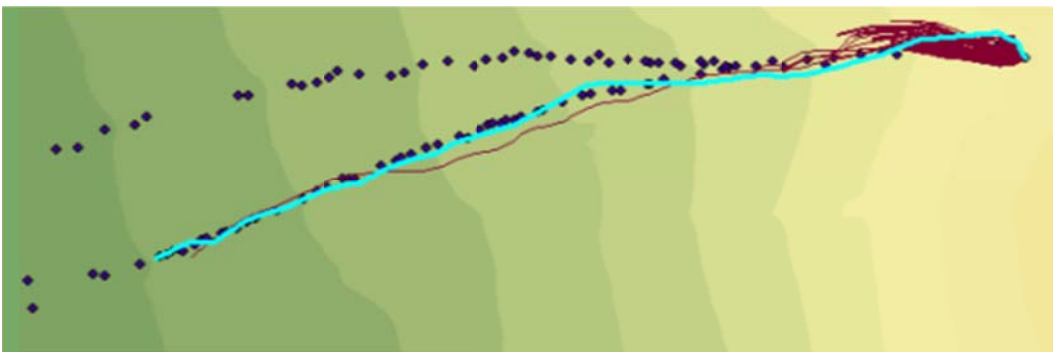


Figure C.53: Rockfall Simulation: $R_n = 0.27$ $R_t = 0.8$; Slope Angle 55° ; Drop Height 70m



Figure C.54: Rockfall Simulation: $R_n = 0.27$ $R_t = 0.8$; Slope Angle 65° ; Drop Height 50m



Figure C.55: Rockfall Simulation: $R_n = 0.27$ $R_t = 0.8$; Slope Angle 65° ; Drop Height 60m



Figure C.56: Rockfall Simulation: $R_n = 0.27$ $R_t = 0.8$; Slope Angle 65° ; Drop Height 70m

Tangential COR is reduced with the normal COR remaining at typical value. The COR values are:

$$\begin{aligned} R_n &= 0.3 \\ R_t &= 0.77 \end{aligned}$$



Figure C.57: Rockfall Simulation: $R_n = 0.3$ $R_t = 0.77$; Slope Angle 45° ; Drop Height 50m



Figure C.58: Rockfall Simulation: $R_n = 0.3$ $R_t = 0.77$; Slope Angle 45° ; Drop Height 60m



Figure C.59: Rockfall Simulation: $R_n = 0.3$ $R_t = 0.77$; Slope Angle 45° ; Drop Height 70m



Figure C.60: Rockfall Simulation: $R_n = 0.3$ $R_t = 0.77$; Slope Angle 55° ; Drop Height 50m



Figure C.61: Rockfall Simulation: $R_n = 0.3$ $R_t = 0.77$; Slope Angle 55° ; Drop Height 60m



Figure C.62: Rockfall Simulation: $R_n = 0.3$ $R_t = 0.77$; Slope Angle 55° ; Drop Height 70m



Figure C.63: Rockfall Simulation: $R_n = 0.3$ $R_t = 0.77$; Slope Angle 65° ; Drop Height 50m



Figure C.64: Rockfall Simulation: $R_n = 0.3$ $R_t = 0.77$; Slope Angle 65° ; Drop Height 60m



Figure C.65: Rockfall Simulation: $R_n = 0.3$ $R_t = 0.77$; Slope Angle 65° ; Drop Height 70m

The previous reduction of the COR values was minor, reflecting typical differences noted in the RocScience tables. A more significant reduction of the values may provide additional insight. The further reduced COR values for this test are:

$$\begin{aligned} R_n &= 0.15 \\ R_t &= 0.5 \end{aligned}$$

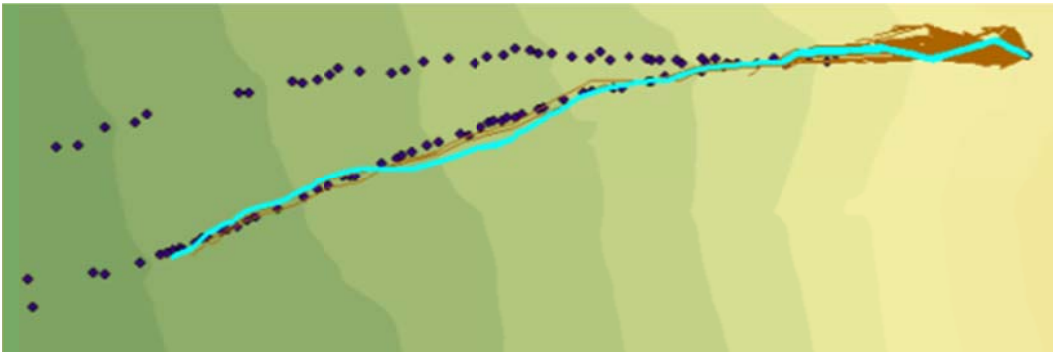


Figure C.66: Rockfall Simulation: $R_n = 0.15$ $R_t = 0.5$; Slope Angle 45° ; Drop Height 50m



Figure C.67: Rockfall Simulation: $R_n = 0.15$ $R_t = 0.5$; Slope Angle 45° ; Drop Height 60m



Figure C.68: Rockfall Simulation: $R_n = 0.15$ $R_t = 0.5$; Slope Angle 45° ; Drop Height 70m



Figure C.69: Rockfall Simulation: $R_n = 0.15$ $R_t = 0.5$; Slope Angle 55° ; Drop Height 50m



Figure C.70: Rockfall Simulation: $R_n = 0.15$ $R_t = 0.5$; Slope Angle 55° ; Drop Height 60m



Figure C.71: Rockfall Simulation: $R_n = 0.15$ $R_t = 0.5$; Slope Angle 55° ; Drop Height 70m



Figure C.72: Rockfall Simulation: $R_n = 0.15$ $R_t = 0.5$; Slope Angle 65° ; Drop Height 50m

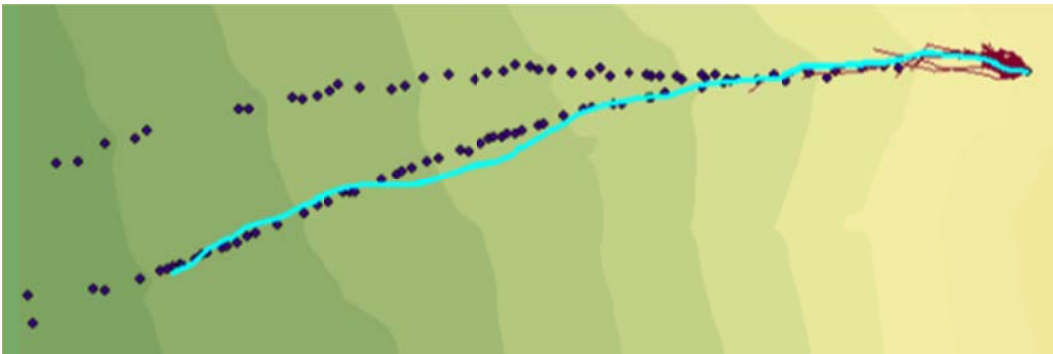


Figure C.73: Rockfall Simulation: $R_n = 0.15$ $R_t = 0.5$; Slope Angle 65° ; Drop Height 60m



Figure C.74: Rockfall Simulation: $R_n = 0.15$ $R_t = 0.5$; Slope Angle 65° ; Drop Height 70m

As with the previous change in COR, a sensitivity analysis should be performed by varying the normal and tangential COR values. The normal COR is reduced first:

$$\begin{aligned} R_n &= 0.15 \\ R_t &= 0.8 \end{aligned}$$



Figure C.75: Rockfall Simulation: $R_n = 0.15$ $R_t = 0.8$; Slope Angle 45° ; Drop Height 50m



Figure C.76: Rockfall Simulation: $R_n = 0.15$ $R_t = 0.8$; Slope Angle 45° ; Drop Height 60m



Figure C.77: Rockfall Simulation: $R_n = 0.15$ $R_t = 0.8$; Slope Angle 45° ; Drop Height 70m



Figure C.78: Rockfall Simulation: $R_n = 0.15$ $R_t = 0.8$; Slope Angle 55° ; Drop Height 50m



Figure C.79: Rockfall Simulation: $R_n = 0.15$ $R_t = 0.8$; Slope Angle 55° ; Drop Height 60m



Figure C.80: Rockfall Simulation: $R_n = 0.15$ $R_t = 0.8$; Slope Angle 55° ; Drop Height 70m

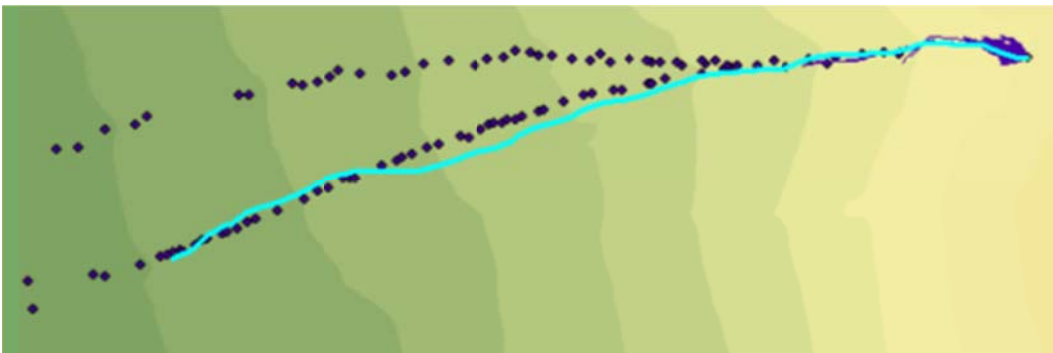


Figure C.81: Rockfall Simulation: $R_n = 0.15$ $R_t = 0.8$; Slope Angle 65° ; Drop Height 50m



Figure C.82: Rockfall Simulation: $R_n = 0.15$ $R_t = 0.8$; Slope Angle 65° ; Drop Height 60m



Figure C.83: Rockfall Simulation: $R_n = 0.15$ $R_t = 0.8$; Slope Angle 65° ; Drop Height 70m

The final section of the analysis is to reduce to the tangential COR by the greater degree.
The reduction of the COR is:

$$\begin{aligned} R_n &= 0.3 \\ R_t &= 0.5 \end{aligned}$$

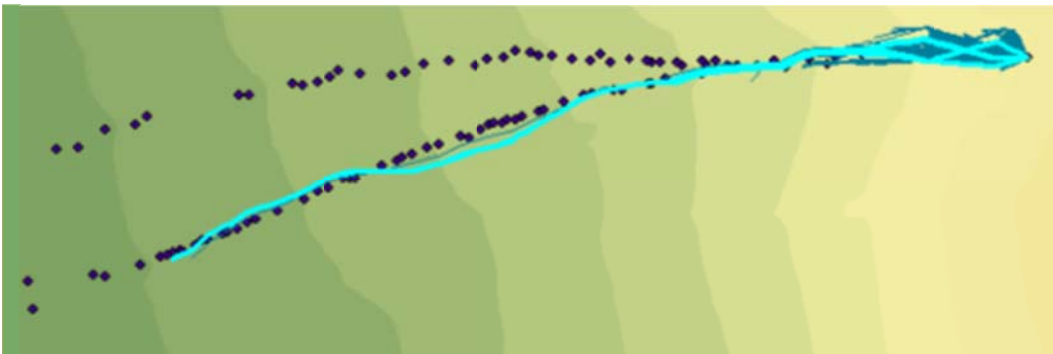


Figure C.84: Rockfall Simulation: $R_n = 0.3$ $R_t = 0.5$; Slope Angle 45° ; Drop Height 50m



Figure C.85: Rockfall Simulation: $R_n = 0.3$ $R_t = 0.5$; Slope Angle 45° ; Drop Height 60m



Figure C.86: Rockfall Simulation: $R_n = 0.3$ $R_t = 0.5$; Slope Angle 45° ; Drop Height 70m



Figure C.87: Rockfall Simulation: $R_n = 0.3$ $R_t = 0.5$; Slope Angle 55° ; Drop Height 50m



Figure C.88: Rockfall Simulation: $R_n = 0.3$ $R_t = 0.5$; Slope Angle 55° ; Drop Height 60m



Figure C.89: Rockfall Simulation: $R_n = 0.3$ $R_t = 0.5$; Slope Angle 55° ; Drop Height 70m



Figure C.90: Rockfall Simulation: $R_n = 0.3$ $R_t = 0.5$; Slope Angle 65° ; Drop Height 50m



Figure C.91: Rockfall Simulation: $R_n = 0.3$ $R_t = 0.5$; Slope Angle 65° ; Drop Height 60m



Figure C.92: Rockfall Simulation: $R_n = 0.3$ $R_t = 0.5$; Slope Angle 65° ; Drop Height 70m

The results of the surveys can be summed up in maximum and median rockfall travel distance. This travel distance is from the chosen seeder point rather than the rockfall source, and is therefore not the total rockfall travel distance. See Table C.3.

Table C.3: Maximum and Median Rockfall Travel Distances Based on COR, Drop Height, and Slope Angle

Bounding COR				Typical COR			
angle	height	median	max	angle	height	median	max
45	50	36.67022	550.6058	45	50	36.5247	508.1911
45	60	65.91832	588.2212	45	60	70.34177	510.587
45	70	99.81419	512.0249	45	70	98.9711	509.4695
55	50	22.79497	511.163	55	50	22.80895	506.1098
55	60	23.41401	510.0409	55	60	23.40733	505.6557
55	70	23.72549	548.985	55	70	23.72042	557.9616
65	50	21.46653	139.9952	65	50	21.45453	139.9687
65	60	26.58127	504.7581	65	60	26.62431	504.6745
65	70	26.53299	548.9012	65	70	26.52253	567.2765
Reduced COR				Reduced Rn			
angle	height	median	max	angle	height	median	max
45	50	36.5247	508.062	45	50	36.5247	515.6812
45	60	70.34177	510.4588	45	60	70.34177	510.4908
45	70	98.30145	509.4914	45	70	98.73693	509.4947
55	50	22.80895	162.7185	55	50	22.80895	162.7074
55	60	23.40733	505.5452	55	60	23.40733	505.5824
55	70	23.72042	509.7089	55	70	23.72042	518.5229
65	50	21.45453	140.005	65	50	21.45453	140.0003
65	60	26.62431	504.6994	65	60	26.62431	504.6481
65	70	26.52253	561.228	65	70	26.52253	561.544
Reduced Rt				Greatly Reduced COR			
angle	height	median	max	angle	height	median	max
45	50	36.5247	508.16	45	50	36.5247	507.0773
45	60	70.34177	510.5919	45	60	70.34177	507.008
45	70	98.98222	509.4846	45	70	89.3853	508.4984
55	50	22.80895	506.0924	55	50	22.80895	295.9142
55	60	23.40733	505.6314	55	60	23.40733	139.4772
55	70	23.72042	559.9309	55	70	23.72042	480.7821
65	50	21.45453	139.9765	65	50	21.45453	504.5076
65	60	26.62431	505.1432	65	60	26.66753	504.8292
65	70	26.52253	559.54	65	70	26.52253	503.985
Greatly Reduced Rn				Greatly Reduced Rt			
angle	height	median	max	angle	height	median	max
45	50	36.5247	507.8538	45	50	36.5247	507.7966
45	60	70.34177	509.6623	45	60	70.34177	510.2735
45	70	89.40888	508.5065	45	70	99.53457	509.4303
55	50	22.80895	508.8037	55	50	22.80895	163.9249
55	60	23.40733	504.753	55	60	23.40733	139.4163
55	70	23.72042	503.3597	55	70	23.72042	492.4543
65	50	21.45453	504.0099	65	50	21.45453	139.9651
65	60	26.62431	507.7078	65	60	26.62431	143.699
65	70	26.52253	505.7289	65	70	26.52253	505.3314

Figures 5.41 through 5.44 are the graphical representation of Table C.3. The following figures look at the same data points individually, rather than together, for greater detail. Refer to Table C.3 to confirm the angle and height of each point.

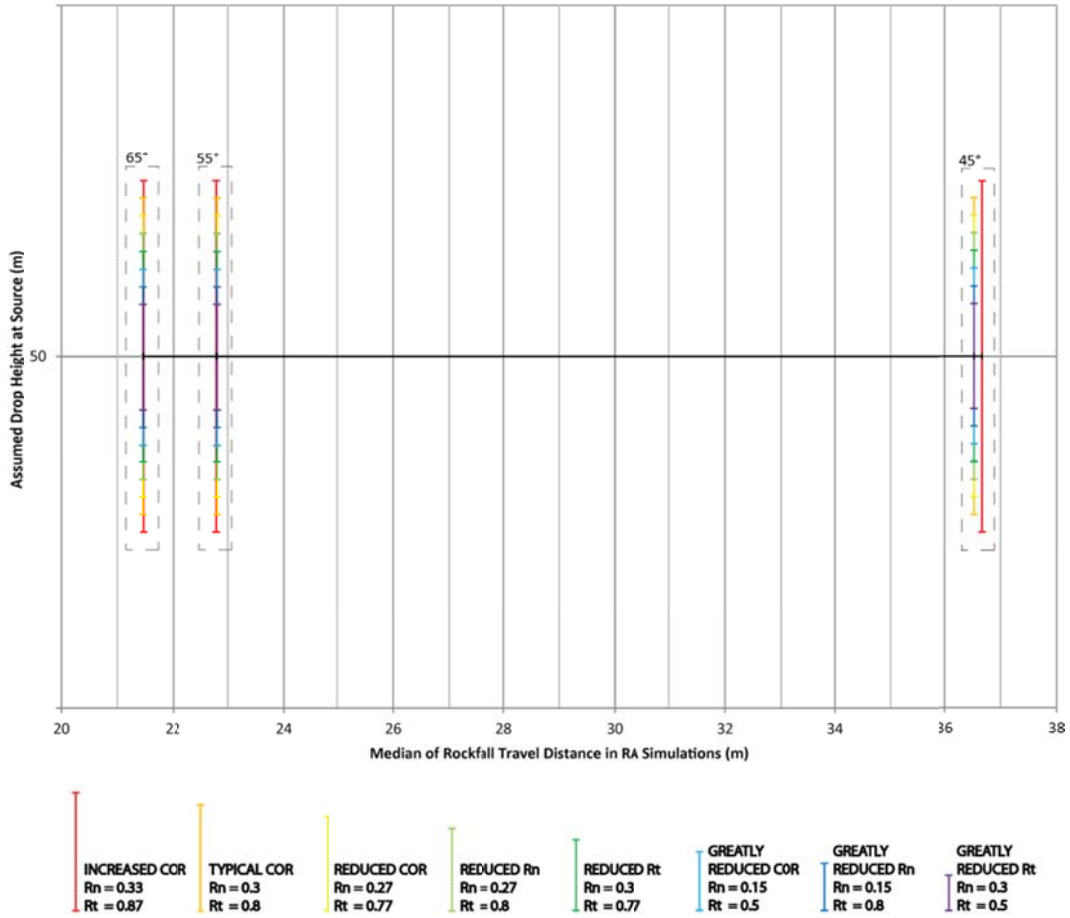


Figure C.93: Median Rockfall Travel Distance at 50m Drop Height

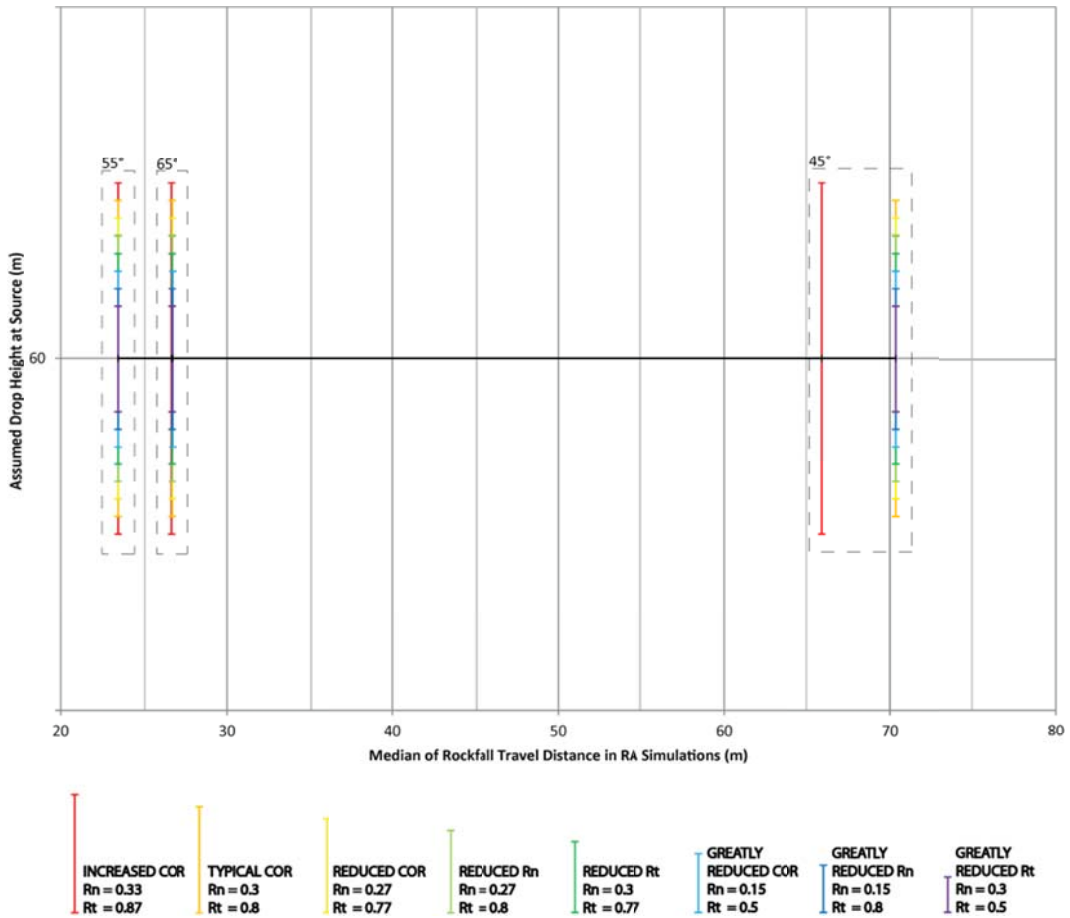


Figure C.94: Median Rockfall Travel Distance at 60m Drop Height

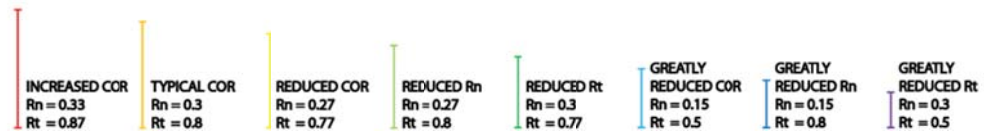
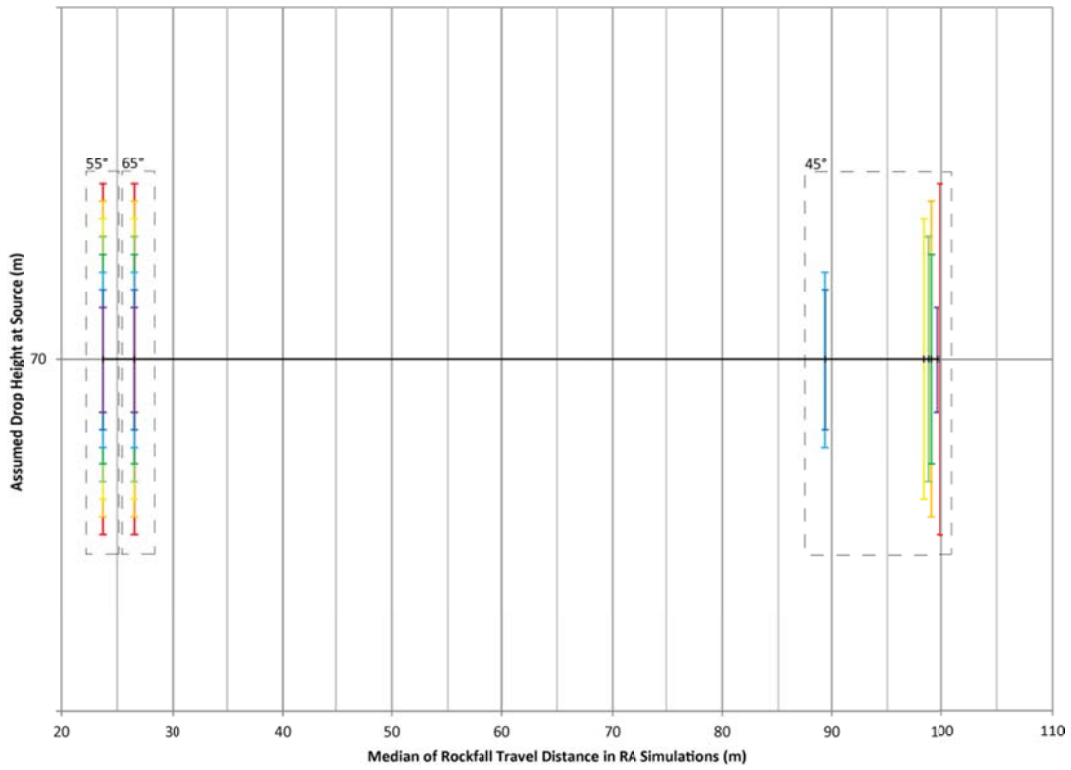


Figure C.95: Median Rockfall Travel Distance at 70m Drop Height

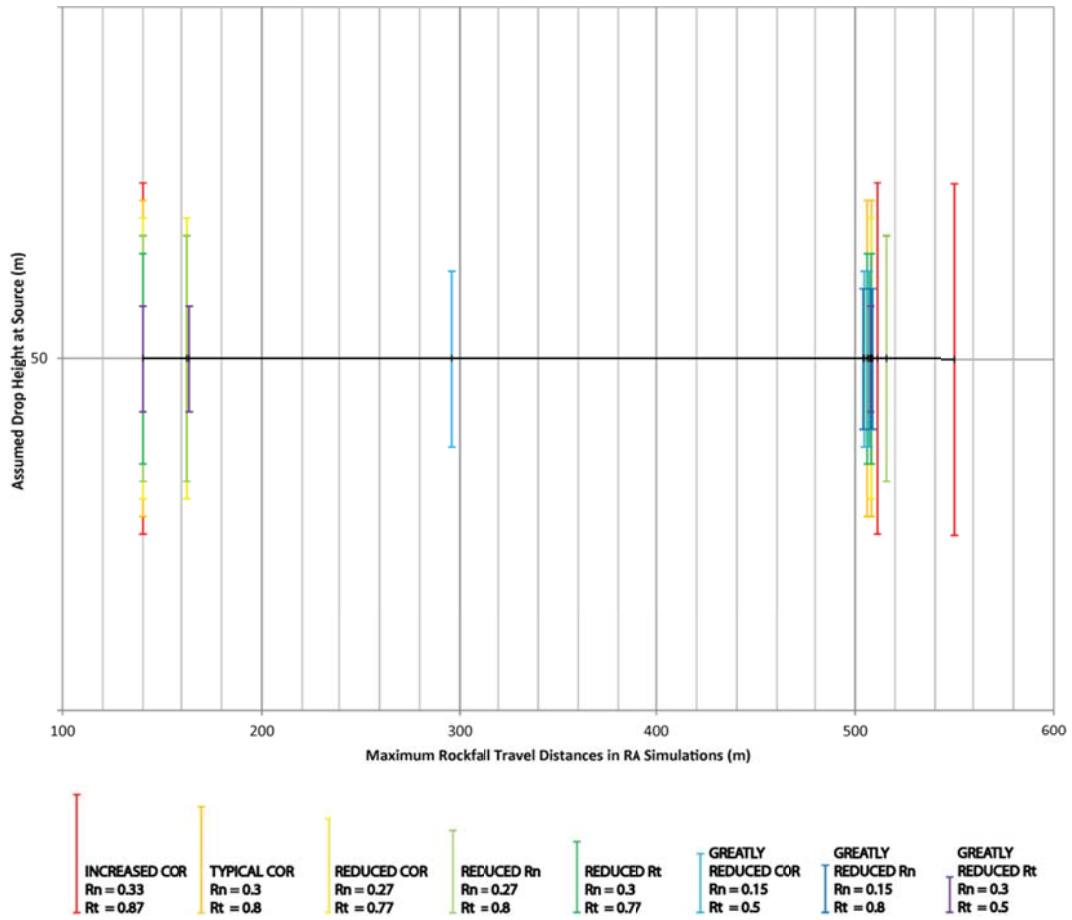


Figure C.96: Maximum Rockfall Travel Distance at 50m Drop Height

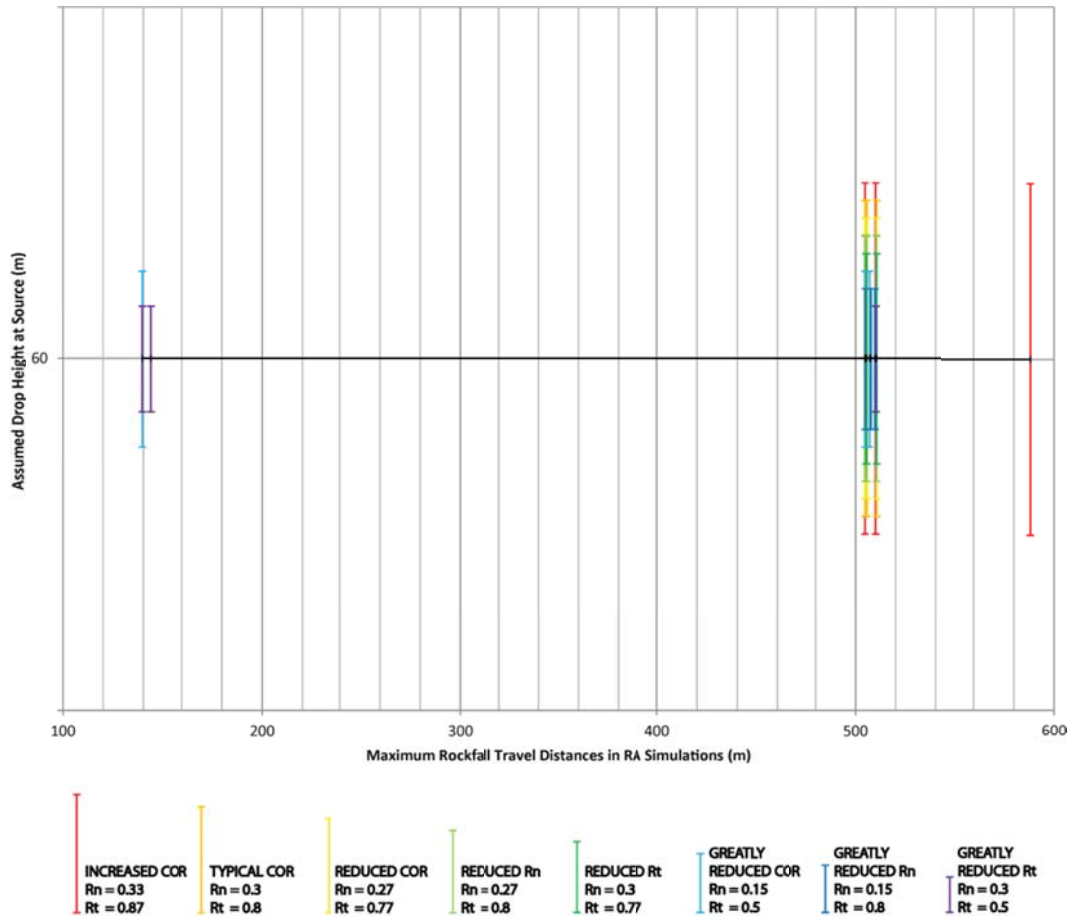


Figure C.97: Maximum Rockfall Travel Distance at 60m Drop Height

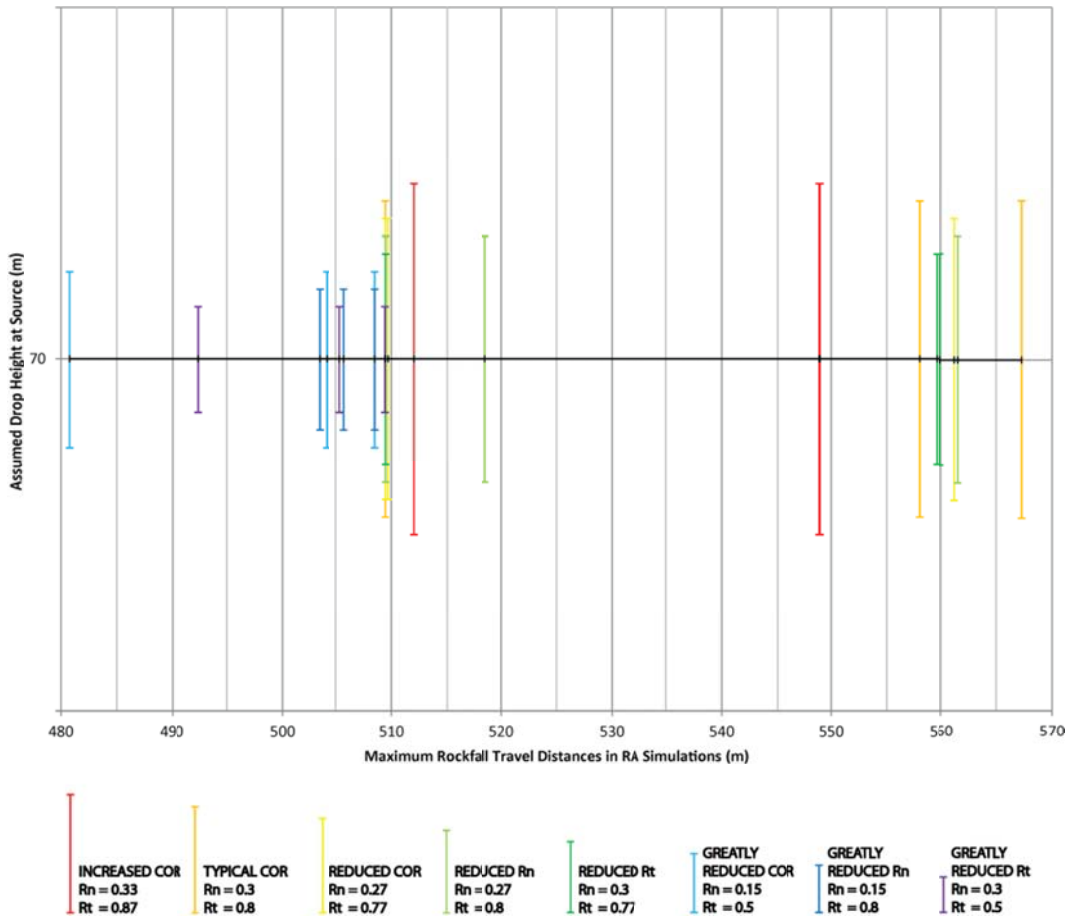


Figure C.98: Maximum Rockfall Travel Distance at 70m Drop Height

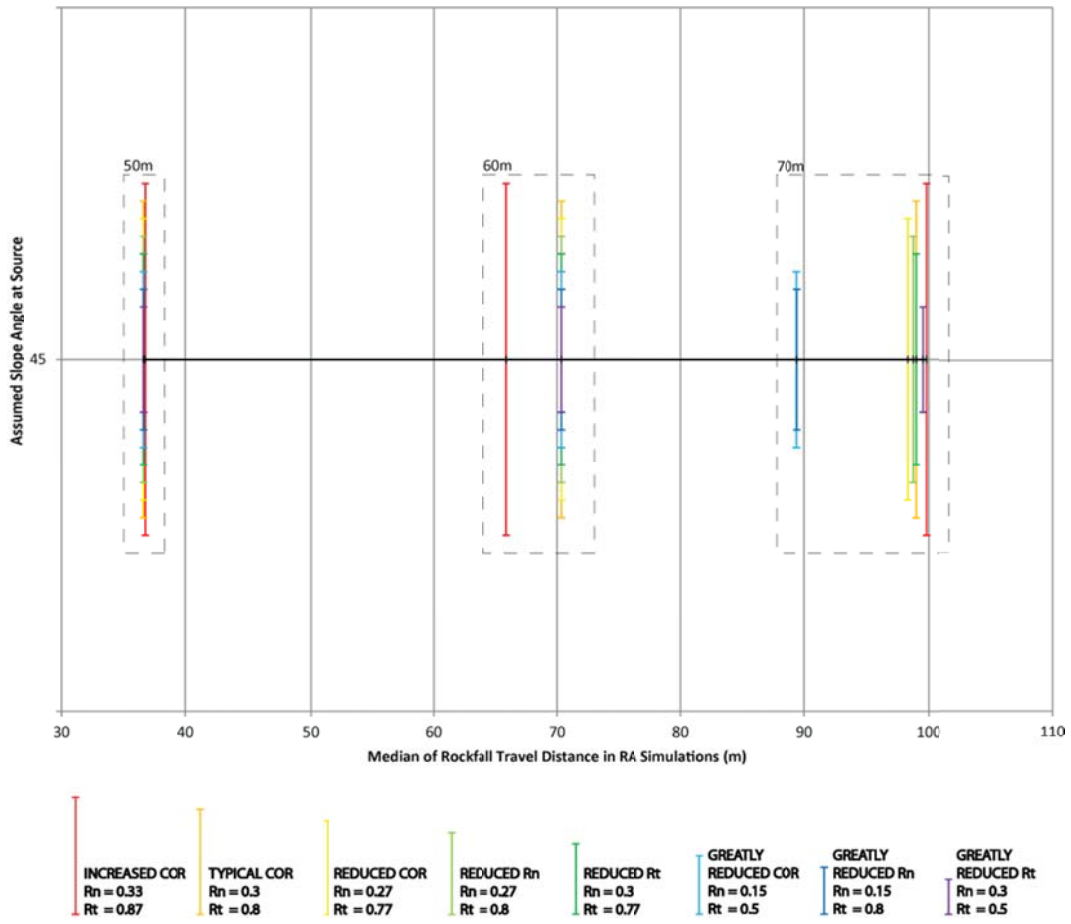


Figure C.99: Median Rockfall Travel Distance at 45° Slope Angle

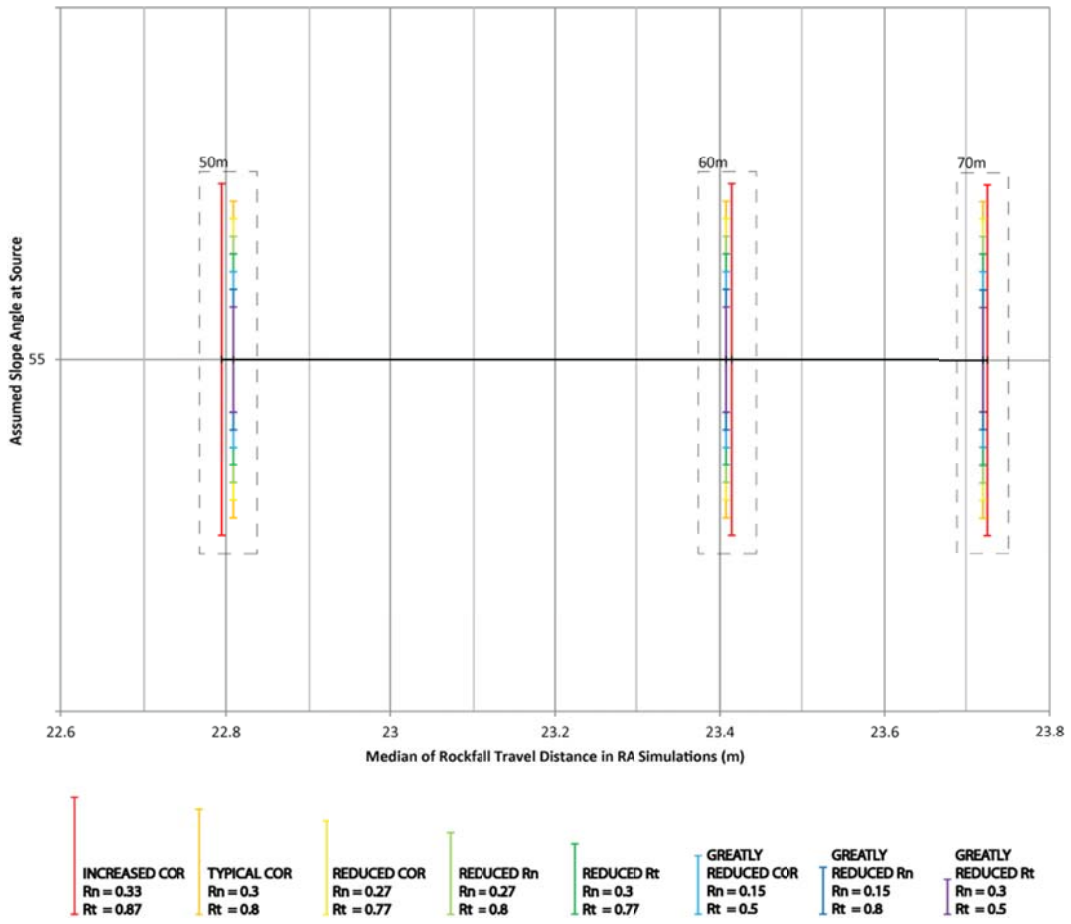


Figure C.100: Median Rockfall Travel Distance at 55° Slope Angle

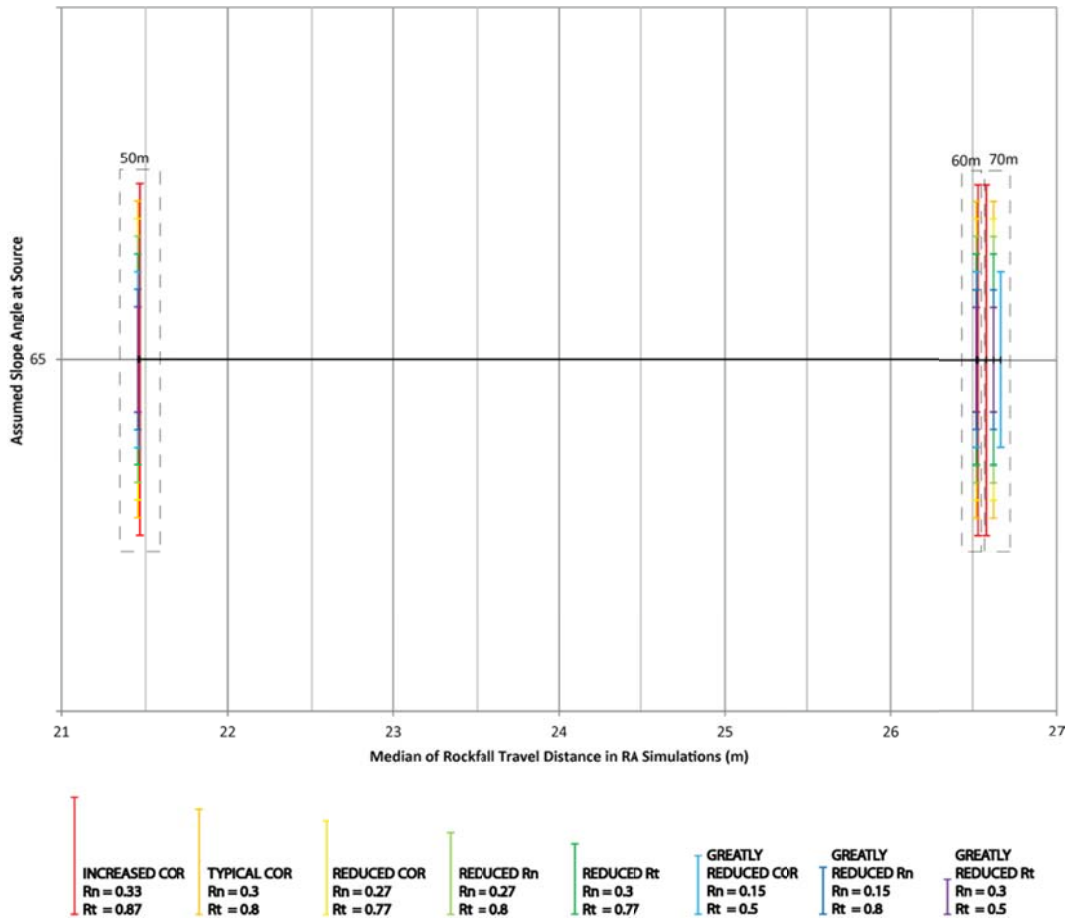


Figure C.101: Median Rockfall Travel Distance at 65° Slope Angle

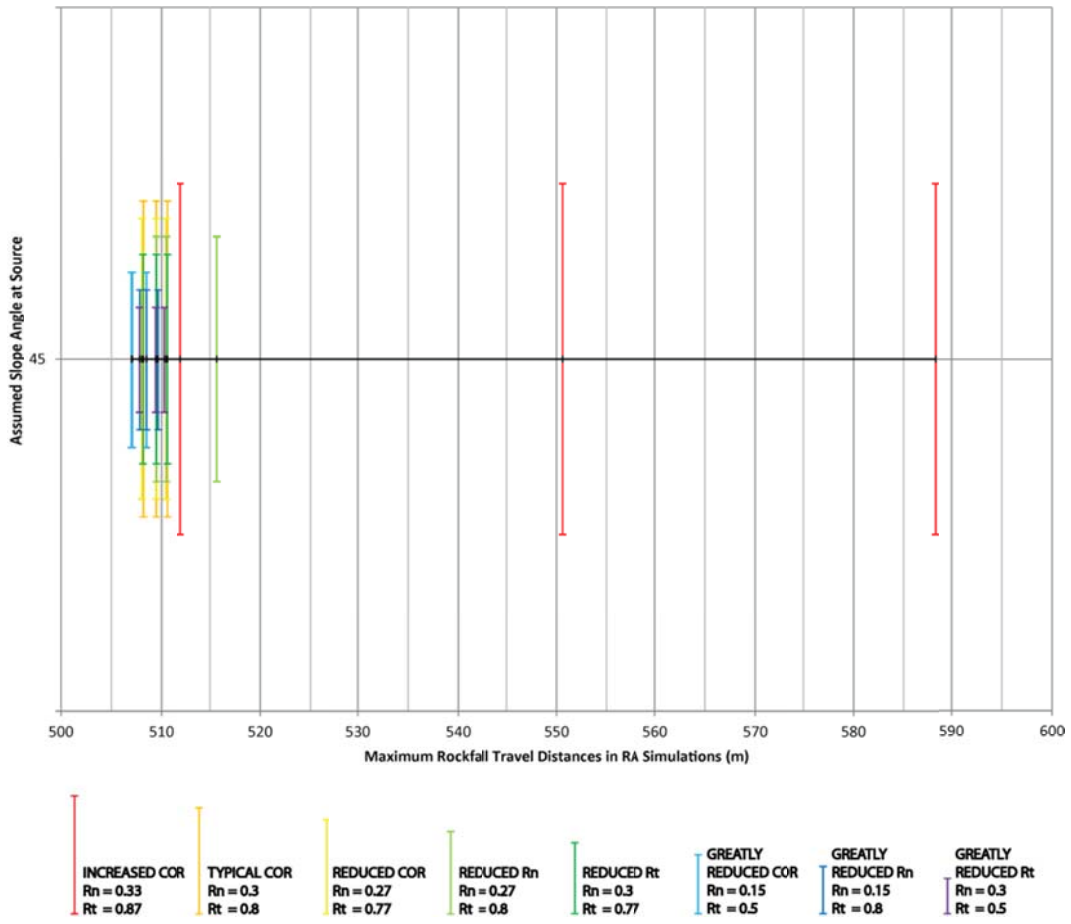


Figure C.102: Maximum Rockfall Travel Distance at 45° Slope Angle

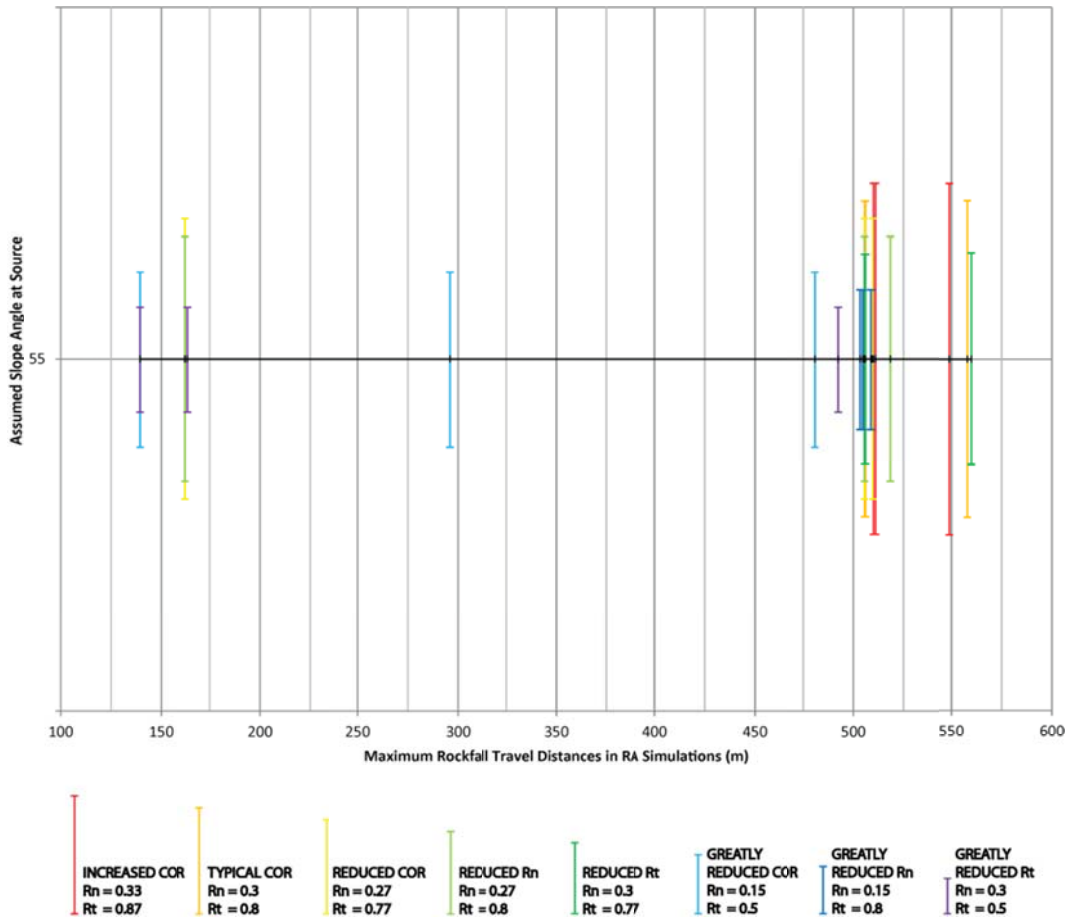


Figure C.103: Maximum Rockfall Travel Distance at 55° Slope Angle

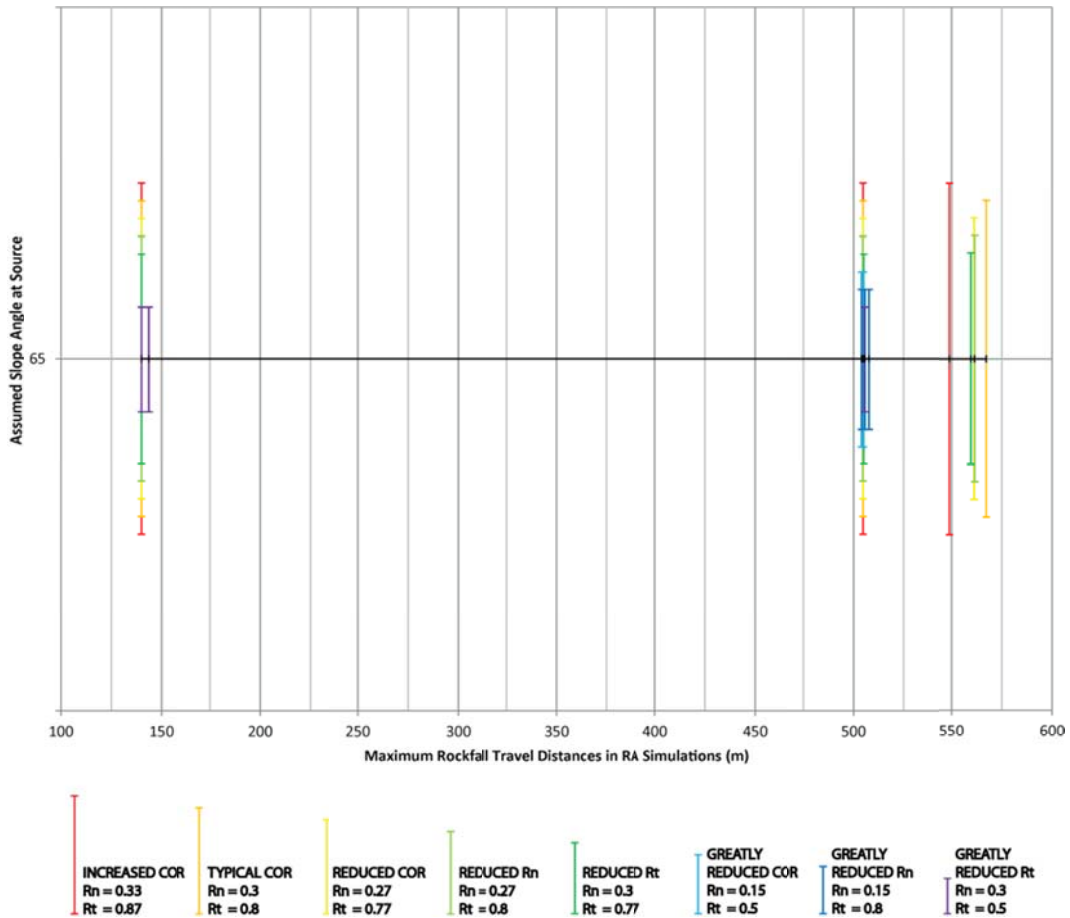


Figure C.104: Maximum Rockfall Travel Distance at 65° Slope Angle

The cumulative distribution curves for the slope length are shown here. The curves for the typical COR values is shown in the body of the document as Figure 5.47.

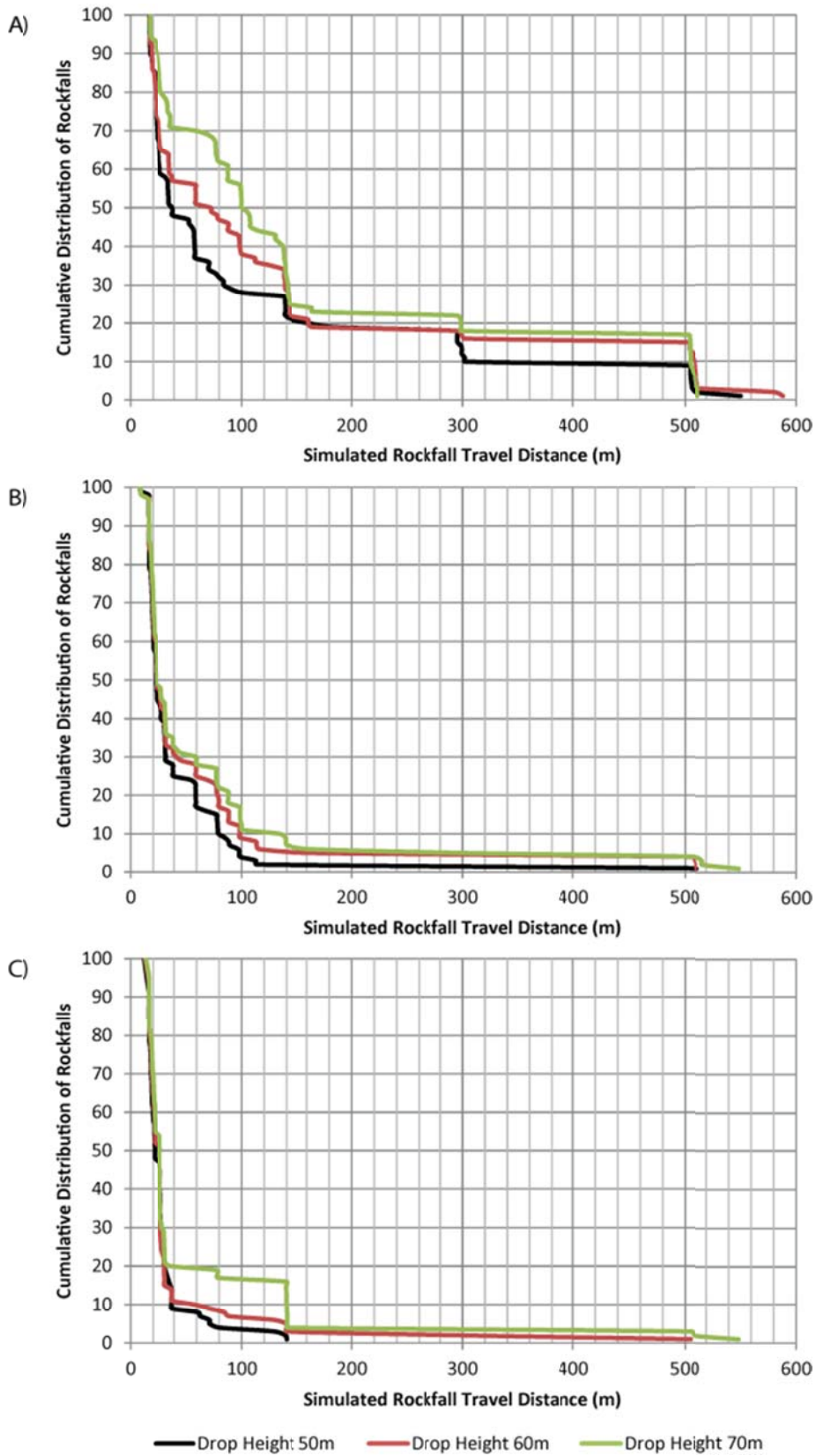


Figure C.105: Cumulative Distribution Curves for Increased COR at Assumed Slope Angles of A) 45°, B) 55°, and C) 65°

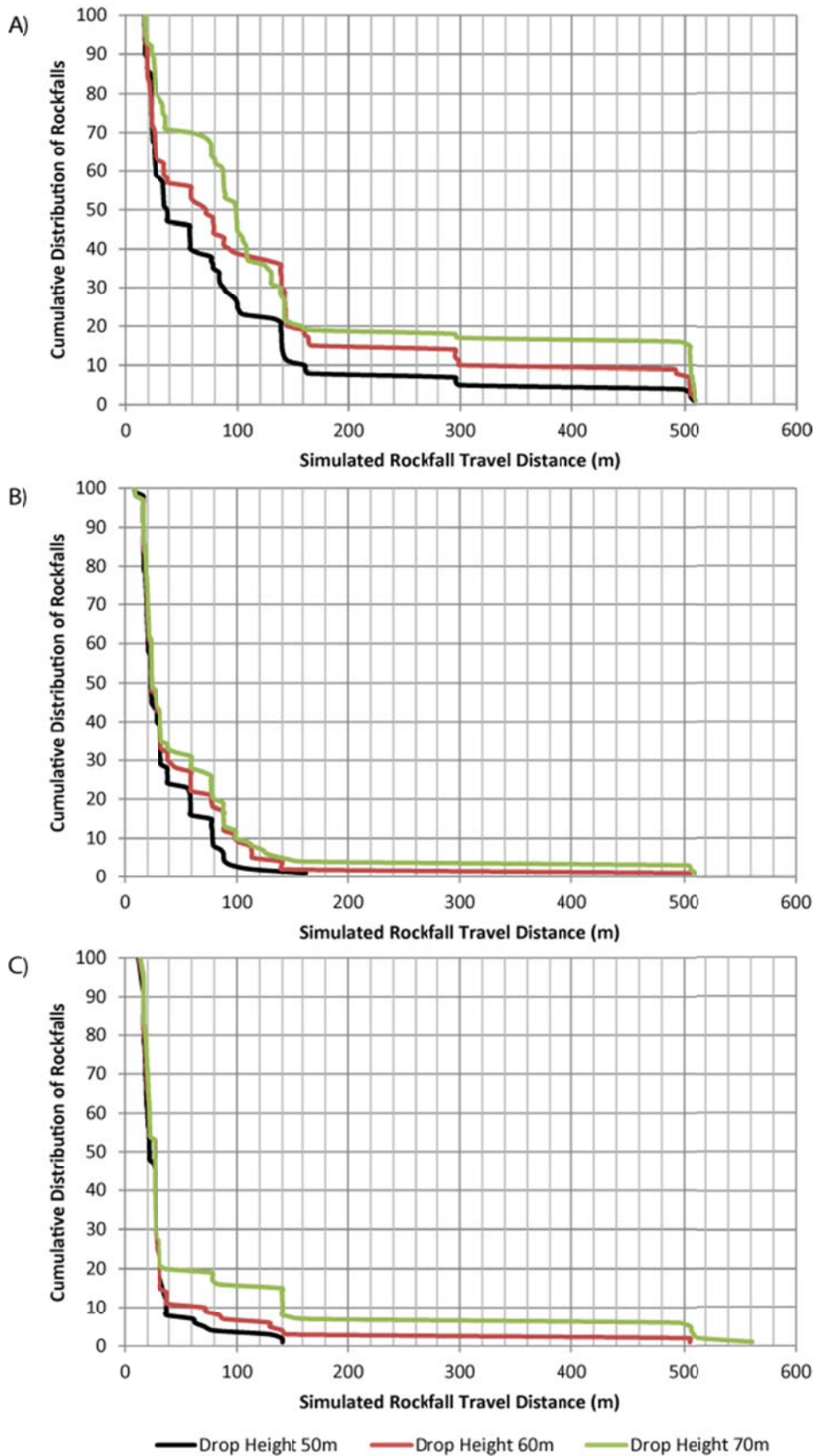


Figure C.106: Cumulative Distribution Curves for Reduced COR at Assumed Slope Angles of A) 45°, B) 55°, and C) 65°

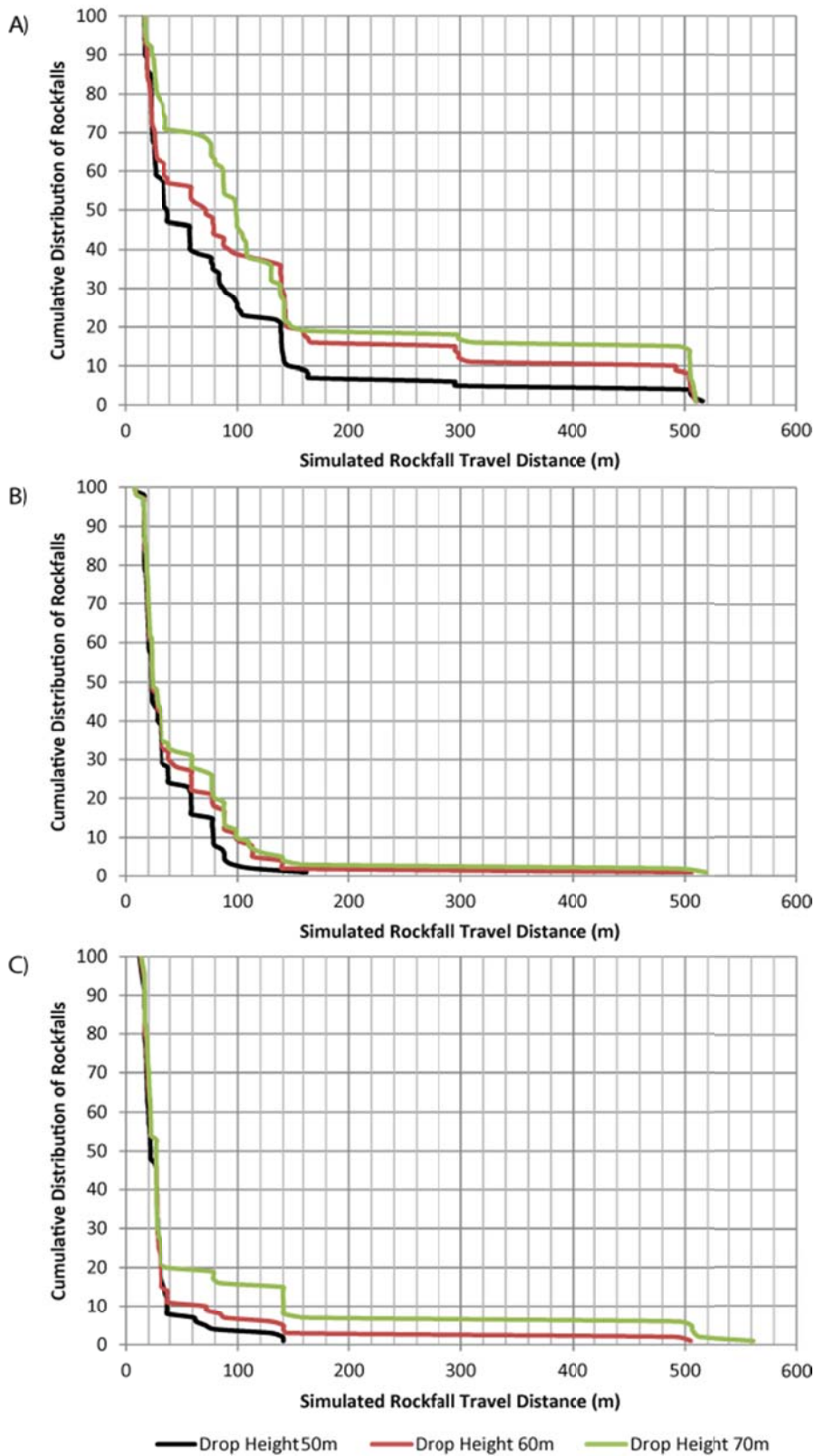


Figure C.107: Cumulative Distribution Curves for Reduced R_n at Assumed Slope Angles of A) 45° , B) 55° , and C) 65°

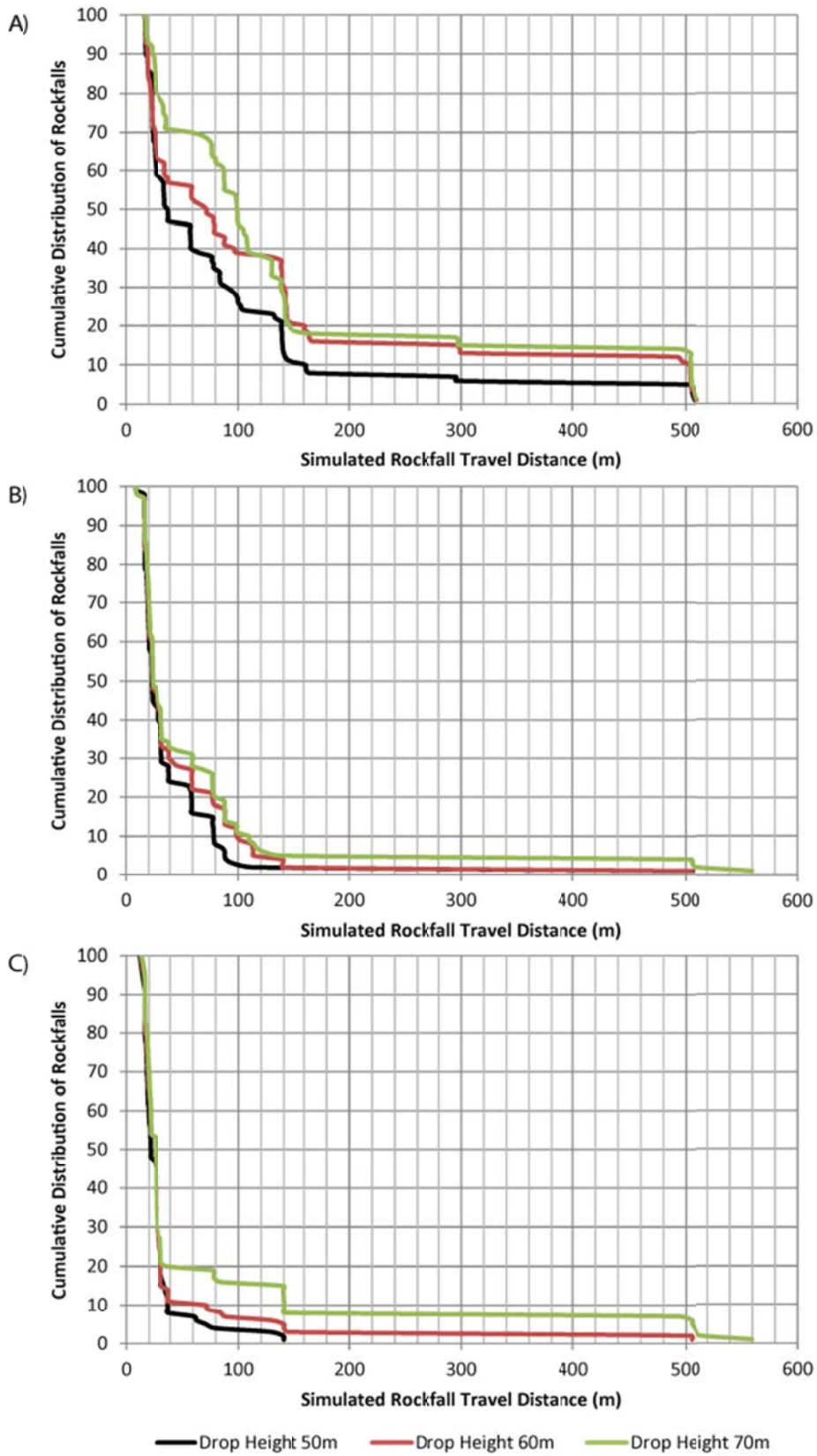


Figure C.108: Cumulative Distribution Curves for Reduced R_t at Assumed Slope Angles of A) 45°, B) 55°, and C) 65°

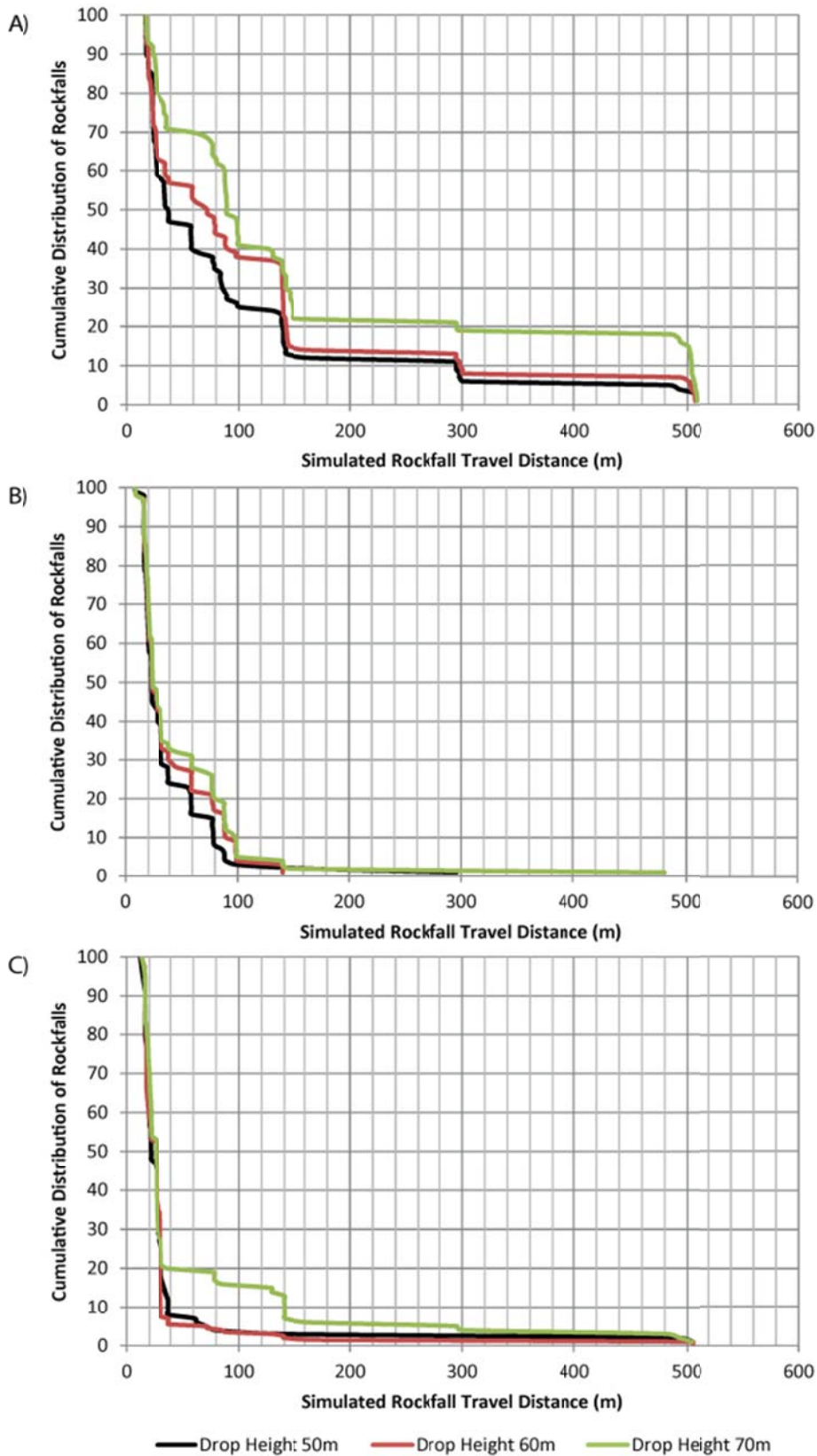


Figure C.109: Cumulative Distribution Curves for Greatly Reduced COR at Assumed Slope Angles of A) 45°, B) 55°, and C) 65°

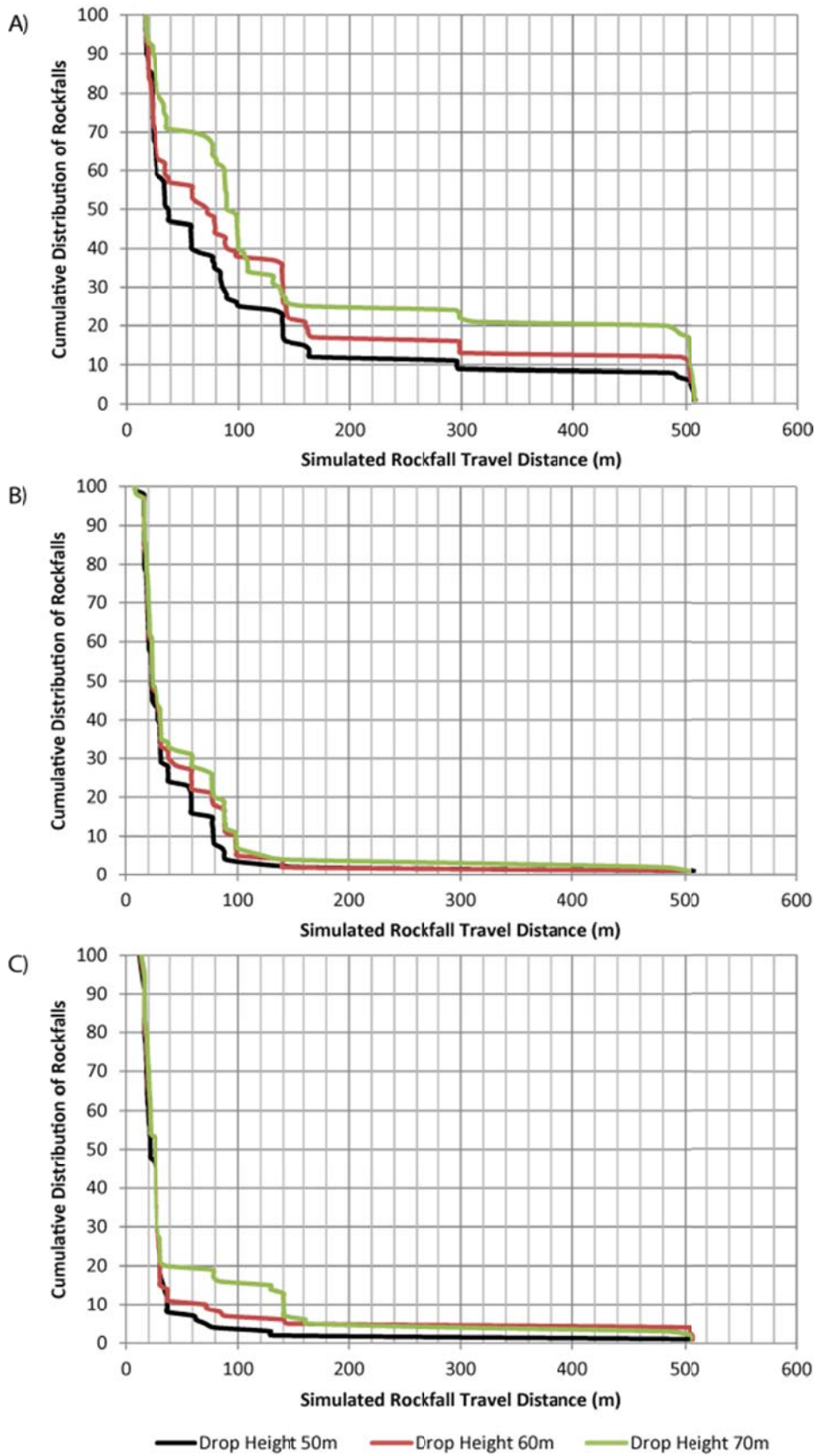


Figure C.110: Cumulative Distribution Curves for Greatly Reduced R_n at Assumed Slope Angles of A) 45°, B) 55°, and C) 65°

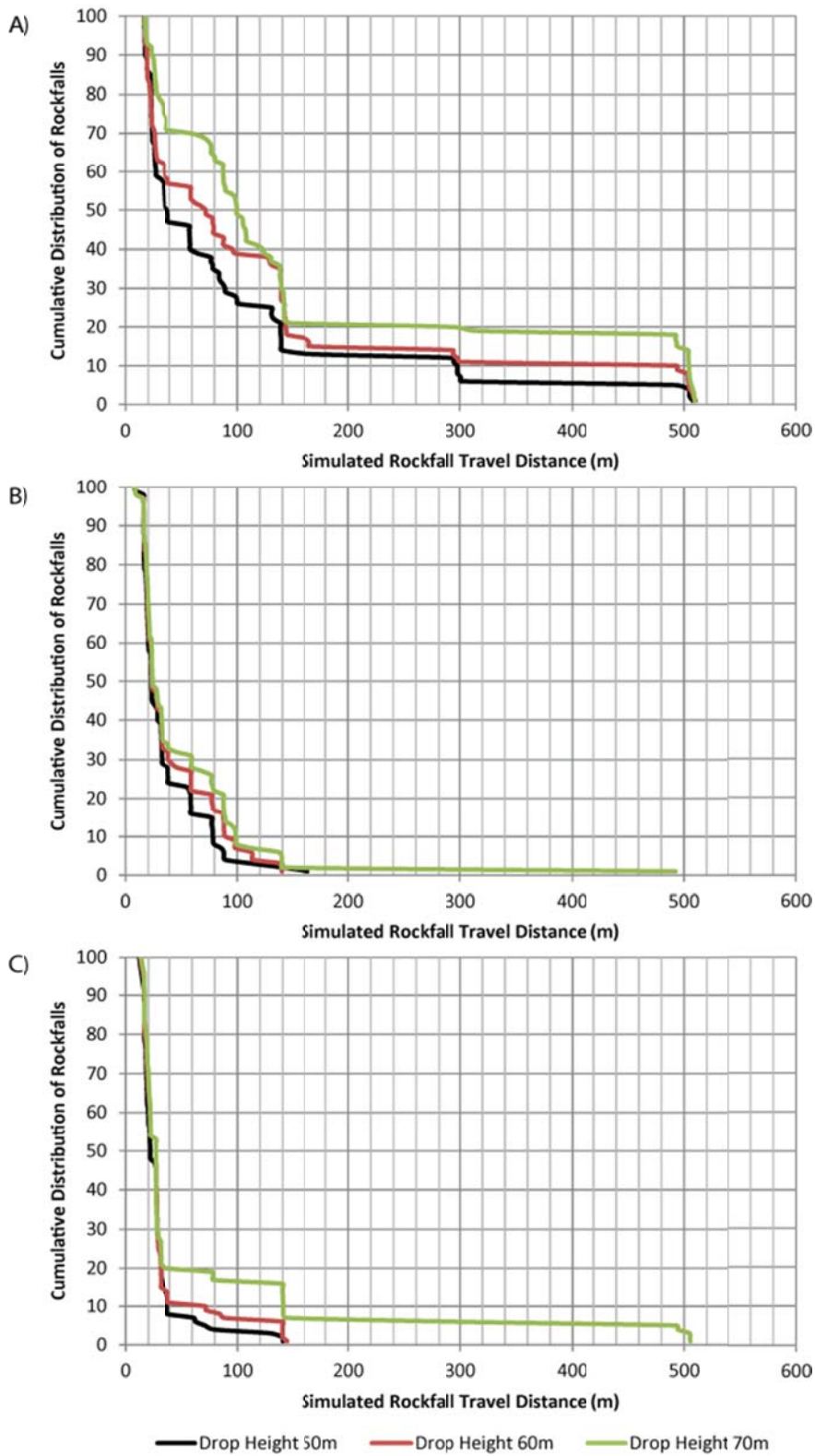


Figure C.111: Cumulative Distribution Curves for Greatly Reduced R_t at Assumed Slope Angles of A) 45°, B) 55°, and C) 65°